Development of a Fabrication Technique for Soft Planar Inflatable Composites

By

Jun Wai Kow

Submitted in accordance with the requirements for the degree of

Doctor of Philosophy

The University of Leeds

Institute of Design, Robotic and Optimisation

School of Mechanical Engineering

April 2020

The candidate confirms that the work submitted is his own, except where work which has formed part of jointly authored publications has been included. The contribution of the candidate and the other authors to this work has been explicitly indicated below. The candidate confirms that appropriate credit has been given within the thesis where reference has been made to the work of others.

The work presented here includes the papers below, and is partly used in Chapters 1 – 6:

- Kow J; Culmer P; Alazmani A. (2018) **Thin Soft layered Actuator Based on a Novel Fabrication Technique.** - IEEE RAS RoboSoft'18. DOI: https://doi.org/10.1109/ROBOSOFT.2018.8404916
- Kow J; Jones D; Culmer P; Alazmani A. (2020) **Adjustable Stiffness Soft Sensor via a Soft Lamination Fabrication Technique** - [Under Preparation]

For the papers above, I was responsible for the technical work carried-out in the listed papers above, the co-authors were responsible for reviewing the papers.

Acknowledgements

I would like to first thank my two, incredibly talented and supportive supervisors – Dr Ali Alazmani and Dr Peter Culmer for their tremendous support and guidance over the course of my research degree and initially paving the way and providing me the opportunity to embark on this journey starting my research degree.

I would also like to thank the people behind the Surgical Technologies research group; past and present within the length of time that I have been part of. It has been a pleasure working with the group in various aspects in the context of research work, collaboration projects as well as student support. Here's to my colleagues; Dominic Jones, Mark Zhang and Dushyant Goordyal for going through this journey with me. A special shout-out to Dushyant, for his ever hyped-enthusiasm in life and vibrant personality that has made the office environment one heck of a roller-coaster ride along with his antics that has positively affected those around him.

Thank you to my family and friends for supporting and encouraging me throughout this journey. I may have not been my best at times but knowing that you would still stand by me is more than I ever could hope for. As we continue to learn and walk in various paths of life, I am truly grateful to have you all.

I would also like to dedicate my thanks to my future partner, wherever she may be. I may have finished this part of my journey with or without you, but certainly you will be hearing the good, bad, ups and down as adventures of this journey soon.

Abstract

Soft robotics is a rapidly growing field in robotics that combines aspects of biologically inspired characteristics to unorthodox methods capable of conforming and/or adapting to unknown tasks or environments that would otherwise be improbable or complex with conventional robotic technologies. The field of soft robotics has grown rapidly over the past decade with increasing popularity and relevance to real-world applications. However, the means of fabricating these soft, compliant and intricate robots still poses a fundamental challenge, due to the liberal use of soft materials that are difficult to manipulate in their original state such as elastomers and fabric. These material properties rely on informal design approaches and bespoke fabrication methods to build soft systems. As such, there are a limited variety of fabrication techniques used to develop soft robots which hinders the scalability of robots and the time to manufacture, thus limiting their development.

This research focuses towards developing a novel fabrication method for constructing soft planar inflatable composites. The fundamental method is based on a sub-set of additive manufacturing known as composite layering. The approach is designed from a planar manner and takes layers of elastomeric materials, embedded strain-limiting and mask layers. These components are then built up through a layer-by-layer fabrication method with the use of a bespoke film applicator set-up. This enables the fabrication of millimetre-scale soft inflatable composites with complex integrated masks and/or strain-limiting layers. These inflatable composites can then be cut into a desired shape via laser cutting or ablation. A design approach was also developed to expand the functionality of these inflatable composites through modelling and simulation via finite element analysis. Proof of concept prototypes were designed and fabricated to enable pneumatic driven actuation in the form of bending soft actuators, adjustable stiffness sensor, and planar shape change. This technique highlights the feasibility of the fabrication method and the value of its use in creating multi-material composite soft actuators which are thin, compact, flexible, and stretchable and can be applicable towards real-world applications.

Contents

List of Tables

List of Figures

Chapter1: Introduction

This chapter introduces the context of the research to be embarked by firstly introducing the general concept of Soft Robotics, a paradigm shift in the field of robotics. The research motivation is then presented to underline the research problem, followed by the research aims and objectives set out to be achieved. Once the contribution of the study is highlighted, the structure of the thesis is presented to summarise the context of each chapter.

1.1 Paradigm Shift in Robotics: Soft Robotics

Conventional robotics as we know to date comprises of mechanically driven joints with robust links and assembled in a rigid structured body. These mechanical machines can be found in industry to the common household, ranging from various sizes and performing specific applications and tasks that in most cases outperforms human capabilities. Built with desired abilities for mobility, perception and cognition; these machines can perform complex tasks autonomously and repeatedly with precision, in staggering quantity and controlled quality. However, conventional robotics lack the adaptability and conformability when interacting with delicate, fragile tasks, along with unknown environments and situation; especially with humans [1, 2].

“Soft Robotics” is emerging as an interdisciplinary field of robotics that combines aspects of mechatronics, robotics, material and biomimetic engineering. The general concept depicts of autonomous systems with unorthodox or biologically inspired characteristics capable of conforming and/or adapting to unknown environments and tasks that would otherwise be improbable or very complex with conventional robotic technologies. It is described as a paradigm shift from conventional robotics, comprising of rigid links to continuum robots that are 'inherently compliant' [3-5]. Subsequently, soft robotics was formally presented as systems built with materials

of a certain degree or magnitude of compliancy and rigidity, ranging from structure to application [6]. As soft and compliant features are inherent attributes that are often exploited by biological systems, most soft system design and application can be seen drawing inspiration from biological systems and nature; some were developed to mimic and/or aid in human movement and interaction in the form of actuation or sensing.

The endless opportunities raised by the development of soft robotic systems in the past decade has led to the apparition of scientific journals dedicated to soft robotics [7]. A significant number of published review articles has justified the continuous growing interest in the field of soft robotics. Where advances in the field of soft robotic systems has seen innovative and complex forms of actuation, sensing and control, such as, mobility over various textures and surfaces, high level precision grasping, as well as adaptability and interaction with its environment [5, 8-11]. The transition of soft robotic systems can be seen shifting away from conventional robotics with rigid structures and incorporating soft features and compliant materials. However, many renown published works in soft robotics research focus solely on the single development of fundamental functionalities (actuation, sensing or control), underlying the development of soft robotics.

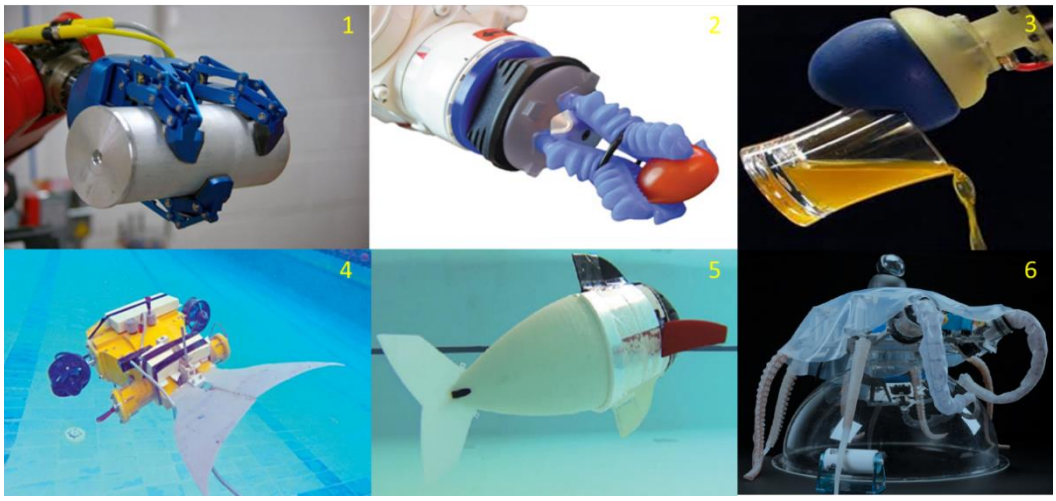

Figure 1.1 Conventional Robotics (1, 4); Soft robotics (2, 3, 5 and 6) ; 1. MIT Robotiq Gripper [12]; 2. mGrip [13]; 3 VERSABALL [14]; 4. DULI Robotic fish [15]; 5. IIT Soft robotic fish [16]; 6. Sant'Anna Italy Soft Robotic Octopus [17]

Despite the achievements of current growing research work on soft robotics, a methodological approach for soft robotic system fabrication have yet to be formulated as compared to its rigid and robust counterparts. Of which, a distinct development methodology exists and is much available commercially as standalone parts with integrable, adaptable components of actuation, sensing and control methods. The limitation of these soft systems lies with the lack of design morphology, fabrication techniques and control methods. The main challenge ahead for the field of soft robotics is to identify a definitive methodology and/or strategy to develop fully functional soft and compliant systems applicable to real world problems. However, the development of soft robotics is currently subjective and dependent to its application and approach, while its components for sensing, actuation, computation and power are sparsely diverse, which presents further challenges for creating soft robotic systems [6, 8, 11, 18].

1.2 Research Motivation

The field of soft robotics is still at an infant stage for development, where fabrication techniques are limited and design morphologies have been empirical. As the field continues to grow, the technological push is seen to be closely tied to the development of new manufacturing techniques and materials [11, 19]. Fabrication of soft robotics plays a central role in the resulting functionality of soft robotic devices. It is often echoed to be considered throughout the design process within the research community, as soft robotic devices are fundamentally dictated by the geometry and properties of its constituent materials compared to its developing application. In result, the behaviour and the motion exhibited by soft robotic devices can be designed relative to the development approach and application.

As reviewed by Laschi *et al*., a number of soft robotic applications have increasingly performant devices with intrinsic soft characteristics [9]. However, these soft robotic devices are typically developed at centimetre or larger scales and largely limited by its production through bespoke manufacturing and fabrication processes. Current study trends suggests a growing demand for smaller, precise, and dexterous soft

robotic devices [20]. This evidence draws its inspiration from biology and micro-organisms, as the emerging challenge aims to follow a 'building-block' or 'cell-structured' design methodology for an integrated approach by combining advance fabrication techniques with different materials and functionalities to invoke the next generation of soft robots. Among many, the approach addresses challenges in diverse areas such as healthcare, manipulation, and rehabilitation [11, 21, 22].

An investigation on soft robotic fabrication techniques to build on existing research opportunities has led the notion that the potential of soft robotic devices exist within the design structure and fabrication method from a (2-D) planar perspective [21]. While soft robotic fabrication from a planar perspective is existent across different scales, from meter-sized soft robots, to millimetre scale microdevices, it is believed that the potential of soft planar devices has yet to be fully explored [23, 24]. Thus, the development of a novel soft fabrication technique is proposed here to develop soft planar inflatable composites.

The main motivation behind this research work is to illustrate the use of soft structures to create functional devices through the development of soft elastomeric composites fabricated through a layer-by-layer process. The design and fabrication approach intends to embed structure and functionality from a two-dimension perspective to transform composites into 3-D structures that can be applicable in real-world robotic problems. By reconfiguring soft materials and innate mechanical properties to form planar structural layers, they can be combined in the form of a composite and be utilised to develop inflatable shape changing structures or actuatable motion. These soft composites are envisioned to be capable of integrating, adapting or going beyond tasks constraints of geometry and interaction of its environment. A range of technologies have been developed that has inspired the course of this research, such as soft interaction and actuation technologies, shape changing structures, flexible and stretchable sensing devices, haptic displays with dynamic stiffness, cognitive textures with tactile surfaces, and interactive augmented shape displays [24-27].

1.3 Aims and Objectives

The research aims to **design and develop a fabrication technique for a soft planar inflatable composite for soft robotics.** In order to fulfil the research aim, the objectives defined to achieve are:

1. To **study the literature and state-of-the-art soft robotics technologies** which would highlight the available techniques and progression within the field of research.

2. To **develop a design method for soft planar inflatable composites** in the form of soft robotic components, such as, actuators, sensors and structures.

3. To **develop a bespoke soft fabrication tool and technique for manufacturing** soft planar inflatable composites.

4. To **understand elastomeric material properties through the characterisation of its fabrication method** and applications.

5. To **model, simulate and potentially optimise the behaviour of soft planar inflatable composite designs** using digital modelling approaches, such as, **Finite Element Analysis (FEA) method**.

6. To **evaluate and demonstrate how soft planar inflatable composites can be leveraged for soft robotic applications** through evaluation of case studies based on soft fabrication methods and applications.

1.4 Thesis Structure

The individual chapters in this thesis is structured as followed along with a summary of its content:

Chapter 1 – Introduction

This chapter introduces the concept of Soft Robotics, a paradigm shift in the field of robotics. The research motivation is presented to underline the research problem. This is followed by the research aims and objectives set out to be achieved. The structure of the thesis is then presented to summarise the context of each chapter.

Chapter 2 – Soft Robotic Literature Review

The chapter introduces the field of soft robotics leading towards fabrication as the focus area to develop the research. The coverage includes the introduction of soft robotics, fundamental fabrication techniques to create soft robots and the progress of soft robotic technologies. The review will then summarise to understand and highlight the need for soft fabrication for soft systems and identify research gap in the field of soft robotics to reflection the research motivation introduced.

Chapter 3 – Soft Planar Inflatable Composite Fabrication Technique

This chapter introduces a bespoke fabrication technique developed by adopting existing additive manufacturing techniques of composite layering and adapting it into a soft fabrication technique to create soft planar inflatable composites. The fabrication method is described from conceptual planar designs to construction and production of soft composites in a planar manner. The fabrication process is described and showcased to highlight the feasibility and applicability of technique and the needed steps for further development

Chapter 4 – Characterisation of Soft Composite Fabrication Technique

The chapter defines the fabrication technique to develop soft planar inflatable composites for soft robotic applications through characterisation of the bespoke fabrication platform. As the fabrication method is described in the previous chapter, this chapter expresses the variability of the technique by characterising the fabrication process to assess its accuracy and repeatability in order to produce design controlled soft layered composites. The chapter first describes characterising of the film applicator based on desired thickness, speed and temperature against the material viscosity. Composite adhesion strength is then investigated to understand material dissociation via lamination. Finally, laser ablation through cutting and engraving of silicone material is described to produce the desired planar shapes from the fabricated soft planar composites.

Chapter 5 – Modelling and Simulation of Soft Composites

This chapter investigates the understanding elastomeric materials through finite element analysis modelling and methods. A modelling strategy is employed to characterise hyper-elastic materials in order to simulate its behaviour computationally. Followed by a design scheme to develop soft inflatable composites in the form of actuators. Evaluation and validation of the computational modelled soft composite actuators were then compared with fabricated soft composite actuators.

Chapter 6 – Case Studies

Combining the aspects of the fabrication technique, the characterisation of the techniques identifying its limitations and its possibilities, and the work illustrated through modelling and simulation through finite element analysis; this chapter presents how the developed soft composites are applicable in real-life applications in the form of case studies. A total of three case studies were performed with the developed soft planar inflatable composite fabrication technique.

Chapter 7 – Discussion and Conclusion

This chapter focuses on the limitations and feasibilities of the research outputs and will be presented with a general discussion along with possible point of improvements based on the research output. The concluding chapter of the research will then present a general review of the design development, fabrication technique and modelling aspect of the research in-line with the research objectives.

Chapter 8 –Future Work

The final chapter discusses the potential future works and improvements to existing work and establishes itself by concluding the research output of this PhD Thesis.

Appendix

An appendix providing further detail to the research carried out, including datasheets of components and materials used in this research.

Chapter 2: Literature Review

The chapter introduces the field of soft robotics as an overview from design to control, leading towards Fabrication of Soft Robotic Devices/Systems as the focus area of the review. The coverage of fabrication techniques for soft robots aims at giving an insight on the current state of the art in soft robotic manufacturing. In reflection, this provides an insight to soft robotic development from fundamental perspective of components, materials to methods and processes used to create soft robots. The chapter will then summarise with the current state of soft robotic fabrication and technologies to understand and highlight the need to innovate fabrication methods dedicated towards soft robotics.

2.1 Introduction to Soft Robotics

In the past decade, a growing area of research, 'Soft Robotics' highlights an informal approach to conventional robotics. The shift in paradigm for robotics no longer consists of rigid links, structurally robust bodies and mechanically solid components, but to continuum, flexible, deformable and 'inherently compliant' machines [1, 2, 18]. Conventional robotics are built with desired abilities for mobility, perception, and cognition. These machines can perform complex tasks autonomously and repeatedly. Advanced in industrial manufacturing sectors, conventional robotics are becoming prevalent and can be used in many tasks and scenarios. However, conventional robotics lacks the adaptability and conformability when interacting in natural tasks and environment, especially its interaction with humans. Cognitive capacities beyond the reach of artificial systems still require the involvement of human manipulation either in direct or collaborative manner. As such, this scientific shift is more than just a trend, but a justified evolutionary solution to one of shortcomings of conventional robotics towards the ability to perform safe physical human-robot interactions [5, 18, 28].

The conceptual imagery of soft robotics depicts of autonomous systems with unorthodox or biologically inspired characteristics. These characteristics are envisioned to be capable of conforming and/or adapting to unknown environments and tasks that would otherwise be improbable or very complex with conventional robotic technologies. A formal definition was agreed upon by The RoboSoft Coordination Action community during its first plenary meeting [29]: "*Soft robots are devices which can actively interact with the environment and which can undergo 'large' deformations relying on inherent or structural compliance*".

The word 'soft' in soft robotics refers to the material composition used to materialise and embody such systems, it can also refer to the compliance of a structure [5, 10, 30]. The context of softness can be interpreted in various ways, where soft robots are built from materials such as elastomeric rubber, silicone polymers, textiles and plastics. This is due to the material compliancy and structural deformity enabling its embodiment for task interaction and adaptation to its environment. Whereas, the actuation of these soft devices opt for the use of pneumatics, hydraulics and/or chemical reactions as compared to electronics and mechanical components such as electrical excitation, motors and gears. The use of pneumatic actuation often compliments soft robotic composition and embodiment, as compressed air is easier to store, readily available and environmentally friendly.

As one of the precursors of soft robotics, most soft system design and applications can be seen drawing inspiration from biological systems, such as animals and insects. As soft and compliant features are dominant attributes often exploited by biological systems, soft robotics strives to incorporate such capabilities through the configuration of mechanical properties in materials [2, 8, 9, 31]. The development of conventional robotic systems follows a distinct developmental methodology. This follows a principal design boundary that is categorised extensively and are design driven towards requirement, performance and capacity of its applications; where its components are much available commercially as standalone parts; such as, actuators, sensors, and control methods. This is then followed by the kinematics and dynamics of its embodiment to achieve its optimum design criteria prior to

manufacturing and assembly to control. Soft robots, however, has yet to achieve such a methodological development at this stage.

From a design perspective, two approaches can be distinguished in developing a soft robotic system; (a) rigid skeletal structure/components enveloped in soft exterior and (b) overall intrinsically soft system with passive characteristics for soft structure/components [9]. However, the current conceptual design constraints for soft robots has generalised its aims to have an all-inclusive, continuous deformable structure that is capable of actuation, sensing and consist of a controllable behaviour comparable to conventional robots. Fundamentally, these components are sparsely limited in development and is commonly application specific, while current systems and devices are heavily relied on inspiration and creativity drawn from biology and nature.

Robotic systems are typically designed with 3D computer-aided design (CAD) software modelling and is mathematically represented using known geometric parametric models. However, these graphical representations were not created with the thought of free-form fabrication processes required in soft robotic systems. Based on material embodiment, the design of soft systems is generally aimed at application and tasks driven due to the lack of design morphology [32].

Soft actuators from a general perspective can be described as a deformable piece of material, capable of holding a homogeneous load applied using some fluidic medium (pressure or hydraulics) to generate a certain behaviour or interaction and motion. This concept is at the core of many soft robotic actuators and their various design implementations. The first design of a soft pneumatic actuator dates back to 1992, demonstrated by K. Suzumori *et al*. [33]. The work featured a pneumatically driven actuator composed in three segments of rubber elastomer, while encased and reinforced by a fibre mesh to manipulate its motion when inflated. The actuator showcased three degrees of freedom followed by a continuous, deformable and adaptive motion driven pneumatically. Following this, a number of ‘soft pneumatic actuator’ were soon developed; such as the McKibben actuator, also known as Pneumatic Artificial Muscles (PAMs), describing a contractile or extensional linear actuator composed of elastomer tubes encased in fibre sleeves [34]. Although a

vague representation of a muscle, these actuators can be fabricated in various sizes and lengths; which can then be mathematically defined to relate the force produced during motion and inflation. Soon after, pneumatic networks (PneuNets) were then introduced as a class for soft actuators featuring a series of channels and chambers inside an elastomer by Whitesides Research Group at Harvard [35-37].

Inherently soft, these actuators are scalable, customisable and widely recognised [38]. However, unlike conventional robotics, the movements of soft bodied robots are difficult to be mathematically confined to planar motions and translations. As soft robots adopts hyper-elastic materials, such as silicone polymers, rubber, hydrogels or comparable materials; an understanding of such materials needs to be define in order to exploit its non-mechanical properties [4]. Hyper-elastic materials as such, are not described in three, but six degrees of freedom (three rotations and three translations about the x, y, and z axes). Thus, the movements of these soft bodied robots cannot be confined to planar motions, as such, elastic materials can produce motions that can bend, stretch, compress and twist.

The kinematic and dynamics of soft robotic systems are unlike of conventional rigid bodied robots that consists of links and joints. The kinematics follows a continuous function with the need for mathematical modelling to take account for material properties [28, 39, 40]. Recently, the function of these systems was introduced to be analysed through its behaviour via finite element analysis modelling [41-43]. Through this method, a mathematical model can be used to analyse the characterisation of the actuator in the form of force, torque, range of motion and speed of actuation. However, this method is widely used as an approximation due to the limited literature for material properties and mathematical models revolving around soft systems for mechanical characterisation [44, 45]. This factor heightens the difficulty and challenges faced moving towards fabrication of soft systems.

The field of soft robotics has grown to a broad research area spreading across multiple disciplines to develop methods of actuation, sensing and control. For such soft machines to achieve its full potential, its means of fabrication also need to advance with its trends. In an early review of soft robotics, Cho *et al.,* emphasised

the need for innovative and advancements to manufacturing and fabrication of soft systems in order to realise and produce new and novel generation of soft robots.

However, the current trend of fabrication techniques used to develop soft robots only adopts a handful of conventional manufacturing techniques compared to an expanding material library.

With a large soft material library, as a means of measurement for softness and rigidity of materials, Young's modulus can be used to compare and characterise the compliancy, elasticity, stiffness and flexibility of materials. The material moduli commonly adopted in conventional robotics stagnates around the order of 10^9 to 10^{12} pascal (Nylon, Wood, Steel, Carbon Fibre and Diamond). Soft robots instead aim to relate and/or imitate biological systems around us, such as tissue cells in the body. As presented by Rus *et al.*, the material moduli range befitting of soft robotic systems sits in the order of 10^4 to 10^9 pascal [10]. As illustrated in Figure 2.1, the material moduli is defined for homogenous components that are subjected to axial loading and stress deformations, as it is a useful scale of measurement for rigidity of materials. It can be utilised as a foundation to build and fabricate soft systems as positively viewed in a number of soft robotic research [46].

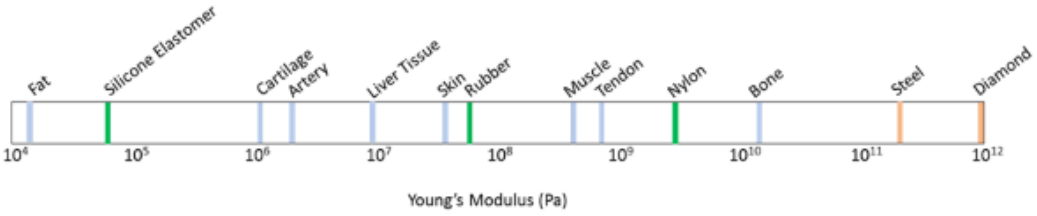

Figure 2.1 Young's modulus scale of engineering and biological materials [10]. As a means of measurement, soft robots are often considered to be under 10^9 pascals. Conventional robots' favours structurally robust materials above 10^9 pascals

As the field of research and technological aspects of soft robots is still young, a significant number of review articles have already been published and are well-known [22]. To date, most innovation and advancements have solely focused on the development of fundamental functionalities, underlying the development of soft robotics to fully functional systems as those forecasts by Majidi *et al.* [8]. However, in the author's opinion, the development of advanced manufacturing process will further push the development of new materials and overall development of soft robotic technologies. Soft robotic review by Cho *et al*., and Laschi *et al*., have also supported this notion as advanced fabrication techniques is needed to realise the next generation of soft robotic devices [11, 47].

Comparing to a review on soft fabrication by Cho *et al.* a decade ago, limited research has focused on soft robotic fabrication methods and techniques [47]. As such, this review proposes an update and insight on the technologies that have been developed and/or used during the last decade of soft robotic development. The review focuses towards the fabrication of components and devices that constitute the realisation of soft robots to find a gap for innovation. Despite the numerous types of soft robotic devices and components (actuators and sensors), the design approach and functionality shall not be discussed in detailed. As their sole functionality and design purpose deserves much more than a section in this literature review. In addition, the research aim is fundamentally dedicated to the expansion and development of soft robotic fabrication and manufacturing.

2.2 Fabrication of Soft Robots

Much to the broad variability in design morphologies, material composition and fabrication techniques are key to the development of soft robotic systems to achieve its desired functionality and capability. However, the fabrication of soft robots is notably the most challenging and unreliable part throughout its development. Often due to the fundamental composition and properties of materials, it is also limited to a handful of conventional manufacturing techniques in contrast to the desired material for its development.

Soft materials such as elastomers are commonly used in soft robots for their elastic and fundamental soft nature relative to the human skin (10^7 to 10^8 Pascals). Such elastomeric material along with other comparable soft materials require a form of pre-processing stage, such as curing, vulcanising, catalyse or solidification; to achieve or form its desired functional state. Fundamental properties of soft materials are commonly known to vary in viscosity (3,000 ~ 40,000 centipoise), can be easily deformed due to external factors, such as thermal alterations and require unconventional approaches with multi-staged steps and complexity. These factors potentially hinder the widespread use of soft systems in real world application and fabrication processes. Soft materials with this initial approach cannot be actively shaped through conventional manufacturing processes, such as machining or sculpting. Instead, they are often moulded, casted or extruded into a predefined passive shape. Thus, the usage and functionality of material present an added challenge in the fabrication processes. Extending towards material engineering for a solution, recent advancements have shown an expanding field of materials for soft robots covering textiles, synthetics, elastomeric polymers, hydrogels, biological materials, and liquid crystals [48-50]. However, it is crucial to highlight the material considerations, constraints and accessibility towards the design and fabrication methods when developing such systems. This is due to the adaptation of different materials increases the complexity and challenges of the development stages. In this review, soft materials and its elements are described as part of soft fabrication. Despite the numerous developing advances in material science, their presentation

would deserve much more than a section in this research context towards soft fabrication.

In order to develop soft systems that are highly capable and functional, the fabrication techniques for soft material construction requires an adaptive and informal approach in order to exploit the compliance and flexibility of material properties. Much to the innovative and advancements made to soft robotic technologies in the form of fabrication, to date the nuance of soft fabrication and material still rely heavily on the use of moulding and casting. It is considered the most fundamental fabrication method for creating soft robots. During the field's infancy, the interest of soft robotics did not intrigue many researchers at the time; while fabrication methods was not disclosed openly in literature. Going back nearly two decades, one of the first soft actuators was developed by Koichi Suzumori in 1991. The work presented an electro-pneumatic driven flexible micro-actuator (FMA) capable of multi-degrees of freedom and was fabricated using various forms of bespoke moulding and casting techniques adopted from a combinative conventional manufacturing technique [51]. Despite the innovative development of the FMA, the McKibben artificial muscles or pneumatic artificial muscles (PAMs), became a more popular choice of interest, albeit its commercialisation in the mid-1990s, it was said to have been developed into 1950s [52]. While both actuators operate with the same principle of using fibres to control the expansion of the cavity in the form of motion and structure, the fabrication of the two are at opposing ends. PAMs can be fabricated through commercially available products, whereas FMAs enlists bespoke machined moulds and industrial use of production tools and equipment. Even so, compared to the flexible micro-actuator, the McKibben actuator could only perform a single degree of freedom based on the directional pattern of the fibres that were wrapped along a membrane for inflation.

More than a decade later, the surge of interest to develop soft robots was ignited with the concept of creating biomimetic robots. Taking inspiration from biology, robot developments took a biomimetic approach to mimic and adopt the behaviour, motion and characteristics found in nature as compared to mechanically driven rigid motions constraint by structural rigid joints and robust metallic exteriors in

conventional robotics. Biomimetic robots such as a wall climbing gecko and cockroach inspired robots led the use of non-traditional manufacturing technique known as shape deposition manufacturing (SDM) [53, 54]. The technique allows deposition of material and machining to include soft and compliant materials along with structural rigid links and the possibility of electronic embedded parts such as actuators and sensors [47]. The technique enlists and combines the concept of rapid prototyping and additive manufacturing techniques even though the developed robotic system were not all-inclusive and intrinsically soft. However, the developed robots are still bound to conventional robotic paradigms. Soon after, additive manufacturing techniques such as stereolithography (SLA), composite layering (CL) and multi-material printing techniques based on fused deposition modelling (FDM); steadily gained immense popularity in soft robotic fabrication [55-57]. These '3D printing' techniques initially employed enabled the creation of intricate and bespoke moulds in a rapid and 'printable', manner without the use of conventional manufacturing techniques (CNC machining). An added advantage is that these techniques can be combined to create composites with programmable material properties, embedded components and composites. However, due to the nature of soft material properties, these fabrication techniques are still constraint to the adaptability to overcome and/or incorporate soft materials while increasing in complexity in overall fabrication process planning.

Illustrated in Figure 2.2, the primary fabrication processes currently adopted in the soft robotic research community can be illustrated as such. The map serves as an overview to illustrate on primary fabrication techniques used to develop soft robotic systems found in literature. As soft elastic materials such as elastomer still requires a pre-processing stage, the technique of moulding and casting acts as a centrepiece for soft fabrication. While other techniques such fused deposition manufacturing (FDM), revolves its technique around casting of elastomeric materials. [10, 58].

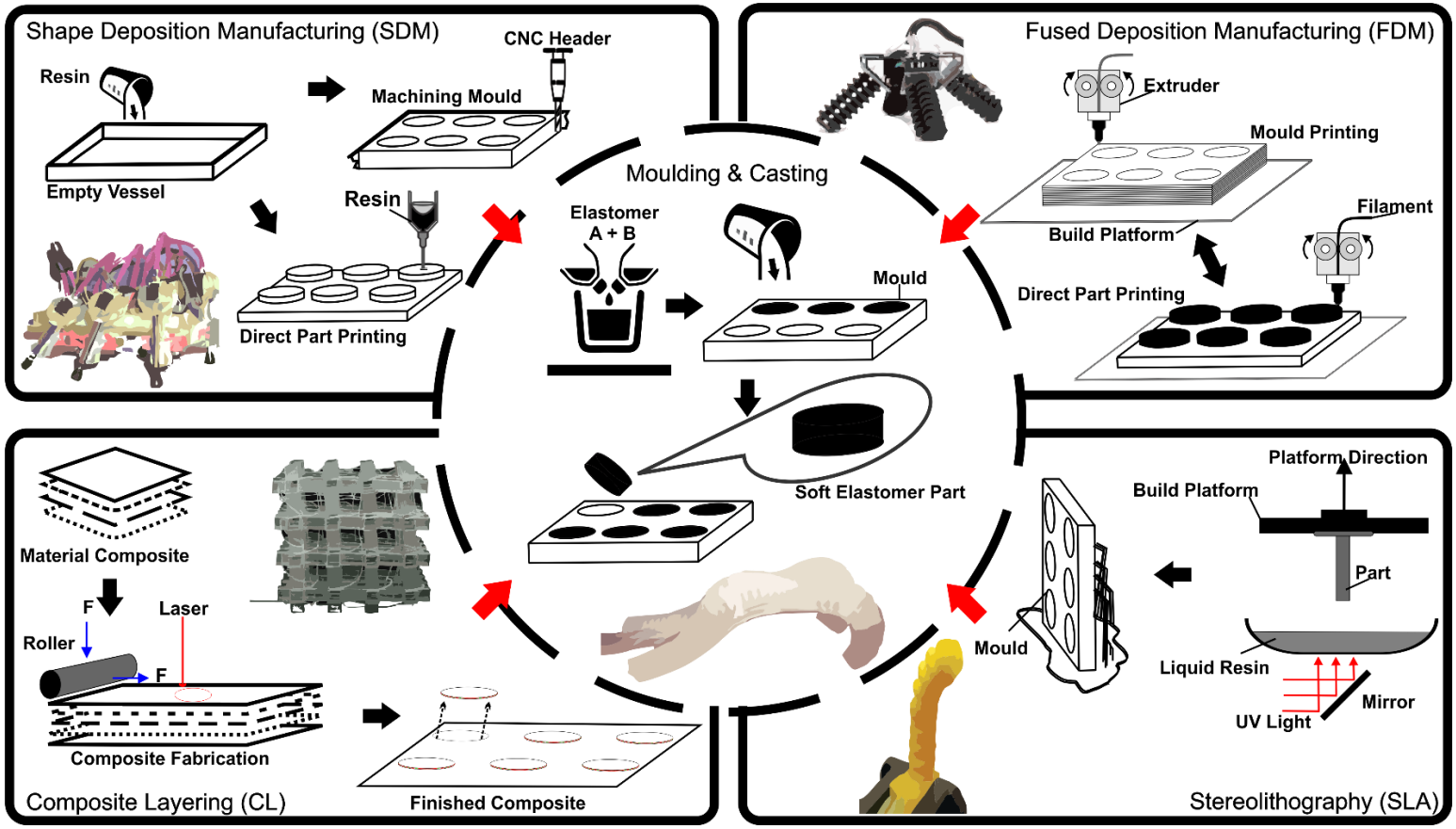

Figure 2.2 Soft Fabrication Map. Illustration of the core manufacturing methods used to fabricate soft robotics. Moulding and casting form the centre technique and core fabrication method of soft robots. The surrounding four types of additive manufacturing methods further assist, enable and advance the development of soft robotic fabrication [35, 59-62].

2.2.1 Moulding and Casting

Compared to conventional manufacturing methods, moulding and casting can be adopted and modified into building micro-to macro scaled soft robots in a rapid, inexpensive and mass producible manner. While there are many forms and types of moulding and casting manufacturing techniques, the difficulty and challenge comes from the material at hand and the desired designed output. This is because, intrinsically soft materials commonly used in creating soft robots such as rubber silicone and/or similar types of commercially available elastomers require to undergo a curing processed prior to forming its semi-soft and elastic state. In its inactive or uncured state, these materials vary in viscosity, highly-adhesive in a gel or liquid form, and are often introduced as two-part polymer ratio. Activation of these materials is needed to catalyse to a solid hyper elastic state. These material parts are mixed together (commonly in 1:1 or 10:1 ratio) and left to cure, cross-link, catalyse, or vulcanise. In this manner, thermal and optical conditions can also inhibit or facilitate the efficacy of the process but depending on the material composition for development.

Moulding is a manufacturing process that shapes liquid or pliable raw material within a solid structured frame known as a 'mould'. While casting is where material in liquid or comparable state is introduced into a mould and left to take on the predesigned shape. Both techniques are co-related and dependable on each other. An illustration of the technique is showcased in Figure 2.2.1. Other forms of these techniques used in industrial production also include extrusion, injection and compression for moulding, while casting includes die and investment techniques.

The underlining technique is fundamental due to its ability and adaptability over soft material compositions as seen in many soft robotics developments. The development of a quadrupedal pneumatic driven robot by Shepherd *et al.*, is a prime example of a fully soft, pneumatically driven robot amongst soft roboticists [35]. At its introduction, the method of fabrication uses custom fabricated moulds made from stereolithography (SLA). Followed by a two-step casting technique of silicone elastomers (Smooth-On EcoFlex™ 00-30 and Sylguard 184 PDMS), each step requires the elastomers to be fully cured prior to progressing to the next stage. Based on a

pneumatic architecture design by Illievski *et al.*, the overall structural stiffness is tuned towards the material composition as two layers (extensible and inextensible) [4]. As such, the difference in strain between the layers results towards a bending motion when pressurised. From there, soft robotic systems such as pneumatic graspers/grippers; bioinspired robotic fish and octopus, and other forms of soft actuators that are capable of elongation, contraction and twisting were also fabricated in a similar manner [4, 63-65]. Marchese *et al.*, presented the forenamed actuation motions through differentiated internal pneumatic structure (ribbed, cylindrical and pleated) and by taking inspiration from other forms and types of moulding and casting [66]. Through this informal approach of using basic commercial material components, such as wax and textiles; underlines the inspiration adopted from investment casting. Despite this, casting of soft materials is often constrained to a two-dimensional plane, as such, the fabricated mould designs tend to be of planar in structure as liquid rubber is poured or injected into the mould and allowed to cure. An advantage to the technique is its durability due to the lack seams and layer separation depending on the method and material composition. Leading to a higher durability and mechanical strength during inflation as the material encapsulates its embodiment. However, bonding materials of different properties in casting is dependent on its composition and does not guarantee a success. Cosmetic faults (semi-cured parts and bubbles) and un-even layer meniscus (concave and convex) can also arise during fabrication that may reduce efficiency of the design function when casting in a two-dimensional plane. In addition, mould material and environmental factors also contribute to the efficacy of the overall development.

The fabrication process incorporates a multi-stage process to incorporate different design aspects, such as, embedded features, channels and cavities. As such, a thorough planning stage from mould design to material composition are key factors prior to fabrication. Although the technique is still the most sought after to date, the design to fabrication process has its limitations. Complex geometries, small-scale and delicate features, and embedded components are difficult to cast and mould. As a result, rapid prototyping methods and additive manufacturing techniques, such as, shape deposition manufacturing (SDM) and stereolithography (SLA) has enabled the development of complex moulds capable of forming intricate and innate geometrical

characteristics for moulding of complex designs. Bespoke developments such as a multi-chamber tube actuator by Wakimoto *et al.*, was fabricated using extrusion moulding method [67]. The technique highlighted a complex multi-channel actuator at micro-scale, fabricated with accurately and efficiently capable of reaching any arbitrary lengths. Other research adopting such industrial techniques also included Zhao *et al.*, with a rotational casting method to directly mould complex and hollow geometries [68].

Solutions in material science have also been sought after, such as material with low viscosities (PDMS or hydrogels), and moulds made using intricate materials, such as photo-curable resins, sacrificial wax, dissolvable and thermal driven plastics [69-74]. As soft fabrication progresses, a form of moulding and casting technique persists in the current state of the art developments. While its limitation steer towards material science or even the use of bespoke or industrial equipment for solutions.

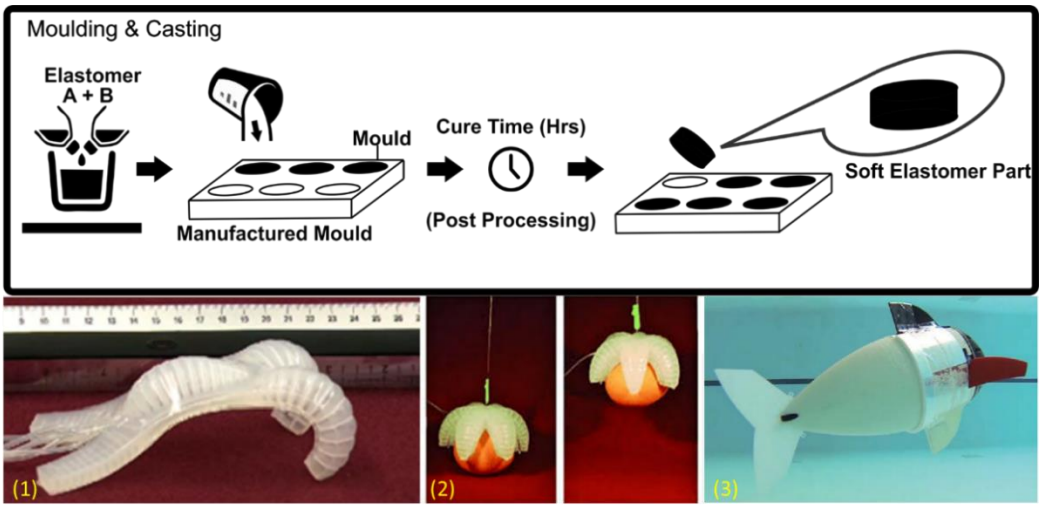

Figure 2.2.1 (Top) Illustration of Moulding & Casting technique to produce soft elastomers for soft robotic applications. (Bottom) (1) Quadrupedal soft robot [35];(2) Soft robotic gripper [4];(3) Soft robotic fish [66]

2.2.2 Shape Deposition Manufacturing

Combining material deposition and machining manufacturing techniques in a single system, a multi-step-single-platform method was coined in the mid-1990s. The technique resurfaced as a potential method for soft fabrication to develop an omni-inclusive biomimetic robots [54, 75]. The technique illustrates the fundamental concept of additive manufacturing through a layer-by-layer deposition technique along with an active application of machining tools for shaping and sculpting. Starting from a digital design, the fabrication method focuses on two aspects, deposition and removal of materials in an enclosed vessel. Often wax or comparable materials, such as clay is casted into a vessel to create a large block. Machining tools such as drills and mills are then introduced to shape the desired vessel into a mould matrix. At this point, sensors, actuators and other embedded materials can be introduced into the mould depending on the desired application. Pourable materials, such as liquid metal, elastomers or resins, are then introduced into specified points of the mould matrix to form the body of the design. The process of casting through material deposition and shape machining is then repeated till the desired design is completed. An illustration of the technique is showcased in Figure 2.2.2.

With the use of this technique, earlier works of biomimetic systems, such as Stickybot by Kim *et al.* demonstrates a robot mimicking the wall climbing capabilities of a gecko [76], and iSprawl by Kim *et al.* for a crawling hexapod [59], illustrate the capabilities of the fabrication technique through incorporation of ‘hard’ and ‘soft’ components. Although not entirely an embodiment and intrinsic soft system, the robots developed are fabricated from structural rigid links with soft compliant features acting as joints, actuators and/or sensing components. The fabrication of these robotic systems takes the advantage and the ability to include external electronic and mechanical components, such as sensors and actuators embedded within its 3D structure [77]. Scalability of the technique has also demonstrated to be capable of fabricating a soft, atraumatic deployable surgical grasper by Gafford *et al.* as compared to macro scaled functional bodied robots [78].

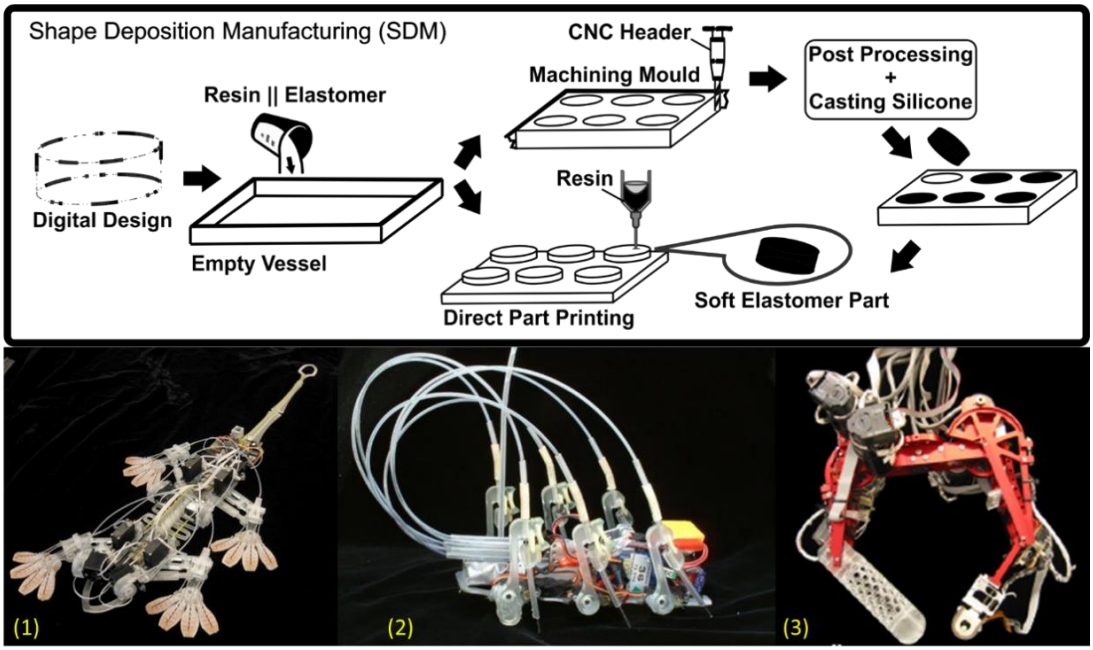

Figure 2.2.2 (Top) Shape Deposition Manufacturing fabrication process. (Bottom) (1) Wall climbing gecko robot [76];(2) iSprawl robot [59];(3) Force control fingertips [79]

The technique was initially seen as a plausible futuristic method for soft fabrication. However, accessibility and popularity of the method is also dependable on its cost in adoptability and technical difficulty in manufacturing. The technique calls for extensive detailed technical planning and breakdown of processes compared to conventional rapid and additive manufacturing methods. Whilst its cost for prototyping does not justify its production ability and efficiency. This is due to the complex workflow and meticulous architecture needed for precise and timed deposition of different material compositions, machining tools and sequence to create structure, features and aesthetic designs.

While the technique allows an entire robot to be sequentially and/or simultaneously fabricated and assembled, the challenge lies with its complexity. Although the key advantage to the technique is its ability to fabricate complex 3D geometries with the inclusion of rigid to soft compliant mechanisms, along with embedded electro-mechanical components. The use of this technique amongst the soft robotics community is not opted when skeletal or structural rigid links/joints are adopted, along with externally embedded mechanical actuators and sensors. It is also noted that certain machining tools are not suited for most soft materials to date, due to its

material mechanical properties and the technique is suitable towards macro structures compared to micro scaled components and applications.

2.2.3 Composite Layering

Composite layering (CL) is a comparatively niche rapid manufacturing process for layering and/or laminating composite films or sheets at millimetre scale. Parts of the technique has been adopted in the field of microelectronics, microfluidics, and micro-electro-mechanical systems (MEMs). While the technique takes a new direction in the fabrication of micro to mesoscale robots capable of electrical actuation for self-configurable and assembly known as 'Pop-up' robots [80-83]. The manufacturing process involves the layering of alternating rigid and compliant layers of micron to centimetre scale planar layers similar to the fabrication of a flexible printed circuit board. Starting off with a planar pattern design, functional layers are stacked upon each other and micro-machined towards its design imprint. The process continues as each layer is gradually bonded together either with heat, adhesives or compression methods until the design configuration is formed. An outline of the fabrication process is illustrated in Figure 2.2.3.

Variations of composite layering techniques are often described either as rod casting, film application, spin coating and film lamination. However, the method results in a controlled thickness substrate (film or sheet) through a layer-by-layer process along with possible incorporation of different materials, such as elastomer, fabric, paper and plastics to produce a functional composite for actuation and/or sensing [71, 84-88].

The technique is no stranger to the use of semi soft compliant materials, such as cardboard, fabric, paper or polymer films; as it is often overlooked as types of packaging in consumer goods. A number of developments has since incorporated the technique, such as an embedded thread actuated deformable wheel on a robot, soft skin strain gauge sensor and a miniature robot capable of self-folding and actuation from a magnetic field [89-91]. The actuation of these small-scale systems has since grown beyond shape memory polymers (SMP) and alloys. Other forms of actuation include, printable inks and hydrogel for programmable thermal actuation,

pneumatic inflatable pouches and fluid driven actuators [85, 92, 93]. This technique for soft fabrication is still predominantly favoured for millimetre scaled applications and/or micro-structures, such as skin or pop-up robotics. Compared to its additive manufacturing counterparts for building completely soft robotic systems, the fundamental concept of adhesion and bonding of thin layers still holds many unique potentials, such as inflatable shape changing surfaces and architected deployable structures.

In recent years, these composite robots have also found inspiration within origami and simple mechanics for the construction of articulated strain-oriented actuation compared to rigid links and joints in conventional robotics. Using origami and mathematical modelling for folded actuation, the fabrication process can be simplified but requires a planar planning process for layering and adhesion along with material mechanical properties. A multi-material self-folding composite can be fabricated using several layers comprising of semi-rigid materials as structural constraint layer and a stretchable material as a flexible layer. Each layer is adhered together with commercially available adhesive after a planar design is laser-cut or micro machined on the subsequent layer. Based on the design, actuation of these structures is often with the use of SMP applied on the articulated flexible links. Overvelde *et al.* presented a pneumatic actuated transformable composite structure with this technique [62]. The developed work was inspired by the concept of snapology origami applied to extruded rhombi forming a unit cell [94]. Fabricated from polymeric plastic sheets, the design follows a 2D planar design of layering and laser cutting to create a composite with articulated hinges. Actuation of the cells were instead fabricated separately using heat pressed polyvinyl sheets and embedded within the sleeves of the structure. The entire process features the use of commercially available materials along with openly available manufacturing techniques.

The development holds potential for miniaturisation at micro-scale for self-assembly for laminate-based mechanisms [21, 91, 95]. In a similar modality, Ou *et al.* fabricated an inflatable fabric composite capable of shape change using heat sealing of fabric and comparable material, such as thermoplastics [96]. The technique also looks into reconfigurable and replaceable inflatable modules as compared to intrinsic soft systems as demonstrated by Natividad *et al.* and Niiyama *et al.* [97, 98]. Despite its potential of programmable inflation, these inflatable modules still lack the mechanical strength and robustness for adapting to external contact factors.

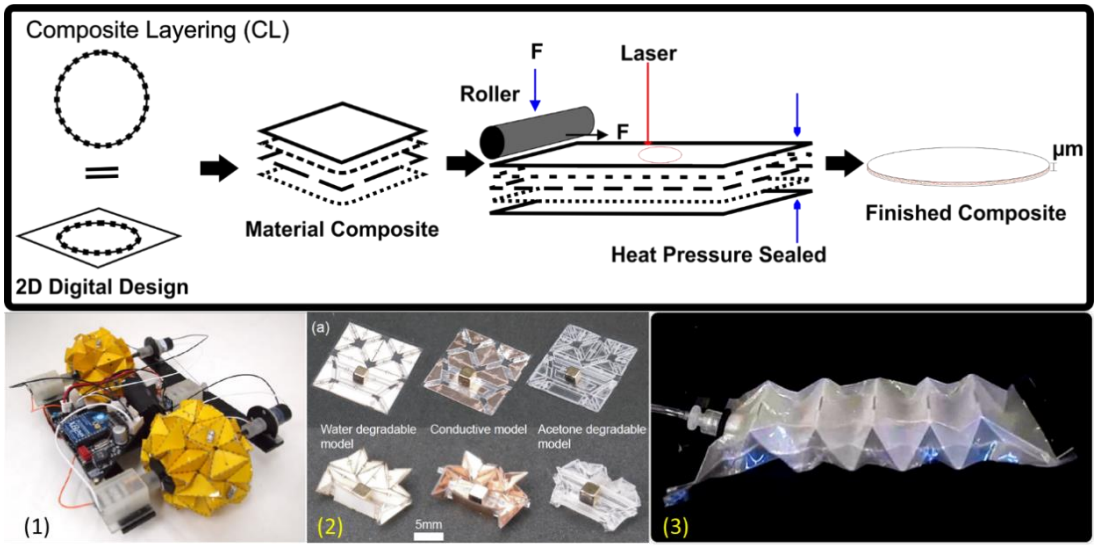

Figure 2.2.3 (Top) Illustration of Composite Layering fabrication method. (Bottom) (1) Deformable wheeled robot [89];(2) Miniature origami robot [91];(3) Fluid driven artificial muscle [93].

2.2.4 Additive Manufacturing (3D Printing)

The technological terminology known as 3D printing refers to a subset of additive manufacturing that directly describes the creation of 3D objects through the formation of layers from digitally designed files. The technology encompasses a range of printing techniques, such as fused deposition modelling (FDM), stereolithography (SLA), selective laser sintering (SLS), and direct ink writing (DIW). The underlying mechanical platform builds from a computer-controlled translation stage with a mounted pattern generating device (laser optics, deposition nozzle or

thermal conductive pin) to form a layer at a time in an additive, repeatable, and precise manner. Its material library is unique to each printing process, from resins, powders, inks or similar compositions are solidified and fused together to yield the desired pattern. Depending on the technique, the research focus has been on improving printing resolution, material durability and compatibility. The following describes 3D printing techniques used in soft fabrication of soft robotic technologies.

2.2.4.1 Stereolithography and Selective Laser Sintering

Stereolithography (SLA) is one of the first 3D printing methods to use light as a source to sculpt object, while another form of light driven printing technique is known as selective laser sintering (SLS). The difference in the two is based on the material composition used and its process, where SLA utilises photo-curable resins, while SLS uses polymeric powders. The term 'soft lithography', introduced by Xia *et al.* dating back to 1998, describes the process of stereolithographic technology for microfabrication in the field of micro-electromechanical systems (MEMs), microfluidics and microelectronics [99]. The fabrication process of soft lithography fundamentally starts with a vat of liquid pre-polymer resin, followed by a rastering laser to selectively photo-polymerise a solid object. The technology exploits the spatial and temporal control of light depending on the technique, as such different illumination sources allow variability in technology, resolution, cost and efficacy. Compared to the layer resolution found in extrusion or deposition in additive manufacturing, the resolution and feature size of SLAs is significantly better, as it can produce layer thickness and features in micrometre scale (>100μm). In a similar manner, the laser in SLS is rastered across a bed of powdered or granular material and effectively fusing the particles together at a certain melting point. Each layer is fabrication sequentially through a uniform distribution of polymer powder, followed by sintering of polymer powder until the entire structure is built. The resolution aspect of an SLS yields a layer resolution and feature size better than SLA. This is typically due to the particle size for curing of liquid resins are typically larger than of sintering granulated powders (10 ~100 μm) and compared to extrusion of thermoplastics when bonding [55, 100]. As such, the potential aspect for soft

fabrication with microscale features, complex geometries and intrinsic soft structures provides an efficient and commercial interest for soft robotic research. [70, 100, 101].

To date, SLA and SLS are still often employed to fabricate moulds with intricate geometries for pneumatic or hydraulic networks since the inception of soft robots [4, 35, 102]. This is due to the low cost for prototyping, ability to produce complex network designs and surface texture are less granulated, which is better suited for investment or die casting of pourable elastomers to produce intrinsic networks for pneumatic or hydraulic actuation. The technique is further enforced with research work, such as a multi-nodal soft pneumatic actuator as presented by Mosadegh *et al.*; Marchese *et al.*, whom presented a foundational recipe for fabricating soft robots using stereolithography printed moulds and Martinez *et al.* on incorporating origami concept on elastomeric actuators fabricated in a similar manner [36, 64, 66]. Despite this, SLA printed moulds are preferably opted, as production time and post-fabrication are faster and less complex as compared to SLS technique.

Similar towards any additive manufacturing technology, direct soft lithographic printing is limited by the ability to produce truly free-form 3D structures that are fully and intrinsic soft and compliant. This primary limitation is due to its constraint fabrication method on a fixed planar morphology. As such, the technique limits soft robotics systems to achieve amorphous forms as in the work presented from Stokes *et al.* and Bryan *et al.* [61, 103]. The lack of available photo-curable material for direct soft robot fabrication is often due to the chemical and molecular compatibility with SLA technology. Despite a growing material library of photo-curable materials that has extended to print towards solvent dissolvable, bio-comparable elastomers and electro-conductive resins; multi-material printing can readily employed through automated resin vat exchange, however, conflict or fouling of unreacted resins has to be taken into account [104-106]. For direct soft printing, custom chemically amended resins towards elastomeric by-product must adhere to the fabrication process and constraints. As such, controllable light spectrum and intensity, resin viscosity and photo-curability at an acceptable timescale are factors that are consecutively progressing in research. In SLS, granular or powder thermoplastic

material have similar material compatibility and printing process to fused deposition modelling technique. However, the technique is often hindered by its extensive production time, cost and printed designs must adhere to fabrication constraints, such as apertures to allow drainage of encapsulated material during fabrication. As such, soft fusible material may not be a venture soon, due to its material complexity direct towards the technology.

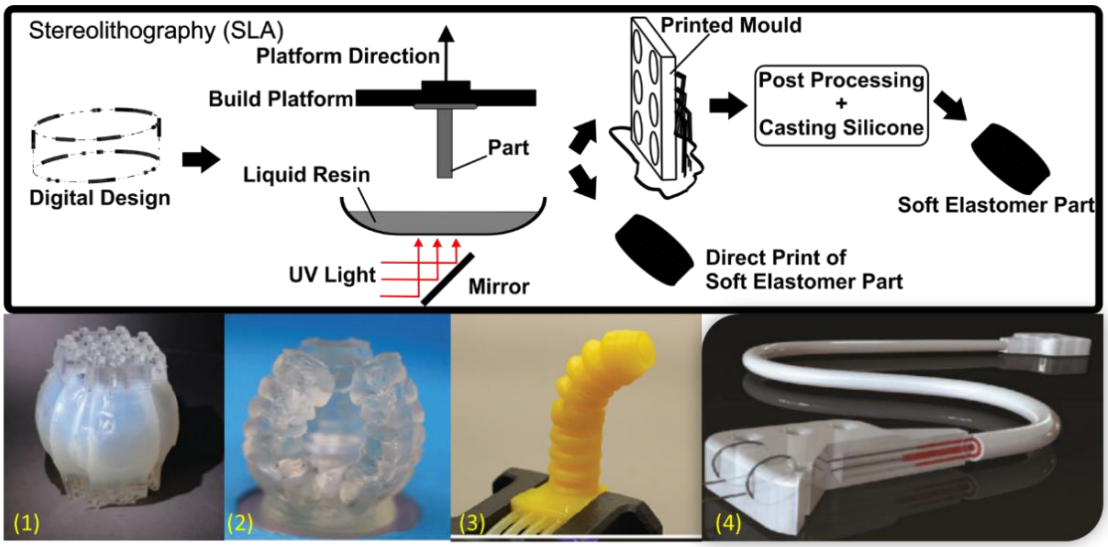

Figure 2.2.4.1 (Top) Manufacturing process of stereolithography (SLA) for soft robotic applications. (Bottom) (1) 'Click-e-Bricks' elastomeric structures [102];(2) UV curable elastomers [61];(3) UV Printable artificial muscles [106];(4) Capacitive soft strain sensors [107].

Figure 2.2.4.1 illustrates the process of stereolithography directed towards mould printing or direct soft printing. From a computer aided digital design, the designed models are computationally broken down into coordinates, pixels or layers. Photo-curable liquid resin is introduced into a reservoir, while an elevated platform will hold the part in place. A light source (typically UV Light for SLA) then shapes the desired parts of the object. As each layer is polymerised, additional material is continuously introduced into the workspace while layers are formed by subsequently linked in the illuminated regions by the light source. The process is then repeated until the desired designed object is completed. Upon completion, the object/model may require post processing methods, such as smoothing, washing, or removal of structural supportive parts.

2.2.4.2 Deposition or Extrusion Manufacturing and Direct Writing

Popular, affordable and commercially available, fused deposition modelling (FDM) refers to materials (often thermoplastics) deposited or extruded through a nozzle across a static or translational bed. Initially ventured towards printable moulds for investment casting and supporting structures, thermoplastics, such as acrylonitrile butadiene styrene (ABS) and polylactide (PLA) are often associated in this technique [73, 108, 109]. FDM printers are capable of resolution up to millimetre range depending on the nozzle diameter (> 0.1 mm), the rate of extrusion or deposition along the translation of material properties and nozzle displacement in real-time also affect the efficacy, resolution and production time.

As such, the technique relies significantly on the thermal conductivity of thermoplastics or equivalent materials for deposition or extrusion. Inherently, the printing process is affected through defects, delamination and voids due to unsuccessful layer fusion or adhesion. Figure 2.2.4.2 illustrates the manufacturing technique tailored to develop soft robotic applications. Where extrusion/deposition type printers are commonly associated with printing moulds and solid parts, while injection/embedded printing directly prints soft materials. In both cases, the object and model require post processing methods, such as smoothing, washing, or removal of structural supportive parts.

While different types of filaments have been explored, the closest results considered suitable for soft robots would be thermoplastic polyurethane (Ninja Flex). An example of the material has been presented in the form of a bi-directional fluidic actuator, capable of withstanding high strain under high blocked force and a functional pneumatic-driven tri-legged robot by Yap *et al.* and Drotman *et al.* respectively [60, 110]. Although its material composition is mechanically more robust, less flexible and elastic than a fully elastomeric counterpart, the printed actuator implicated the direction towards material engineering for solution. Inherently moving away from generic thermoplastic filaments, materials which consist of bio-mechanical properties, solvent dissolvable mechanism, photo-reactive complaint materials, and many more are recent advancements within the field of printable material [111]. Embedded electronics on soft materials, such as electro-

conductive inks, particles and plastics, are also entering the playing field of printable materials [55].

As such, the technical aspect of the technology has also extended to ink/injection direct writing/printing, where material of liquid state or less viscous components are directly patterned onto a substrate in the form of droplets, continuous fluidic ink, or gel-like state. Portrayed as a form of multi-material printing, it can incorporate material in an aqueous to molten-like state with added composition consisting of carbon, wood, liquid, rubber or even conductive particles [112-114]. The technique is capable of adaptation to incorporate different forms of deposition methods and materials ranging from device type for multi-nodal deposition to direct injection or printing of liquid substances [112, 115, 116].

Given the accessibility of the technology today, portable desktop 3D printers or custom-built printers can be adapted and directed for soft system applications [117, 118]. As such, the technology has enabled innovative fabrication techniques, such as Wehner *et al.*, who presented an integrated design and fabrication strategy by embedding patterned catalytic chambers on to a casted elastomer of an Octopus design mould [119]. The technique takes inspiration from microfluidic and direct ink writing for fabrication and chemical catalytic reaction for actuation. Another form of the technique featured a bending pneumatic actuator capable of sensing strain through microfluidic patterned conductive inks [120]. Such techniques were inspired by earlier forms of the fabrication method, including printing biomimetic micro-vascular networks embedded within a hydrogel matrix by Wu *et al.*, hydrogel structures for bio-structure constructs by Melchels *et al.*, and bioactive carbon nanotube as flexible electronics by Shin *et al.* [121-123]. The conceptual idea of direct printing of 3D elastomeric structures are still highly aimed at. Morrow *et al.* recently demonstrated the feasibility of directly printing of consumer available elastomer (EcoFlex 30, Smooth-On), on a custom adapted RepRap-Ingentis designed FDM printer [124].

Due to the innate material properties of elastomer, the presented work only hinted the feasibility of direct printing. Compared to other printing techniques, the printed actuator had clearly defined limitations, such as print quality varying significantly in

repeated prototyping fabrications, and resolution of layer is highly dependable on the curing speed and ambient temperature. In addition, additives such as thickeners or deadeners may alter the fabrication time, quality and process. However, recently Yirmibesoglu *et al.*, revealed to have achieved direct printing of two-part commercial elastomers through a bespoke extrusion mechanism [125]. The extrusion print-head presented consists of an internal mixing component and a convection heating element. However, it was reported that the printed actuators did not perform better and showed delamination at certain layers than cast-fabricated actuators under high pressures. Despite this, the research is still in progress as its printed characteristics have yet to be fully defined.

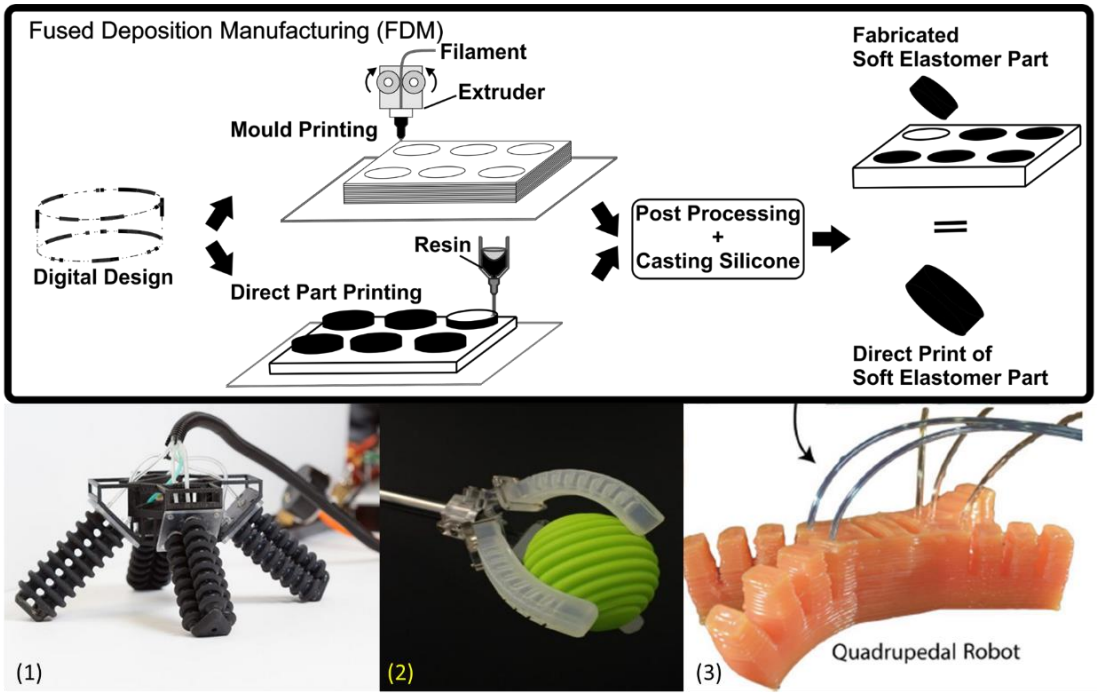

Figure 2.2.4.2 (Top) Manufacturing process of fused deposition manufacturing (FDM) for soft robotic applications. (Bottom) (1) Printable pneumatic actuators [60];(2) Soft somatosensitive actuators [120];(3) 3D printing of silicone elastomer [125].

2.3 Progression of Soft Fabrication

A review in soft robots in 2016, Laschi *et al.* pointed out the need for a combination of such fabrication techniques in order to fully tackle the mechanical and material limitations in soft fabrication [9]. While material engineering contributes towards more than half of the problems in soft robotics, the mechanical manufacturing techniques and tools currently used to realise soft systems still needs a more defined strategy to adopt soft material limitations and design constraints. Based on the existing techniques used for soft robotic fabrication, a recent review of soft fabrication by Schmitt *et al.*; noted that current fabrication of soft systems has shifted towards its heavy reliance of additive manufacturing and rapid prototyping technologies, either through integration and innovation of the technique or through a combinative merge of advantages each technique possesses [19]. This shift in soft fabrication technique illustrated in Figure 2.3.1, evolves from the initial approach of soft fabrication map in Figure 2.2.

Relating back to Figure 2.2, early works in soft fabrication primarily converge towards the use of moulding and casting technique as soft material is often casted onto a mould as the final process. These moulds were manufactured either through conventional manufacturing methods, deposition or stereolithography as showcased by literature, e.g. Shepherd *et al.* [35]. These methods of manufacturing often involves two or more step-processes to reach its desired development. The use of 3D printing technology (SLA, SLS or FDM) to develop complex moulds with embedded designs for channels and/or cavities were then popularised and much sought after due to the accessibility and availability of the technology. While moulding and casting are still proprietary for fully soft and elastomeric materials as seen in 'Zero-Volume' flat pneumatic actuators by Park *et al.*, and shape morphing actuators by Sun *et al.* [37, 126]. Integration of additive manufacturing techniques has since opted in soft fabrication processes. Embedding materials and technique using FDM technology, such as conductive inks and comparable materials were then sought after. This led to fabrication of stretchable sensors and interactive designs as showcased by Muth *et al.* and Overvelde *et al.* respectively [62, 111].

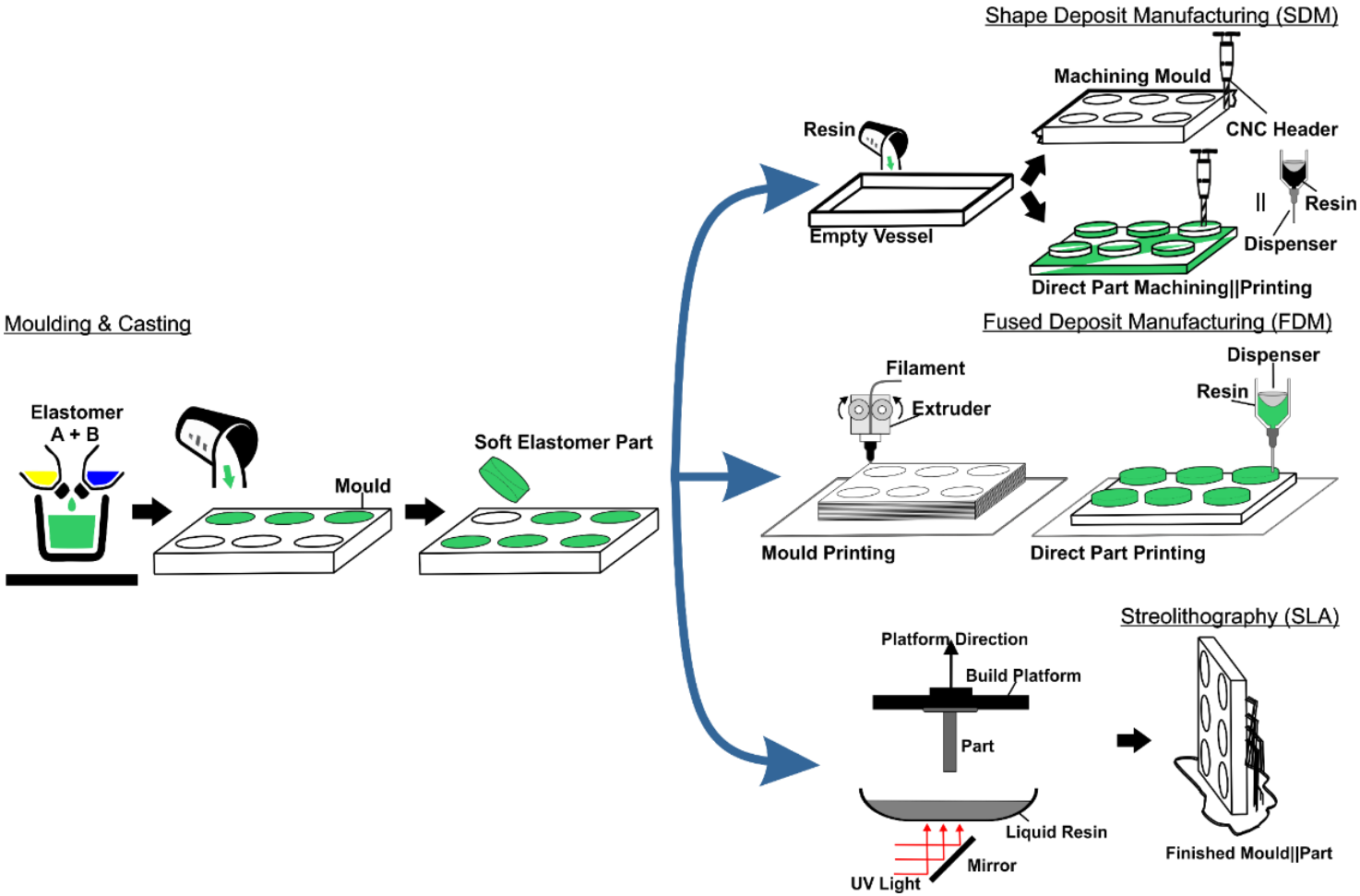

Figure 2.3.1 Shift of soft fabrication techniques in relation to the fabrication map Figure 2.2. From moulding and casting, the technique is advanced through various means of additive manufacturing methods

The main advantage to the shift in soft fabrication techniques is its ability to be adopted and/or combined into a multi-step process, capable of creating a variety of complex soft bodied systems. A recent fabrication approach developed by Wehner *et al*. builds on this advantage, featuring a combinative fabrication technique that enables programmable actuation and assembly within a completely soft, autonomous robot through means of casting, stereolithography and deposition of materials [119]. However, its fabrication strategy involves several bespoke tools and approach, requiring complex planning and high-level technical understanding.

Despite this, soft fabrication techniques have seen the increase adaptation of rapid prototyping and additive manufacturing techniques. These techniques have mostly been adopted due to the popularity within the research community as compared to the innovation and advantages each technique has to offer in order to define a fabrication strategy as illustrated by Wehner *et al*. [119].

Based on a systematic review of state-of-the-art soft robotics, the trend in soft fabrication research can be mapped out based on two distinct characteristics, (1) production and technical complexity and (2) manufacturing time. The two characteristics were derived from the study of *complexity in engineering design and manufacturing* by Waguih *et al*. [127]. While each field of science and engineering defines and views complexity in different ways, the unifying concept or general complexity can be described based on a score-classification method followed by the evaluation within each score addressing a set defined characteristics. It is an estimated and quantifiable classification based on interpretation of literature, published data as well as the author's opinion [127]. Table 2.3.1 illustrates a score classification of 1 to 5, designed to classify technical complexity and manufacturing time towards soft fabrication approach. Each score refers to an evaluated understanding of soft fabrication relating to the two characteristic defined. Attributes such as technicality, costs, and accessibility were used as sub-classes within the characteristic of production and technical complexity. While manufacturing time is described as a non-quantitative value reflecting on the production and technical complexity of any fabrication technique employed. These

attributes were tailored to each score and based on manufacturing development approaches.

Table 2.3.1 Score classification of production and technical complexity, and manufacturing time towards soft robotic development.

Value	Production and Technical Complexity	Manufacturing Time
1 (Easy)	Technicality: • Designs are of simple geometries • Fabrication techniques are easily adopted Costs: • Common consumer/hobbyist consumables Accessibility: • Commercially available materials • Fabrication tools are adaptable to consumer use	• Within hours (Depending on materials and tools) • Requires less than two manufacturing tools • Designs are of simple constructs
2 (Practical)	Technicality: • Designs uses combination of geometries • Fabrication techniques require technical planning Costs: • Common consumer/hobbyist consumables • May require industrial available consumables Accessibility: • Requires certain level of technical understanding	• Within hours (Depending on materials and tools) • Requires two or more manufacturing tools and stages • Designs are adaptable
3 (Difficult)	Technicality: • Design ties geometry designs to theoretical validation • Fabrication technique may require non-commercial methods Costs: • Requires non-commercial materials and tools Accessibility: • May require bespoke tools and materials • Materials are uncommon	• Within a day (Depending on materials and tools) • Requires three or more manufacturing tools and stages • Designs may require a form of planning
4 (Complex)	Technicality: • Designs are bespoke tied with theoretical needs. • Involves complex designs and bespoke tools for development Costs: • Materials and tools are industrial level and/or bespoke Accessibility: • May require bespoke tools and materials	• Within a day or two (Depending on materials and tools) • Requires forms of bespoke manufacturing tools and stages • Designs requires a form of planning
5 (Intricate)	Technicality: • Designs are very complex and bespoke • Involves multi-step designs and bespoke tools for development Costs: • Completely bespoke materials and tools towards development Accessibility: • Requires bespoke tools and materials	• Within a week (Depending on materials and tools) • Requires bespoke manufacturing tools and stages • Designs requires detailed planning

The score classification can then be used to evaluate a number of selected state-of-the-art soft robotic developments featured within this review. The result of this is presented in Table 2.3.2, a number of aforementioned soft robotic developments were classed with its used fabrication techniques and scored based on the characteristics of (1) production and technical complexity and (2) manufacturing time.

Table 2.3.2 Evaluation of production and technical complexity, and manufacturing time of selected state-of-the-art soft robotic system based on a systematic review [35, 59, 62, 64, 78, 91, 106, 111, 119, 128-130].

Soft Robotic System	Used Fabrication Techniques	Production & Technical Complexity (1 - 5)	Manufacturing Time (1 - 5)
Multi-gait Robot	Moulding & Casting Stereolithography (Creating molds)	1	1
Transformable Cubes	Composite Layering	1	1
Origami Elastomers	Moulding & Casting Composite Layering	3	2
Foldable-thermo	Composite layering	3	2
Origami Graspers	Composite layering Stereolithography (Molds)	2	1
E-skin	Moulding & casting Injection printing	3	3
SMA heart	Moulding & casting	3	3
Metamaterial printing	Fused deposition manufacturing	4	4
Direct resin printing	Stereolithography	4	4
Octopus	Injection printing Stereolithography	4	4
Resin printing	Stereolithography	5	5
i-sprawl	Shape deposition manufacturing	5	5

A number of state-of-the-art soft robotic developments were assessed and evaluated based on their published data metrics. In line with the score classification in Table 2.3.1, the current trend of soft fabrication approach can then be illustrated in a graphical manner highlighting the increasing complexity of fabrication against manufacturing time taken to develop these soft devices as shown in Figure 2.3.2. This illustration not only serve as a representation of the trend in soft fabrication for soft robotic development, but also highlights adaptability and integration of additive manufacturing methods towards soft fabrication techniques across the given selected examples of state-of-the-art soft robots.

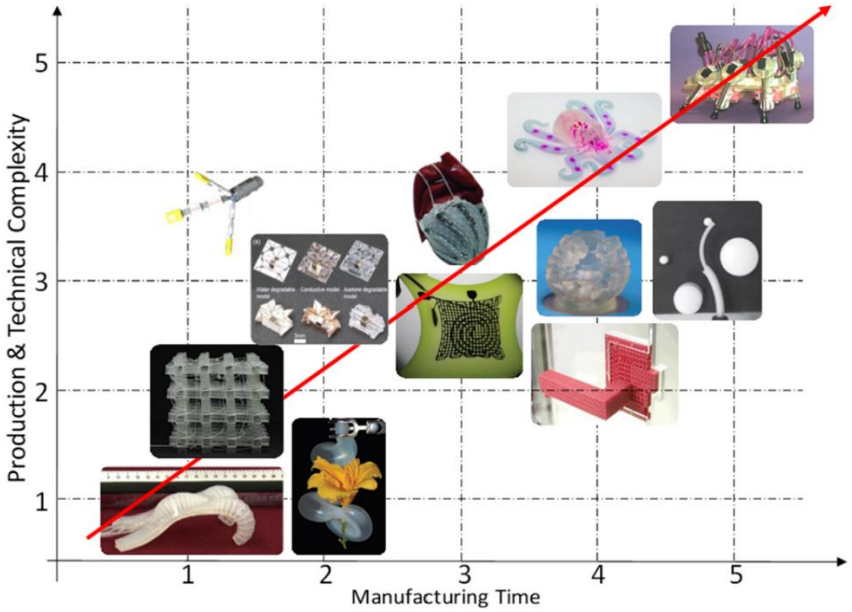

Figure 2.3.2 Soft fabrication trend of soft robotic systems represented as Production and Technical Complexity vs Manufacturing Time [35, 59, 62, 64, 78, 91, 106, 111, 119, 128-130]

In line with manufacturing time, as the production and technical complexity increases, it is evident that advances in soft fabrication techniques will help push for increasingly performant and intricate soft robots to be developed. However, there is a distinct need to innovate current fabrication techniques to reflect soft robotic development approaches. The underlying factor would also help reduce the number of processes and simplify the complexity faced with free form fabrication. Other crucial factors also includes cost of materials, fabrication accuracy, resolution, repeatability, external intervention and discrete time taken for fabrication compared to manufacturing time.

As it stands, advance fabrication techniques for soft robotics can be seen incorporating and encompassing a growing multi-disciplinary field of engineering with new approaches for soft fabrication techniques. However the techniques described in this review forms the fundamental fabrication technique used to create the current state-of-the-art soft robotic applications. As Table 2.3.3 illustrates, there is no single-solution based on a fundamental fabrication technique, as each development is dependent on its intended design, application and other attributes.

Table 2.3.3 Selected list of soft fabrication techniques used in this review to illustrate application suited approach for development. [11, 19, 131]

Fundamental Fabrication Technique	Class of Fabrication Technique	Part Scale (mm)	Application	Pros	Cons
Moulding & Casting	Gravity moulding	1-10^3	Fluidic Actuators	Low Implementation Cost	Degassing; Casting time; Rheological properties
	Vacuum moulding	10^3-10^1	Microfluidics	High precision details	Complex design and manufacturing of moulds
	Spin casting	1-10^2	Microfluidics	Planar moulds	Thickness control; Limited details on moulds
Stereolithography (SLA)	SLA for Mould Printing & Direct Part Print	10^-2-10^1	Prototyping of moulds; UV curable resins for soft device fabrication	Large range of material (UV Curable Resins); Mould has low surface roughness	Single material use in vat; Long manufacturing time;
	Selective Laser Sintering	10^-2-10^2	Prototyping of moulds; Direct Part fabrication	Fabricated moulds are robust; Large complex models applicable	Limited range of material; Cost of manufacturing
Fused Deposition Manufacturing (FDM)	Fused Deposition Moulding	10^-1 - 10^2	Prototyping of moulds;	Large range of materials (Filaments);	Poor mechanial properties; Low accuracy; High surface roughness on moulds
	Inkjet/Direct Printing	10^-2 - 10^1	4D printing; Conductive Applications	High precision; Multi-material aqueous patterning	High material cost; Long manufacturing time; Complex manufacturing design
Shape Deposition Manufacturing (SDM)	Combination of Moulding & Casting, Fused deposition manufacturing and Machining	10^1 - 10^3	Biomimetic robots; Multi-stage fabrication including machining	High precision; Complex designs and development	Complex manufacturing technicality; High manufacturing cost; Long manufacturing time
Composite Layering	Spin Coating	10^-4 - 10^-1	Thin Film; Microfluidics	Planar design; Large material library	Limited scale; Thickness Control;
	Lamination	10^-1 - 1	Thin Film; Film Composites; Pop-up Robotics	Planar designs; Low cost implementation	Thickness Control; Material library limited to planar sheets

Recent advancement still presents an unorthodox approach towards fabrication and material integration. This is due to the limitation of existing fabrication techniques to overcome and incorporate soft material libraries. A greater understanding of soft materials is required to address the limitation and integration of different materials (soft, rigid, solid and aqueous). Along with pre-existing techniques utilised and adopted, enabling techniques such as micro-moulding, multi-material embedded 3D printing, and self-configurable composites have highlighted promising potential in advance soft fabrication techniques.

2.4 Conclusion of Review

The review initially provided an overview of Soft Robotics from a methodological development route. This starts with the principle design boundaries of soft robotics and was described with its approach towards computational aid, while relating to soft robotic actuators and its material constituents. Among them, the term of "soft robotics" was described based on different interpretations and classification of 'soft' and 'compliant' features found in soft materials [2, 3, 5, 10, 11, 58, 131]. As the review progressed, fabrication of soft robotics is noted as the main fundamental development point. Soft fabrication was highlighted as notably the only way to produce these envisioned soft robotic devices. By identifying and classifying the core manufacturing methods used in soft fabrication, the review outlined its technique along with its innovation, advantages and disadvantages.

The shift from conventional manufacturing techniques has seen evolving from common moulding and casting techniques to explore arbitrary printing technologies adopted and innovated from additive manufacturing methods (shape deposition, fused deposition and soft lithography). Such methods have become increasingly common in soft fabrication with recent advancement, but still presents unconventional approaches towards fabrication and material integration. This is due to the adaptability of existing fabrication techniques to overcome and incorporate soft material libraries.

The configurability of soft material and mechanical properties towards the physical design and/or embodiment of microstructures is believed to be combined to develop shape changing features in order to interact with its environment. The main challenge still lies in the development of fully soft and compliant systems. While the research community has popularised printing technologies as the future of soft fabrication, there is a noticeable lack of innovation and applications generated towards thin-film fabrication methods for fully soft and complaint devices. Compared to the other three fundamental soft fabrication techniques mentioned in this review, the depth of composite layering applications have yet to see a fully soft and complaint device. Existing state-of-the-art devices that is fabricated fundamentally through composite layering exploit the use of semi-compliant materials, such as fabric, paper, plastics and extensible films of millimetre thickness. Techniques adapted from thin-film manufacturing are necessary to be manufactured at precise controlled thicknesses and homogeneous across the layer of material. However, to-date a fully elastomeric, small scale (millimetre), inflatable and programmable soft robotic device has yet to be formulated.

As such, a soft fabrication method to develop soft planar composites, capable of programmable inflation is found to be a research gap in soft robotic development. The design and fabrication approach intends to embed structure and functionality from a two-dimension perspective to transform composites into 3-D structures that can be applicable in real-world robotic problems. The following describes a methodological approach to be taken in aspects of design, fabrication and control, for the development of soft planar inflatable composites.

With the growing development of new inflatable designs for soft actuators, there has been an increasing interest in utilising digital design means for predictive soft models in numerical methods. This is intended to predict the capabilities and performances of soft robotic devices due to its non-linear behaviours and interaction of materials that constitute to the unique motion and ability they possess. Analytical models, such as finite element analysis of soft actuators as seen in literature, can simulate the material effects and design behaviours. Prior to the time taken for trial

and error design and fabrication processes, finite element modelling may be capable of assessing its functionality, performance and capabilities in order to optimise and further develop soft robotic components.

The research aims to adopt the use of composite layering technology to develop a soft inflatable composites for various functionality and modalities. The fundamental technology is viewed to be closely relatable and most suitable point of development. Using soft materials and innate material mechanical properties, the use of laminar techniques can enable the means to generate soft pliable thickness-controlled layers that can be reconfigured to form functional composites. Furthermore, bespoke fabrication tools to enable such developments can be adopted or constructed along the development. While most soft materials mentioned in the review are either costly, difficult to acquire or bespoke, the use of platinum cured silicones are commercially available and easily acquired. The choice of elastomers is often used by the soft robotic research community as depicted in the review. Custom pneumatic control methods will be employed and developed to actuate the fabricated soft inflatable composites. As the aim of the research focuses towards the fabrication of a soft planar inflatable composite, the review has provided an in-depth insight and understanding of soft robotic fabrication.

Chapter 3: Soft Planar Inflatable Composite Fabrication Technique

This chapter introduces a bespoke fabrication technique developed by adopting existing additive manufacturing techniques of composite layering and adapting it into a soft fabrication technique to create thin elastomeric sheets to form soft composites in a planar manner. The fabrication method is described from a conceptual manner of construction and production of soft planar inflatable composites (SPIC). A SPIC fabrication process is designed to describe the process and applicability of technique. In addition, a development build of a bespoke fabrication set-up to enable the creation of SPIC fabrication is described and the needed characterisation steps for further development.

Work contributing to this chapter was published in RoboSoft'18 (Soft Robotic Conference 2018).

Kow J; Culmer P; Alazmani A. (2018) Thin Soft Layered Actuator Based on a Novel Fabrication Technique. IEEE RAS RoboSoft'18.
DOI: https://doi.org/10.1109/ROBOSOFT.2018.8404916

3.1 Introduction to Soft Planar Inflatable Composite Fabrication

Soft robotic fabrication has seen a shift from conventional 'moulding and casting' methods to explore a range of rapid prototyping techniques, including additive manufacturing, shape deposition manufacturing and combinative techniques. However, the research community has since favoured printing techniques as a point of innovation and has since developed many fascinating, intricate and complex soft robotic developments, including solutions within the field of material engineering. Despite the shift in manufacturing method, moulding and casting is still considered one of the fundamental techniques for fabricating soft devices. As casting of soft materials is subjected to a two-dimensional plane designs constraints, fabricated mould designs tend to be planar in structure and the structural complexity of soft components producible at millimetre and/or smaller scales is constrained by the manufacturability of moulds and its technique [64]. Moulds created from additive manufacturing techniques such as fused deposition manufacturing and stereolithography allows nearly arbitrary geometries, but the compatibility of soft materials and limited resolution produces static devices due to the innate material composition and properties [56].

Taking inspiration from 'Pop-up robotics' and the current advances for composite based soft robots, a novel approach to build fully soft, stretchable, self-reconfigurable and functional robotic device is introduced here. The conceptual idea depicts thin, soft, inflatable and fully configurable robotic composite component that can actively deform to their pre-programmed state when actuated. Based on the fabrication technique of composite layering, the design of the development focuses towards a planar two-dimensional (2D) plane. The technique proposed here, adopts film application and microfluidic approaches that have seen soft components fabricated across centimetre to micrometre scales [86, 87, 119]. The fundamental technique enables dense micrometre features capable of fluidic computation and planar layer building as widely demonstrated in the field of microfluidics. Despite a limited material library and non-conventional process within its fabrication

technique, its layer-based fabrication technique can be adopted and have shown potential of creating planar 'skin-like' soft components [132, 133]. Figure 3.1 illustrates two conceptual ideas of possible planar, soft and pneumatically driven controllable composites. The first features a circular disc able to fold outwards when actuated; while the second shows a flat composite of rectangular shape capable of collapsing at desired points into a zig-zag motion.

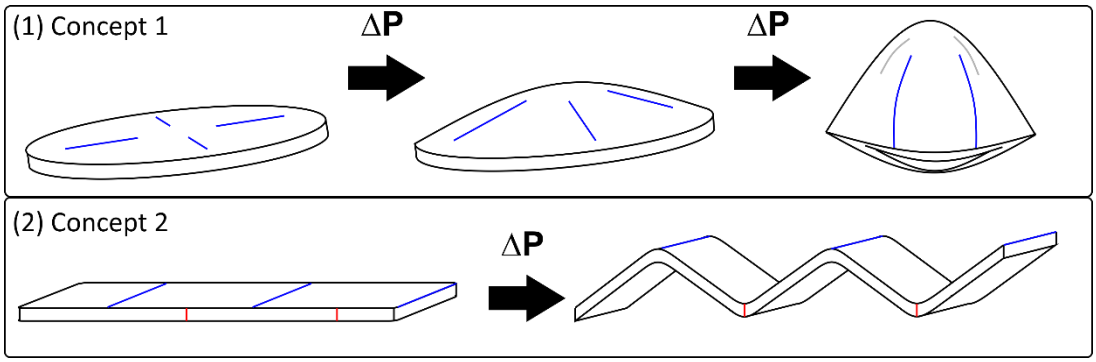

Figure 3.1 Taking inspiration in 'Pop-up' robotics and adopting soft robotic features, two conceptual designs were envisioned to propose the development. (1) A composite of circular disc shaped is actuated and undergo shape change. (2) A rectangular composite with embedded mechanical features deforms into a collapsing motion when actuated at desired points into a zig-zap motion.

A novel fabrication technique is proposed for designing and fabricating soft planar inflatable composites (SPIC) in a planar manner. The technique takes from creating millimetre-scale laminar material sheets and stacking them through a layer-by-layer process. By reconfiguring soft materials, such as thermoplastics, fabric and soft viscous elastomers; they can be combined to form structural layers for soft composites, of which can be utilised to develop shape changing structures/surfaces in order to interact, adapt or conform to its environment. The overall material composite shall consist of strain limiting layers for embedded mechanical programming and mask layers for inflatable cavities. This would then serve as the base foundation and development for functional, programmable soft inflatable composites to be applied in various applications.

3.2 Conceptual Design of Soft Planar Inflatable Composites

The fundamental concept of the design focuses on materials in a planar manner, such as sheets and films; stacked through a layer-by-layer process in a form of composite layering as its fabrication technique. Through this process, materials can then be reconfigured to form functional composites through its material and/or structural design in order to develop thin, soft, inflatable components. As soft layered composites, the overall design follows a 2D planar manner. Upon actuation, these flat-laminar structures will undergo shape change through cavities formed through 'mask layers'; while its morphology is controlled through embedded mechanical programming with the use of strain-limiting materials (constraint layer) and/or its overall material embodiment. Figure 3.2.1 illustrates the conceptual design of a thin soft inflatable composite.

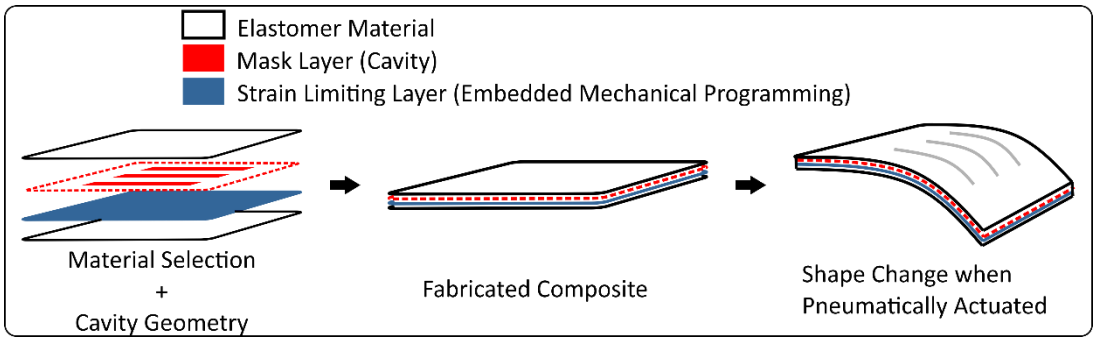

Figure 3.2.1 Conceptual design of a soft planar inflatable composite. Configured in a layer-by-layer method, the composite inflates through the mask layer and deforms to the shape of the embedded strain limiting layer, while the elastomer material is the embodiment of the composite.

The conceptual design of an inflatable soft planar composite can be described into two main design parameters; (i) Selective material layering, and (ii) Structural geometry variation; as shown in Figure 3.2.2. Starting with selective material layering, the configuration of various laminar materials forms the basis of the composite. Soft elastomeric sheets are used to form the overall material layers for

these soft composites; of which can then be inflated and formed through mask layers introduced in its fabrication process. Such a development is plausible through 'Zero-Volume' cavities via soluble materials, such as paper, oil, or wax; as introduced by Park *et al*. [37]. Inflated (actuated state), its morphology can then be controlled through embedded mechanical programming with the use of strain-limiting materials, such as paper, fabric or elastomers of higher stiffness and of similar properties. Types of fabric such as spandex or similar material with patterned configurations to adjust its tensile ability is proposed to be used in this development based on configuration 2 and 3, as shown in Figure 3.2.2.

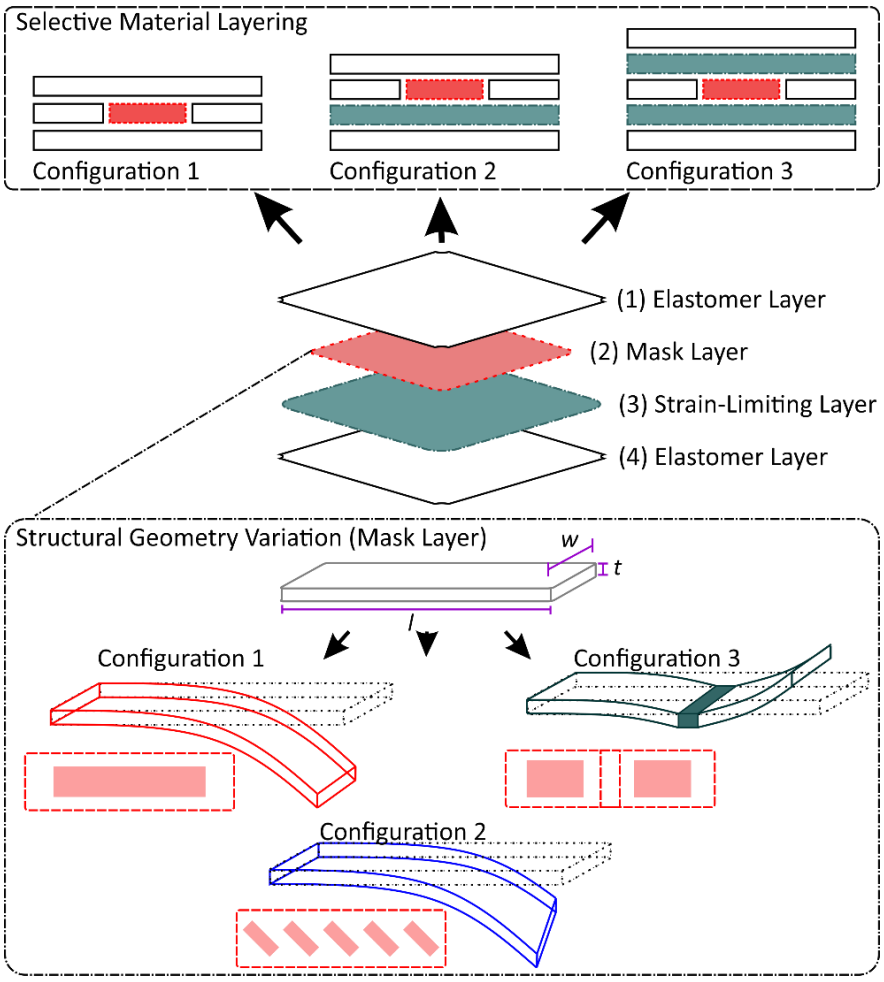

Figure 3.2.2 Design parameter to develop a soft, inflatable composite for actuation. Selective material layering and Structural geometry variation provide the fundamental design parameters to fulfil. Proposed configurations illustrates the conceptual idea of soft planar inflatable composites to take shape.

The second design parameter investigates the structural geometry variation of its mask layer. As each layer is configured, its inflation characteristics introduces a 'zero-volume' void that can be structured towards creating cavities, channels and chambers. The interaction of the design of the mask layer, strain-limiting layer and overall elastomer embodiment relies on each other to produce the desired inflation characteristics. With the creation of zero-volume cavities and its overall material selection, its design aspect will require further development beyond its fabrication means. In this entire development, water-soluble paper (Sulky Solvy Stabilizer, Sulky Burel LTD, UK) is used to introduce the mask layers for inflation. Other means of mask layer materials have been explored, such as wax, foam, and printing paper; however, the use of water-soluble paper was a more accessible and cost-friendly choice in this development to ensure a defined thickness cavity (0.1 mm) is embedded during fabrication. Computer aided software and graphical illustration tools for design morphology and finite element analysis for modelling and behaviour simulation will be used to extend its design development and will be detailed and explored in Chapter 5.

Basic soft materials such as elastomers require a form of curing process to form its semi-solid and elastic state. Often introduced as a two-part polymer ratio, these materials vary in viscosity in its uncured (pre-polymerisation) state; are then mixed and left to cure (polymerise) and catalyse into a solid hyper-elastic state. While, thermal and optical external factors can also facilitate the curing process depending on its material composition. In this development, platinum cured silicone is proposed to be used as the building layers to embody the concept of 'soft composite' as the overall fundamental material. With an extensive and progressively expanding soft material library, elastomers are by far the most common category of used material in soft robotic research as depicted in the review. Platinum cured silicones such as, Smooth-On-EcoFlex™, DragonSkin™; Wacker Elastosil®, are commercially inexpensive and available, easily assessible and acquired. The material is versatile, compliant and plausible for certain silicone materials to adhere and/or bond to its cured counterpart or other material of similar properties without the use of

adhesives to form the composite. With the choice of material set, the development adopts film application technique as the fabrication method of thin laminar elastomeric sheets. A number of techniques were investigated to achieve elastomeric film fabrication, such as, spin coating, rod casting, and even injection moulding into an enclosed cavity with a defined thickness [134]. However, these methods were found to be unsuitable due to, limited workspace and production capability, difficulty to incorporate and/or integrate external fabrication processes, and the cost and accessibility of such techniques, including free form material library (e.g. paper, wax, fabric, powders). Thin film techniques commonly use material for micro-electronics, e.g. Sylguard 184 PDMS, are costly, requires specific fabrication methods for processing and are difficult to incorporate. As such, the technique of film application was ventured to enable the designed fabrication process. The technique benefits from its integrable applications and customisation suited towards the intended conceptual design and fabrication technique. A fabrication process was then designed to integrate film application technique to develop the proposed soft planar inflatable composite. The technique encompasses a step-by-step process from fabrication to removal of patterned designs of the soft composites via laser ablation and post-processing, such as cleaning and inflation.

As the complexity to create a homogenous film thickness of millimetre thickness were based on the conceptual design, a form of automation for film application technique was sought after to reduce and remove possible fabrication errors. A bespoke platform was designed and built to enable automation of the film application process to remove fabrication errors, such as, applicator spread speed and applied pressure. The specifications and requirements of the film applicator in this development, along with the manufactured build platform is described in Section 3.4. Theoretical characterisation of film application is detailed and discussed in Chapter 4 to evaluate the fabrication of desired elastomeric film thickness for soft composite feasibility.

3.3 Fabrication Technique of Soft Planar Inflatable Composite

The conceptual design drove the development of the fabrication method which aims to exploit a configuration of elastomeric planar layers into a soft functional composite. The fabrication technique of soft planar inflatable composite (SPIC) proposed here follows a step-by-step process as illustrated in Figure 3.3.1, and is described in the following context.

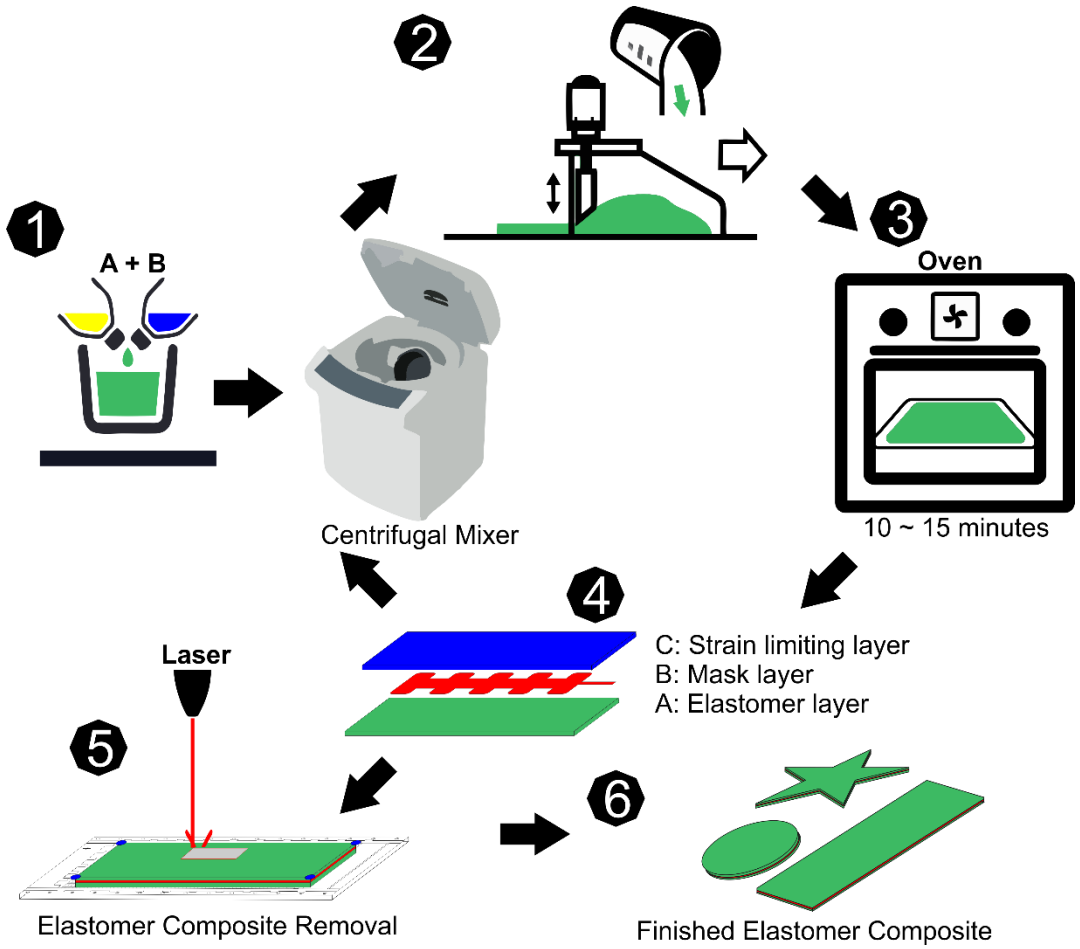

Figure 3.3.1 Illustration of soft planar inflatable composite (SPIC) fabrication process. A step-by-step process is described in the following context in reference with the number headers in the figure. (1) Preparation of elastomeric material; (2) Film application of elastomeric material; (3) Curing of elastomeric material; (4) Material composite is build; (5) Laser ablation of completed soft composite build; (6) Post-processing of finished soft elastomer planar composites.

As shown in Figure 3.3.1, a step-by-step process describes the proposed SPIC fabrication process. Each step is associated to the figure in a numerical manner and is named accordingly to the technique executed. The following describes an overview of the workflow involve to produce the desired technique in each step as illustrated in Figure 3.3.1.

(1) Preparation of elastomeric material

Elastomeric material of desired properties is mixed (1:1 common ratio for two parts - platinum cured silicones) in a centrifugal mixer (ARE-310, Thinky Inc., Japan) to enable a catalytic reaction. As the centrifugal mixer automates the process of mixing viscous material while degassing at the same time, the elastomer is ensured to be uniformly mixed in a timely manner prior to total catalytic reaction (curing) based on its material properties.

(2) Film application of elastomeric material

A film applicator is set to the desired layer thickness and pre-polymer elastomer is poured towards the spread-plate of the applicator. The applicator is then dragged across the build plate at a desired set speed, spreading the elastomer across the platform to produce the desired thickness. A bespoke film applicator platform was designed to assist the development of the fabrication by automating the spread process of the film applicator at set speeds and applied pressure across the build plate.

(3) Curing of elastomeric material

Once the elastomer has been spread across uniformly, the build plate is then removed and placed into an oven to cure for a set amount of time and temperature depending on the type of elastomer and its material specifications. (i.e. 10 ~ 15 minutes @ 75°C).

(4) Material composite build

Strain-limiting materials (i.e. fabric or elastomers of higher stiffness) or patterned masks layers are then added to the layer before and/or after the elastomer has been cured and cooled. As heat reduces the handling time of elastomer prior to curing, it is crucial to allow a cooling stage after removal of build platform from the oven. Further layers of elastomer or embedded material are introduced by repeating stages (1)-(4) based on the desired designed layer configuration as illustrated in Section 3.2, Figure 3.2.2.

(5) Laser ablation of completed soft composite build

Once the desired composite structure is achieved, the build plate is placed into a CO_2 laser cutter (VLS3.50 Universal Laser Systems) to cut out the desired shape using pre-defined alignment features. The selective laser cutting process can be used not only to cut the fabricated composite sheet and separate it from the base build platform, but also to pattern (engrave) individual layers to produce desirable features and profiles (depth) through ablation. The profiles (depth) of these patterns can be controlled by adjusting the laser power and speed settings.

(6) Post-processing of finished soft elastomer planar composites

The fabricated composites are then removed, cleaned (using isopropanol or soapy water bath), and fitted with pneumatic airlines ready to be actuated. The final composite can also be cleaned using a pressurised airgun and then a sonicator consisting of isopropanol or a soapy water bath, to remove any debris and soot from the fabricated soft planar composite. This will provide a clean surface for safe handling and possible further fabrication use either through integration or adaptation.

From the proposed fabrication technique, each step provides a key role into developing a soft, compliant and functional elastomeric layer. Despite the use of specialised equipments, such as centrifugal mixer, oven and CO_2 laser cutter to facilitate the fabrication of the elastomer layers. Commercial automated film applicators were not an accessible and available option, due to its high cost and pre-built form with little to no option for integration with third party solutions. Apart from the high cost, commercial film applicators are often pre-set with limited range of settings, such as spread speeds, thickness range for pre-built fixtures and build plate production size. In order to adopt a cohesive material library and conceptual fabrication design parametric needs, a bespoke applicator platform was designed and built to facilitate and enable the fabrication of thickness-controlled elastomer layers. A batch manufacturing process is opted to potentially reduce the overall fabrication time. This includes cleaning and layer alignments to create the desired composite configuration in an optimal and efficient process.

3.4 Development of Bespoke Applicator Platform

Fabricating layers of elastomers with a uniform thickness is extremely important in this development to fabricate soft inflatable composites. The composite layering technique of film application was adopted base on its ability to produce controlled thickness substrates (film or sheets) over the nature of soft materials in a viscous state. Film applicators are often manufactured as metal bars to high tolerances to provide a consistent, repeatable and even coating of a substance over a substrate. Despite the high manufacturing tolerances, the thickness of any coating that remains after application can vary from 50% to 90% of the actual desired thickness. This theoretical phenomenon is known as '*wet film thickness*' based on ASTM-D823-95 and ISO 2808 standard practice, and is addressed in detail in Chapter 4 [135, 136]. While there are multiple types of applicators with varying forms and functionality, common factors that can affect the quality and fundamental mechanics of the fabricated films are: (1) applicator set relative gap, (2) applicator spread speed, (3)

ambient and effective temperatures, and (4) applicator substrate. It is noted that these factors are dependent on material viscosity subjected to the type of application method. Initial prototypes featured a casting rod technique using a metal rod affix to a controllable position relative to a substrate via micrometric stage. However, it was observed that the viscosity and rheological property of elastomeric materials are directly linked to the accuracy of thickness producible by the relative gap set. As the control of the rod distance relative to the substrate was not of robust construction, the development expressed further need to produce a sustainable method to produce quality, accurate and repeatable layers of elastomeric material. Looking towards film applicators, it is understood that small variations in speed and applied pressures are inevitable in manual applicators. While automatic film applicators may vary in their construction, the build assures consistent speed and pressure applied to the applicator, providing repeatable results. Taking into consideration of the cost of such an equipment, a commercial manual applicator was favourable. However, a bespoke platform consisting of a linear drive stage was opted to emulate the spread speed and applied pressure on a commercial manual applicator.

An extensive range of manual applicators are commercially available to accommodate different standard requirements. In this development, the choice of manual applicators was based on three criteria's, (i) range of producible film thickness (0 to 3 mm), (ii) thickness resolution (< 0.1 mm) and (iii) film width ($100 < x < 300$) mm. Several commercially available manual film applicators were compared, from baker film applicators, casting blocks to casting knife applicators as illustrated in Figure 3.4.1. From the conceptual design, a batch manufacturing process is opted based on the producible film width of the applicator, which potentially reduces the time needed for alternating designs and enable fabrication of various component designs with changes in geometry. While a small thickness resolution is favourable, often these applicators are not equipped with producing a large range of film thicknesses. After reviewing several applicators, a 20 cm casting knife applicator was chosen as it fulfils the main criteria set as described and can be easily adapted into the design of the bespoke applicator platform.

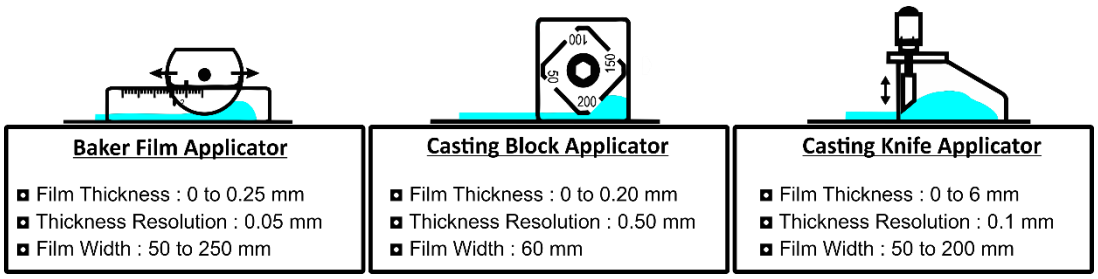

Figure 3.4.1 Choices of film applicators and specifications. Left: Baker film applicator; Centre: Casting block applicator; Right: Casting knife applicator.

Based on the chosen manual applicator and the fabrication process as introduced in Section 3.3, the build plate (applicator substrate) was opted to be made of solid anodized aluminium sheet (Alloy 3003) and is machined towards a specific size (Width: 280 mm, Length: 450 mm, Thickness: 4mm). Anodized aluminium was chosen as the substrate material as it is commonly used as a standard laser cutting material support surface in industry. Often these standard laser support surface consists of a thin-wall aluminium honeycomb-core pattern evenly supported by an underlying hollow structure. This surface structure is common due to the choice cutting material, such as plastic, paper or fabric, to reduce excess laser power which can damage the lower surface of the target material as it reflects off the support surface. However, a solid aluminium surface standard is also available for materials with higher resistance to heat and non-reflective properties, such as wood and silicone rubber, where excess laser power is not a concern and/or is absorbed in an unfocused state. As such, the choice of material and fabrication method can be directly placed into the laser cutter. In addition, a mobile build plate with a solid surface is preferable as elastomeric material can be easily removed from the build plate after fabrication and its ability to withstand temperatures up to (600°C) when using external thermal source for elastomer curing (Oven).

The design of the build plate was based on the choice and method of manual film applicator, while its size was to accommodate a various production designs over a single fabrication process. In addition, alignment features and drain lines were designed into the plate to assist the method of application and to enable direct laser ablation (cutting and/or engraving) onto the fabricated composites with addition of

mask layer and constraint layers patterning. Figure 3.4.2 shows (a) graphical illustration of the designed build plate with dimensions, and (b) picture of manufactured build plate.

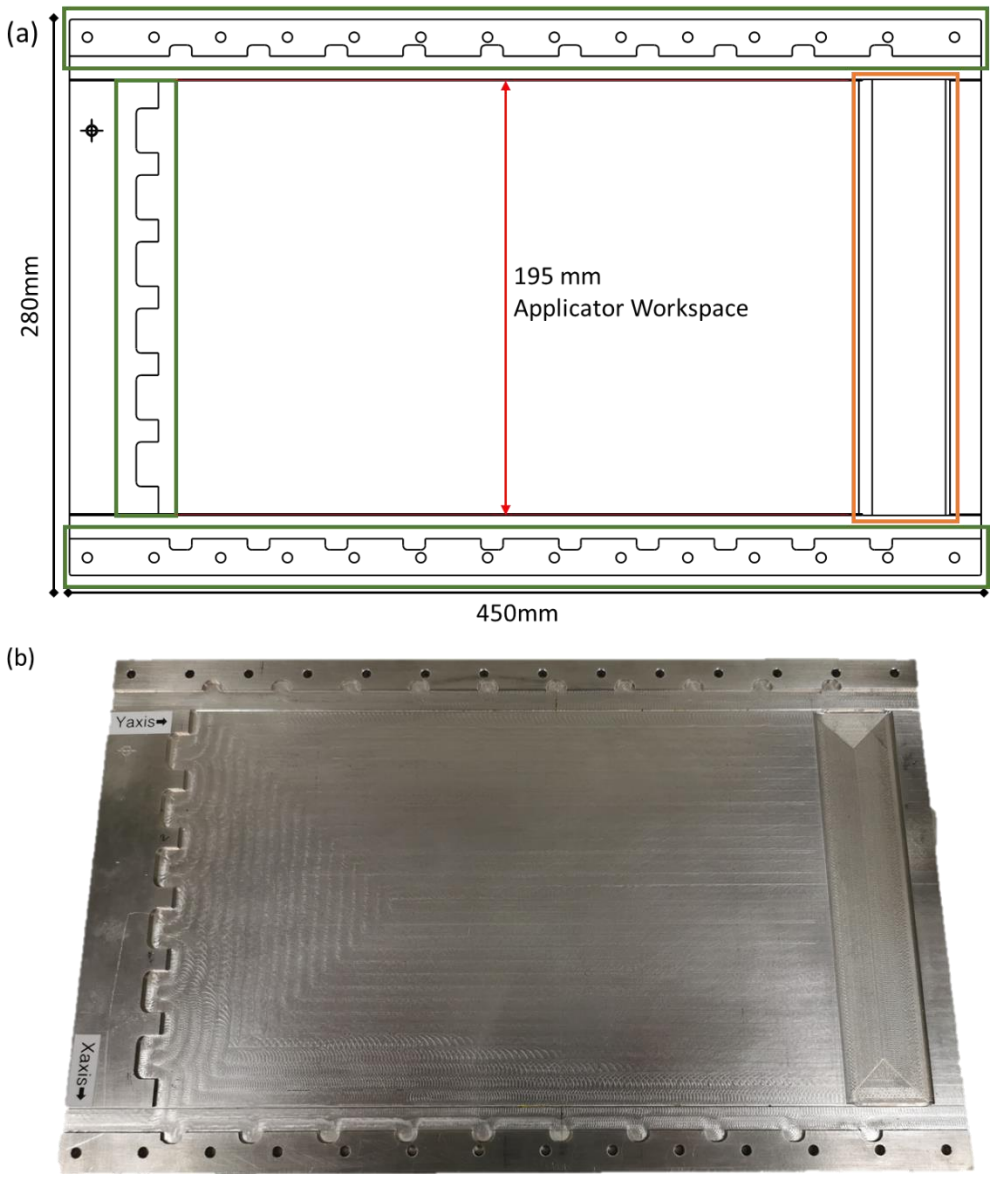

Figure 3.4.2 (a) Graphical illustration of designed SPIC build plate; (b) Machined build plate for SPIC fabrication (Width: 280 mm, Length: 450 mm, Thickness: 4mm). Ridges are formed on the side of the build plate to be used as alignment features (Green Box). A drain feature is incorporated into the design to remove excess elastomers during fabrication (Orange Box).

Commercially available automated film applicators are often pre-set with a range of application speed, type of applicator fixtures and designed build plate. Despite the various form of construction and number of features or functions, the spread speed and direction are the two main functions that serve the fundamental build of automatic film applicators [135]. In order to emulate such functions, the bespoke fabrication platform is fitted with a single-axis linear drive actuator (C-Beam® Linear Actuator, Open Build) of 300 mm travel distance above the carriage with a custom attachment to apply a constant pressure and drive the manual applicator across the build plate. The placement of the linear drive actuator was to ensure a level platform for the build plate and fabrication to occur as compared to conventional film applicators. The linear drive actuator is equipped with a stepper motor capable of a 1.8^{o} step angle (Nema17 Bipolar Stepper Motor) and connected to a lead screw (8 mm diameter, 2 mm pitch) with the custom attachment to push the manual film applicator.

Controlled with a microcontroller (Arduino Mega D3) and motor driver (Digital Stepper Controller 2DM542), the linear stage is programmatically designed to drive the manual film applicator across the build plate at controllable set speeds from 1 mm/s to 50 mm/s at 1 mm/s step-resolution. The design and build of the linear drive actuator is shown in Appendix 3, along with the program code used for control. Controls for the bespoke applicator was also designed to be comprehensible with actuatable tactile controls and visual aid through an LCD screen. A program flow chart describes the controls developed for the bespoke applicator platform in Figure 3.4.3. Compared to commercial automated film applicators, the custom built applicator platform benefits most from a high resolution of driving speeds and an adjustable workspace and configuration. This set-up essentially automates the technique of film application at desired set speeds and accessibility in comparison to an automatic film applicator that were not designed and built for the proposed application. Relative to the material viscosity and properties, characterisation of the technique against its intended working material is still needed and is investigated in Chapter 4.

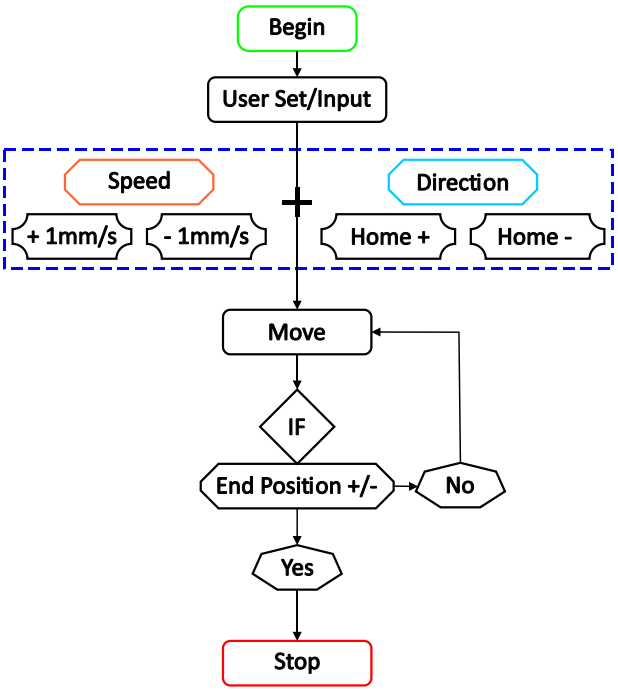

Figure 3.4.3 Bespoke applicator platform program control flow chart. The control algorithm is programmed to provide the two main functions ('Speed' and 'Direction') as controls to drive the linear stage emulating commercial automatic film applicators.

In summary, the bespoke film applicator platform was designed and built to accommodate a 20-centimetre-wide manual film applicator (Elcometer 3520 Casting Knife Film Applicator, UK). Capable of producing films of 0.1 mm thick, on a bespoke set up with a linear drive actuator (C-Beam® Linear Actuator, Open Build) of 300 mm travel distance above a build plate made of machined aluminium (W: 280 mm, L: 450 mm). Automated and controlled by a microcontroller (Arduino Mega D3), the linear actuator is capable of driving the manual film applicator across the build plate at variable set speeds from 1 mm/s to 50 mm/s at 1 mm/s step-resolution. The manual film applicator is able to adjust the height of the spread-plate relative to the build plate to produce elastomeric sheets of desired thicknesses ranging from 0.1 mm to 6 mm at a resolution of 100 microns (0.1 mm) using two integrated micrometric screws. Figure 3.4.4 illustrates the assembled bespoke applicator platform, while an expanded view and build of material is shown in Appendix 3.

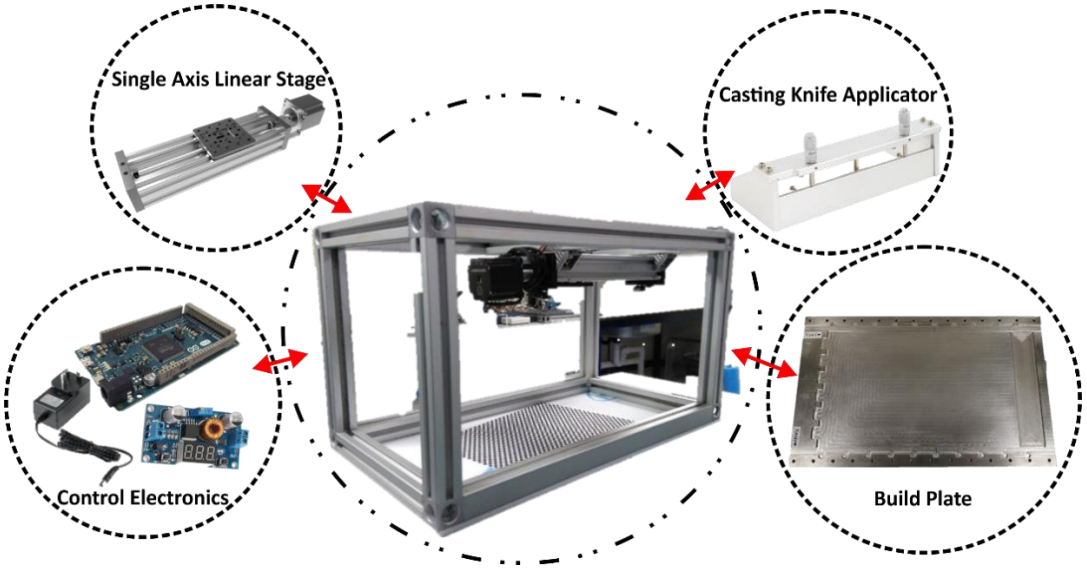

Figure 3.4.4 Overview illustration of developed bespoke applicator platform to assist development of SPIC fabrication with categorised components. Build of materials and expanded assembly of bespoke applicator platform is shown in Appendix 3.

3.5 Summary

From the literature review, a distinct research gap was identified in soft fabrication towards composite layering fabrication methods for fully soft and compliant devices.

In order to develop a soft, planar and inflatable composite, a bespoke fabrication technique was developed by adopting existing industrial additive manufacturing techniques of composite layering and soft fabrication techniques to create functional soft planar inflatable composites for soft robotic applications. The fabrication method was introduced from a conceptual design manner drawing inspiration from 'Pop-up' robotics [80-83] and Snapology Origami [94].

Based on the conceptual design, the fabrication technique of soft planar inflatable composite (SPIC) was proposed and enabled through the construction and use of a bespoke applicator platform and adopted soft fabrication techniques found in literature. The fabrication technique aims to enable controlled thickness of elastomeric films to be produced, along with mask layers for inflatable cavities and constraint layers for embedded mechanical programming. The fabrication technique

is described in a process manner starting from mixing of elastomeric materials to the creation of desired thickness soft composites in a continuous, repeatable, lamination technique of elastomeric material. To enable such a development, a bespoke applicator platform consisting of a commercial manual casting knife film applicator, a machined aluminium build plate and a controllable stage actuator was assembled to assist the fabrication technique. Preliminary and exploratory work surrounding soft fabrication paved the way for the proposed SPIC fabrication technique. As the technique was developed, time taken for each layer to be fabricated has been reduced significantly to 25 minutes. This includes preparation and cleaning such as set-up of fabrication platform, layer settings, thermal event for enhance catalytic reaction (10-15 minutes in oven) and laser ablation for composite removal (time dependent on the workspace and patterned design). The technique has also progressed to be less labour intensive as certain processes has been optimised, such as alignment features and design processes.

Controls for linear stage actuators of the bespoke applicator platform were not discussed in great length as the electronic build and programming are rather basic and fundamental method in assembly and construction in most electronic control devices. Functionality of the linear stage is only limited to position and speed of travel of the applicator across the build platform. The machined aluminium plate was not manufactured with high tolerances and has found certain defects in alignment and its machining production. Although these errors will be a contributing factor in the technique's fabrication overall efficacy and ability, these errors can be reduced through manual interaction or design changes to accommodate these during fabrication. The structural build of the bespoke applicator platform comprises of Rexroth aluminium rectangular struts of 30 x 30 mm and is assembled to suit the size of the linear drive build and applicator platform. The assembly of the platform was not discussed in detail as the Rexroth struts only provided a means of structure to the applicator platform.

With the use of elastomeric materials, its varying viscosity in its uncured state will affect the production ability of film thickness being produced. This factor is present in most microfluidic development as the rheological property of viscous material,

gravitational-mechanical interaction and environmental temperature will affect the end-result of the thickness prior to forming a solid hyper-elastic state. As such, characterisation of elastomeric films is investigated in terms of applicator set thickness, applicator spread speed, and curing temperature in relation towards the viscosity of elastomeric material. The characterisation of the fabrication technique for controlled thickness of elastomeric layers and controlled depth ablation via laser cutting of composite is detailed in Chapter 4. Overall fabrication limitation was found to be the incorporation and use of water-soluble paper as mask layer. This limitation focuses on two aspects, during fabrication and after. During fabrication, application of the water-soluble paper may dissociate and buckle as uncured elastomeric material is layered on-top of the mask layer. This factor is often due to elastomeric material entering the gaps between the elastomer layer and the mask layer. Micro-bubbles can also form when curing if the mask layer is not aligned properly with the build plate. This will lead to undesired gaps that may possibly affect the inflation profile of the composite as well introduce a leak when inflated. When a successful composite is fabricated, the mask layer is removed by introducing water through the inflation channels of the design. A flushing mechanism is opted for the design to allow the mask layer to dissolve. However in some cases, residues of the water soluble paper remains within the cavity, of which can change the inflation behaviour of the composite and cause blockage to the inflation channels. Removal of the mask layer is necessary as it is fundamentally a structural layer used to form the cavity. If the mask layer is not removed, a change in inflation behaviour is expected as it acts as a strain-limiting layer.

Two design parameters were denoted to influence the interaction and functionality of the overall composite design and material composition, (1) Selective material layering and (2) Structural geometry variation. The parameters are sought to be key features aimed at producing desired inflation characteristics and fundamental to its functionality. Its inflation characteristics and behaviour will require further development and investigation beyond its fabrication means with the use of computer aided design tools and finite element analysis. This development is further explored in Chapter 5 of the thesis.

Chapter 4: Characterisation of Soft Planar Inflatable Composite Fabrication Technique

The previous chapter introduced a novel conceptual design and fabrication technique of soft planar inflatable composites through the process of film application of elastomeric material. The technique of fabrication detailed a step-by-step layering process to create functional soft composites in a planar manner adopted from additive fabrication methods. Within the technique, a bespoke applicator platform consisting of a commercial manual film applicator, a machined aluminium build plate and a linear drive system to facilitate the applicator across the platform at controlled set speeds and thickness, enables the creation of soft inflatable composites.

As such, the characterisation of the production of the fabrication is to assess the production capability, accuracy, repeatability and quality of the intended thin elastomeric films. This is necessary in order to achieve controlled desired thickness of material being laminated into composites. The composites are also evaluated in terms of material lamination bonding strength (mechanical adhesion strength via lamination of material), as this provides an understanding towards material de-lamination (peeling) and material compatibility to enable pneumatic or hydraulic expansion through the embedded cavity design for actuation. In addition, the concept of laser ablation of elastomeric material through cutting and engraving was characterised to enable controlled and precise removal and patterning of elastomeric material.

4.1 Characterisation of Fabrication Technique

Chapter 3 introduced a novel conceptual design and fabrication technique of soft planar inflatable composite (SPIC). The fabrication technique detailed a step-by-step layering process to create functional elastomeric embodied composites, consisting of an inflatable volume for pneumatic actuation, and configurable layers of strain-limiting layers for mechanical programming. A bespoke applicator platform consisting of a manual film applicator, an aluminium machined build plate and a linear drive stage was designed with the intention to drive the film applicator across the platform.

As to any material, the intended films to be produced adopts commercially available platinum cured elastomeric materials. Often producible in two parts, these elastomeric materials are mixed at a 1:1 ratio and are left to catalysed (cured). When mixed, the material viscosity would vary the performance and production of film through its viscoelastic flow based on material properties, rheological affects due to spread speed, gravitational forces and material shrinkage when cured. As such, these factors are sought to be addressed through the characterisation of material viscosity against film application of elastomeric materials.

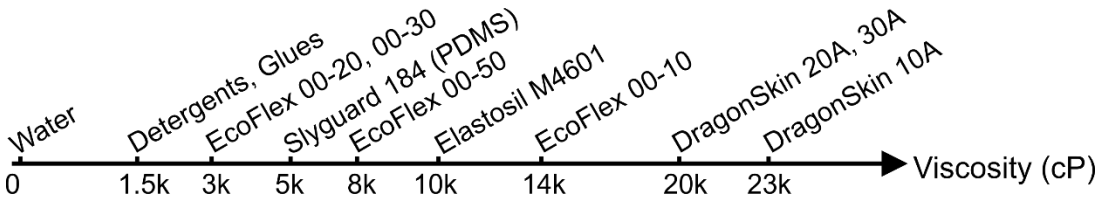

Figure 4.1.1 Scale of viscosity (centipoise (cP)) of elastomeric materials (Smooth-On-EcoFlex™, DragonSkin™; Wacker Elastosil® M4601; Dow Crowning - Sylguard™ 184). Water, Detergent, and Glues provides a relatable baseline for comparison.

Figure 4.1.1. Illustrates the scale of viscosity of elastomeric materials to be characterised based on the selected elastomers chosen and described in Section 3.1. To provide a comparable and relatable baseline, water, detergent, and glue were added onto the spectrum to provide a contrast to the viscosity of mixed elastomers

listed. Popularly and commonly used in soft robotic research, EcoFlex™ series (00-10, 00-20, 00-30, and 00-50) make up of high number of soft robotic developments. The elasticity and/or stiffness of material (shore hardness) is often indicated in its name. Next on the line-up is DragonSkin™ series (10A, 20A, 30A) and then followed by Elastosil® M4601. While almost all the elastomeric material listed above is capable of curing below 100°C under an average recorded time of 15 minutes; Sylguard™ 184 does not comply with the list of elastomers and the designed fabrication method. Its recommended curing temperature is 100°C at 60 minutes based on its material datasheet and must be handled with extreme care. Although the material is widely and often used in the field of microfluidics, microelectronic and medical applications, it is not adaptable into the designed fabrication technique which opts for a much shorter curing time for each layer to enable a repeatable and continuous laminar process.

In order to evaluate the efficacy, performance and applicability of the fabrication technique of film application, understanding of the mechanics of film application or coating of materials is necessary in relation to the material properties. Based on this concept, the thickness of any material coating that remains after application (spray-gun, rod-casting, casting knife and etc) is governed by the theoretical phenomenon of '*wet film thickness*' (WFT) [137]. The theory depicts that, despite high manufacturing tolerances of applicators, material coatings after application can vary from 50% to 90% from the actual desired thickness. Wet film thickness itself is the measured thickness of any applied liquid based materials. Its principle use is often fundamental for applications using paints, varnishes and materials that consists of solvents that evaporates after application. The material thickness that remains, is then known as the dry film thickness, of which is the desired thickness to achieve. As the liquid based material evaporates in a coating, the material solids that remain can be expressed as a volume percentage of solids. As such, the WFT theory can then be expressed as a simple mathematical formulae:

$$Wet\ Film\ Thickness = \frac{Dry\ Film\ Thickness \times 100}{\%\ Volume\ Solids} \qquad \text{(Eq.4.1.1)}$$

The WFT measurement and method itself is fundamental as it enables coating or application to be adjusted or compensated to achieve the desired dry film thickness based on the type of applicator/coater. However, the intended mathematical formulae is not fully applicable for materials without complete accessibility to its base formulation, such as the elastomers featured within this study. Despite this, standard practices (ASTM D823-95 and ISO 2808) depicts and addresses the characterisation of applicators to determine the film thickness produced without reliant of material composition formulation [135, 136].

In Section 3.4, common factors that can affect the quality and fundamental mechanics of film application were described as: (1) applicator set relative gap, (2) applicator spread speed, (3) ambient and effective temperatures, and (4) applicator substrate. These factors are described and reflected in characterisation standards for film applicators [135, 136]. Based on these factors, the effects can be illustrated to provide understanding to the mechanism of film application and its direct relationship with material viscosity in order to experimentally characterise the technique. Figure 4.1.2 illustrates the factors that can hinder the fundamental concept of film application.

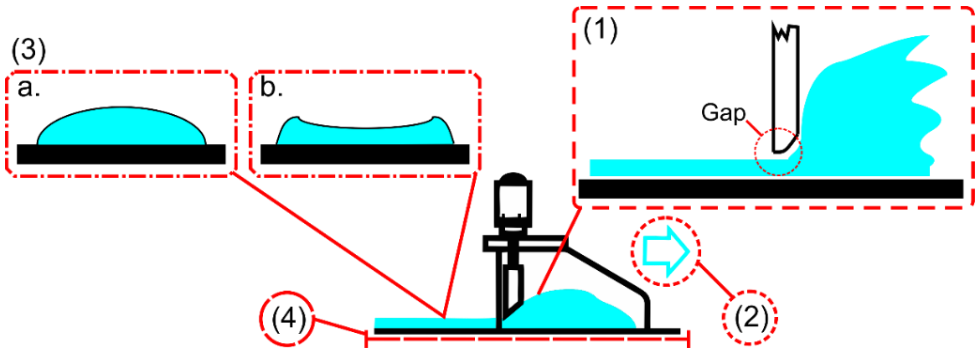

Figure 4.1.2 Illustration of film application technique and factors that can hinder the fundamental concept of film application in relation to the viscous property of materials. (1) Applicator set thickness; (2) Applicator spread speed; (3) Curing temperature (3a) convex meniscus (3b) concave meniscus ; (4) Applicator substrate.

As shown in Figure 4.1.2, a number of common factors dictate the quality and accuracy of film production regardless of the type of applicator. The following describes the factors that can hinder the fundamental concept of film application.

(1) Applicator Set Thickness

Despite being manufactured to high tolerances, depending on the material's viscosity and rheological properties, the thickness that remains after film application can vary as depicted by the concept of 'theoretical wet film thickness'. This phenomenon points at the relative gap between the substrate (build plate) and the applicator blade as materials with higher viscosity is less affected by the spread gap of the applicator compared to materials with low viscosity.

(2) Applicator Spread Speed

As the applicator is being drawn across the platform, the spread speed can also greatly affect the flow of material and relative gap between the substrate and the applicator as the material settles due to rheological and gravitational influence of fluid over time.

(3) Curing Temperature

Effective temperature acting on the material can also cause the material to deform in ways after spreading as it starts to solidify and cure. The temperature affecting the material can be ambient or relative to the substrate and material.

(4) Applicator Substrate (Build Plate)

In relation to the applicator, the surface resistance and levelling of the substrate can also hinder the travel rate of the applicator and spread material compatibility. Despite manufacturing tolerances, the quality of surface roughness is often dismissible while the levelling of the build plate is considered as it could obstruct the relative gap of the applicator.

A custom in-house anodized aluminium machined build plate with alignments features is manufactured for this development under a number of key-factors; (a) non-stick to elastomeric materials; (b) provides a smooth, levelled and robust platform for the film applicator; (c) capable of withstand temperatures up to 100°C; (d) non-affected by CO_2 laser ablation. Figure 3.4.2 in Section 3.4, illustrates the design of the custom manufactured build plate. It is noted that the surface roughness and resistance of the build plate was not considered as it has dismissible effects towards the overall fabrication.

Distinct thickness measurements were performed across the surface of the build plate to ensure a levelled plane to reduce the error of relative gap between applicator blade and build plate surface. The characterisation process focuses on factors (1) to (3) as highlighted above towards the first layered of fabricated-film in Figure 4.1.2. Following a standardise method of practice fundamentally aimed at film applicators (ASTM D823-95 and ISO 2808), the method evaluates various types of film applicators despite the difference and variation of materials and its innate properties [135, 136]. Adopting the method to evaluate the production of thin elastomeric sheets through film application, the designed fabrication technique is mainly characterised in terms of:

- Applicator Set Thickness against Elastomer Viscosity
- Applicator Spread Speed against Controlled Applicator Thickness
- Curing Temperature for Controlled Applicator Thickness

As such, the following describes the experiment settings to be characterised, starting the with applicator set thickness. The thickness resolution of the casting knife applicator is known to be 100 microns (0.1 mm) and can reach up to 6 mm in relative gap with the adjustment of two micrometric screws. As such, the applicator is designed to be tested at a set range of 0.1 mm (100 microns) up to 0.5 mm (500 microns) set thickness.

The linear drive stage can drive the film applicator at 1 mm/s up to 50 mm/s at 1 mm/s step resolution. As the spread speed of the applicator forms a variability in generating controlled set thickness, a range of spread speeds were tested to identify the optimal spread speed for the desired elastomeric materials. Based on preliminary tests, the drive stage is set to be tested at 2mm/s intervals from a minimum range to 2 mm/s up to 10 mm/s spread speeds. Spread speeds higher than 10mm/s is not recommended as the casting knife blade is seen to be dragged across the build plate at an angle due to insufficient pressure applied. In addition, higher spread speeds would reduce efficacy and influence the rheological flow of material over time.

One of the fundamental factors of the designed fabrication technique is the thermal reaction applied to the elastomeric materials to quicken the curing process as it sets. From the recommended material datasheet and gathered published data, it is indicated that higher curing temperatures significantly aid the curing process of elastomeric materials. With average temperatures set at 40°C across all elastomeric materials, the curing time is reduced significantly as it reaches 100°C. From the literature gathered, the curing temperature is then designed to characterise at 40, 50, 75 and 100 °C; at a total time of 15 minutes to provide a suitable benchmark to be adopted into the designed fabrication technique. Table 4.1 summarises the listed characterisation factors to be experimentally carried out, along with its settings at each experiment.

Table 4.1 Characterisation of the film applicator to be experimentally carried out with the listed factors and their settings.

Applicator Characterisation Experiment Settings	Set 1	Set 2	Set 3	Set 4	Set 5	Constant Variable
Applicator Set Thickness	100 µm	200 µm	300 µm	400 µm	500 µm	@ 2 mm/s, 75°C
Applicator Spread Speed	2 mm/s	4 mm/s	6 mm/s	8 mm/s	10mm/s	@ 200 µm, 75°C
Curing Temperature	40°C	50°C	75°C	100°C	-	@ 200 µm, 2 mm/s

4.1.1 Characterisation Experimental Protocol

Based on the fundamental characterisation needs following standard practices (ASTM D823-95 and ISO 2808), this section describes the experimental protocol [135, 136]. The characterisation investigates addressing the performance, applicability and limitation of the fabrication technique by evaluating the control, accuracy and production capabilities of the film applicator in relation to the elastomeric materials chosen. This enables the fabrication of desired thickness of elastomeric films to be composed in a layer-by-layer method to form the desired functional composites. Each characterisation aspect (applicator set thickness, spread speed and curing temperature) is experimentally fabricated and measured. First the fabrication protocol is illustrated and described, followed by the measurement technique employed to evaluate the elastomeric sheets fabricated.

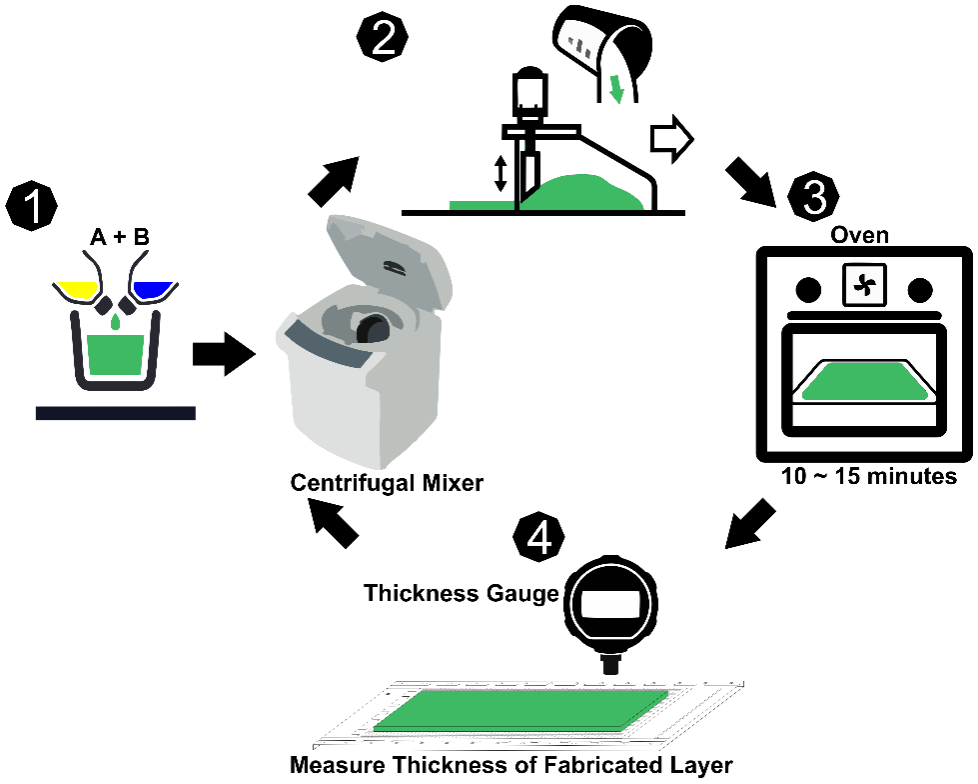

Figure 4.1.3 Fabrication process designed for characterisation of film application of elastomeric material and fabrication technique. (1) Preparation of elastomeric material; (2) Film application of elastomeric material; (3) Curing of elastomeric material; (4) Material measurement.

The following describes the fabrication process as illustrated in Figure 4.1.3. Each characterisation aspect (applicator set thickness, spread speed and curing temperature) is actively monitored and set based on the experiment. Each step is associated to the figure in a numerical manner and is named according to the steps annotated in Figure 4.1.3.

(1) Preparation of elastomeric material

Elastomeric material at a constant volume (80g total weight) is measured and mixed in a centrifugal mixer to enable a catalytic reaction for a total of 2minutes and 30 seconds (Pre-set at 1 minute for mixing at 2000rpm and 1 minute and 30 seconds for degassing at 2200 rpm).

(2) Film application of elastomeric material

Once mixed, the **film applicator is set to the desired thickness** and pre-polymer elastomer is poured onto the build plate of the applicator. The **spread-speed of the applicator is set**, allowing the linear drive stage to drive the applicator across the platform at the set desired speed (Default at 2 mm/s).

(3) Curing of elastomeric material

After the elastomer has been spread across the build plate, it is removed and placed into an oven to cure for a set time and temperature (Default 75°C for 15minutes).

(4) Material measurement

The build plate is then removed from the oven after the set time and left to cool for handling and measurement purposes. Once cooled, a thickness gauge (Mitutoyo Absolute IDS 543-692, Mitutoyo Ltd, UK) is used to measure and record the fabricated elastomer film thickness on set points on the build plate assisted by alignment features as shown in Figure 4.1.4. The fabrication experiment is repeated three times for each layer and renewed once the produced elastomeric sheet has been measured and recorded.

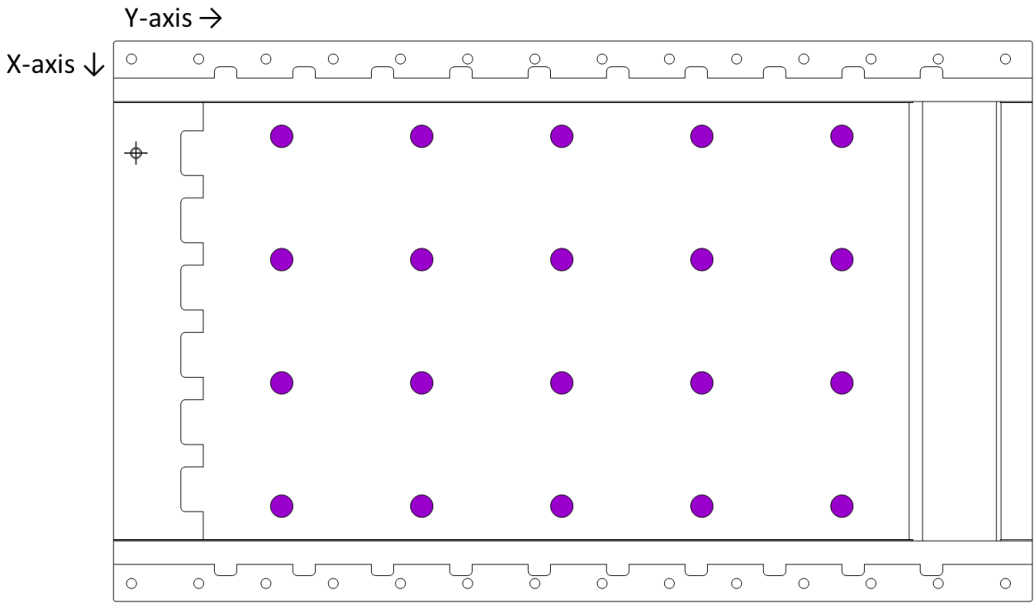

Figure 4.1.4 Measurement points on build plate for characterisation of produced elastomeric films. Indicated across the build plate, the purple dots signify the measured points to evaluate the elastomer thickness.

The produced elastomeric sheets were measured using a manually operated digital thickness gauge (Mitutoyo Absolute IDS 543-692, Mitutoyo Ltd, UK). The gauge features a manually operated contact piston with a 0.01mm resolution, 0.03048 mm accuracy, and 12.7 mm operating range. It has been modified with its internal spring mechanism removed to ensure little to no contact pressure is applied to the elastomer film produced. In addition, a flat acrylic piece with a diameter of 12 mm and thickness of 2 mm was fitted onto the tip of the thickness gauge in replacement of a ball-point tip. This is done to ensure that the gauge would not damage to fabricated samples and to allow a greater surface area to be measure as compared to numerous fine points across an extensively large workspace. Contact pressure is then measured via a digital weighing scale of 0.01 grams resolution, the piston fitted with the contact plate is recorded to be at 0.0536 Newtons. This is dismissible and not pressurise the surface of the film and impede the characterisation measurements.

Based on the designed build plate, designated points (20 points in total) were placed across the build plate to quantify the thickness measured as shown in Figure 4.1.5. All material samples for every layer were experimentally fabricated and characterised three times, while every layer is measured five times for every point (Figure 4.1.4) across the build plate. The data recorded were then correlated and computationally fed into MATLAB® to provide the appropriate results settings based on the measured thickness across the three main characterisation factors. Given the number of measured data points and the sheer number of elastomer sheets to be fabricated at the designed characterisation experiment of applicator set thickness, spread speed and curing temperature; the data is configured to be presented in the form of quadrants for quantifying and simplifying the information for processing. Each quadrant (Q1 – Q5) is based on a collective plot measurement of 6 points (P1 – P6), as illustrated in Figure 4.1.5. The average of each quadrant is used to represent the homogenous film thickness achieved. While the standard deviation and relative error were calculated to indicate the variance presented by each quadrant and the level of accuracy achieved. This approach enables aid to visual and analytical processing to present the measured data.

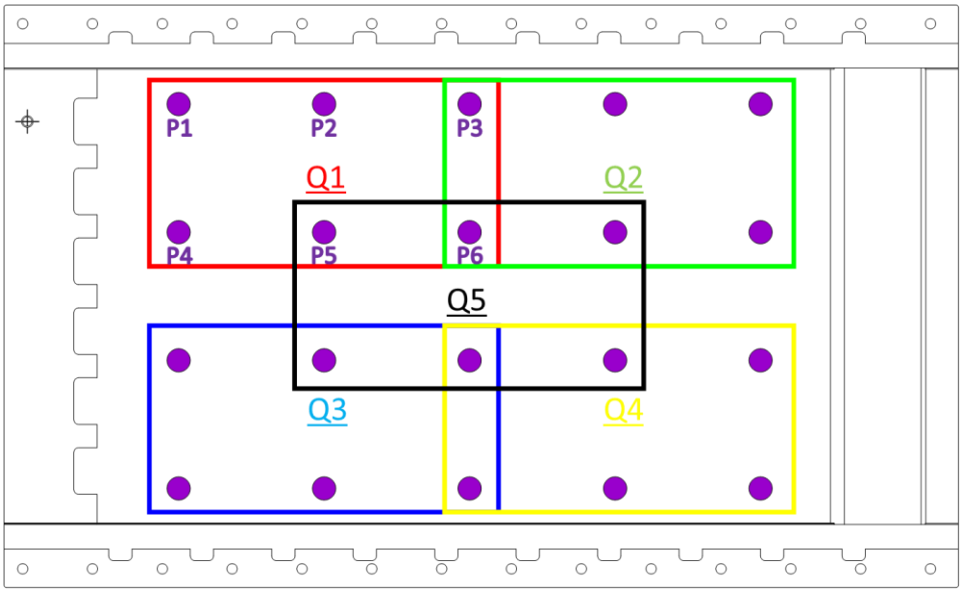

Figure 4.1.5 Illustration of quadrant classification of measured data points for characterisation of controlled applicator thickness. (Q1 – Q5: Quadrants, P1 - P5: Points)

4.1.2 Applied Set Thickness, Spread Speed, and Curing Temperature

A total of 8 elastomeric materials were tested based on the characterisation experiment described in Section 4.1.1. Three elastomers, EcoFlex™ 00-30, Elastosil® M4601, and DragonSkin™ 30A were selected to be presented within the context for all the characterisation experiments. Across the three series of elastomers, the choice was based on the effects and relationship of material viscosity and film application characterisation factors of thickness, speed and temperature. The complete result of elastomers, including those presented in this study context can be found in Appendix 4.

As described previously, each characterisation setting summarised in Table 4.1 were fabricated and measurements were recorded accordingly to the experimental protocol in the previous section. First, Figure 4.1.6 presents the characterisation of applicator set thickness from 100 microns to 500 microns. Each graph illustrates the results of the characterisation with measured thickness as the Y-axis, and the elastomeric material and its quadrants is indicated on the X-axis. The graphs are annotated with its heading as the intended applicator set thickness, followed by the desired applicator set thickness illustrated as a solid line threshold. This is reflected in the rest of the characterisation experiments.

Starting with the characterisation of set applicator thickness in Figure 4.1.6, it is evident that the effects of material viscosity, gravitational force and relative gap of the film applicator resulted in the data shown. Initial deduction based on theory depicts materials with higher viscosity is less affected by the spread gap of the applicator compared to materials with low viscosity. This is seen as evident, as shown in the material trends across all the set applicator thickness in Figure 4.1.6.

Table 4.1.1 lists out the analytical values of Figure 4.1.6 in terms of average thickness achieved based on all five quadrants, the standard deviation of the averaged quadrants and the relative error to depict accuracy. As the relative gap of the applicator increases, EcoFlex™00-30 at 100 microns and 500 microns exhibited a similar achieved thickness range with Elastosil®M4601 and DragonSkin™30A. While in all cases, both Elastosil®M4601 and DragonSkin™30A displayed a close range to each other. The standard deviation for all three elastomeric materials, shows that as

the set applicator thickness increases, the variance increases. The relative error shows a similar deduction that the error increases as the relative applicator gap is increased.

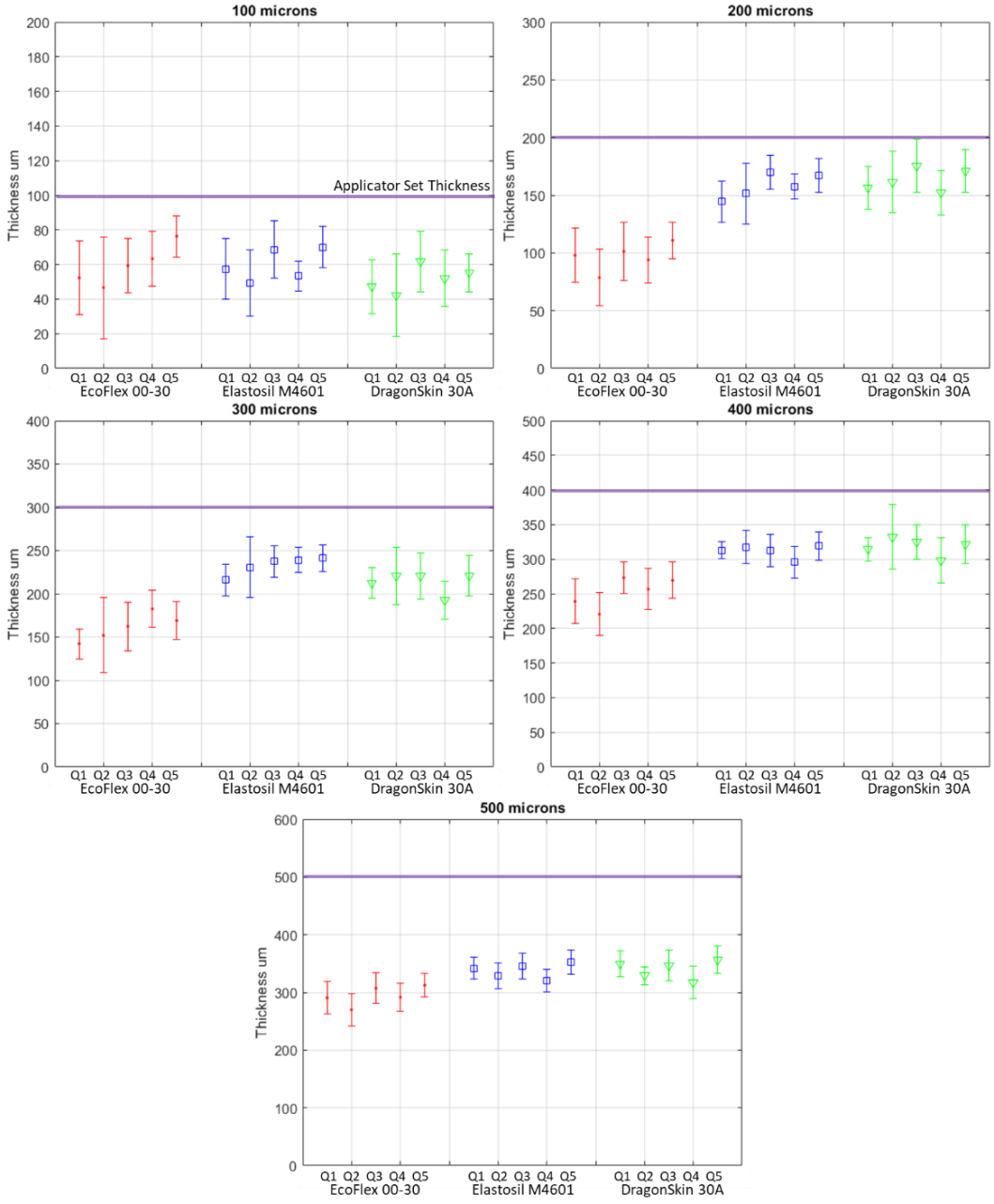

Figure 4.1.6 Characterisation of applicator set thickness from 100 microns to 500 microns with applicator spread speed of 2 mm/s and curing temperature 75°C. Materials presented: EcoFlex™00-30, Elastosil®M4601, and DragonSkin™30A.

Table 4.1.1 Analytical values of characterisation of applicator set thickness from 100 microns to 500 microns in Figure 4.1.6. Materials presented: EcoFlex™00-30, Elastosil®M4601, and DragonSkin™30A.

Material	Thickness (µm)	Average Film Thickness	Standard Deviation Average Sheet Thickness	Relative Error
EcoFlex 00-30	100	59.60	11.34	-0.41
	200	96.60	11.83	-0.51
	300	161.67	15.51	-0.46
	400	251.78	21.98	-0.37
	500	294.40	16.62	-0.41
Elastosil M4601	100	59.73	9.22	-0.40
	200	158.27	10.59	-0.21
	300	232.93	10.26	-0.22
	400	311.53	9.32	-0.23
	500	337.87	13.29	-0.32
DragonSkin 30A	100	51.73	7.41	-0.48
	200	163.33	9.89	-0.18
	300	213.33	12.28	-0.29
	400	318.33	12.80	-0.20
	500	330.87	15.99	-0.32

Following the characterisation of applicator set thickness, the following describes the results of applicator spread speed as shown in Figure 4.1.7. With a set applicator thickness of 200 microns, the spread speed is varied from 2 mm/s to 10 mm/s in 2 mm/s intervals, and cured at 75^{o}C.

Based on the overall results of Figure 4.1.7, it can be seen that the spread speed of the applicator significantly influence the achieved film thickness. As the spread speed increases, a similar trend in all three elastomers in thickness is achieved across all five tests. However, the accuracy of the achieved film thickness reduces (as the relative error increases), as the spread speed increases, as listed in Table 4.1.2. Within each elastomeric material, the influence of applicator spread speed is reflected in the calculated average measured film thickness.

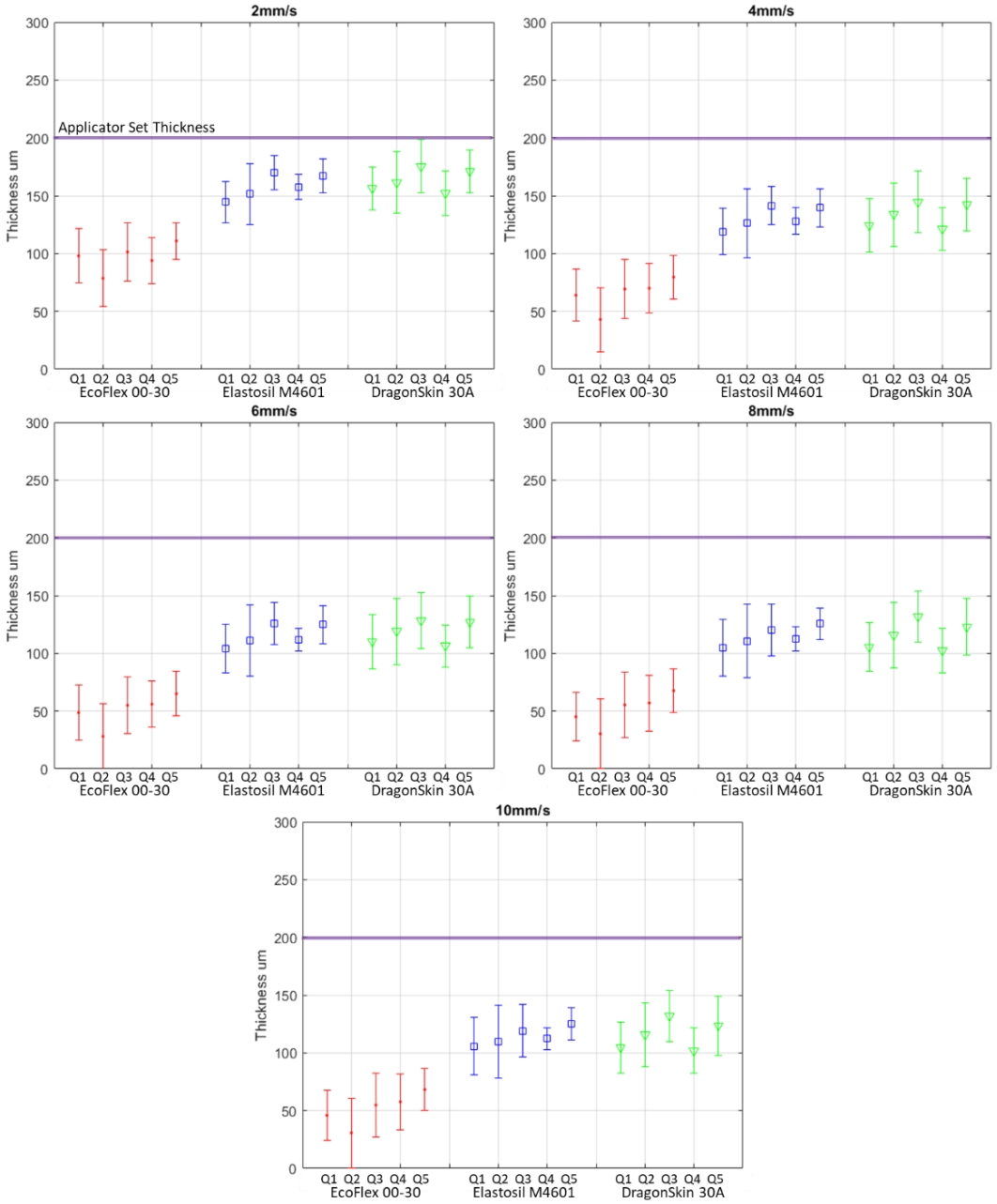

Figure 4.1.7 Characterisation of applicator spread speed of 2 mm/s to 10 mm/s with 2 mm/s intervals with 200 microns applicator set thickness and curing temperature 75°C. Materials presented: EcoFlex™00-30, Elastosil®M4601, and DragonSkin™30A.

Table 4.1.2 Analytical values of characterisation of applicator spread speed from 2 mm /s to 10 mm/s at 2 mm/s intervals in Figure 4.1.7. Materials presented: EcoFlex™00-30, Elastosil®M4601, and DragonSkin™30A.

Material	Speed @ 200 µm	Average Film Thickness	Standard Deviation Average Sheet Thickness	Relative Error
EcoFlex 00-30	2 mm/s	96.60	11.83	-0.51
	4 mm/s	65.20	13.63	-0.67
	6 mm/s	50.53	13.87	-0.74
	8 mm/s	51.07	14.10	-0.75
	10 mm/s	51.40	14.13	-0.74
Elastosil M4601	2 mm/s	158.27	10.59	-0.21
	4 mm/s	130.87	9.44	-0.34
	6 mm/s	115.53	9.45	-0.42
	8 mm/s	114.80	8.18	-0.43
	10 mm/s	114.43	7.75	-0.43
DragonSkin 30A	2 mm/s	163.33	9.89	-0.18
	4 mm/s	133.27	10.42	-0.34
	6 mm/s	118.13	9.86	-0.41
	8 mm/s	115.67	12.29	-0.43
	10 mm/s	115.51	12.63	-0.41

From the characterisation of applicator spread speed, the following describes the results from characterisation of curing temperature as shown in Figure 4.1.8. The applicator relative gap is set towards 200 microns and spread speed at 2 mm/s. Here, the curing temperature is characterised at 40°C, 50°C, 75°C and 100°C, as described in the experiment protocol. In Figure 4.1.8, higher temperatures (75°C and 100°C) resulted in a higher accuracy of desired film thickness compared to lower temperatures (40°C and 50°C). Comparing between 75°C and 100°C (higher temperatures), the differences in achieved film thickness indicated minor to dismissible differences, as shown in Table 4.1.3 highlighted in red. This is also seen when comparing between 40°C and 50°C (lower temperatures), however, the achieved film thickness at lower temperatures resulted in a lower accuracy. Based on the relative error calculated, it can be deduced that at higher temperatures, the accuracy increases.

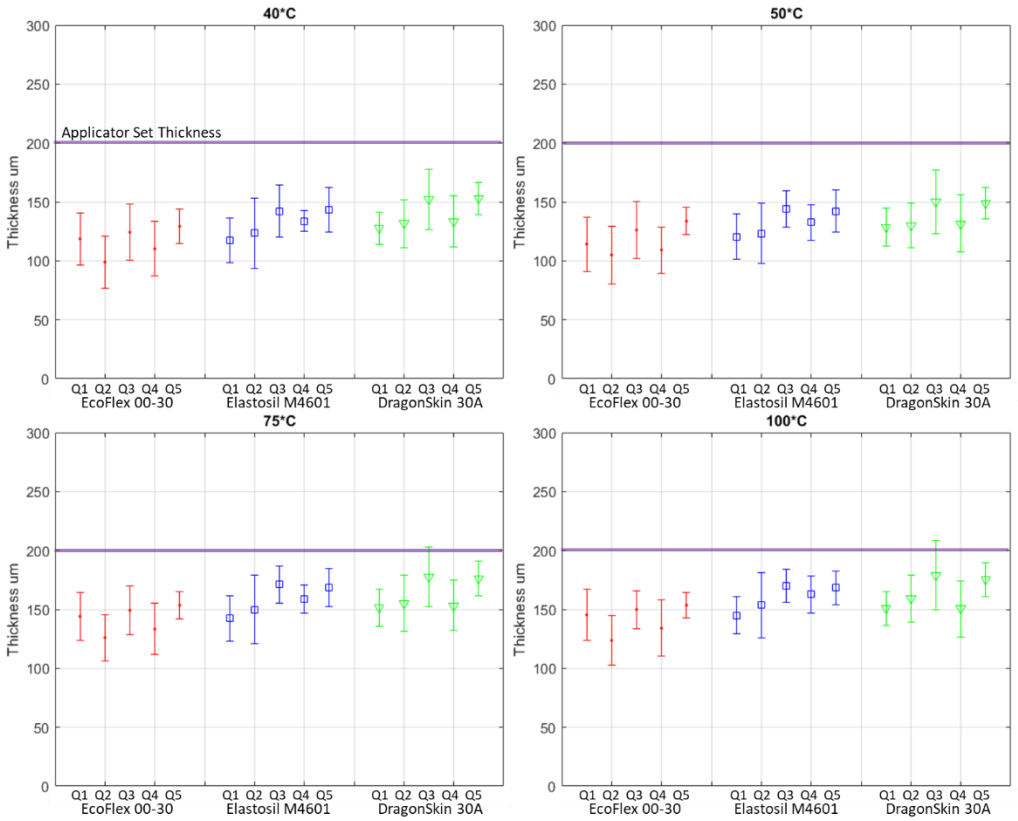

Figure 4.1.8 Characterisation of curing temperature from 40°C, 50°C, 75°C and 100°C for 200 microns applicator set thickness with spread speed of 2 mm/s. Materials presented: EcoFlex™00-30, Elastosil®M4601, and DragonSkin™30A.

Table 4.1.3 Analytical values of characterisation of curing temperature from 40°C, 50°C, 75°C, and 100°C in Figure 4.1.8. Materials presented: EcoFlex™00-30, Elastosil®M4601, and DragonSkin™30A.

Material	Temperature	Average Film Thickness	Standard Deviation Average Sheet Thickness	Relative Error
EcoFlex 00-30	40 °C	116.27	12.01	-0.42
	50 °C	117/62	11.97	-0.42
	75 °C	141.20	11.41	-0.29
	100°C	141.33	12.31	-0.29
Elastosil M4601	40 °C	131.94	11.48	-0.34
	50 °C	132.54	10.73	-0.34
	75 °C	158.16	12.15	-0.21
	100°C	159.92	10.52	-0.20
DragonSkin 30A	40 °C	139.57	12.02	-0.30
	50 °C	137.86	10.67	-0.31
	75 °C	162.80	13.03	-0.19
	100°C	162.97	13.38	-0.19

4.1.3 Discussion of Characterisation of Controlled Thickness, Spread Speed and Curing Temperature

Based on the results, a precise and predictive production of elastomeric films may not be feasible at this stage. This is due to the need of fine experimentation on viscosity and rheological properties of the materials around the theoretical wet film thickness. Further fine measurements and experimentation may be required to provide a definitive performance and accuracy to produce desired elastomer thickness. From the characterisation experiments, a spread speed of 2 mm/s was used as default in applicator set thickness and curing temperature experiments. Results have also shown that a relative slow spread speed produces a smaller error compared to a higher speed. In addition, curing temperatures have been set at 75°C as an optimal point, as higher temperatures (100°C) yielded no significant changes based on the results obtained in Figure 4.1.8 and Table 4.1.3. The selected temperature was also due to reduce cooling time and handling purposes.

The results have also illustrated a question of levelled plane caused by the build plate. As the build plate is manufactured in-house, manufacturing tolerances and surface finish needs to be further tuned to provide a smooth and levelled build platform. While pre-fabrication measurements of the build plate were performed to provide an offset to the measured elastomer thickness, results have indicated a slight unlevelled plane. While it was not possible to manufacture another build plate, the error produced was considered minimal and acceptable to further progress in the research development.

The use of a manually operated thickness gauge for measurement may have contributed to the errors in the result. However, this was mainly due to limited options in measurement choices suitable during the time of study. Other high-advance methods of measurements such as laser-displacement sensors, optical microscopes and image processing units have been investigated and preliminarily tested. However, the surface of the elastomeric sheets fabricated are often translucent and reflective. Even with colour dyes under ambient lighting, the translucent surface gave a reflective and glossy finish, thus impeding the use of light and/or optical based sensors. With the use of a manually operated thickness gauge,

the measurement points have been kept to an optimal number due to the sheer number of experiments performed.

The initial aim of the characterisation was to define the fabrication technique and produce layers of elastomers at desired thickness However, fine tuning of the characterisation is required along with extensive measurements methods and experimentation is needed to produce an in-depth and qualitative method for the production of controlled thickness of elastomers. Currently, a method of step-repeat compensation is opted to sufficiently produce the desired elastomer thickness and not hinder the performance of the applicator and fabrication technique. To showcase this method of compensation, the characterisation of set applicator thickness was repeated under the same conditions as before. However, in this step-repeat compensation method, an added layer of elastomer is added onto the initial fabricated layer without changing the volume of elastomer used, the set applicator thickness, spread speed and curing temperature. This would result in an added layer to form a single film of elastomer. The method is made possible as the elastomeric library in this study are capable of adhering to its cured counterpart to form a single piece of film of desired thickness.

Presented in Figure 4.1.9, the step-repeat compensation method of applicator set thickness was experimentally carried out and characterised. The analytical results of the compensation method is listed in Table 4.1.4. From the results, the maximum relative error was found to be about 15%, with the lowest at 5%. One of the significant difference found in the step-repeat result would be the small variance calculated from the standard deviation. A significant difference from this approach was found that a homogenous film thickness was achieved across the quadrants regardless of material. Although an added step is required to achieve a higher accuracy of film thickness, a complete desired film thickness is still not achieved. This can be due to the rheological property in liquid based material and material shrinkage due to the curing temperature.

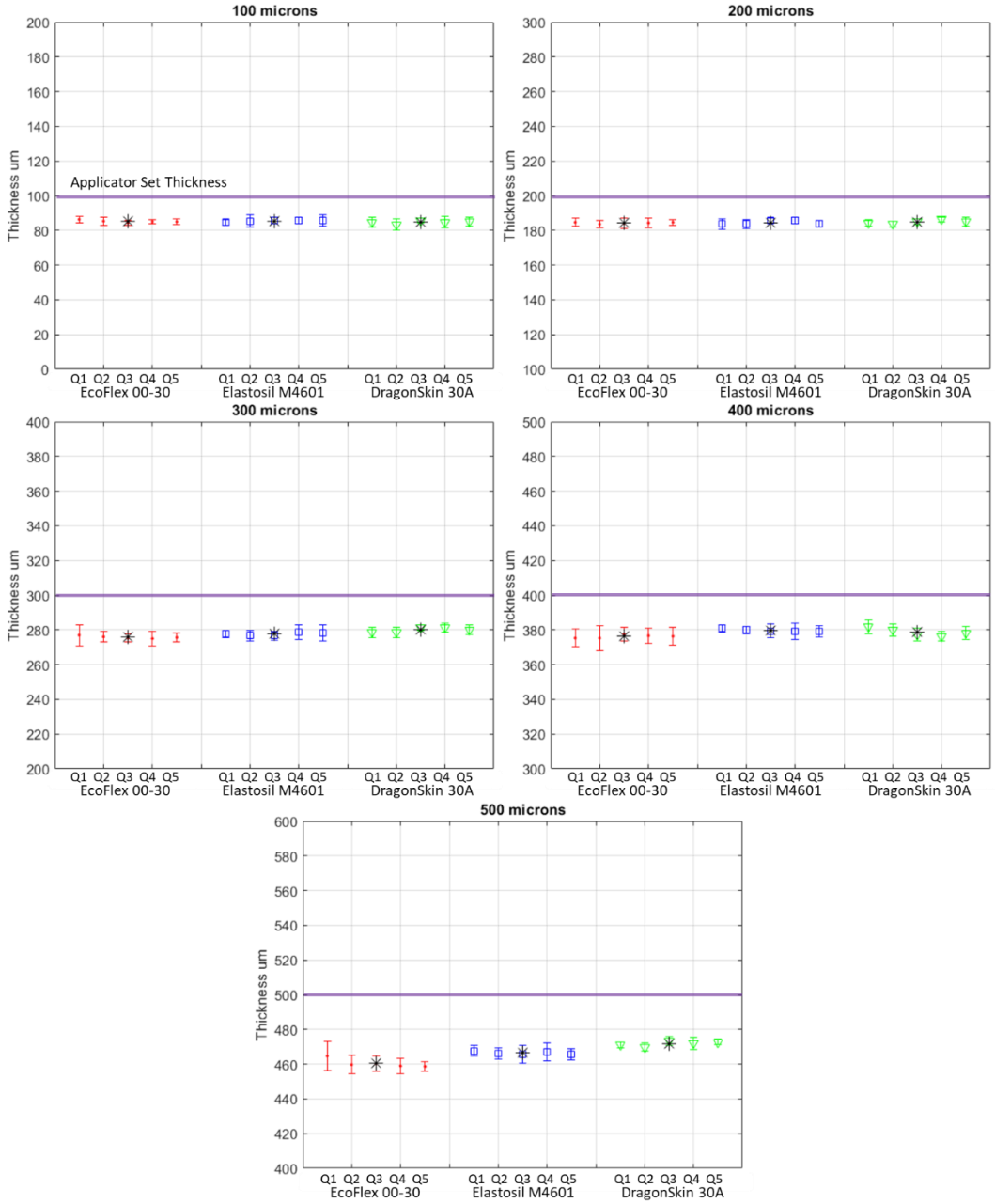

Figure 4.1.9 Characterisation of step-repeat of applicator set thickness from 100 microns to 500 microns with applicator spread speed of 2 mm/s and curing temperature 75°C. Materials presented: EcoFlex™00-30, Elastosil®M4601, and DragonSkin™30A.

Table 4.1.4 Analytical values of characterisation of step-repeat of applicator set thickness from 100 microns to 500 microns in Figure 4.1.9. Materials presented: EcoFlex™00-30, Elastosil®M4601, and DragonSkin™30A.

Material	Thickness (µm)	Average Sheet Thickness	Standard Deviation Average Sheet Thickness	Relative Error
EcoFlex 00-30	100	85.20	0.73	-0.15
	200	184.27	0.43	-0.08
	300	275.80	0.77	-0.08
	400	376.27	0.98	-0.06
	500	460.47	2.43	-0.07
Elastosil M4601	100	85.40	0.43	-0.15
	200	184.53	1.04	-0.08
	300	277.60	0.93	-0.07
	400	379.67	0.84	-0.05
	500	466.40	0.89	-0.07
DragonSkin 30A	100	84.67	0.85	-0.15
	200	184.87	0.99	-0.07
	300	280.00	1.33	-0.06
	400	378.73	2.12	-0.05
	500	471.73	1.44	-0.06

In conclusion, the performance and applicability of the fabrication technique of film application is governed by the wet film thickness (WFT) phenomenon. As the theory suggests, despite the use of high manufacturing tolerances of applicators, the material coating that remains after application can vary from 50% to 90% from the actual desired thickness. The results of the characterisation of set applicator thickness is evident of this, as the presented elastomers fall within the theoretical range of liquid based materials. However, a uniform thickness was achieved due to the added layer of material. Without the use of a step-repeat method, further characterisation is required to characterise the wet film thickness of elastomeric materials. Despite the lack of information revolving elastomeric volume solids, further information provided by its commercial body would need to be pursued to enable the full use the wet film thickness theory. Despite the current use of step-repeat method to ensure fabrication of controlled set thickness, the overall fabrication technique can still be progressed to further develop its design approach.

4.2 Mechanical Adhesion Strength

The mechanical bonding strength of elastomeric laminar composites reflects the conceptual design of soft planar inflatable composites. As described in Section 3.2, the choice of elastomeric material was based on its versatility, compliancy and plausible ability to adhere and/or bond to its cured counterpart or material of similar properties without the use of additives or adhesives. In addition, the concept of inflation of the soft composites resides from the 'zero-volume' cavities embedded during fabrication. However, during inflation of the fabricated composites, it is unknown if the expansion of the internal volume may cause de-lamination or a form of mechanical disassociation due to high internal pressures at points of composite lamination. As such, the study here investigates the mechanical adhesion strength is conducted to evaluate the material lamination strength of elastomers to assess the its material feasibility for lamination to form soft inflatable composites.

Based on several industrial standardised characterisation techniques, several standard test methods were compiled and incorporated to suit the aim of the study here with respect to the material and fabrication process. A related standard practice (ASTM F2256) describes the method used to compare and characterise different types of adhesives and for manufacturing quality-controlled tissue adhesives based medical devices or plastic composites for specific developments [138]. Other common standards aim to measure the mechanical bond (adhesion strength) of two laminates are, D42903 (Adhesion to Rigid Substrates by 180° angle) and D90398 (Adhesive Bonds, Peel or Stripping by Unidirectional 90° angle)[139, 140]. However, these were not suitable as the mechanical dissociation test was based on single-face direct to a rigid surface, while the concept of the experiment was the dissociation of two laminate surface in a composite manner. The method found in 'tissue adhesive by T-Peel testing' (ASTM F2256) is suitable for the application and concept [138]. Incorporating the method, an experiment was designed to investigate the mechanical adhesion strength of the elastomeric lamination based on the fabrication technique. Figure 4.2.1 illustrates the different test methods described to evaluate adhesion strength.

Figure 4.2.1 A range of standard test methods to evaluate mechanical adhesion strengths based. D42903 (Adhesion to Rigid Substrates by 180° angle); D90398 (Adhesive Bonds, Peel or Stripping by Unidirectional 90° angle); F2256 (Tissue Adhesive by T-Peel testing) [138] [139, 140].

4.2.1 Experimental Design, Fabrication and Procedure

The experiment was designed based on incorporating the three mentioned standard methods to the sample design and testing method. The experiment adopts 'T-Peeling' method as illustrated in Figure 4.2.2, in order to characterise the strength of lamination and possible dissociation from its cavity during inflation. For each elastomeric material, a total of 10 samples is produced in a single batch due to the size of the build plate. Each sample is designed towards the dimension of 25 x 125 x 2 mm (width x length x height) and consists of a flap of 25 x 25 (width x length) embedded during fabrication. The flaps acts as fixture points for peeling, while emulating the cavity as the point of expansion during conceptual inflation. An Instron-5943 tensile tester with a 1kN load cell is used to displace the samples at a set travel speed of 2.5 mm/s across a 200 mm distance. It is also noted that, a pneumatic grip force of 7 bars with a fixture size of 25 x 25 mm is used to secure the samples in place. Illustrated in Figure 4.2.2, the test samples are presented along with its dimensions and listed procedure listed in Table 4.2.

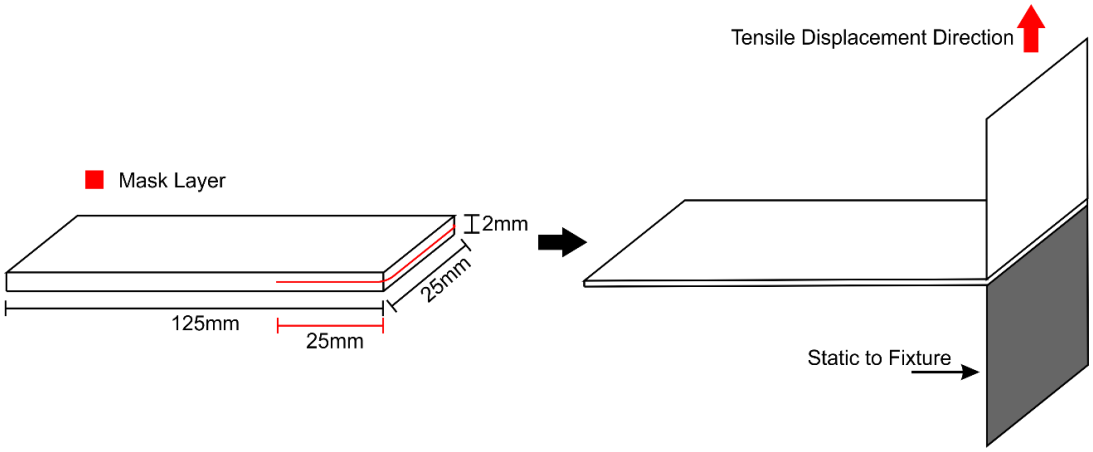

Figure 4.2.2 Design of test sample for mechanical adhesion strength (Peeling) test. Dimensions are listed in millimetres (mm). The thickness of the samples is 2 mm.

Table 4.2.1 Test Procedure for Mechanical Adhesion Strength (Peeling) Test.

Specimen		Tensile Tester Method	
Width	25±0.1 mm	Fixture Size	25 x 25 mm
Length	125 mm	Travel Speed	2.5 mm/s
Thickness	2 mm	Travel Displacement	200 mm
Number of Samples	10 pieces	Fixture Grip Force	7 Bar

The fabrication process entails in the similar manner as previous iterations for steps (1) to (3), as illustrated in Figure 4.2.3. Based on the sample designs, step (4) to (6) is modified to correspond to the designed experimental protocol. (4) The designed samples are layered in such a way that the mask layer (cavity) is centred within the sample. The layering process is repeated from steps (1) to (4) until the desired designed material layer is achieved. (5) The samples are then cut out via laser to the specifications as described and set in Figure 4.2.2 and Table 4.2.1. The samples are then cleaned with the water soluble papers removed and prepped accordingly for mechanical testing. (6) The fabricated samples are then tested based on the described test procedure in Section 4.2.2 and Table 4.2.

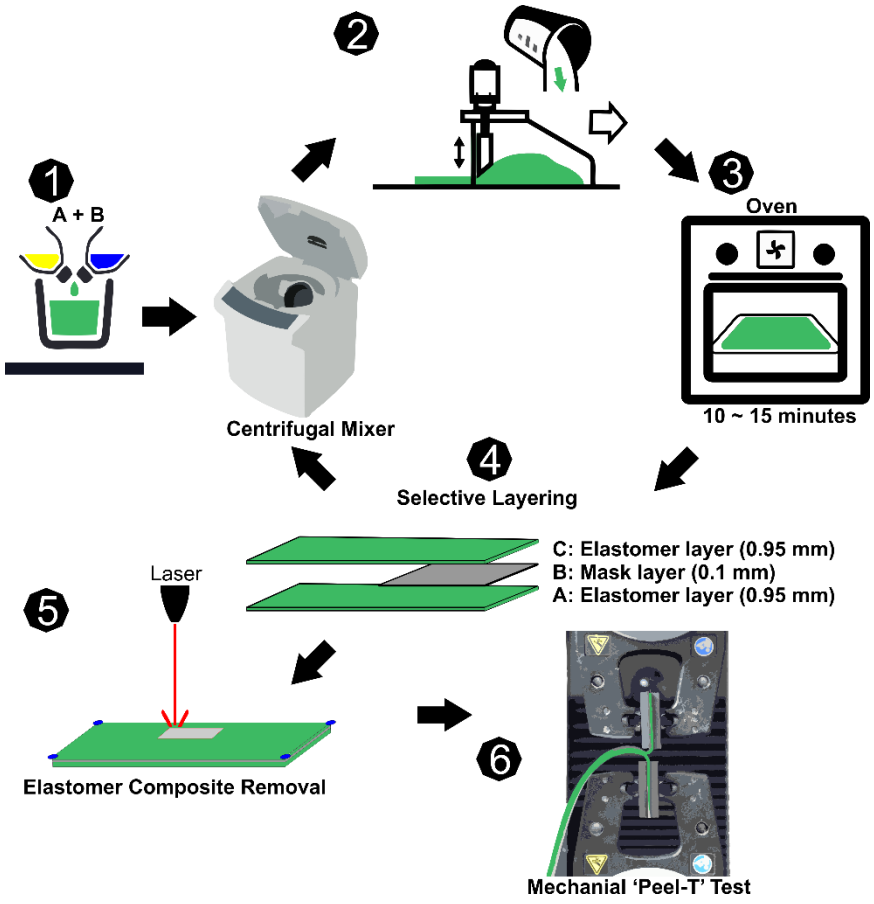

Figure 4.2.3 Fabrication process for characterisation of mechanical adhesion strength of elastomeric materials. Steps (1) to (5) follows the SPIC fabrication method; (6) illustrates the mechanical 'Peel-T' test of the fabricated samples.

4.2.2 Results and Discussion

Each material set consists of a total of ten samples. As a point of comparison from the previous characterisation of elastomeric film-thickness experiment, EcoFlex™ 00-30, Elastosil®M4601 and DragonSkin™30A is presented to show the difference in material composition related to its elasticity, stiffness and shore hardness of the material. EcoFlex™00-50 is included in this study to highlight a number of results in order to further illustrate the findings. Figure 4.2.4 illustrates the execution of mechanical adhesion strength (peeling) test on a piece of elastomeric sample. In this case, the EcoFlex™ 00-50 test sample, was loaded onto the machine pneumatic grips as shown in Figure 4.2.4 (1). As the machine displaces vertically upwards, the

material is stretched in a 'T' motion from the point of its embedded cavity during fabrication. As the displacement progresses to the maximum point of 200 mm, the material is seen to be stretched and focusing its stress at the point of layer lamination in Figure 4.2.4 (4). Due to the nature of the material, EcoFlex™ 00-50 is very elastic and has a lower tensile strength as compared to Elastosil® and DragonSkin™, which corresponds to the visual representation shown in Figure 4.2.4 and Figure 4.2.7.

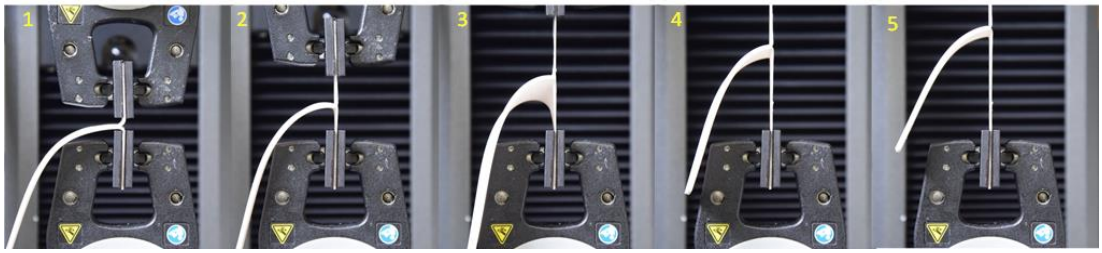

Figure 4.2.4 Characterisation of mechanical adhesion strength (Peeling Test) of EcoFlex™ 00-50. Illustration represent the experiment progressions from (1) to (5) as material is displaced.

From the experimental frames shown in Figure 4.2.4, the recorded graphical result is shown in Figure 4.2.5 for EcoFlex™ 00-50. As the material (EcoFlex™00-50) is displaced, the recorded samples shown in Figure 4.2.5 corresponds to the characteristic of hyper-elastic strain of elastic material during its initial phase. However, a second phase is shown to induce at a displacement range of 80 to 100 mm and below the force threshold of < 8 Newtons. This occurrence is seen to be material stripping or tear as the designed sample has reached its maximum tensile strength point. As the samples are displaced at the rate of 2.5 mm/s, the material does not fully break, but a third phase is exhibited with the occurrence of layer disassociation. The layer disassociation was found to not occur at the point of lamination of the composite but across a random break/tear point at the point of lamination. This can be seen in Figure 4.2.5(3), at the stretched cavity point as the material twists due to uneven layer displacement.

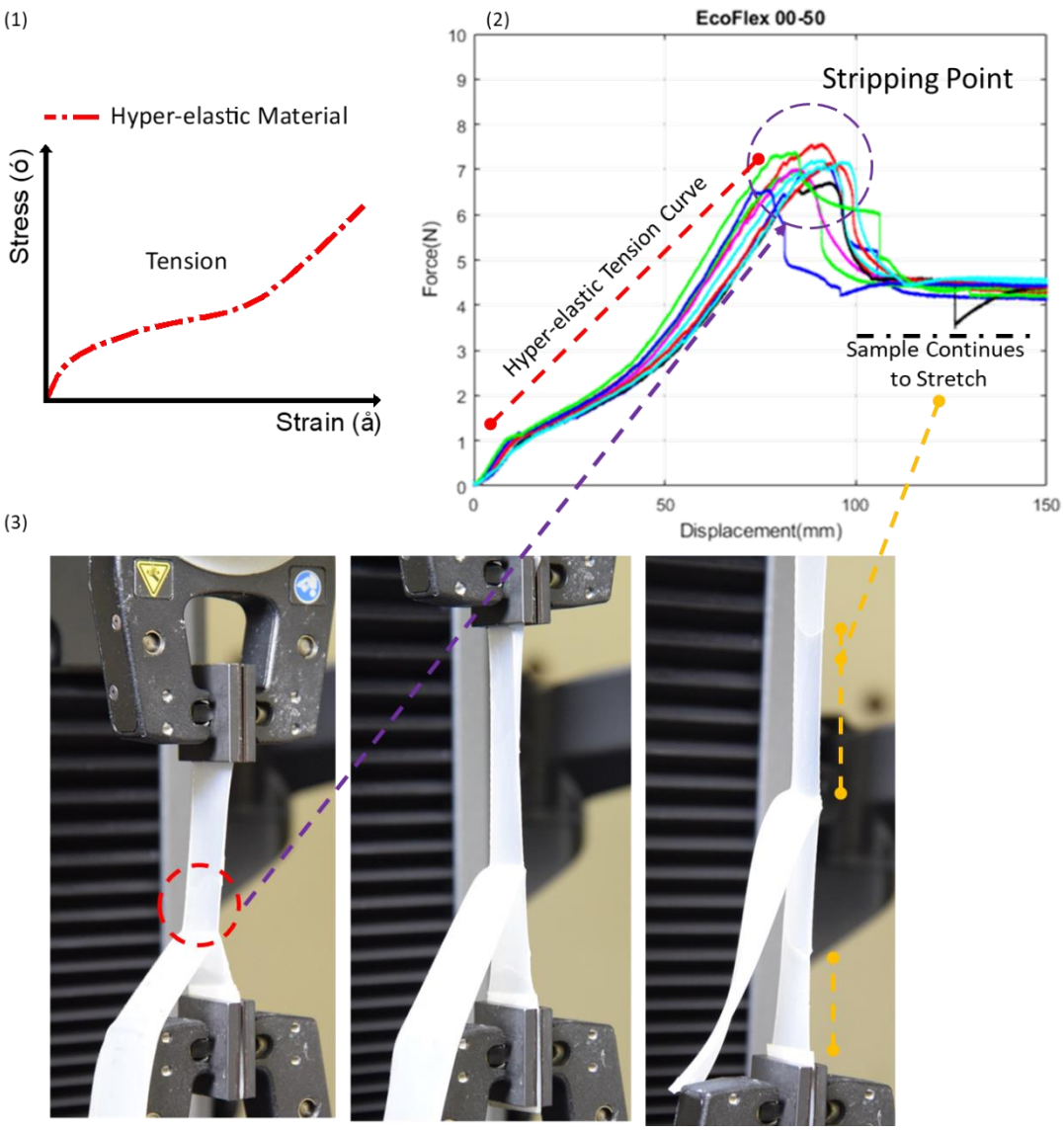

Figure 4.2.5 (1) Illustration of hyper-elastic material strain curve under tension of elastic material. (2) Graphical result of EcoFlex™00-50 under force against displacement test. (3) Stripping point of material as material dissociates while sample continues to stretch.

The result shown in Figure 4.2.5, is distinct to its sample and material of EcoFlex™00-50. While the hyper-elastic material strain curve is expected to be seen in almost all of the elastomeric samples, this is not the case based on the recorded data. The following presents the recorded data for EcoFlex™--30, Elastosil®M4601 and DragonSkin™30A in Figure 4.2.6. Annotations were made on the graph to indicate the deduction based on the data recorded.

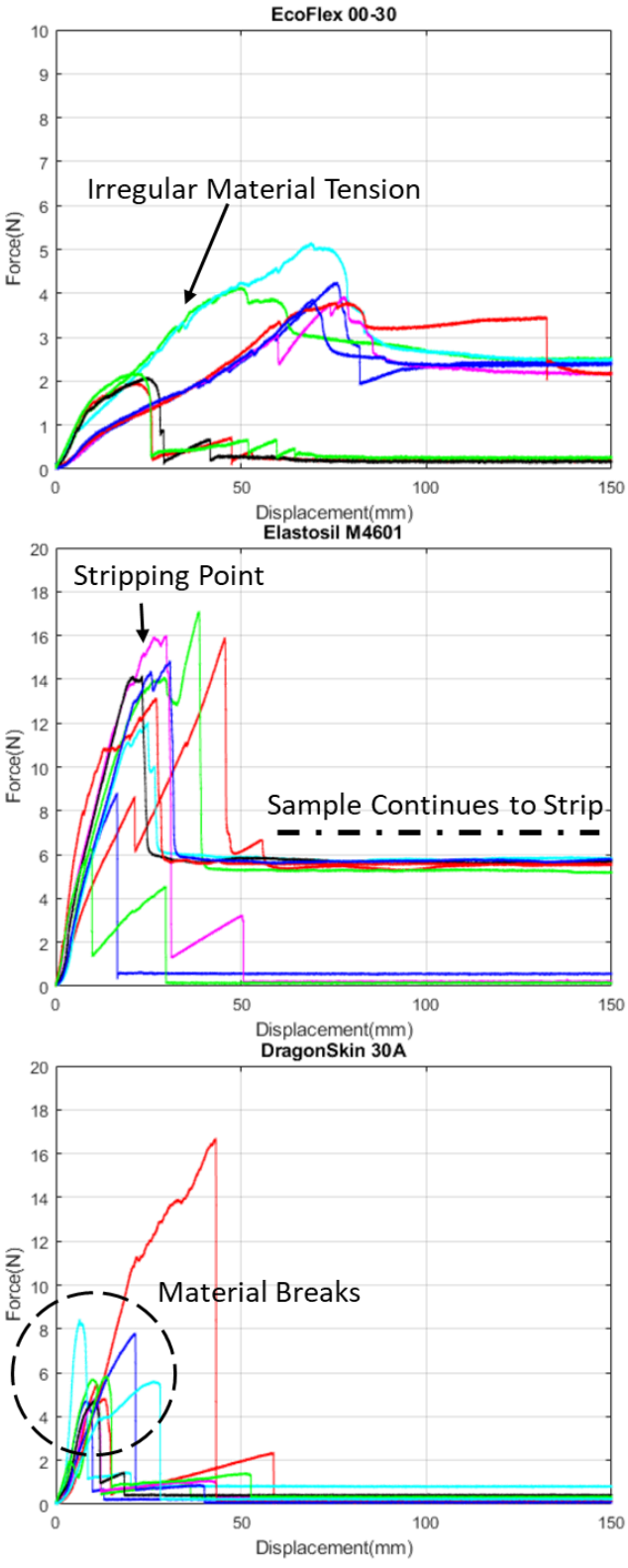

Figure 4.2.6 Force against displacement result for EcoFlex™ 00-30, Elastosil® M4601 and DragonSkin™ 30A, from top to bottom respectively, for mechanical adhesion strength test. Graphical result are annotated to reflect context description.

Based on the results shown in Figure 4.2.6, the overall deduction can be seen that irregular stripping of material or material dissociation is occurring at different points for each of its given material. Compared to Figure 4.2.5 and the material EcoFlex™00-50, the result of EcoFlex™00-30 showed a similar hyper-elastic strain curve for a number of samples. However, irregular material tensions were recorded, while 3 samples encountered material breakage at an early stage of < 2 Newton threshold. Despite the tension irregularities, the material of EcoFlex™00-30 were subjected to repeats to ensure no introduction of fabrication error. However, similar occurrences were recorded while EcoFlex™00-50 displayed similar findings that ruled out fabrication errors. The visual comparison of tensile strength between the two EcoFlex™ materials were also closely related as depicted in its material datasheet despite its shore hardness.

Progressing towards Elastosil®M4601, the material resulted in a higher tensile force at a range of 12 N to 17 N and its displacement < 50 mm, before the material either breaks in a few samples, or starts to strip/tear at the cavity point. The layer dissociation then gradually continues across the T-sample until a total breakage occurs. Despite its material shore hardness, it is expected to have DragonSkin™ to have a lower tensile force compared to Elastosil®M4601 based on the material datasheet. For DragonSkin™30A, the results depicted complete breakage of material at the average force threshold of 6 N, this is further shown in Figure 4.2.7. When comparing between the two stiffer material of Elastosil® and DragonSkin™, the material elastic difference does influence the rate of breakage as shown in Figure 4.2.6 and Figure 4.2.7 to illustrate the breakage.

Initial investigation was aimed to ensure the efficacy of lamination of elastomeric material to avoid potential dissociation of layers through internal pressures brought by inflation of soft composite. However, the occurrence of lamination dissociation is not evidently seen throughout all the experimentally characterised samples of elastomeric materials. The deduction from the recorded data suggests possible material composition changes, unknown fabrication error or external factors that may have resulted in presented data here.

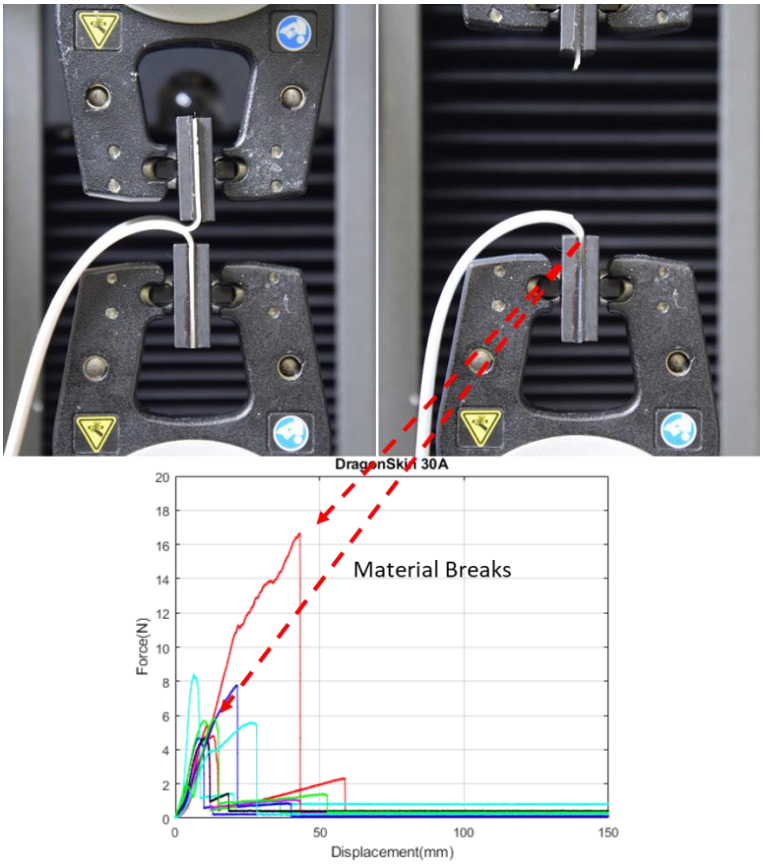

Figure 4.2.7 Example of material mechanical breakage at endpoint of cavity for DragonSkin™30A. Annotation indicates the point of breakage in-line with the picture for reference.

In conclusion, the study of mechanical adhesion strength of elastomeric lamination has provided a potential point of insight to the possibility of layer-dissociation due to internal pressures at the point of lamination. Currently, limited analytical deduction is drawn from the graphs due to the irregularities recorded and material breakage at variating points within each material. Potential solution may lie within modelling and simulation of the experiment to shed light on the stress points and possible delamination of layers. It was deduced that a different approach may be required to investigate the mechanical adhesion strength between the elastomeric layers at this point. In addition, further experimentation and development may be required to fully understand and characterise the material property of hyper-elastic material and the composition of layer-based lamination as compared to complete material curing.

4.3 Laser Cutting and Engraving of Elastomers

Industrial machining tools are known to be not suitable to actively shape soft pliable materials. However, the use of certain specialised tools such as laser ablation have been used in a few soft robotic developments. With the earliest by Yehoshua *et al.*, in an attempt to create complex channels on PDMS [141]; while others have only used it as a two-dimensional shaping tool [90]. Although most initial developments were applied towards microfluidic applications, laser ablation of elastomers have since been only lightly ventured. In contrast to those developments, the use of a CO_2 laser cutter (VLS 3.40, 50 Watts, ULS) in the designed fabrication technique was aimed at patterning features and removal of designed elastomeric composites. Previous published works have only highlighted the feasibility of complex cutting of elastomeric materials, but the material compatibility and machine capabilities are not openly shared as device specifications of different laser systems tend to produce different results depending on its manufacturer.

Here, the capabilities of the laser cutter is characterised towards the same elastomeric library featured within the fabrication technique of the thesis. The functions of the laser cutter were first reviewed through the manufacturer datasheets and preliminary tests. The laser cutter consists of two distinct functions; (1) Vector cutting and (2) Raster engraving. Vector cutting performs the action of cutting an outline (Vector), while raster engraving refers to an image to be imprinted on a surface. A third option known as 'etching' is achieved through a vector image in a raster mode and differential power and speed settings are deployed. In order to control the laser cutter, the proprietary software (ULS) provides the user access and control over power, speed and pulse per inch (PPI) settings. The power and speed of the laser is represented in the form of percentage levels (0: 100%), while PPI refers to the pulses generated by the laser per linear inch of travel distance within a scale of 0 to 1000. With this, a characterisation experiment is designed to investigate the effects of the laser power and speed settings on elastomeric material.

4.3.1 Experimental Design, Fabrication and Characterisation Method

As shown in Figure 4.3.1, a graphical design profile is conceptualised to experimentally characterise power and speed settings of the laser on different elastomeric materials. A geometrical design with a diameter of 12 mm of an octagon combined with a semi-circle was used as the centrepiece within the profile to highlight the main characterisation of differential power and speed on the elastomer, including laser point accuracy and ablation effects which results in ablated depth. In addition, small vector circles (holes) ranging from 0.1 to 1 mm in diameter and 2 mm length incisions with width sizes of 0.1 to 0.5 mm were also designed to test the capability and performance of the laser cutter. It is noted that 'Hairline' indicates a vector width which corresponds to a graphical illustration software (CorelDRAW®) that is used to design the profile. It is translated as the smallest focal point of the laser vector performance, which is approximately 0.07mm based on the equipment commercial build specifications.

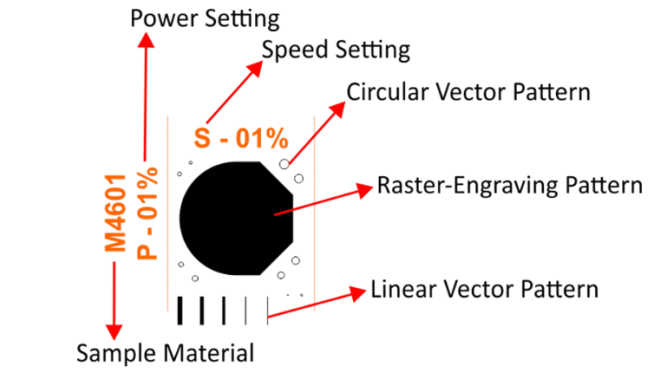

Linear Vector Pattern (mm)	Circular Vector Pattern (θ mm)	
• 0.5	• 1	• 0.4
• 0.4	• 0.9	• 0.3
• 0.3	• 0.8	• 0.2
• 0.2	• 0.7	• 0.1
• 0.1	• 0.6	
• 0.07 (Hairline)	• 0.5	

Figure 4.3.1 Design profile for characterisation of laser ablation on elastomeric material. Profile consists of key notations, (1) Power setting; (2) Speed setting; (3) Raster-engraving pattern; (4) Linear vector pattern; and (5) Circular vector pattern. Circular vector patterns are populated across the profile at known points while linear vector patterns are placed in an incremental range from 'Right to Left' of the profile.

From the design profile, a characterisation matrix was designed to pan out the experiment for each elastomeric material available. The matrix is conceptually designed as a single strip of elastomer material focusing on a single power setting of the laser. Within the matrix, the speed setting of the laser is then differentiated in an ascending order from left to right for each cell. Based on preliminary tests, the power and speed settings of the laser to be characterised are set starting from 1%, 5% to 50% with 5% intervals, followed by 10% intervals from 50% to 100%. While the list of elastomer samples follows the characterisation of film applicator. Figure 4.3.2(3) illustrates the design of the characterisation matrix for laser ablation/patterning. From the matrix design, the elastomer sample is designed as shown in Figure 4.3.2(2); along with the design of the mould to fabricate the elastomer samples in 4.3.2(1).

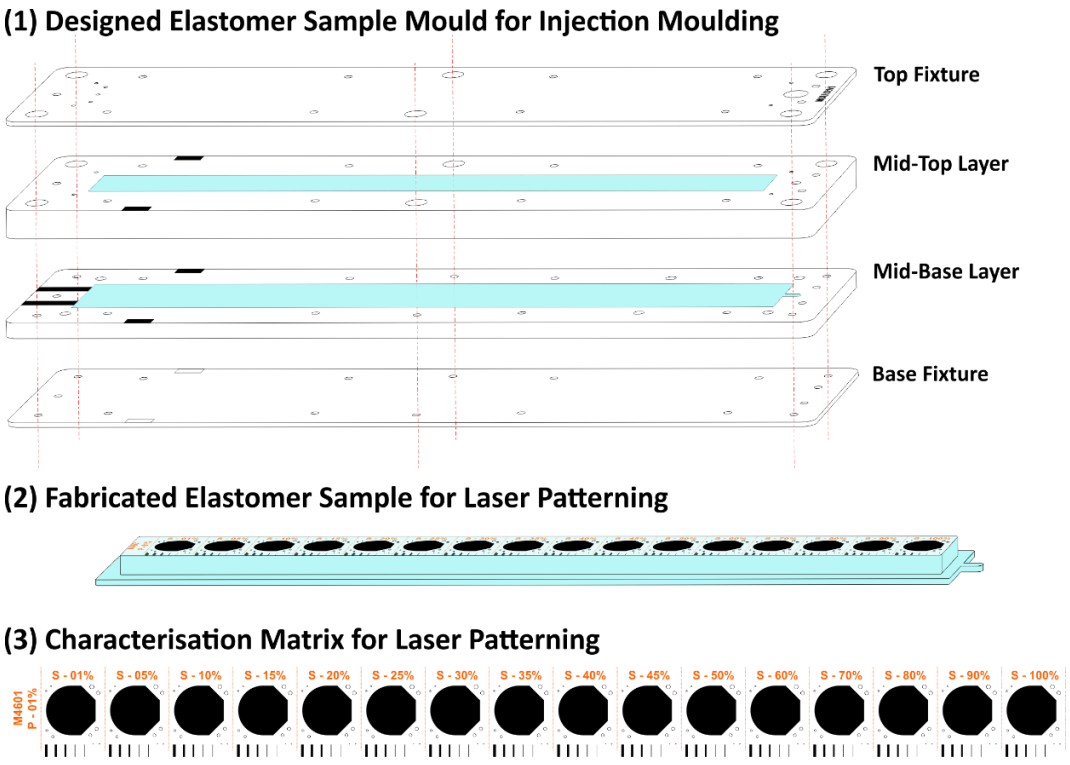

Figure 4.3.2 Experimental method featuring an orthogonal view of the mould and the experimental steps. (1) Exploded view of designed elastomer sample mould for injection moulding; (2) Illustration of fabricated elastomer sample for laser patterning; (3) Top view of laser ablated characterisation matrix.

Injection moulding was selected as the fabrication method to create the elastomer samples for laser ablation and patterning. The fabrication method uses a closed mould design with an inlet for elastomer injection. The technique itself focuses on removal of micro-bubbles and shape irregularities to provide a consistent and repeatable sample for the experiment compared to open mould designs. Figure 4.3.3 illustrates the fabrication process that enabled the characterisation of laser ablation/patterning of elastomeric materials.

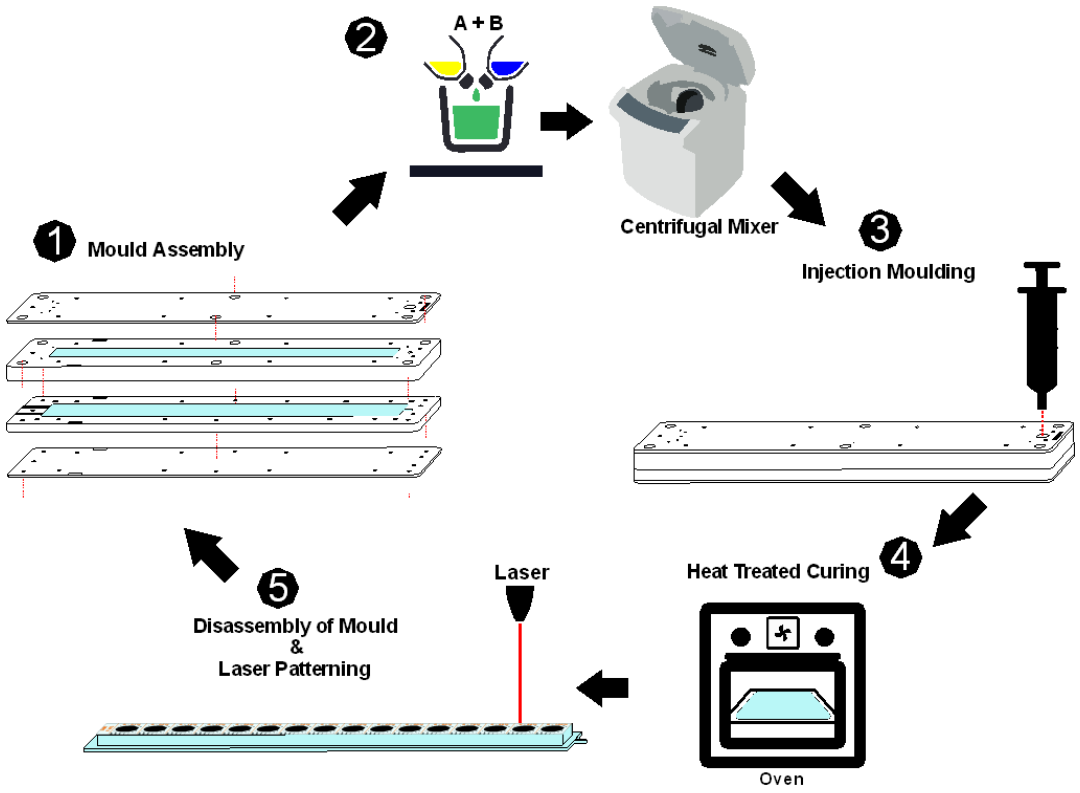

Figure 4.3.3 Fabrication protocol for laser ablation for elastomer patterning. (1) Assembly of designed mould; (2) Preparation and mixture of elastomeric materials; (3) Injection of elastomeric material in mould; (4) Thermal treatment for accelerated curing of elastomer samples; (5) Disassembly of mould and laser patterning of elastomer materials.

The fabrication protocol of the elastomer samples for laser ablation is as followed:

(1) **Assembly of designed mould:** The designed mould is cleaned and assembled with screws at designated points to produce a closed and sealed mould assembly.

(2) **Preparation and mixture of elastomeric materials:** Desired elastomer material is weighed (70 grams in total weight) and mixed in a centrifugal mixer to enable a catalytic reaction for a total of 2minutes and 30 seconds (1 minute for mixing, 1minute 30 seconds for degassing; both at 2000 rpm and 2200 rpm respectively).

(3) **Injection of elastomeric material in mould:** Once mixed, the elastomer material is poured into a syringe barrel and encapsulated with a plunge cap piston. The piston is then manually pressurised, allowing elastomer to inject into the mould. The injection process is continued till elastomer material fully occupies the space inside the mould and pushes the air out of the mould through designed outlets for exhaust. It is essential that the method of pouring does not incorporate air-bubbles to ensure no cosmetic faults.

(4) **Thermal treatment for accelerated curing of elastomer samples:** The filled mould containing elastomer material is then placed into the oven at 75^{o}C for 20 minutes to ensure material is fully cured. Mould is removed and left to cure prior to handling and next steps.

(5) **Disassembly of mould and laser patterning of elastomer materials:** Once cured, parts of the mould are removed, revealing the elastomer sample surface to be ablated. The elastomer sample is then placed into the laser cutter via designed alignment point to begin laser patterning. Based on the designed matrix, the elastomer sample is then left till completion of patterning. The now patterned elastomer sample is then cleaned using isopropanol and pressurised air gun. The remainder of the mould is disassembled and cleaned to be reused for the remainder of the material samples.

Two methods were then used to characterise the samples fabricated, a thickness gauge to measure the ablated depth of the profiles and an optical microscope for vector cut, raster engraving performance along with visual quality and measured accuracy. The next section presents the results and discusses the characterisation performed.

4.3.2 Results and Discussion

The thickness gauge (Mitutoyo Absolute IDS 543-692, Mitutoyo Ltd, UK) used as the measurement apparatus in Section 4.1.1, is used in this study to measure the ablated profiles with five repeats and is recorded. All characterisation settings for each elastomer material fabricated were correlated and computationally placed into MATLAB® to provide a comprehensive look-up table of settings based on the measured ablated depths of each material. Figure 4.3.4 presents the collected measured laser ablation depth profiles through controlling the power and speed of the laser cutter for EcoFlex™ 00-30, EcoFlex™ 00-50, Elastosil®M4601 and DragonSkin™ 30A.

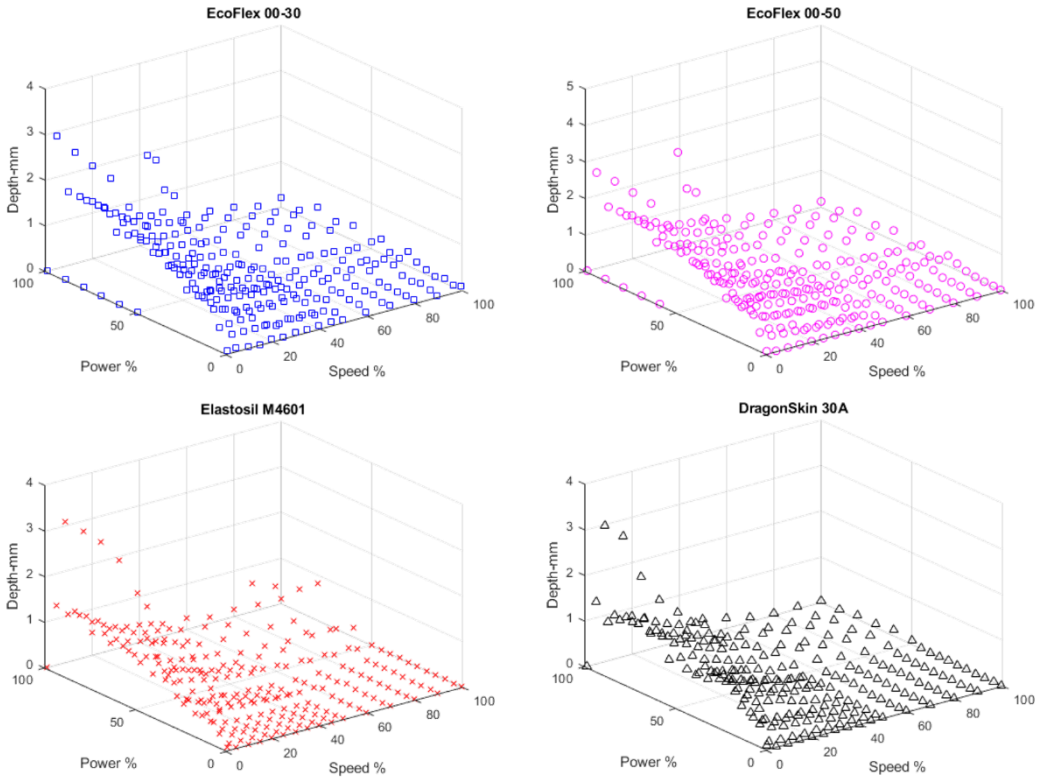

Figure 4.3.4 Three-dimensional plots of compiled measured depth data for laser ablation for materials EcoFlex™ 00-30, EcoFlex™ 00-50, Elastosil®M4601 and DragonSkin™ 30A.

Serving only as a visual perspective, Figure 4.3.4 illustrates that a degree of control can be achieved through varying the power and speed settings of the laser to enable depth ablation of elastomers. From an overview across all material, it can be seen that at power levels under 50% and speeds above 50% generated little to no

ablation. While depth ablations > 1 mm occurs when the speed level are kept < 40%. The ablated profiles suggest that the depth of ablation can be controlled using the differentiated power and speed settings of the laser system.

From a 2D view of Figure 4.3.4 for depth against speed levels, as presented in Figure 4.3.5, the depth of ablation recedes as the travel speed of the laser carriage increases at the power setting for 10%, 50% and 100% along with the chosen elastomers. EcoFlex™ 00-50 is added into the graph to compare towards its material series of EcoFlex™ 00-30, and is found to produce shallower depths across the power settings. It can be deduced that the effects of laser ablation does not relate to the shore hardness of material, but rather its composition. This is evident, as DragonSkin™30A was able to achieve the similar depth range of EcoFlex™00-30 at power levels of 50%. The measured laser settings for the presented materials are listed in Appendix 4.5. It is noted that at 100% power, for all elastomers and at speeds of 1% and 5%; the data zeroed as the material was completely damaged due to the excessive energy deposited by the laser exceeding the thickness of the sample (5 mm) and in return damage the mould and the surrounding sample profiles.

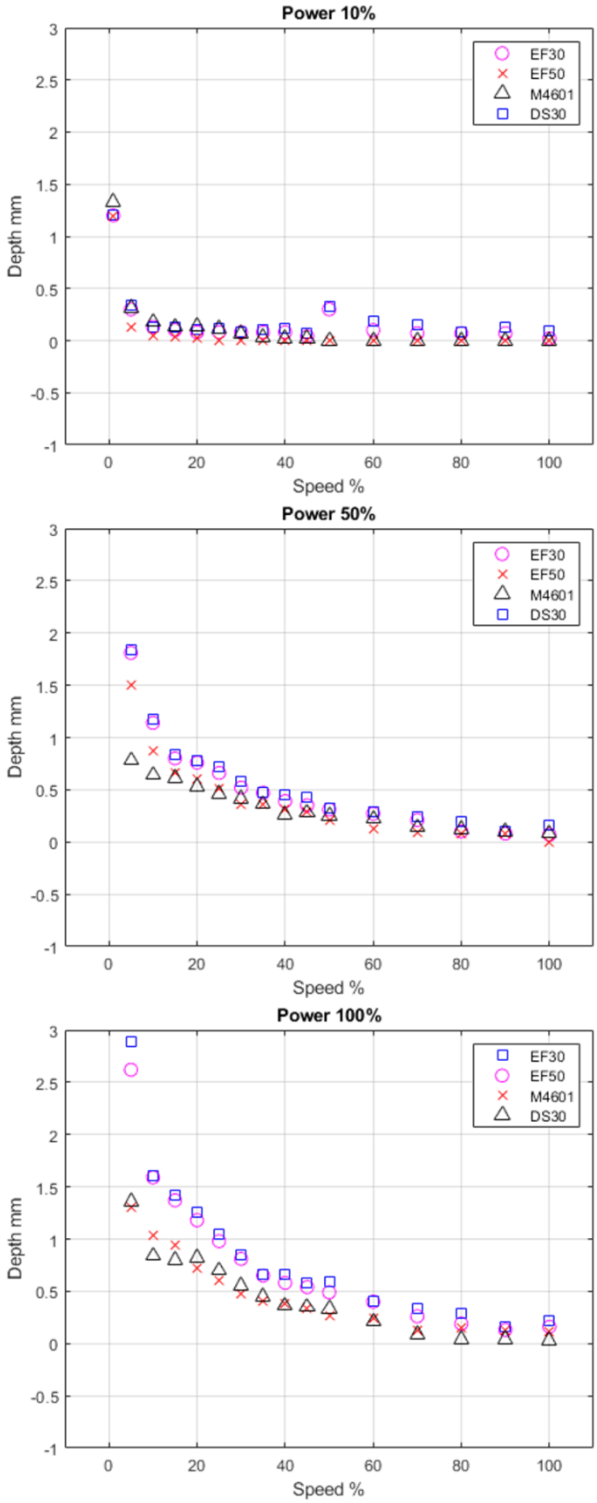

Figure 4.3.5 Measured ablated depth against speed setting (1% to 100%) for EcoFlex™ 00-30, EcoFlex™ 00-50, Elastosil® M4601 and DragonSkin™ 30A, at different levels of power settings (Top 10%; Centre 50%; Bottom 100%)

An optical microscope (VHZ-6000 Series Digital Microscope, KEYANCE LTD, UK), was used to visually capture and optically measure the performance and quality of vector profiles of the patterned by the laser. The matrix for all elastomeric samples were measured twice for optical accuracy and error comparison. Figure 4.3.6 presents a visual comparison view of Elastosil® M4601 at a set speed of 10% with power settings of 10%, 50% and 100% to illustrate the effects of laser ablation on elastomer.

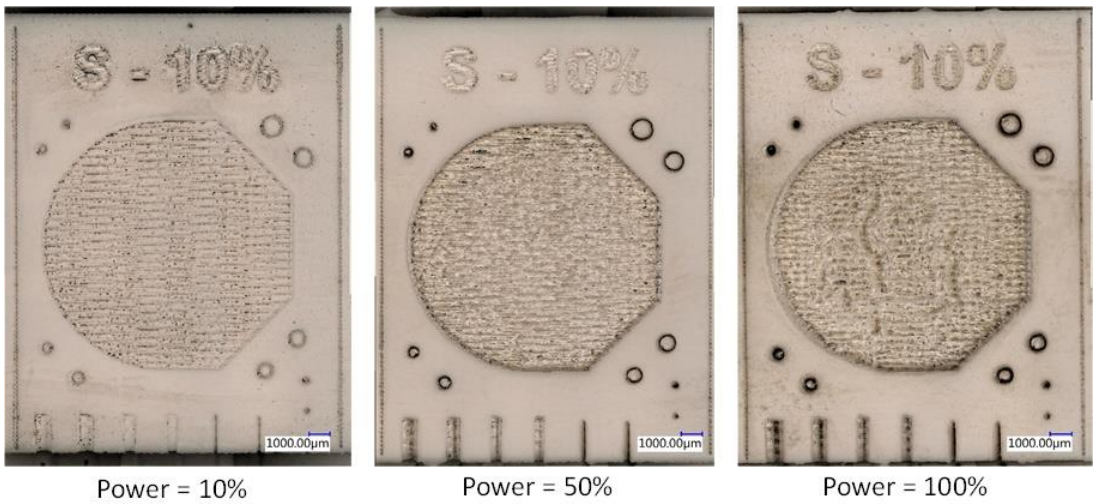

Figure 4.3.6 Laser ablated profiles under an optical microscope for Elastosil® M4601 at a set Speed of 10% with Power settings of 10% 50% and 100%.

As shown in Figure 4.3.6, it can be visually noted that as laser power is increases from 10% to 100%, the effects of the energy deposited by the laser increases along. In return, soot and debris is generated from the ablated material as this can be seen forming around and within the designed profiles. It is a common factor that the focal point of laser systems is designed with a certain degree of angle enabling the cutting process as compared to a complete vertical beam perpendicular from material surface to focal point of the laser. In addition, the generated and accumulation of soot and debris within the profile during ablation could potentially hinder the ablation process to be less effective as compared to affecting the depth measurements. This is due to the heat of the laser during ablation can calcify the carbon back into the surface of the ablated material.

Depending on the type of elastomer, the accuracy, quality and reproducibility of the laser ablated can be controlled through selective laser settings. The use of laser ablation enables the removal of designed composites in a planar manner through controlled depth cutting of the composite. Current results enabled a maximum depth cut of < 2mm depending on material and laser settings. However, further extensive characterisation in precise differential power and speed settings may be required. A form of linear regression was initially conducted to refine the laser power-speed levels towards the elastomers, however, this was not possible, as the results indicated. Within the context of the study, the results is deemed sufficient and optimal to aid and progress the development into the next phase, as a degree of optimal power-speed settings were achieved to enable removal of fabricated composites.

4.4 Summary

This chapter of characterisation was to assess the control, accuracy and performance of the developed SPIC fabrication technique. Characterisation of SPIC fabrication technique were based on elastomer material property against the film applicator's relative gap (applicator set thickness), spread speed and curing temperature as adopted in standard test methods. Based on the collective results of the characterisation experiments, a repeat-step-compensation is opted as the form of fabrication method to sufficiently produce the desired elastomer thickness and not hinder the performance of the applicator and fabrication technique. A spread speed of 2 mm/s and a curing temperature of 75°C is to be set as default to carry out the production of any thickness of elastomer as an optimal setting. The choice of curing temperature was evaluated between 75°C and 100°C, as the results are comparable with a ±5 micron tolerance, 75°C was opted to reduce the fabrication time between building elastomeric layers. The spread speed choice of 2 mm/s was based on the results indicating a gradual reduction of desired thickness of material as speed is increased.

A predictive metric was initially aimed for controlled elastomer thickness based on the theoretical wet film thickness. However, due to the vast set number of experiments performed, it was deduced that the measured results did not provide a concrete indication that this was possible. One of the limitation lies with the measurement technique employed via a manually operated thickness gauge, as other methods of measurements (laser or optical) were not applicable to the characterisation needs due to material. Despite the limitation in accuracy of the thickness gauge, the forces acting on the contact point of the gauge may potentially hinder the results obtained. In addition, laser and optical measurement technique were explored options during the characterisation. However, the employed techniques found inaccurate results due to the reflective and translucent surface of the fabricated elastomers reduced the efficacy of the techniques.

Making use of the experimented data, further investigation compared the results towards industry standard tests and equipments, however, it was found that large tolerances were often adopted as the coating of any material is highly dependent on the fluidic property of materials. In addition, reproducibility and tolerances are significantly affected by applicator spread speed and relatively applicator gap regardless of applicator specifications and precision which further increases the complexity to ensure production of desired thickness of any material. As such, industry and micro-fluidic fields often practice ‘step-compensation’ to achieve the desired thickness of a coating depending on criteria. As shown, a step-repeat method experimentally carried out yielded a higher accuracy and uniform thickness across the materials when compared to the initial characterisation of set applicator thickness. Analytically, the experiment results provided an insight understanding towards the concept of theoretical wet film thickness and the investigative measures to characterise film applicators. A higher precision measurement technique is needed be able to quantify the production of desired elastomeric thickness followed by an in-depth characterisation at micron-level for each elastomeric material based on the effects of wet film thickness. While there is a need to further improve the measurement technique, the results was comparable to manufacturing standards (ASTM D823-95 and ISO 2808) [135, 136].

Building from the characterisation of producing controlled thickness of elastomeric films, the mechanical adhesion strength of laminated elastomer films was experimentally investigated. The experiment was aimed and designed at assessing the lamination strength of two elastomer layers adhered during fabrication through an embedded cavity wedged between the layers. The assessment was based on stress-induced expansion within an inflatable cavity and theoretically, this would cause breakage and/or delamination between the layers. However, there is currently no comparable method to evaluate and validate the experiment designed. The results of the experiment entails intriguing possibilities for further research. However, further experimentation and detailed understanding of material properties may be required to fully understand the characteristics of the study. Due to limitation of analytical deduction drawn from the results, modelling and simulation of the experiment may provide an insight to the irregularities recorded. Upon further investigation, it was deduced that a different approach may be required to investigate the mechanical adhesion strength between elastomeric layers formed in SPIC fabrication.

The concept of laser ablation of elastomeric material through cutting and engraving was characterised to enable controlled and precise removal and patterning of elastomeric material. The characterisation experiment was designed to evaluate and investigate the effects of laser power and speed levels on a range of elastomeric materials. As such, a graphical design profile was designed to enable evaluation of the laser ablation and patterning ability, accuracy and precision. This is followed by a novel matrix design for fabrication of elastomeric samples. The elastomeric samples were then fabricated through a intricate mould design with the use of injection moulding to create repeatable and aesthetically robust samples for laser ablation. The samples were designed to be of 5 mm in thickness, based on preliminary experiments to accommodate higher laser power levels and build of residual heat from lower operating speeds. The fabrication process was then described in a step-by-step manner in similar to the SPIC fabrication process for ease of understanding. Measurement of the ablated depth of raster-engraved pattern used a manually operated thickness gauge, while linear vector and circular vector patterns were characterised using an optical microscope.

From the results, it can be concluded that laser ablation can be controlled and used to cut and pattern elastomeric materials through differential power and speed settings of the laser. Precision cutting and be performed at tested settings of power and speed, however, this is also dependent on elastomeric material tested. The range of laser power and speeds experimented were opted to provide an overview prior to fine-tune adjustments, however, further extensive characterisation of the effects of laser may be required to provide a definitive laser setting metric against elastomer material. There is a need to further characterise these features extensively, however due to scope of the study, the technique and characterisation of laser ablated depth was deemed optimal to aid and push the development of the research, while future works may continue to provide an in-depth characterisation of the technique.

Chapter 5 Modelling and Simulation of Soft Composites

Following the development progress, this chapter investigates a cohesive design method to model, simulate and analyse digital soft device designs to develop inflatable soft components towards reconfigurable programmable composites. The design method utilises computer aided design and finite element analysis software to increase the functional feasibility and understand the complexity of soft component designs to enable the creation of articulated mechanisms with up to sub-millimetre scale, embedded features and innate capabilities for a range of potential applications in soft robotic research as well as planar type soft components. In-line with the designed fabrication technique to produce thin soft composites, this chapter aids the development through introducing an iterative computational design process as compared to trial and error design and fabrication process.

5.1 Introduction to Soft Modelling and Simulation

The development design process of soft robotics is often left to the imagination and creativity of many researchers. Designs are often application specific and new components have little to no fundamental specifications and theoretical rules to provide a general development baseline compared to conventional robotic design process. Design tools currently employed are typically towards computer-aided design software used to elaborate the morphology of a concept. While this allows researchers to rapidly visualise and modify conceptual designs, existing means to simulate, predict and/or evaluate the performance and capability of a design is still sparse.

Soft robots are often expressed as a continuous deformable media, and can best be modelled as such; however, analytical models are complex and difficult to derive for non-linear geometries and behaviours as soft materials are classified as hyper-elastic. Soft actuators for specific applications have been analytically modelled either towards rigid-body kinematics and dynamics or over-simplified entities with known degrees-of-freedom. However, these linear models are limited to simple configurations and is hindered by its theoretical simplification of hyper-elastic material properties. Examples of analytical modelling is most known towards fibre-reinforced bending actuators and fibre-reinforced elasto-fluidic enclosures [142, 143].

While analytical modelling is difficult to derive for soft robots exhibiting geometric and behaviour non-linearity, the function of these systems are slowly being introduced to be analysed through finite element analysis modelling [144, 145]. Through this method, a mathematical model can theoretically be used to analyse the characterisation of the soft component in the form of force, torque, range of motion, speed of actuation and attributes in behaviour. Computationally in-expensive, finite element methods are often adapted towards design check validity of a closed-form model or provide comparative results with experiments as the method is widely used as an approximation due to the limited literature for an adaptive hyper-elastic material properties and general mathematical models revolving around soft systems

for mechanical characteristics. To date, an extensive and detailed modelling framework directed towards multi-variant soft pneumatic components has yet to exist. An example of an application specific modelling method, is of a soft bending actuator configured towards a pneumatic network design by Moseley *et al*. [43].

The sections that follows attempts to provide a cohesive design method directed towards modelling and simulating soft, thin, inflatable composites based on the designed fabrication technique via finite element analysis method. Prior to that, the proposed route has often been limited to specific materials, geometries and applications; and due to the complexity involved in modelling high-strains and continuum deformations in finite element, understanding of soft materials (hyper-elastic material properties) is needed to provide a reliable and accurate simulation of soft material behaviour. Progressing forward, the use of hyper-elastic material properties is required to be used to deduce quasi-static solutions needed to simulate the response of soft embodied inflated matrix designs. Building from the design parameter introduced in Chapter 3, the structural geometry of a functional soft thin actuator can then be modelled, evaluated and optimised in design, feasibility and possibly introduce new developments to aid soft robotic research.

5.2 Soft Material Characterisation, Modelling and Simulation using Finite Element Analysis

Soft materials, such as elastomers, are classified as hyper-elastic materials [146]. Which means, its elasticity (stress-strain curve) or elastic behaviour is not linear compared to conventional Hook's law (linear elasticity). Elasticity is defined as an impermanent distortion of an object from its original shape due to external and/or internal forces [147]. In a practical sense, predicting and replicating elasticity in a numerical method is needed for deformation (loading condition). While Hooke's law defines a one-dimensional linear relationship, between force, distance and a stiffness constant; the relation is only applicable for small range of strains and would not be valid for multi-dimensional strain and non-linear attributes.

In order to predict non-linear elasticity, general hyper-elastic mathematical models have been identified in literature and are widely recognised [43]. These prediction models are expressed towards non-linearity in elastic materials by considering the strain energy in a material. They typically fall into two broad categories: (1) phenomenological models based on descriptions of observed material behaviour, and (2) mechanistic models derived from information about the underlying material structures. The strain energy stored in a material can be elaborated not just as the force to distort the material, but the internal stress (stress symbol) and strain (strain symbol) that serves as the fundamental principle for hyper-elastic models. Figure 5.2.1 illustrates the stress-strain curve for a hyper-elastic model. Within this fundamental principle, all hyper-elastic equations must be endeavoured to replicate/mimic the elastic relationship (stress-strain curve) from any hyper-elastic experimental data [148-150].

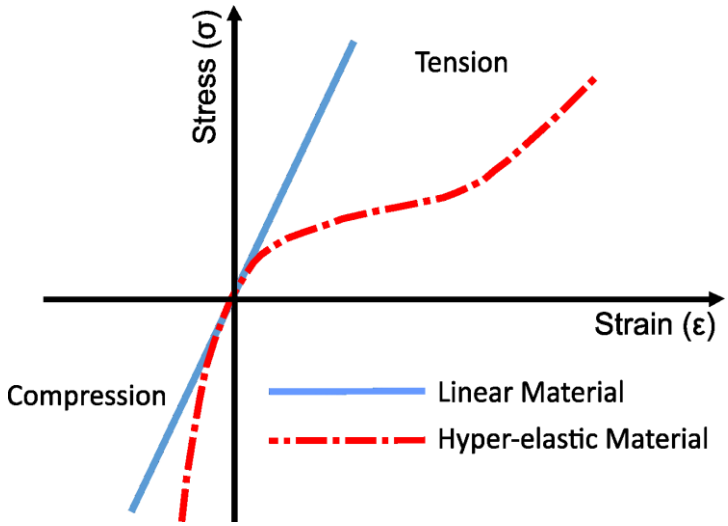

Figure 5.2.1 Hyper-elastic material stress-strain curve [151, 152]. Illustration depicts the tensile and compression curves of a hyper-elastic material compared to a linear material.

The fundamental expression of a hyper-elastic model relating the strain energy (*W*) to normalised stress and strain is given in Equation 5.2.1 and Equation 5.2.2:

$$W = f(l_1, l_2, l_3) \qquad \text{(Eq.5.2.1)}$$

$$l_1 = \lambda_1^2 + \lambda_2^2 + \lambda_3^2;\ \ l_2 = \lambda_1^2\lambda_2^2 + \lambda_2^2\lambda_3^2 + \lambda_3^2\lambda_1^2;\ \ \ l_3 = \lambda_1^2 \times \lambda_2^2 \times \lambda_3^2; \qquad \text{(Eq.5.2.2)}$$

W is denoted as the strain energy, which is a function of invariants (l_1, l_2, l_3) of Green deformation across a tensor. Each invariant is defined by a principle stretch ratio (Equation 5.2.2) in each direction. While the principle stretch ratio $(\lambda_1, \lambda_2, \lambda_3)$ is defined by the ratio of deformed distance to its original point in each direction. Based on this, the principle stresses and strain relationship can then be derived and formulated; however, the relationship and formulation are not expressed in great detailed in this study as existing hyper-elastic mathematical models are already in place. Often used phenomenological models are Ogden and Yeoh models, which yields good results for soft materials and is widely used [153, 154]. Mechanistic models, such as Arruda-Boyce and Van-der-Waals; are applicable and suitable for smaller strain models and not complex models where material behaviour are determined through multiple modes of experimental testing [155, 156].

Hyper-elastic model properties of soft materials are typically determined through relevant strain and stress tests across a specific design criterion. Several standardized methods exist to achieve this (International Organisation for Standardization (ISO) or American Society for Testing and Materials (ASTM)) [157-160], while these tests focus on material characterisation for tension and compression in the uniaxial, biaxial and planar directions. Uniaxial and planar tests are often performed with standard engineering test equipments, while biaxial requires specialised equipment in order to achieve equilibrated two directional strains. In this study, uniaxial and planar tests in tension and compression is enough to provide an understanding for development.

As soft robotic components are commonly inflated and deformed, they can be represented as forms of tension and compression. From experimental data obtained in terms of tensile and compression tests, hyper-elastic models can then be used to replicate the physical behaviour. Based on a relative error (R^2) of prediction/fitting curve to experimental data points, hyper-elastic models can then be evaluated and expressed in FEA software. From there, the selected hyper-elastic model can then be adopted into material properties within a CAD model and simulated to exhibit soft material properties through finite element analysis. Figure 5.2.2 illustrates an overview approach detailing the experimental material characterisation process towards modelling and simulation of soft robotic components.

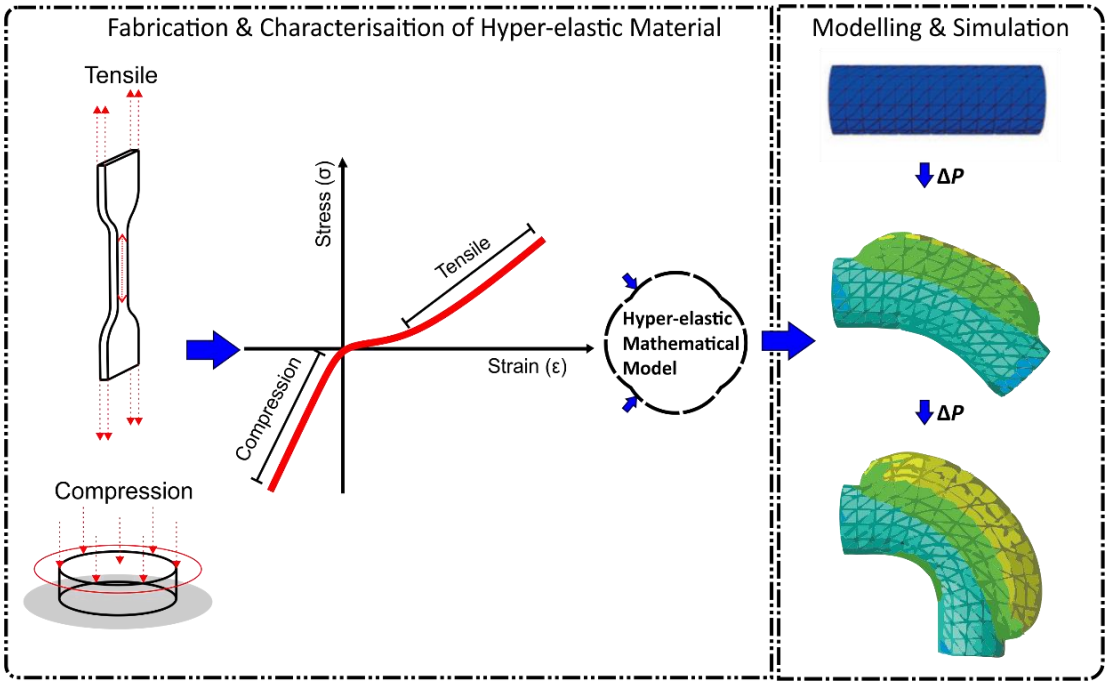

Figure 5.2.2 Illustration of experimental material characterisation process for modelling and simulation of soft robotic component. From material testing of tensile and compression, the obtained data is then characterised with hyper-elastic mathematical model and then used as coefficients for finite element analysis.

To date, there is no established library directed towards the material properties of hyper-elastic models and their mathematical model coefficients. While many researchers have investigated the performance of many hyper-elastic models (i.e. Ogden, Yeoh and etc.), the community still opt to use different methods for elastic material testing and elastomeric materials. These data reported often results in different numerical coefficient derived and sparse material library support. Within the time of study, it was not plausible to create such an extensive library to aid and contribute the development of soft robotics due to limitation of equipment. Instead, published data from literature was obtained through a quantitative review of hyper-elastic modelling of soft robotic components. Table 5.2.1 lists the hyper-elastic model stiffness coefficient constants for Elastosil® M4601 as an example, while an expanded list of other used elastomers is listed in Appendix 5.1.

Table 5.2.1 Table of Hyper-elastic model stiffness coefficient constants of Elastosil® M4601 for. Ogden, Yeoh [153, 154].

Coefficients	**Elastomeric Material**	
(MPa)	Elastosil® M4601	EcoFlex™ 00-30
Yeoh		
$C10$	0.112	0.008
$C20$	0.019	0
$C30$	0	4.03×10^{-7}
Ogden		
μ_1	-3.646	0.024
μ_2	0.619	6.67×10^{-5}
μ_3	7.00×10^{-6}	4.54×10^{-4}
α_1	2.49×10^{-6}	1.714
α_2	3.39×10^{-6}	7.068
α_3	2.34×10^{-6}	-3.366

Based on Table 5.2.1, a commercial finite element method (FEM) software Abaqus (Abaqus FEA, SIMULIA, Dassault Systemes®) is used to model and simulate the designed soft robotic components. Following a general modelling framework directed toward soft pneumatic bending actuators, the choice of software and modelling process were adopted from the 'Soft Robotics Toolkit' [161]. The soft robotics toolkit is an open-source resource directed towards the field of soft robotics. Figure 5.2.3 illustrates an overview of the modelling process to simulate a soft robotic actuator.

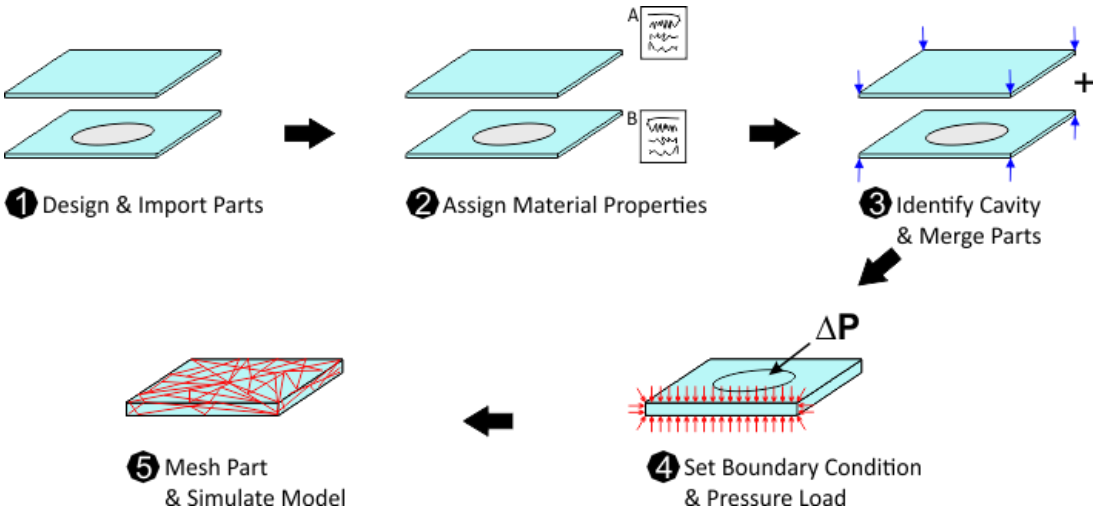

Figure 5.2.3 Illustration of modelling and simulation of a soft component via Finite Element Analysis. (1) Design and import parts from CAD; (2) Assign material properties to parts; (3) Identify cavity and merge Parts into a composite; (4) Set boundary condition and pressure Input for actuation; (5) mesh model and simulate for analysis.

The modelling and simulation process describes a general step-by-step method as introduced in the 'Soft Robotics Toolkit'. It is noted that the software does not interpret units, as such, it is crucial to ensure a baseline of system units (SI) is consistent and adhered towards. In this study, the SI units is as dictated in Appendix 5.2.The general procedure shown in Figure 5.2.3, to model and simulate a soft robotic component is as described:

(1) Design and Import Parts

Part or components are drawn from a CAD software are converted into the appropriate file settings (.STEP file) and imported into the software. It is crucial to follow a consistent dimensional system unit to ensure modelling results is objective and rational. A table of SI units is shown in Appendix 5.2.

(2) Assign Material Properties

Material properties are assigned to each part or overall model. This does not only include hyper-elastic material properties, but also static and other materials that are incorporated into the design for modelling.

(3) Identify surface of inner cavity and Merge Parts

A surface/face to be subjected to actuation (pneumatic or hydraulic) is highlighted and identified to the software.

(4) Setting Boundary Conditions and Load

Boundary conditions, such as constraints and gravitational effects (optional), are placed along with the load for actuation (pneumatic or hydraulic) and is set towards the identified cavity.

(5) Mesh and Simulate

The model is then subjected to a 'Mesh', in order to allow the software to calculate the quasi-static solutions and simulate the behaviour of the model. Once the simulation has completed, the results can be visualised and analysed.

Additional steps and settings are used to enable the success of the simulation, such as denotation of static or boundary conditions, mesh solution type (Hybrid-Tet) and size (Global size of 2). These settings are not material specific or case study related but purely computational modelling and software oriented as depicted. An understanding of finite element analysis and its associated software features may aid the achievability of desired modelling results. However, a series of trial and error is still fundamentally required to enable a analytical deduction to evaluate the results obtained.

Once the simulation completes, the results can be analysed in several ways. It is noted that explicit characterisation and analysis of the simulated soft models were not performed, such as blocked force, component stress-strain, and other complex characteristics. This was due to the diverse challenges listed require an in-depth investigation and understanding, which is be beyond the scope of the research during the time of study. In addition, the obtained coefficients from published data only supported basic modelling and simulation needs, while an insight of material properties and finite element modelling require further in-depth study. However, the design feasibility and inflation behaviour along with other modes of characteristics, such as, internal pressure expansion, height of inflation and design functionality of the soft models were evaluated. In addition, selected models were fabricated and compared against its simulated counterpart in terms of inflation profile and bending angle to further evaluate the development of soft actuators via the designed fabrication technique of SPIC.

5.3 Soft Modelling and Simulation using Finite Element Analysis

Reflecting to Chapter 3, the fundamental design of the proposed SPIC fabrication method follows a two-dimensional (2D) design method to create soft, planar, and inflatable composites that can actively deform to their pre-programmed state when actuated. The objective of this section is to expand on the design of the development of soft planar inflatable composite based on a two-parameter design method (i) Selective material layering, and (ii) Structural geometry variation; towards a design method using finite element analysis. By reconfiguring these parameters towards the design of a soft bending actuator, a type of soft planar continuous bending actuator can be designed and optimised based on a ratio scheme introduced.

5.3.1 Conceptual Design

The fundamental design is based on a continuous bending actuator structure consisting of a rectangular shaped chamber/cavity. Upon pressurisation, the cavity is designed to be inflating uniformly along its length (X-direction), leading to a continuous bending behaviour. As illustrated in Figure 5.3.1, the design of the soft planar inflatable continuous bending actuator (SPICA) is introduced along with its designed dimensions consisting of actuator length (50 mm), cavity width (35 mm) and its total composite thickness of 1mm. The width of the actuator (A_w), is then set towards 5 mm, 10 mm and 20 mm.

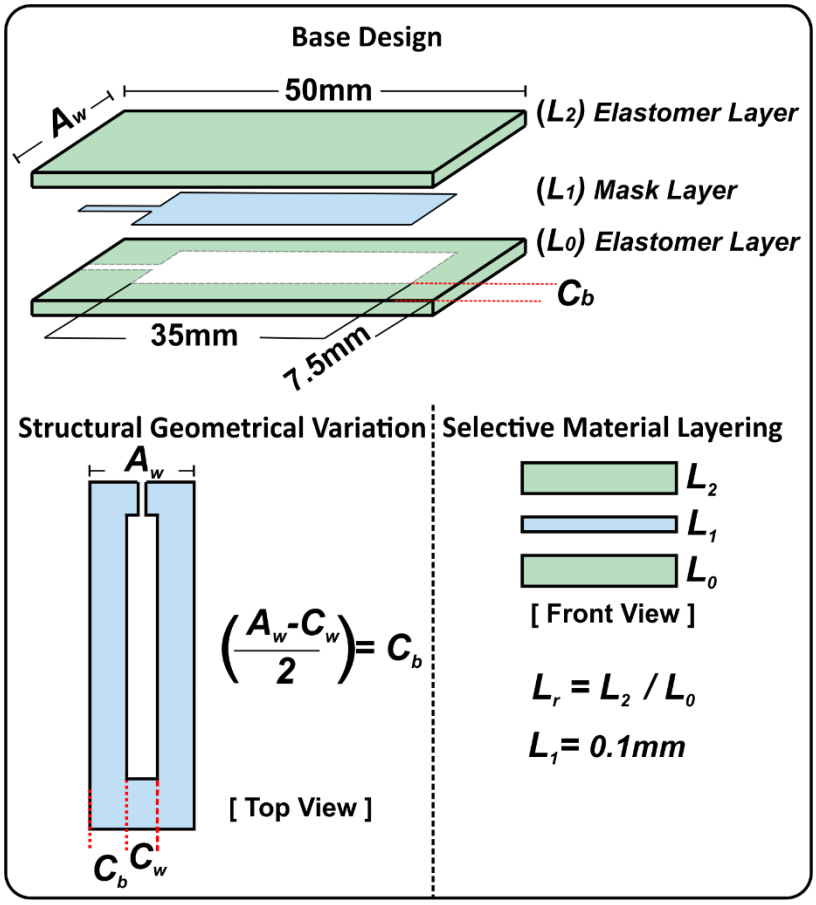

Figure 5.3.1 Design parameter to develop soft planar inflatable continuous bending actuators. Base design provides a schematic overview of the proposed actuators including the static dimensions. Structural geometry variation provides a top view of the actuator including a proposed numerical method to calculate the cavity band (C_b). Selective material layering provides a front/side view of the actuator and introduces the layer ratio (L_r) deduced from the total layers of material enlisted.

The SPICA design is then subjected to the proposed two-parameter design method. In selective material layering, a single soft elastomer forms the overall composite material, of which is inflated through a mask layer via paper based soluble material of a certain thickness (approximately 0.1 mm). The overall thickness of the composite is set at 1 mm thick, and the layers are divided into 3 layers. Introduced here, the layer ratio (L_r) is the thickness ratio of the top layer (L_2) over the bottom layer (L_0). As the cavity thickness is set at 0.1 mm, 0.9 mm of the remaining thickness is equated into a relative layer ratio for simplification purposes. In structural geometrical variation, the design of the cavity is set to a rectangle shaped cavity. With a set cavity length, the cavity width becomes the variable component in the design. As such, cavity band (C_b) is introduced here as a scheme to design and vary the cavity width (C_w) of the actuator. Relative to the selected actuator width (A_w), the cavity band (C_b) is the width space between the cavity and the actuator as shown in Figure 5.3.1.

5.3.2 Modelling and Fabrication of Soft Planar Inflatable Actuators

The conceptual design of the soft planar inflatable continuous bending actuator was carried out based on the modelling technique as depicted in Section 5.2. All the models were subjected to the use of Yeoh hyper-elastic material model (Table 5.2.1) with Elastosil® M4601; along with pneumatic inputs up to 10 psi and mesh size of 2. With each of the actuator modelled and simulated, its response is arranged in the form of a matrix, as illustrated in Figure 5.3.2. Illustrated in Figure 5.3.2, corresponding with the conceptual design, 5 mm actuator width (A_w) is displayed in two viewpoints, side (X) and top (Z) from a planar perspective with its inflated response at 10 psi. The matrix is arranged with the row consisting of the Layer ratio (L_r) and columns indicating the cavity ratio and the cavity width in respect to the actuator width (A_w). The Abaqus input data along with the matrix consisting of all actuator design is listed in Appendix 5.3.

Actuator Width [*Aw*] = 5mm Designs Thickness Layer Ratio [*Lr*]	*Cw* = 4mm *Cb* = 0.5mm		*Cw* = 3mm *Cb* = 1mm		*Cw* = 2mm *Cb* =1.5mm		*Cw* = 1mm *Cb* = 2mm	
	X	Z	X	Z	X	Z	X	Z
L2: 0.45mm L0: 0.45mm *Lr* =1.00	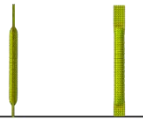		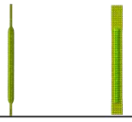		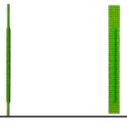		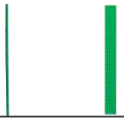	
L2: 0.35mm L0: 0.55 mm *Lr* = 0.63	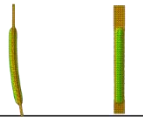		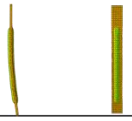		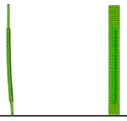		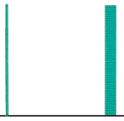	
L2: 0.25mm L0: 0.65 mm *Lr* = 0.38	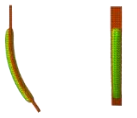						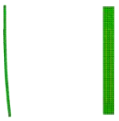	
L2: 0.15mm L0: 0.75 mm *Lr* = 0.20	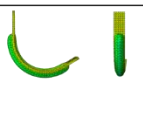		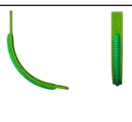		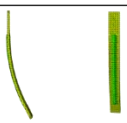		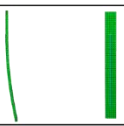	
L2: 0.10mm L0: 0.80 mm *Lr* = 0.125	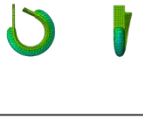		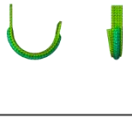		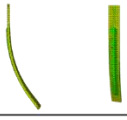		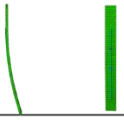	

Figure 5.3.2 Matrix scheme of the modelled and simulated soft planar inflatable continuous bending actuators of 5 mm actuator width (A_w) at 10 psi.

From the matrix, the inflation responses indicate the feasibility of the bending actuators in respect to the layer ratio (L_r) and cavity band (C_b). Compared to a direct design and fabrication process, the matrix provides an insight to the design process to the proposed continuous bending actuators. Based on Figure 5.3.2, the layer ratio (L_r) of 0.2 with a cavity band (C_r) of 0.5 to 2 mm, was chosen to be fabricated and evaluated. Compared to the layer ratio (L_r) of 0.125, the layer was deemed too thin despite the film applicator's ability as presented in Chapter 4, while the layer ratio (L_r) of 0.38 and above showed minimal actuation capabilities, and therefore not considered for fabrication. The fabrication of the actuators is as presented in Chapter 3, while the material of choice to model and fabricate is Elastosil® M4601 with respect to the availability of published hyper-elastic data. A total of 12 actuators at the selected layer ratio (L_r) of 0.20 is to be produced for actuator width (A_w) of 5, 10 and 20mm, and cavity bands (Cb) of 0.5 to 2 mm at 0.5 mm intervals as presented in Figure 5.3.2. A complete matrix scheme of the described actuators can be viewed in Appendix 5.2.

5.3.3 Characterisation and Evaluation of Soft Inflatable Composites

A custom pneumatic control set-up was developed to characterise the samples across a range of controlled input pressures of 0 to 10 psi. For each test, the actuators are inflated using a custom built pneumatic control box consisting of a pneumatic regulator (SMC ITV10010) and an analogue absolute pressure transducer (15 PSI SSC Series Absolute Pressure Transducer, HoneyWell, USA); connected to a data acquisition device (NI-USB 6002 DAQ) for digital control and data acquisition of pressure sensor. Figure 5.3.3 illustrates the pneumatic control set-up schematic diagram used in this study. A second custom pneumatic control set-up without data acquisition functionality featured in this thesis is found in Appendix 2, along with its generic build of material.

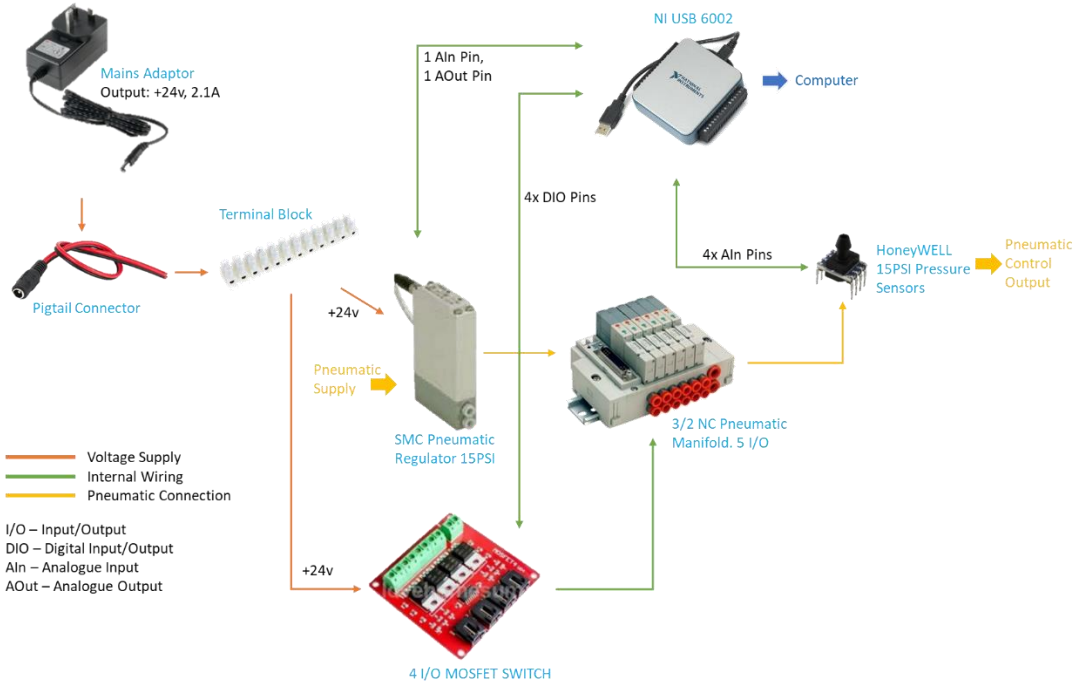

Figure 5.3.3 Schematic diagram of custom pneumatic control set-up assembly and build. Connections and operations are based on the intended use of components listed can be found with it associated reference material and datasheets.

In soft pneumatic actuators, its pneumatic induced cantilevered actuation generates deflections in the longitudinal and transverse directions and cannot be estimated using the traditional mechanics beam theory [162, 163]. Soft pneumatic actuators generate large deflections which generate geometrical and material non-linearities in their mechanical output as shown in Figure 5.3.4 [42, 163]. As the internal pressure of the soft actuator is increases, the actuator deforms in a curling motion resulting in an angular displacement of the tip of the actuator. A method to characterise the bending angle is through vision system to record the deflection behaviour of the soft actuator as it is pressurised incrementally without the need for deriving accurate physical and material models [22, 39, 142, 163]. As shown in Figure 5.3.4, the bending angle (θ) is measured as the angular displacement of the actuator tip from its static fixture point.

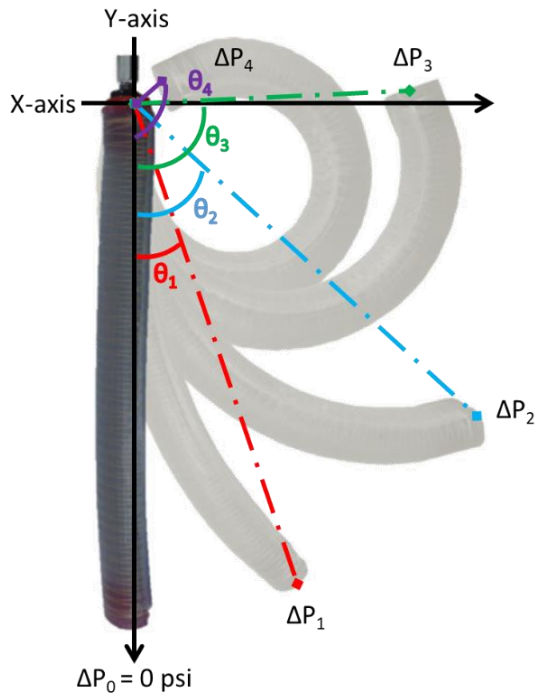

Figure 5.3.4 Characterisation of a soft pneumatic actuator to measure bending angle (θ). As ΔP : Internal pressure difference increases, the bending angle is measured as the angular displacement through the tip of the actuator. Soft actuator image based on Fiber-Reinforced Actuators [22, 164]

In this study, as the control input pressure is incremented, the inflation profile of the actuators is recorded using a high definition camera (D5300, Nikon, Japan) along with a measurable calibrated backing pattern (5mm x 5mm) for post-image processing. Post processing of the images are subjected to an open-source image analysis program (ImageJ, Image Processing and Analysis in Java) in which the Cartesian X and Y coordinates of the actuator tip were tracked, and the resultant total bending angle was measured. This is then compared towards simulated designs to evaluate the bending angle, as well as behaviour efficacy and accuracy of the model. It is noted that the initial deflection in the actuators under zero pressure is considered zero degrees in angle as shown in Figure 5.3.4.

Given the millimetre scale thickness of the actuators, preliminary characterisation for blocked force resulted in rupture of the cavities in a number of samples. This is due to the result of over-expansion caused by internal stress of inflation pressure. Based on recorded data of preliminary results, a maximum input pressure of 10 psi was not able to produce a force > 1 Newton. This is due to the size of the actuators including the thickness of the configurated layers. It is also noted that the load-cell available at the time of this study was only up to 10 Newtons with a relative resolution of 1 Newton. Theoretically, an extensible layer of fabric or mesh may aid the structural integrity and limit the possibility of over-inflation of the actuator. However, this study did not include any embedded mechanical programming layers in order to simplify and assess the feasibility of soft modelling a continuous bending actuator from a single elastomer material perspective.

The following figures (Figure 5.3.5 – 7) illustrates the inflated profiles comparing fabricated actuators and its simulated counterparts models. A table consisting of the measured bending angles of fabricated actuators and simulated models are listed below each corresponding figure. Each sample presented here were selected based on its performance and feasibility. While repeats were fabricated to ensure validity, hindering factors such as fabrication error, material limitation and time constraints were affected as this study were carried out.

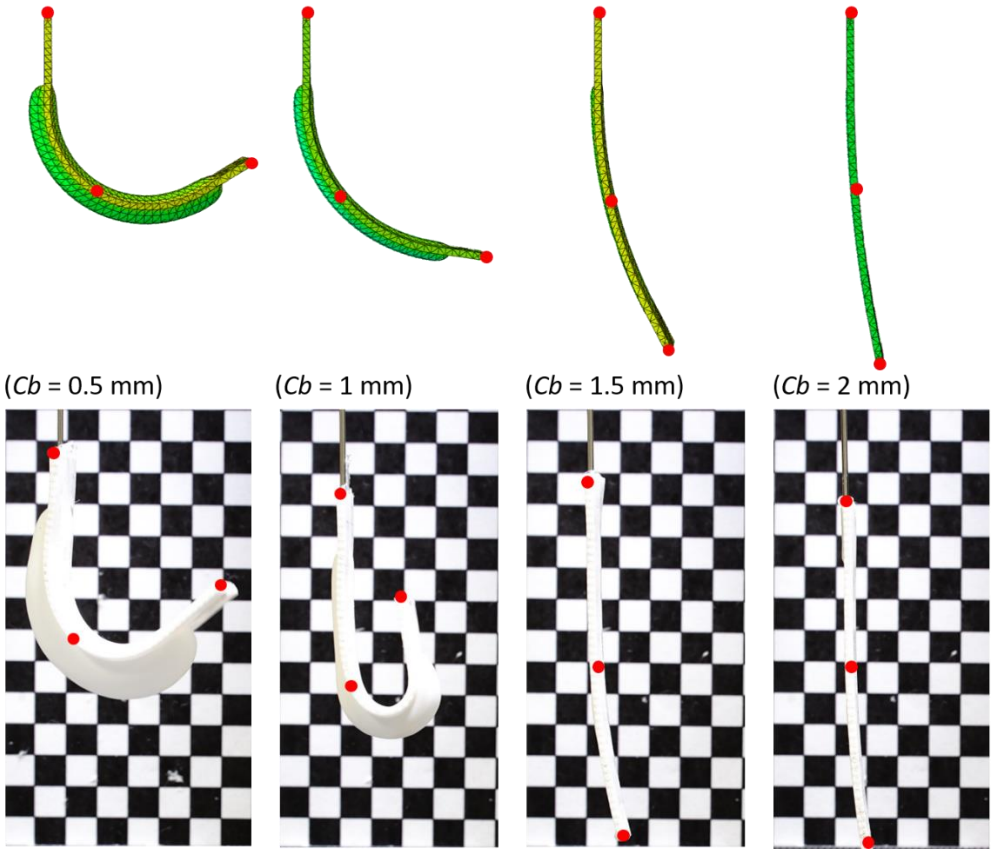

Figure 5.3.5 Comparison of fabricated and simulated models of SPICA 5mm actuator width, L_r = 0.2 at 10 psi.

Table 5.3.1 Measured bending angle and simulated bending angle of SPICA 5mm actuator width, L_r = 0.2 at 10 psi; Based on Figure 5.3.5

Cavity Band (Cb) (mm)	0.5	1	1.5	2
Simulated Angle Ø (°)	87.66	75.73	20.31	11.80
Measured Angle Ø (°)	106.66	102.06	13.67	9.90
Difference Δ (°)	-19.00	-26.33	6.64	1.9

Figure 5.3.5 illustrates a visual comparison of the simulated and fabricated models, while Table 5.3.1 presents the measured bending angles of the corresponding actuators. The inflation profile for the fabricated actuators displayed a similar referenced behaviour compared to its modelled counterpart. However, in the C_b = 1, the inflation profile of the fabricated actuator behaved in such a manner due to incomplete removal of mask layer material. Repeats of the sample were made, however, this resulted in a series of fabrication errors due to material limitation. This occurrence presented here provides an opportunity to visually highlight one of the limitations during the fabrication of soft composite, which links to the incomplete

removal of the mask layer material as described in Section 3.5. In Table 5.3.1, the measured angle reflects the results presented in Figure 5.3.5 as stand-alone bending angles. A cumulative result of average measured bending angles and standard deviation was not included due to the limitation of fabrication during the study.

In Figure 5.3.6, the fabricated and modelled 10 mm actuators visually provided a comparable inflation profile. Reflected in Table 5.3.2, the measured bending angles of Figure 5.3.6, indicates a similar difference of < 30^{o} when comparing towards the simulated model as reference.

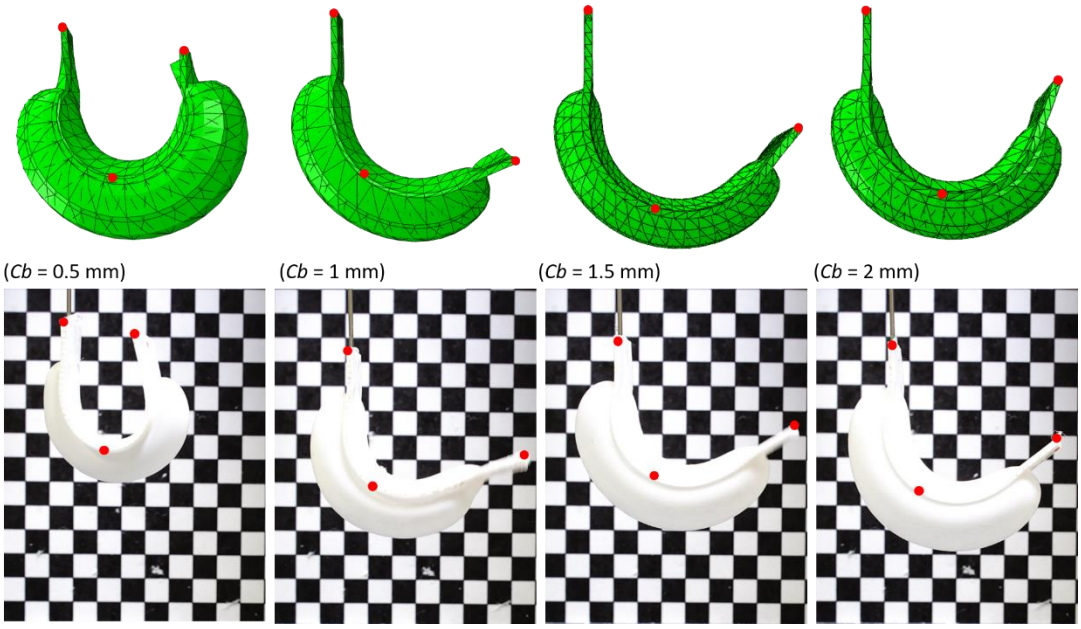

Figure 5.3.6 Comparison of fabricated and simulated models of SPICA 10 mm actuator width, L_r = 0.2 at 10 psi

Table 5.3.2 Measured bending angle and simulated bending angle of SPICA 10 mm actuator width, L_r = 0.2 at 10 psi; Based on Figure 5.3.6

Cavity Band (Cb) (mm)	0.5	1	1.5	2
Simulated Angle Ø (°)	154.23	135.10	122.39	109.08
Measured Angle Ø (°)	146.95	109.07	102.28	100.36
Difference Δ (°)	154.23	135.10	122.39	109.08

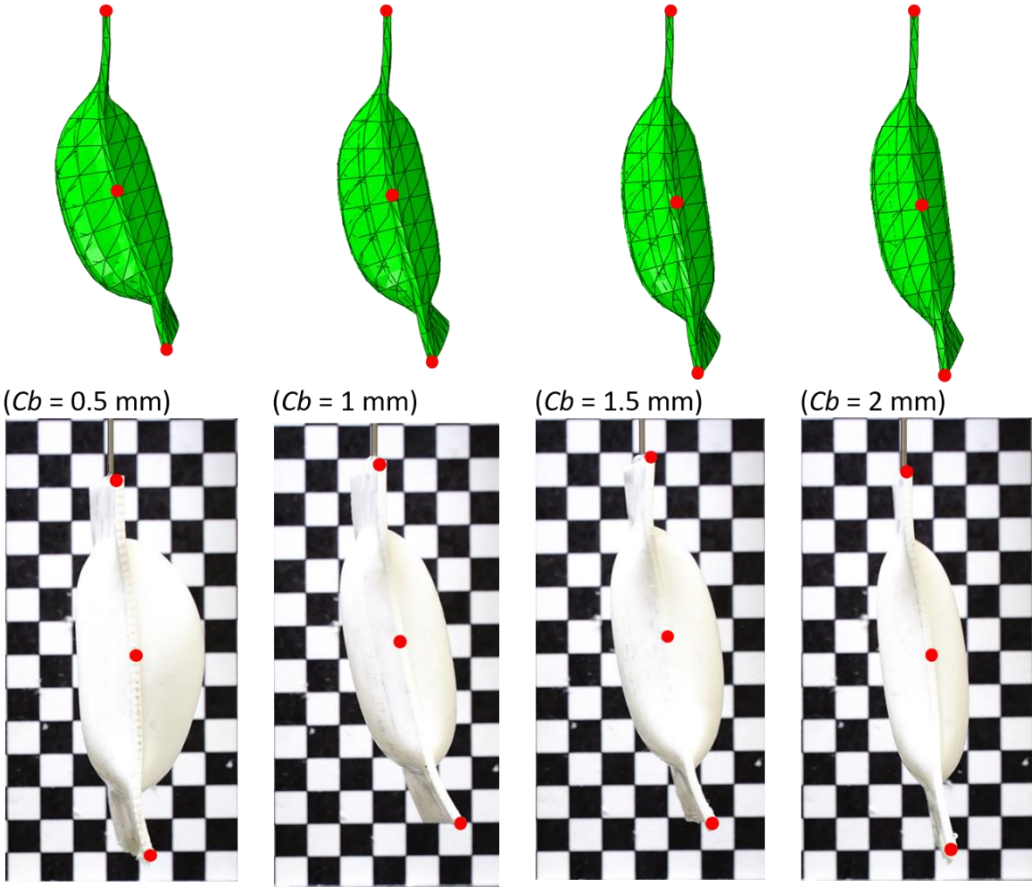

Figure 5.3.7 Comparison of fabricated and simulated models of SPICA 20 mm actuator width, L_r = 0.2 at 10 psi.

Table 5.3.3 Measured bending angle and simulated bending angle of SPICA 20 mm actuator width, L_r = 0.2 at 10 psi; Based on Figure 5.3.7

Cavity Band (Cb) (mm)	0.5	1	1.5	2
Simulated Angle Ø (°)	20.32	19.93	16.79	17.31
Measured Angle Ø (°)	19.13	12.42	10.49	12.92
Difference Δ (°)	1.19	7.51	6.3	4.39

In Figure 5.3.7, the simulated models presents a similar inflation behaviour in a different manner as compared to the fabricated models. Two factors were deduced to have led to this occurrence, which includes incomplete removal of mask layer material, and twisting viewpoint of fabricated model during inflation. Despite the inflation behavioural difference, the measured bending angles as shown in Table 5.3.3 displayed a smaller difference of < 10^{o} compared to the measured simulated model angles. Based on the collective results of the three actuator widths (A_w: 5mm, 10mm, and 20mm), it is noted that, the visual efficacy of the simulated model may

be subjected to assumptions and unrealistic values due to material properties set computationally under ideal conditions. Despite the use of published data as hyper-elastic material properties, other configurations and properties were not configured, such as, gravitational acceleration. As such, the simulated models only serve as a visual aid and inflation behaviour efficacy rather than complete accurate prediction of the fabricated models. In most cases, the inflation profile at under controlled pressure exhibited a visually comparable model between fabricated and simulation. While measured actuator bending angles were within a 30^{o} angle difference to its modelled counterpart, the modelling and simulation process still served as a fundamental development tool to assist further development and designs for bending actuators.

5.3.4 Soft Planar Inflatable Discrete Actuator (SPIDA)

Compared to soft pneumatic actuators (SPAs), the geometrical design of the cavity omits the use of bellows to cause an additive effect causing a bending upon pressurisation as shown in Figure 5.3.8. The proposed soft planar inflatable continuous bending actuators exhibited a similar prolific inflation with its rectangular shaped design. Due to the parametric component of cavity band (C_b) and layer ratio (L_r), an array of thin (1 mm), soft planar inflatable continuous bending actuator were fabricated and evaluated.

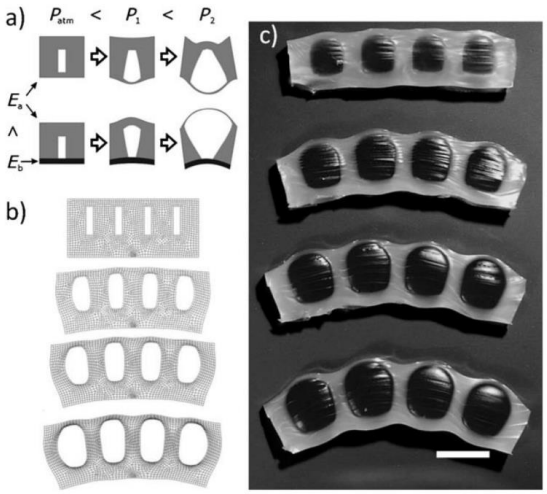

Figure 5.3.8 Soft pneumatic actuator inflation effect due to geometry of the chamber and material properties of the material surrounding the chamber by Ilievski *et al.* [4]

The development of SPICA and modelling is further progressed with the introduction of soft planar inflatable discrete bending actuators (SPIDA). The design of the actuators drew inspiration from Ranzani *et al*. [165]. Based on the development of SPICA previously obtained, a joint-like bending actuator is proposed as compared to a curled continuous bend. Figure 5.3.9 illustrates the design of the actuator, along with its dimensions and set thickness of 1mm composite. The cavity design follows a triangular shaped cavity, with a set cavity band of C_b = 1 (cavity width (C_w = 3)), and a layer ratio of L_r = 0.2.

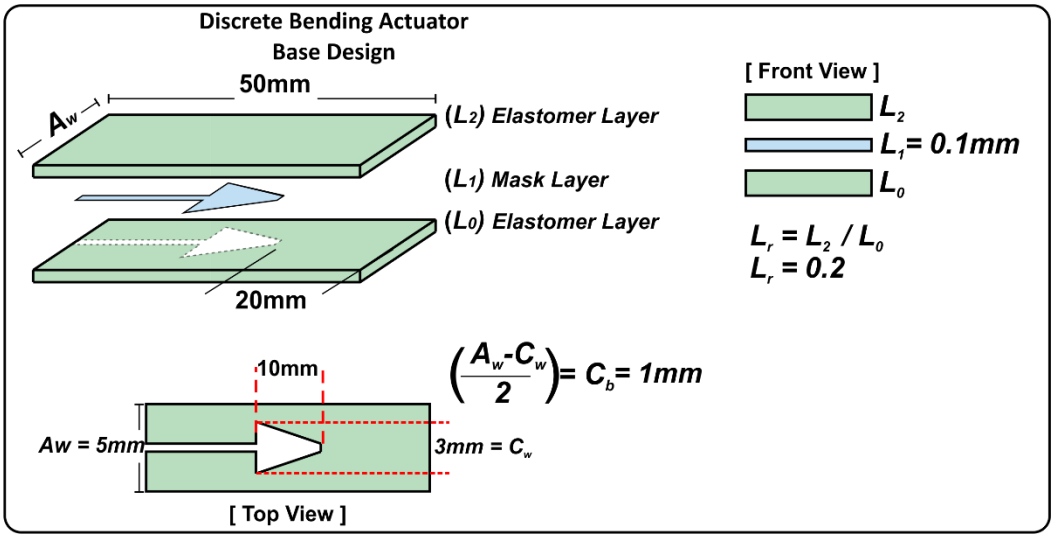

Figure 5.3.9 Design parameter for discrete bending actuator of SPIDA 5mm actuator width (A_w), 3mm cavity width (C_w), cavity band (C_b) of 1, and layer ratio (L_r) of 0.2

The designed discrete bending actuator shown in Figure 5.3.9, SPIDA, was subjected to the same modelling and fabrication process as the development of SPICA. A total of 5 samples were fabricated for the SPIDA under the design parameters shown in Figure 5.3.9.

A pressure step-frame diagram of the fabricated SPIDA is shown in Figure 5.3.10, while comparing to its simulated model. With a maximum input pressure of 15 psi set computationally through FEA simulations, the fabricated actuator was subjected to the same input pressure range. The designed discrete bending actuator exhibited an intended joint-like bending inflation profile based on its design and simulation. At

0 psi, the fabricated actuator is slightly deformed due to initial inflation and removal of the mask layer. Without a rigid structural layer, the actuator deforms towards it bend angle with respect to its layer ratio. Upon pressurisation the actuator exhibits a joint-like profile and is relatable to its modelled counterpart at controlled input pressures. Comparing its bending angles in Table 5.3.4, the averaged measured angles indicates a difference of < 8°, while the standard deviation of the sample indicate a maximum of 4. At this point the SPIDA development has presented its efficacy in its ability to simulate the proposed design parameters compared to conventional soft bending actuation designs. However, further work is required to progress the development to advance the cavity design approach, assimilate the modelling of soft composite and improve the limitations in fabrication.

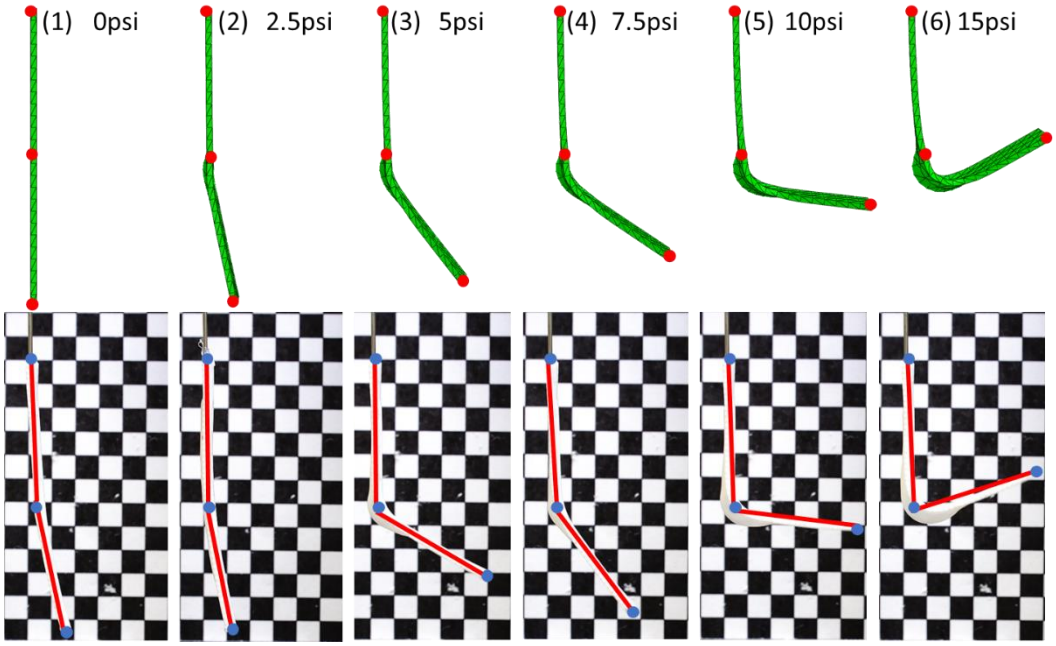

Figure 5.3.10 Comparison of fabricated and simulated soft planar inflatable discrete bending actuator.

Table 5.3.4 Comparison of fabricated and simulated models of soft planar inflatable discrete bending actuator; Based on Figure 5.3.10

No.	1	2	3	4	5	6
Simulated Angle Ø (°)	0	10.17	35.54	55.04	77.89	108.32
Average Measured Angle Ø (°)	8.00	13.35	36.21	55.35	77.78	106.16
Difference Δ (°)	-8.00	-3.18	-0.67	-0.31	0.11	2.16
σ Average Measured Angle (°)	0.233	1.232	2.516	4.000	1.191	0.698

5.4 Summary

Existing design concepts and configurations are based on experiences and creativity of an individual researcher regardless of digital design tools and graphical illustration software. As a result, conceptual designs of any component must endure many time-consuming steps, consisting of design, prototyping, evaluation and optimisation, to fulfil and achieve the desired criteria or specification. A cohesive design method was approached with finite element analysis towards modelling and simulating of soft planar actuators based on the designed SPIC fabrication technique.

The proposed route starts with investigating and characterising elastomeric material properties. The understanding of soft material properties was then reviewed from a computational method of hyper-elastic mathematical models to define continuum deformations in a finite element space. The concept of soft material characterisation was discussed with the use of curve fitting of hyper-elastic models to obtain hyper-elastic coefficients. There is currently no established cohesive library of common elastomeric materials often used by the soft robotic research community with their hyper-elastic coefficients. However, such research are being conducted with a sparse number of published data have investigated the performance and characterisation of several hyper-elastic models and methods. It is noted that reported differences in numerical coefficient derived from several sources are often due to differences in testing equipment, methodology and also sparse material choice and vague FEA solutions from authors. The collected data from published works only serve as a reference point to enable the modelling approach. Future work within this study has plans to create a hyper-elastic material model library to aid and contribute the development of soft robotics.

The modelling process is then described as a step-by-step method to analyse soft inflatable robotic components within an FEA environment. FEA solutions and software inputs were highlighted that additional steps and settings used to enable the success of simulation is often conducted through trial and error. These settings were found to be not material specific but method oriented in terms of computational analysis and software features. A general procedure can still be

utilised to conduct soft modelling approaches, however, further understanding of finite element analysis may be required to provide a cohesive deduction of modelling methodology and evaluation of simulated results.

From the understanding of soft modelling and simulation presented, the design parameters based on SPIC fabrication method introduced in Chapter 3 is revisited. The two design parameters, (1) selective material layering and (2) structural geometry variation were further developed in this chapter by presenting a number of variables and a numerical method to quantify them. A layer ratio (L_r) was introduced based on a general 3-layered configuration consisting of a mask layer between two elastomeric layers. The layer configuration omitted the use of strain-limiting layers to instil simplicity and act as a fundamental point of development. With a defined mask layer thickness of 0.1 mm, the layer ratio can be calculated based on the desired overall composite thickness. In structural geometry variation, a numerical method was introduced to define cavity band (C_b). Of which, derives from the desired actuator width (A_w) and cavity width (C_w), while the length is subject to preference. To illustrate the structural geometry variation of the cavity, a design was presented towards the concept of a soft planar inflatable continuous bending actuator, SPICA. Through a matrix modelling method scheme, a set of design parameters were enlisted and a series of SPICA were chosen to be fabricated and evaluated to validate the modelling approach.

Results from comparing simulated and fabricated SPICA from a visual aspect showed the efficacy and viability of the modelling approach and SPIC fabrication method. It is noted that the measured bending angles from simulated and fabricated models were not comparable. However, the results can still serve as a fundamental development tool to assist further development and designs for the actuators. The comparison of all SPICA, provided a visual comparison of the simulated and fabricated models. However, some fabricated models differ in inflation profile due to possible incomplete removal and residue of mask layers obstructing within the cavity of the actuators. Despite this, the bending angles measured were not conclusive to the simulated models either. However, this is noted that the visual efficacy of the simulated models may be subjected to assumptions, unrealistic values

and omitted cases (e.g. gravitational forces). As such, the simulated models only serve as visual aid towards the expected behaviour of the fabricated models. Hence, the efficacy and feasibility of soft modelling of SPIC was deemed acceptable while further development is still required to fully expand the capabilities possible in this study.

The development was followed by the design of a soft planar inflatable discrete bending actuators, SPIDA. The design of the SPIDA drew inspiration from Ranzani *et al*., to exhibit a joint-like bending as compared to a continuous bending and curling [165]. The SPIDA design differs in cavity shape compared to the SPICAs, but retains in overall actuator dimensions for actuator width of 5 mm, elastomer material and layer configuration. Upon characterisation, the modelled and fabricated bending angles were comparable in both visual and measured bending angles. Measured difference in modelled and fabricated angles marked at < 8^{o}, while standard deviation of the average bending angles logged at 4. The actuators were capable of displaying a distinct bending structure similar to folding a semi-rigid structure (i.e. paper or plastic). Comparing Razani *et al.*, the study here adopted its conceptual parametric study on layer configuration, however, the fabrication method, elastomeric material and variable introduced in the SPIC actuators presents a novel approach. Further characterisation, such as blocked force, were initially considered. However, due to the sheer size of the actuator, the smallest load cell of 10 N available was not able to detect any force from the fabricated SPICA and SPIDA. In addition, increasing the pressure during blocked force test has resulted in breakage of the actuators due to the 0.15 mm layer thickness and may have exceeded the possible strain percentage due to the conflicting forces. Further characterisation and development of soft modelling FEA approaches could potentially provide solutions to the analysis above with potential to include embedded mechanical programming layers. In summary, the chapter has showcased the feasibility and viability of soft modelling approach via FEA techniques and the SPIC fabrication technique to develop soft planar inflatable bending actuators. Further development and improvements are still being made. However, a complete hyper-elastic material library and further extensive understanding of finite element method may further expand and aid the modelling approach and the research in the field of soft robotics.

Chapter 6 Case Studies

This chapter presents how the developed fabrication technique of soft planar inflatable composites (SPIC) are applicable in real-life applications in the form of case studies. The first case study showcases the design applicability compared to conventional soft pneumatic actuator design for bending motion. The study is presented from a conceptual design, fabrication technique and performance characterisation of the actuator. The second case then presents an adjustable stiffness soft sensor. Based on previous research studies within the research group, a magnetic based soft sensor is redesigned with the developed SPIC fabrication technique. The study is presented from a conceptual design, fabrication technique and characteristics of sensor capabilities. A third and final case study then showcases several soft inflatable composite robots to further highlight the potential of SPIC. Several soft planar inflatable composite robot proofs of concepts done in this case study are, a quadrupedal soft robot, a foldable petal and a cube. The study presents the use of multi-material layering as oppose to single material layer optimisation and cavity design.

Work contributing to this chapter was published in RoboSoft'18 (Soft Robotic Conference 2018).

Kow J; Culmer P; Alazmani A. (2018) Thin Soft layered Actuator Based on a Novel Fabrication Technique. IEEE RAS RoboSoft'18. https://ieeexplore.ieee.org/abstract/document/8404916.

Kow J; Jones D; Culmer P; Alazmani A. (2020) Adjustable Stiffness Soft Sensor via a Soft Lamination Fabrication Technique - (To-be-submitted)

6.1 Case Study – 01: Thin Soft Layered Actuators

Soft actuators, such as pneumatic networks (PneuNet) [36] and fibre-reinforced pneumatic artificial muscles (FPAM) [37, 164] have inspired variants of soft pneumatic actuator (SPA)'s designs over the years, all of which uses a form of moulding or casting in their fabrication process. Attempts have been made to build smaller SPAs based on 3D printed moulds, despite the feasibility, due to design and geometrical constraints of moulding techniques, the ability of these actuators to operate in applications with narrow and limited space are somewhat limited due to its general design parameters, scale (centimetres) and overall actuation behaviour around a workspace [130, 166, 167]. Moreover, as described in Chapter 2, moulding-based fabrication techniques are inherently limited in the geometries they can produce, which consequently limits the functionality of the actuators they produce.

As soft pneumatic actuators are not typically designed in a planar manner, the cavity design of the thin soft layered actuators follow an empirical design manner of PneuNets [4]. As a class of soft actuators defined by Whitesides Research Group (Illievski,2011), its design is made up of a series of parallel chambers embedded in an elastomer body. When pressured through a single source of pressure, the chambers inflate in an expanding manner like the inflation of a balloon. As each chamber inflates due to the internal pressure, the external surrounding silicone starts to deform in shape and contacts the adjacent chamber. Due to the overall geometrical shape of the actuator and the difference in structural modulus, a 'bending' and 'elongation' motion is caused by the additive effect of the actuated network of pressured chambers. Figure 6.1.1 illustrates the describe motion of a PneuNet actuator by Ilievski *et al*. and Polygerinos *et al*. [4, 168].

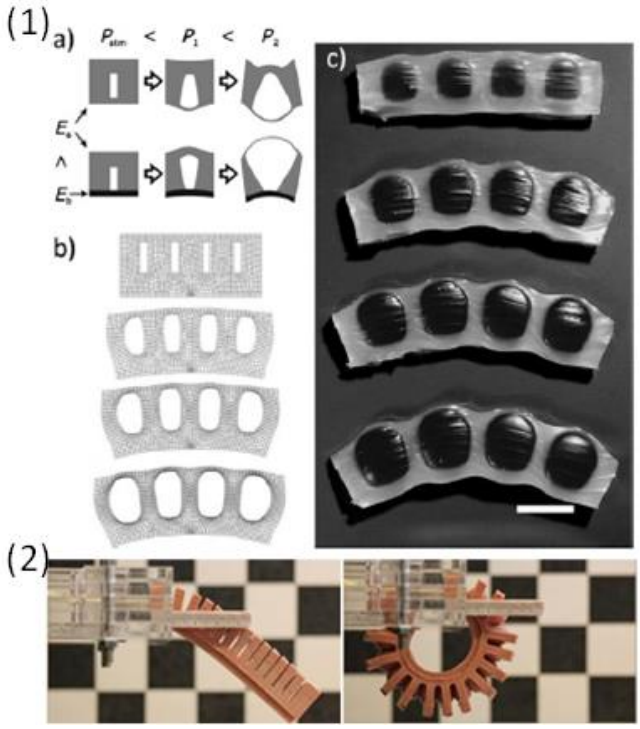

Figure 6.1.1 Pneumatic inflation effect due to geometry of the chamber and material properties of the material surrounding the chamber by Ilievski *et al*. [4];(2) Soft Pneumatic Actuator-Polygerinos *et al*. (2013) [168]

In order to address the shortcomings of conventional SPAs, there is a need for a wider flexible fabrication methods that can easily produce soft actuators at small scales (millimetre range) with precise features and functionalities that can be easily designed. In this study, the concept of soft planar inflatable composite (SPIC) and its fabrication technique developed was initiated with this study and development of a millimetre-scale soft layered pneumatic actuators (SLPA). As such, the conceptual designs, fabrication capabilities, and overall development is considered stand-alone within this study. Prior to the use of soft modelling FEA techniques and the implementation of the design parameters expressed in Chapter 5, initial actuator development follows an empirical design manner that is reflected and referenced against published soft pneumatic actuators within the field of soft robotics.

6.1.1 Conceptual Design

The proposed SLPA consists of soft elastomeric layers, strain-limiting layers and mask layers stacked on top of each other to form a composite build, as shown in Figure 6.1.2(a) and (b). The design follows a common composite build as introduced in Chapter 3. Without the use of FEA modelling and simulation, the incorporation of a strain-limiting layer is introduced for embedded mechanical programming in this study. The stiffness of the overall elastomeric layers must be less than that of the strain-limiting layer such that it bends or deforms readily. A stiffer elastomer or inextensible material (i.e. fabric, paper, and polyethylene terephthalate (PET) film) can be used for strain-limiting layers. The strain-limiting layer acts to resist various types of strains in one or multi directions until its yield strength is reached. Upon actuation, expansion of the inflatable layer is directed by the strain-limiting layer, causing a bending motion or resultant force which can be exploited for actuation.

Using this concept, the stiffness, overall thickness, inflation profile and geometry of the soft actuator can be manipulated layer-by-layer, with the selection of appropriate materials, profiles and consideration of their configuration relative to each other.

Prior to the conceptual design parameter of SPICs, preliminary designs of SLPAs were focused on two key design parameters of the actuator; (1) channel configuration and (2) cavity width, from an empirical manner from conventional soft pneumatic actuator design. Two channel configurations were designed to investigate the effect of placing pressure lines in different locations (DL: Dual-line channel, SL: Single-line channel), while the total channel width of 3 mm remained constant between different configurations. As shown in Figure 6.1.2(c), a nominal spacing between cavities was set at 5 mm for two cavity width configurations of 5 mm and 3 mm. In addition, the total thickness of the actuators is noted to be set at 3mm, its layer configuration can be referenced in Figure 6.1.2(b).

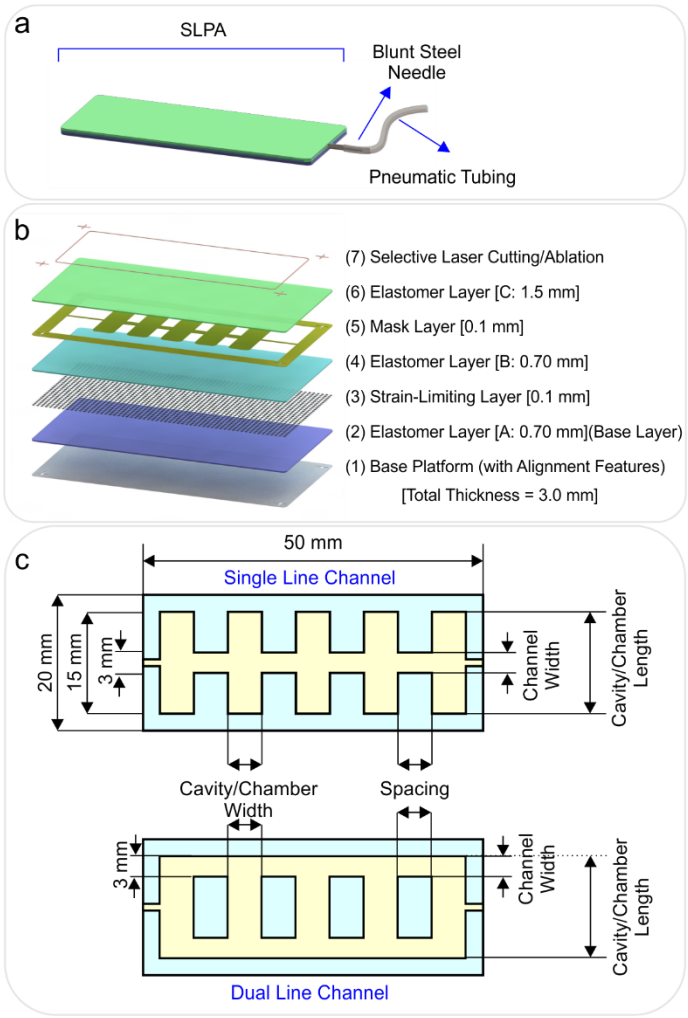

Figure 6.1.2 (a) Conceptual design of the SLPA; (b) Schematic diagram of SLPA, including layer thickness (orthogonal view); (c) Conceptual design and features of SLPA.

6.1.2 Fabrication Technique

As presented in Chapter 3, a step-by-step schematic provides a sequential fabrication process for the proposed actuator. In this case, the fabrication of each soft layered pneumatic actuator, SLPA, follows a similar process and is described below:

(1) Pre-polymer elastomer is prepared, in this instance EcoFlex™ 00-50 is mixed for a total of 2 minutes and 30 seconds in a centrifugal mixer. (2) Once mixed, the applicator is set to the desired applicator thickness and pre-polymer elastomer is poured towards the spread plate and dragged across the platform at 2 mm/s spread speed. A fabric mesh with a known thickness is then placed on top of the pre-

polymer elastomer layer to embed into the actuator; acting as a strain-limiting layer at the configured layer stage. (3) The platform is then removed and placed into an oven at 75^{o}C for 15 minutes. (4) Once the elastomer layer has been cured, the platform is adjusted to compensate to the new layer height and another layer of elastomeric material is applied to the composite. This step is repeated over several times which will include a mask-layer which creates a cavity for pneumatic or hydraulic actuation, strain-limiting layer for shape change morphological reaction and elastomeric material for encapsulation. (5) After the final layer stage of elastomer is cured, the fabricated actuator is then removed from the platform using laser cutting. The mask layer is made of water-soluble paper is removed from the fabricated actuator by flushing with water, leaving a 'zero-volume' chamber for actuation, or in this case pneumatic inflation.

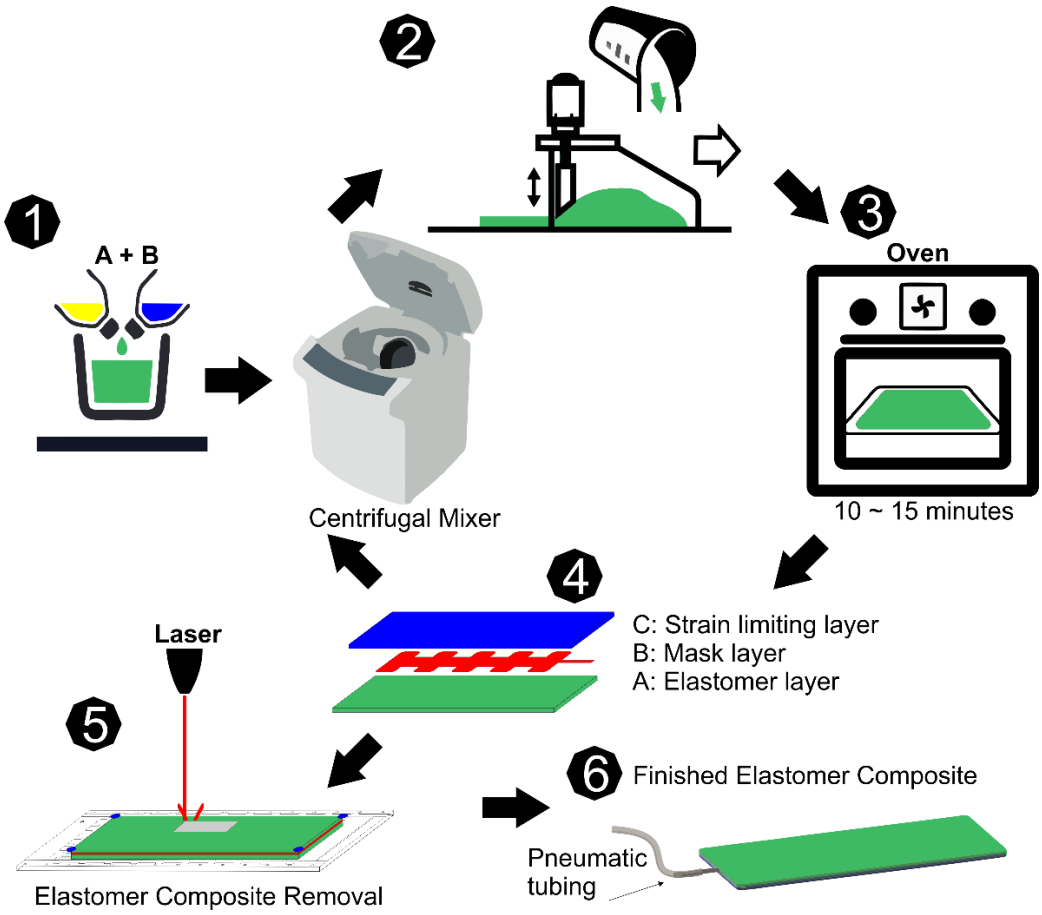

Figure 6.1.3 Illustration of SPIC fabrication process for SLPA. A step-by-step process is described in the context above.

6.1.3 Experimental Design

A custom experimental test set-up was assembled to measure block force and bending angle of each SLPAs across a range of controlled input pressures (0 to 5 psi). For each test, the actuators are inflated using a custom syringe driver consisting of a linear stage of 175mm travel distance and a 50ml syringe.

An analogue absolute pressure transducer (30 PSI SSC series absolute pressure transducer, HoneyWell, USA) was used to monitor and regulate the pressure applied to the actuator. A 6 axis loadcell (Nano25, ATI Industrial Automation, USA) was used to measure the block force generated by the SLPAs. The actuator side surface was placed in contact with a rigid Perspex plate to minimise nonlinear effects due to bending. The pressure inside the actuator was then incrementally increased and normal force exerted by the SLPA's tip was recorded. Each experiment was repeated 5 times to assess accuracy and repeatability. A custom program was developed using LabVIEW (National Instruments, USA) to acquire the measurements from the loadcell and pressure transducer, while controlling the syringe pump at the set static input pressures.

The bending profile of the SLPAs at controlled input pressures were recorded by using a high definition camera (D5300, Nikon, Japan) along with a measurable calibrated backing pattern (5 mm x 5 mm Grid). Intrinsic calibration of the system was conducted to mitigate lens distortion effects and verify measurement accuracy. Post-processing of the images was performed using an open-source image analysis program (ImageJ, Image Processing and Analysis in Java), in which the Cartesian X and Y coordinates of the actuator tip were tracked, and the resultant total bending angle was calculated.

6.1.4 Results and Discussion

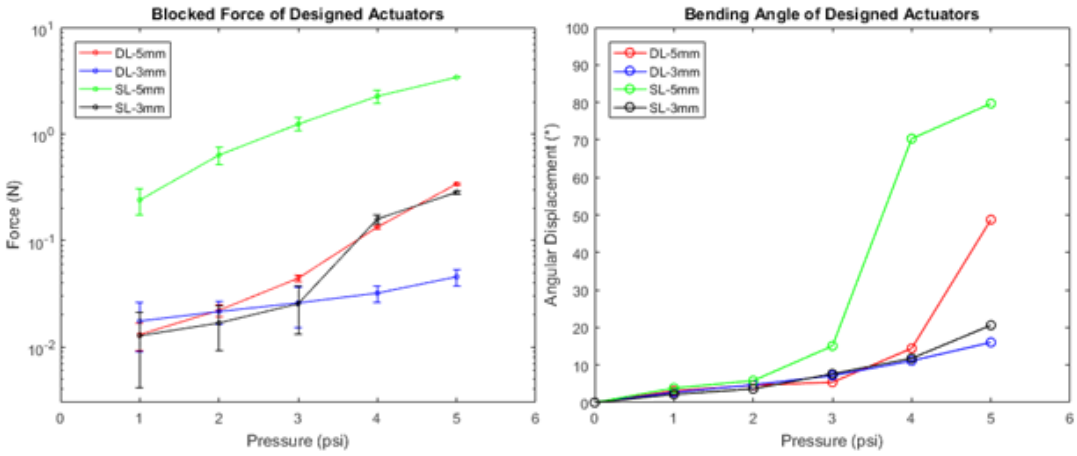

Figure 6.1.4 Results of the blocked force (left) and bending angle (right) response for the SLPAs at five static input pressures between 0 and 5 psi.

Table 6.1 Results of the blocked force and tip bending angle response for the SLPAs at five static input pressures between 0 and 5 psi.

tSLA Designs	Blocked Force (N)					End Tip Angel (deg)				
	1 psi	2 psi	3 psi	4 psi	5 psi	1 psi	2 psi	3 psi	4 psi	5 psi
SL – 3 mm	0.0127	0.0168	0.0254	0.1586	0.2830	2.1890	3.6500	7.6480	11.7800	20.6160
SL – 5 mm	0.2390	0.6313	1.2340	2.2548	3.3974	3.8400	5.8300	15.0830	70.3470	79.6950
DL – 3 mm	0.0175	0.0215	0.0259	0.0320	0.0455	2.7440	4.7300	7.1930	11.1340	16.0420
DL – 5 mm	0.0130	0.0220	0.0441	0.1334	0.3381	3.1110	4.6280	5.4040	14.4450	48.7410

The range of prototype actuators were evaluated using static pressure tests in which the actuator's blocked force and bending angle were measured. All SLPAs were subjected to static pressure between 0 and 5 psi at 1 psi increments and all completed these tests without failure. The experimental results for the blocked force of the SLPAs are shown in Figure 6.1.4. In all designs, the blocked force generated by the SLPAs increases with input pressure. The actuator showing the best performance (5 mm chamber width, single channel) showed a maximum blocked force of 3.5 N at 5 psi static input pressure. The SLPAs with 5 mm chamber width obtained significantly higher blocked force output when compared to the narrower 3 mm chamber design across all input pressures. As shown in Figure 6.1.4 and Table 6.1, the channel design (single line in the centre or double lines on the sides) can have significant influence on force generation. From our results, the blocked force

increased by 10-fold for the 5 mm chamber width in the single-line channel design when compared to the double-line.

The free response of the actuators shows that the SLPA bending angle increases with pressure across all designs as shown in Figure 6.1.4 and Table 6.1. Similar to the blocked force experiment, the bending angle of the tip is significantly higher for the 5 mm chamber width design. The channel design is also influential, for the same cavity width, double lined configurations show lower bending. It was noted that there was expansion of the double channels at either side of the actuator which resisted the bending moment of the SLPA, hence constraining the bending of the actuator in comparison to a single channel configuration.

The sensitivity of the actuators to input pressure exhibits a noticeable non-linear response. For input pressures up to approximately 3 psi, small changes of bending angle were observed per unit pressure change. A possible explanation is that, in this pressure regime, the SLPAs stiffens by first expanding against the strain-limiting constraint fabric layer. Beyond this point, small changes in input pressure generate far larger changes in bending angle and these effects are amplified based on the cavity width. Following these initial investigations, the prototype SLPAs were subjected to additional testing to explore the bending characteristics across a range of pressures. The results for the 3 mm chamber width and single channel configurations are presented in Figure 6.1.5, showing the Cartesian position of the actuator segments and corresponding images from which, these measures were obtained. The non-linear response of the actuator across the pressure range is again evident in this response. For pressures up to 3 psi the actuator produces a near-linear response with low curvature. Beyond this, at 4 and 5 psi, there is a marked change in the form of the actuator, with higher curvature which increases toward the tip. Inspecting the images shown in Figure 6.1.5(a) shows this is linked to expansion of the zero volume chambers and is a factor which could be controlled through manipulation of the constraint layer.

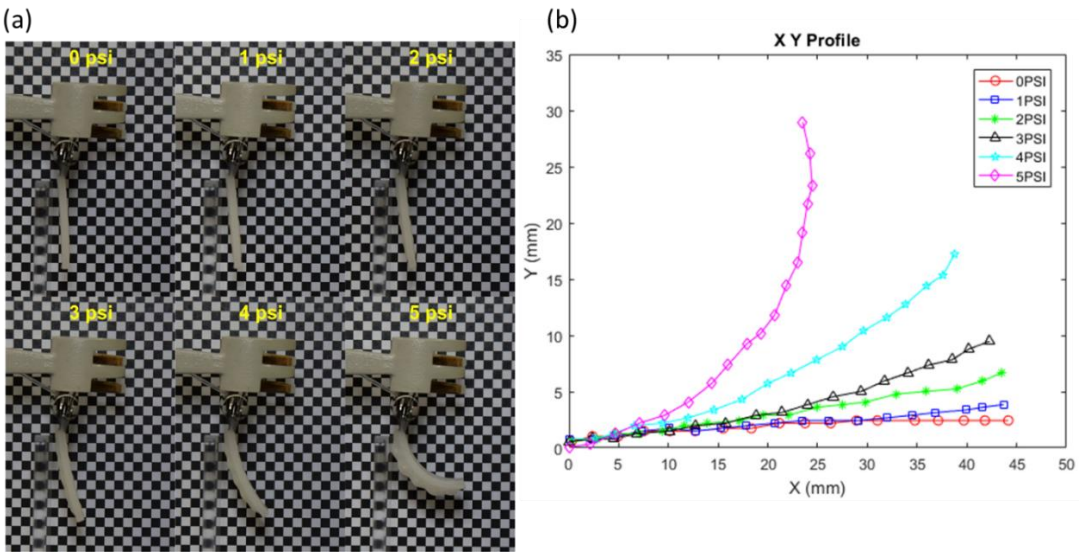

Figure 6.1.5 A prototype SLPA with 5 mm chamber width and single line channel design; (a) Side view of this actuator at 0 to 5 psi input pressures, (b) Calibrated X-Y profile of the actuator

6.1.5 Conclusion

In this study, the developed soft layered pneumatic actuator (SLPA) fabrication technique was used to demonstrate a series of soft layered pneumatic actuators, SLPA, based on empirical design of soft pneumatic bending actuators. Using SPIC fabrication, the thickness of each layer can be carefully controlled using a film applicator. This study also incorporates a strain-limiting layer as commercially available film/sheet (i.e. polyvinylidene chloride (PVDC), polyethylene terephthalate (PET), Kevlar), which can be incorporated into the fabrication process without additional resizing or pre-processing. These design features of SLPA fabrication aid repeatability of the process and enable smaller features to be embedded within soft robotic systems, hence, offering the possibility of reducing the overall scale of soft systems. Compared to an empirical bellow cavity design as seen from generic soft bending actuators, such as PneuNets, FPAM or other SPA variants; there is a need to introduce a new design approach for the soft layered pneumatic actuators. As evident in the study presented in Chapter 5, the design of soft planar inflatable composites (SPICs) highlights the possibility of thinner (< 2 millimetres thickness) and performant actuators possible. Nevertheless, this study reinforces the possibility and opportunity for millimetre-scale soft composite devices with precise operation

which can be readily tailored for application specific requirements. The study was conducted prior to the advancement and progression of the current fabrication platform proposed in Chapter 3 and the design parameters and modelling approach introduced in Chapter 5. As such, the case study is projected as a progression case which contributed to the main research development and advancements.

6.2 Case Study – 02: Adjustable Stiffness Soft Sensor

Previous work within the research group have presented the base work towards a magnetic field based soft tri-axis tactile sensor known as MagOne [169]. The working principle of the sensor takes effect when an external force (normal and/or shear) is applied to the surface of the elastomer and effectively displacing the embedded magnet within the elastomeric body. By measuring the magnetic field vectors through the Hall-effect sensor, the displacement of the magnet can be obtained in three-axis. The force applied to the elastomeric body can then be extracted based on the structure's mechanical behaviour. The development provided a low cost, readily adoptable fabrication method and a robust sensitive force measurement in a calibrated operating range based on different silicone material and dimension. In addition, a toolkit was developed to calibrate and tune the magnetic and force characteristics for optimisation purposes [170].

However, due to material properties of different elastomeric materials, the sensitivity of the overall sensor system is problematic for applications which involves both high sensitivity and the ability to measure a wide range of forces. The sensor's range for different applications can be fabricated from materials of different material compliances (shore hardness or Young's modulus). However, when stiffer elastomeric properties are adopted it leads to a lower sensitivity of the overall sensor system. As such, high sensitivity and dynamically increasing forces are not ideal due to the innate characteristics of the elastomer, sensor and optimisation.

To remedy this limitation, a variable compliance sensor was developed in the form of a dome with a hollow cavity that can be pressurised through a pneumatic supply

[171]. By varying the cavity pressure of the dome, this created an artificial change in the overall stiffness of the sensor, allowing dynamic control of its mechanical compliance without changing the material composition. This allowed the sensor's range and resolution to be dynamically varied without changing the elastomer, thereby overcoming the limitation of the previous sensor iteration. The variable stiffness enables a dynamic range of controllable sensitivity, enabling use in a wider variety of applications and situations. However, due to the innate structure of the dome, the action of applying pressure causes a 'ballooning' effect where the surface rapidly expands toward a spherical shape. This is particularly evident in softer elastomers. In this state, the accuracy and compliancy of the structure would effectively be hindered due to the uncontrollable shape change when pressurised.

Following previous contribution research works in soft magnetic-field based tactile sensor and soft magnetic tactile sensor with variable stiffness, the fabrication technique adopted a conventional moulding and casting technique. As such, the geometrical aspect of the sensor drove the working principle of the overall capability and performance. Compared to a fully soft silicone body coupled with a 3D Hall-effect sensor for measurement of normal and shear forces, this study present a novel flat soft tactile sensor capable of variable mechanical compliance and shape change through soft planar inflatable composite (SPIC) fabrication technique to create soft composites pads, as illustrated in Figure 6.2.1 [88, 169, 171] .

6.2.1 Conceptual Design

The concept of soft variable stiffness sensor pad designed to exploit the SPIC fabrication technique to generate a multi-layered composite structure based around an elastomeric zero-volume chamber with strain limiting layers and an embedded magnet as a sensing target, as shown in Figure 6.2.1(b). The chamber may be pressurised across a range of pressures to modulate the structural stiffness of the sensor and thus the overall sensing range. The strain limiting layer acts to limit the structural shape of the inflation to avoid a 'ballooning effect' or exceed maximum strain of material.

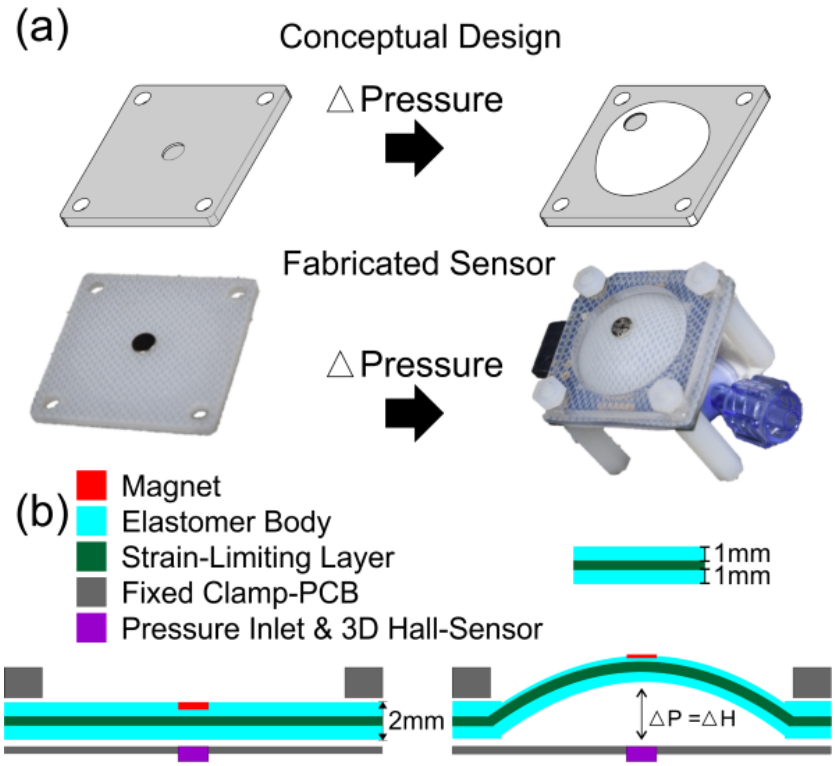

Figure 6.2.1 (a) Conceptual design and fabricated sensor illustration (b) Layer schematic of flat magnetic sensor pad

The initial state of the elastomeric composite is composed of a flat sheet of silicone of 2 mm thick with a fabric constraint embedded along the centre. When the soft pad is clamped and pressurised, a shape change is induced and would continue to expand given the hyper-elastic nature of the elastomer. The fabric constraint prevents this expansion, acting as a strain limiter to control and reduce the magnitude of inflation. The inflation profile is dependent on the material properties of the constituent layers of the soft sheet: the elastomer shore hardness and the tensile strength of the constraint layer. Through this method, the mechanical compliance of the material is dynamically varied by the variable pressure induced.

The working principle is illustrated in Figure. 6.2.2. This would produce a sensor with controllable levels of sensitivity and dynamic range, enabling it to be used in several applications towards tactile sensing. In addition, different elastomeric material based on shore hardness (EcoFlex™00-30, 00-50 and DragonSkin™ 30A) is used to highlight the shift in compliancy due to change in pressures. In result, different

elastomeric materials of varying mechanical compliance will produce different stress curves due to its hyper-elastic properties.

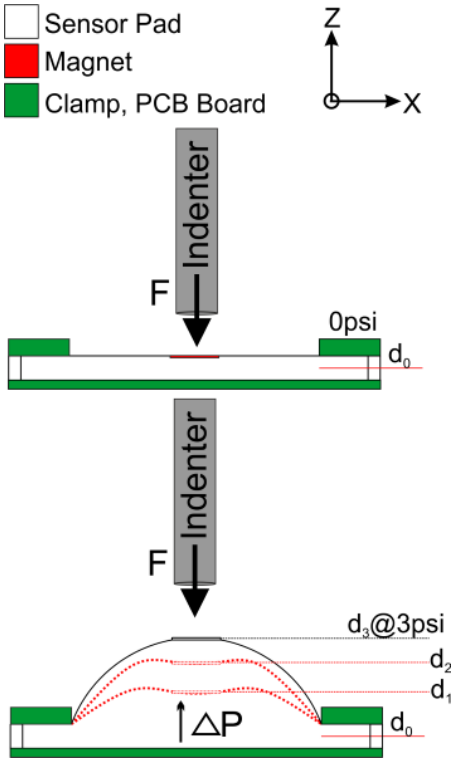

Figure 6.2.2 Illustration of sensor working principle. (Top) Sensor is not pressurised; (Bottom) Sensor is pressurised and actively displaced the magnet from its initial position.

6.2.2 Fabrication Technique

The fabrication of the flat-magnetic sensor pads uses the SPIC fabrication process as described in Chapter 3. An additional design step is added to introduce the permanent magnet to act as the sensor core. Based on the conceptual design, fabrication technique and the layer schematic of the sensor, a step fabrication process is as shown in Figure 6.2.3; and is described as followed: (1) Elastomeric material of desired properties are mixed (1:1 ratio) in a centrifugal planetary mixer for 1 minute and 30 seconds at 2000rpm. (2) Once mixed, the applicator is set to the desired applicator thickness and pre-polymer elastomer is poured towards the spread plate and dragged across the platform at 2 mm/s spread speed. A fabric mesh with a known thickness, is then placed on top of the pre-polymer elastomer layer to

embed into the actuator; acting as a strain-limiting layer at the configured layer stage. (3) The platform is then removed and placed into an oven at 75°C for 15 minutes. (4) Once cured, steps (1)-(3) is repeated until the desired layer configuration is achieved. (5) Once the composite structure is achieved, it is placed into a 50W laser cutter (VLS3.50 Universal Laser Systems) to cut out the desired shape using pre-defined alignment features on the build platform. (6) The sensor is then removed from the sheet, cleaned, and ready to be used.

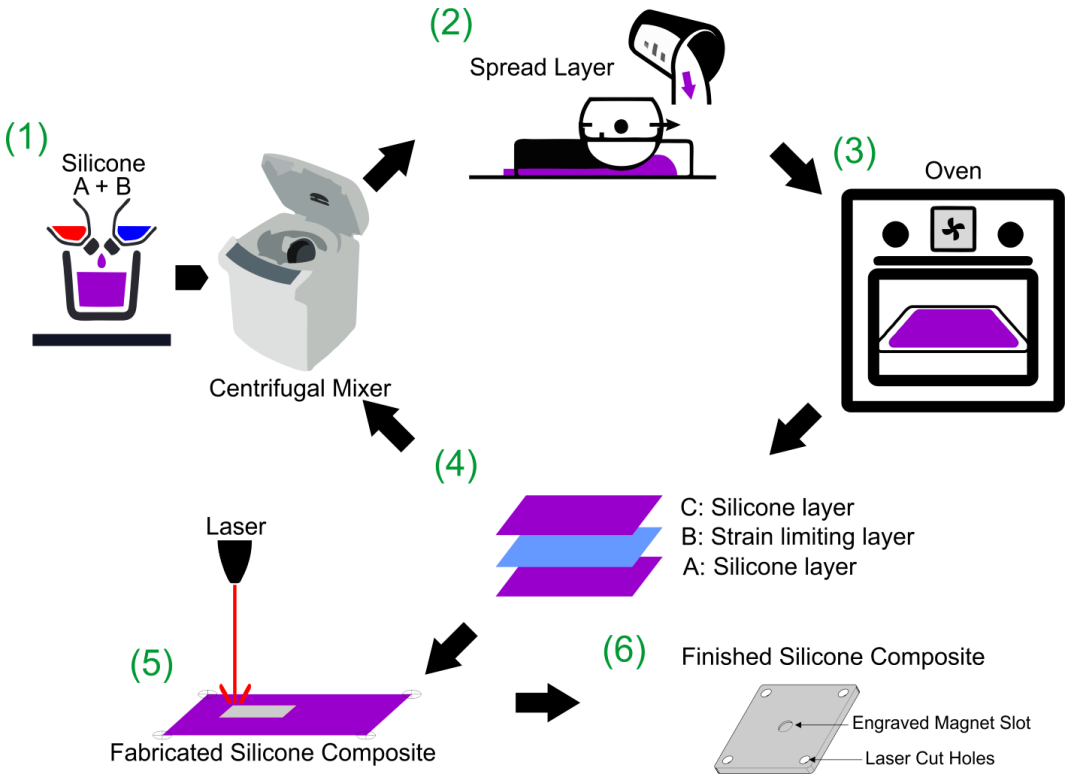

Figure 6.2.3 Illustration of sensor fabrication process. A step-by-step process is described in the context above.

The magnet slot on the surface of the sensor is engraved by the laser based on the thickness of the magnet to be embedded. The selective laser cutting process can be used not only to cut the composite sheet and separate it from the base build platform, but also to cut individual layers and/or patterns to produce desirable features, such as engraving the magnet slots on the silicone.

The settings for the selective laser cutting process is as described and obtained in Chapter 4. The fabricated sensors are then cleaned (using isopropanol or soapy

water bath) and left to dry prior to embedding the magnet. The magnet is then embedded with epoxy (E41 Elastosil, Wacker Silicones) and left to cure. Once cured, the sensor samples can then be mounted on a bespoke test rig to be clamped and actuated for characterisation and testing.

6.2.3 Experimental Design and Characterisation

Characterisation of the flat magnetic variable pressure sensor prototypes were performed to consider the effect of two key design parameters on the sensor behaviour; (1) the measurement range based on pressure change and (2) mechanical compliance due to material change.

As shown in Figure 6.2.4, a custom experimental test rig was assembled to characterise the sensor(s) performances and properties. For each test, the sensor was pressured across a range of controlled input pressures of using a pneumatic control unit operated by electronic servo-valves (SMC ITV0010-15PSI Pressure Regulator, SMC, Japan). The internal pressure of the sensor is monitored and regulated using an analogue absolute pressure transducer (15PSI SSC series absolute pressure transducer, HoneyWell, USA). Two linear stages (T-LSR75B, Zaber technologies Inc, Vancouver, Canada) were arranged in the Z- and Y-axes relative to a pin mounted (indenter) load cell and sensor mount. The sensor was then mounted and subjected to a vacuum to remove any air encapsulated along the tube, before measuring the position of the top surface of the magnet. The sensor was then inflated and compressed along the Z-axis with an indenter from its inflated position until the magnet reached a set point (d_0, 1mm from the surface of the pad); (i.e. d_3 to d_0), as illustrated Figure 6.2.2. The indenter was mounted on a 6-axis loadcell (Nano17, ATI Industrial Automation, USA) to measure the force applied to the sensor throughout the compression, shown in Figure 6.2.4 and illustrated in Figure 6.2.2.

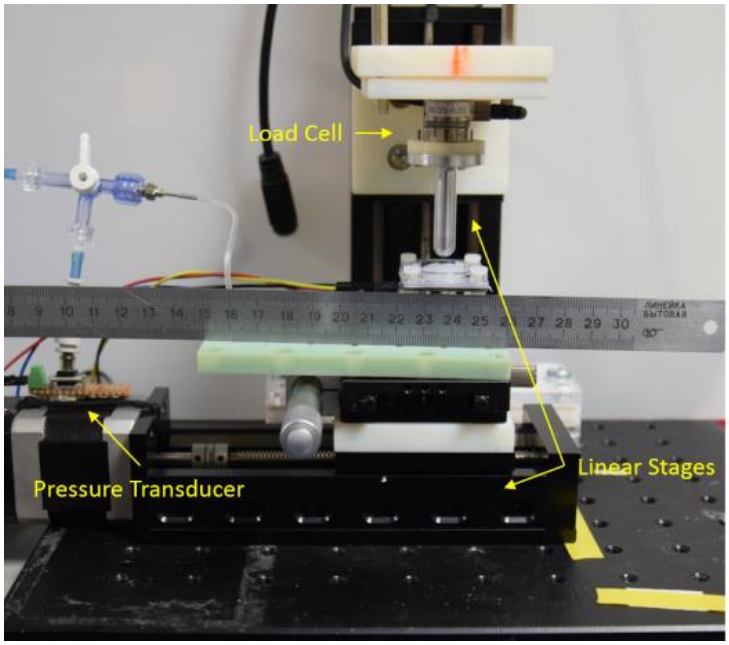

Figure 6.2.4 Experimental set-up used to characterise the sensor

To investigate the effect of pressure, the compression tests were conducted by pressuring the sensor across a range 0 psi to 3 psi in 1 psi increments. This pressure range was selected based on preliminary tests to avoid exceeding the strain limit of the fabric spandex at higher pressures of 4psi for softer silicone materials. To investigate the effect of the elastomeric material properties, the sensor was fabricated using three different silicones (EcoFlex™ 00-30, EcoFlex™ 00-50 and DragonSkin™ 30A). Four samples were fabricated for each material. Each sensor sample was then tested across four repeats to assess repeatability of the sensor. Each test consisted of 5 cycles to investigate factors of hysteresis, magnetic drift and material creep.

During each test, the inflation profile heights were recorded using a high definition camera (D5300, Nikon, Japan). As the sensor is pressurised, the sensor undergoes shape change, as such, a larger displacement of the magnet is achieved, along with the stiffness change due to pressure induced in the cavity. Post processing of the images was performed using an open-source image analysis program (ImageJ Processing and Analysis in Java) in which the Cartesian Z and Y coordinates of the sensor inflation profile can be tracked and the displacement height of the magnet from the Hall-effect sensor can be calculated.

6.2.4 Results and Discussion

At each compression test, the stage is lowered to the point of contact to the sensor body and used as a starting point. At 0 psi (no controlled pressure) for all sensors of different materials, 1 mm was the set threshold displacement acting on the Z-axis (d_0), as illustrated Figure 6.2.2. The force acting upon the sensor at this point is directly indicating of pure compression of silicone on a solid backing (mounting board) and is used as the maximum threshold point for each sensor. In Figure 6.2.5(b), as the range of pressure increases, the results shows linearity towards mechanical compliance. Following that, to provide a force measurement range based on mechanical compliance as pressure is introduced and incremented, the inflation profile is calculated and/or the loadcell is lowered to the point of contact. Figure 6.2.5(a) shows the results obtained from the above mentioned, while Table. 6.2, lists the maximum force achieved at each pressure.

At higher pressures, softer elastomeric material (EF30: EcoFlex™ 00-30) shows a higher force compression as it gets closer to the maximum range of the sensor compared to its stiffer counterpart (DS30: DragonSkin™ 30A). This is due to the material compliancy in less stiffer material providing a stronger feed-back force as the internal pressure of the sensor is reflected by compression. Table. 6.2.1 highlights the maximum force point at different set pressures for different elastomeric materials.

Table 6.2.1 Maximum compression force at variable pressures

Material	Shore Hardness (ASTIM D-2240)	Max Force (N)at Pressure:			
		0psi	1psi	2psi	3psi
EcoFlex™ 00-30	00-30	2.389	1.059	1.973	3.293
EcoFlex™ 00-50	00-50	4.652	1.194	1.781	3.025
DragonSkin™ 30	30A	9.835	1.114	2.070	2.730

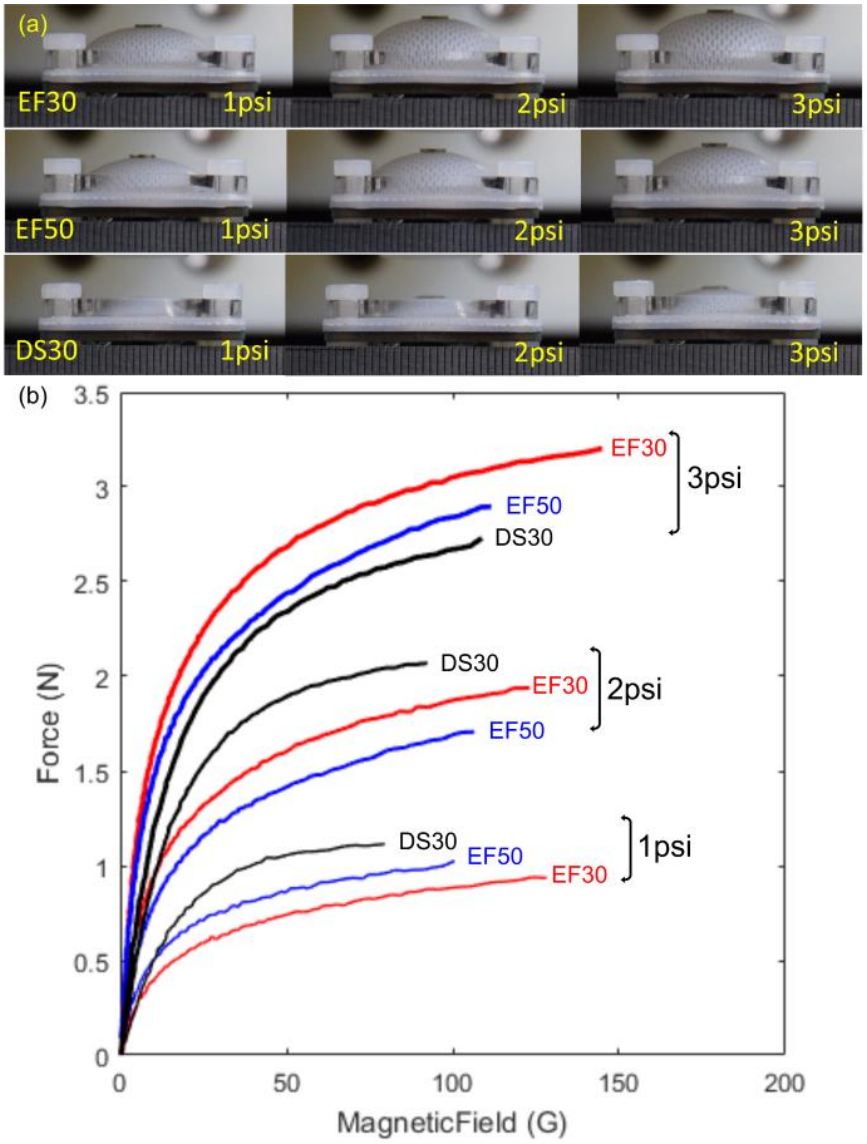

Figure 6.2.5 (a) Inflation profile of sensor pad based on range of materials (EF30 = EcoFlex™ 00-30; EF50 = EcoFlex™ 00-50; DS30 = DragonSkin™ 30A); (b) Stiffness change of the sensor when pressure is induced.

The sensor body mechanical properties can be split into two phases. The initial phase is compression on the elastomer given a pressurised cavity between the elastomer pad and the mounting board. The second is when the elastomer is being compressed to the board, showing the characteristic loading curve of a hyper-elastic material, illustrated in Figure 6.2.6. Owing to the varying inflation profile between pressure cases, the indentation displacement was varied between cases to limit the investigation to the first loading case, where the load is predominantly borne by the

pressurised chamber. Each sensor, regardless of material was treated as fully compressed when the magnet reached the same position as it was in the unpressurised sensor (d_0). Given that the sensor is clamped and then pressurised, the clamping force is approximately adjusted equally for all materials to provide an equal contact displacement for all sensors at zero pressure. As such, the second phase characteristic were omitted as the resultant force was due to pure elastomer compression against the mounting board as shown in Figure 6.2.5. While in Figure 6.2.6, the figure illustrates the overall mechanical properties changing phases at set pressures. Highlighted within Figure 6.2.6, when the elastomer begins to compress on the board, the shift in force curve can be seen across all three elastomers.

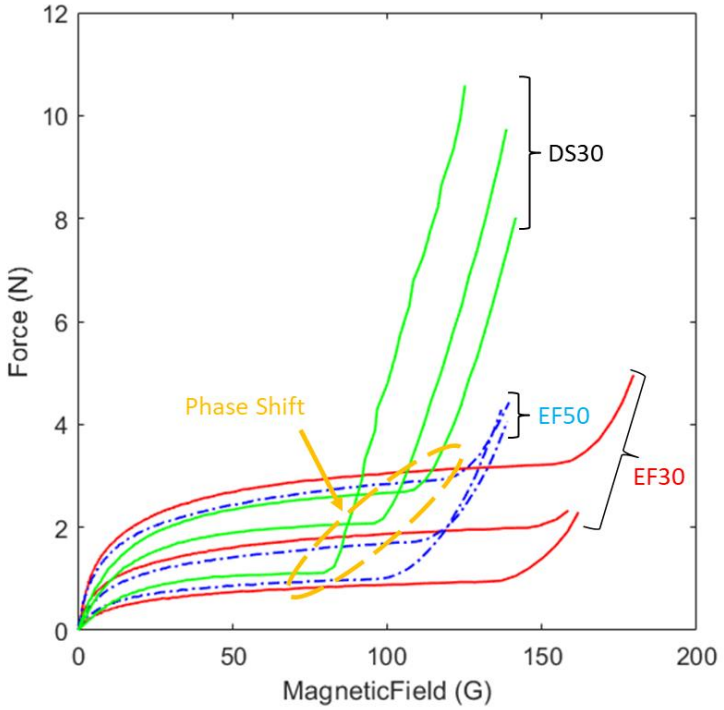

Figure 6.2.6 Inflation profile shift in mechanical properties displaying characteristic loading curve of hyper-elastic material. (EF30 = EcoFlex™ 00-30; EF50 = EcoFlex™ 00-50; DS30 = DragonSkin™ 30A)

Results in terms of displacement and magnetic force indicates that the sensor(s) performances are suitable for low force applications to provide high sensitivity. This is backed by the stiffness against pressure as shown in Figure 6.2.7(b). Depending on

elastomeric material choice, this highlights a feasible variable compliance and controllable stiffness sensor can be adjusted to distinct sensing applications.

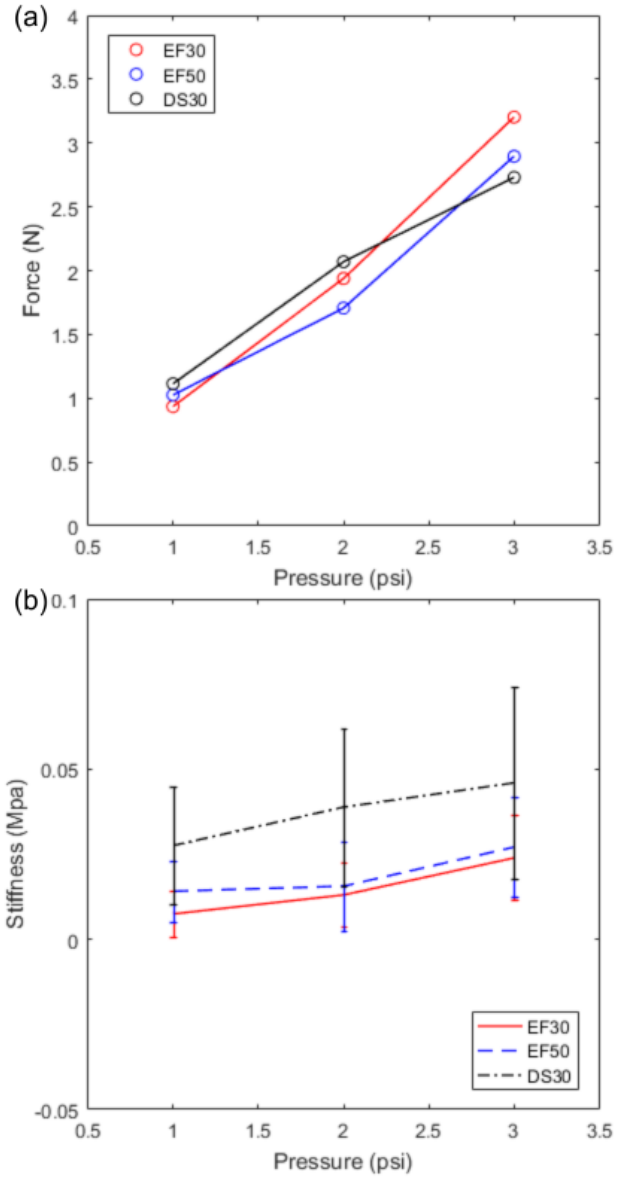

Figure 6.2.7 (a) Force range of the sensor when pressure is induced; (b) Stiffness change of the sensor-based pressure induced. (EF30 = EcoFlex™ 00-30; EF50 = EcoFlex™ 00-50; DS30 = DragonSkin™ 30A)

A maximum characterisation pressure range of 3 psi was set based on preliminary results. At 4 psi and above, there is a higher risk of tearing the embedded constraint material while leaving the elastomer intact, caused by the increasing tension within the constraint. These tears will lower the effectiveness of the strain limiting layer

and cause an uneven inflation across the sensor. Further to this, higher pressures may also cause pressure leakage from the edges of the pad as the clamp only effectively seals the pad at lower pressures.

The increasing elastomer stiffness affected both the range and sensitivity of the pressurised sensor. The stiffer DragonSkin™ 30A sensor exhibited a lower sensor resolution than the softer EcoFlex™ counterparts, owing to the reduced inflation and therefore lower magnet displacement under operation of the sensor. This means that smaller form-factor sensors may be produced from stiffer silicones in applications where higher sensitivity is not required.

By introducing pressure, the mechanical compliancy of the material was shown to be variable dependent on the pressures applied; with higher pressures inducing a higher overall stiffness to the sensor. When compared to compression on a fully elastomer sensors of similar shape (i.e. no air cavity) the pressurised sensor exhibits a different loading response. Under no load, each sensor of different elastomeric materials were pressured to 3 psi and its maximum inflation height was recorded, as shown in Table 6.2.2. The recorded inflation heights were then re-created through computer aided design to fabricate its equivalent moulds. Under moulding and casting technique, the equivalent materials were then fabricated as pure elastomer models and fitted with a magnet for sensing as shown in Figure 6.2.8.

Table 6.2.2 Maximum inflation height of sensor pads at 3 psi input pressures

Material	EcoFlex™00-30	EcoFlex™00-50	DragonSkin™30A
Height at 3 PSI (mm)	7.87	6.92	3.56

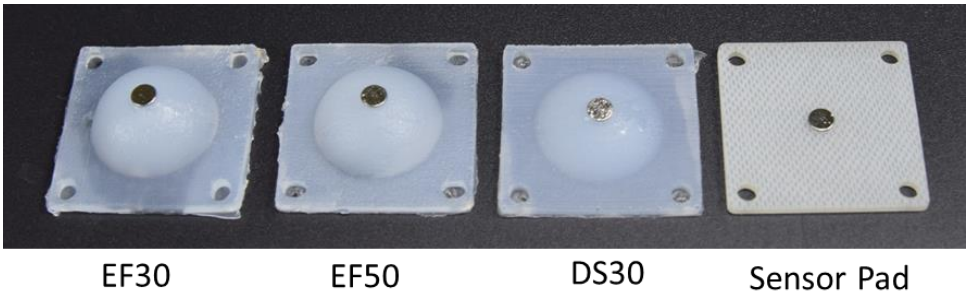

Figure 6.2.8 Visual presentation of fabricated elastomer models based on inflation profile detailed in Table 6.2.2. (EF30 = EcoFlex™ 00-30; EF50 = EcoFlex™ 00-50; DS30 = DragonSkin™ 30A)

The fabricated pure elastomer models were the experimentally subjected under the same characterisation method in terms of compression over a linear displacement. Shown in Figure 6.2.9, a comparison between a flat sensor pad of different elastomer materials at 3 psi and its fabricated pure elastomer models of equal inflation height as its flat counterpart for displacement and magnetic field against force. The comparison of the two modalities highlights that the shift in sensitivity based on compression on pressurised cavity compared to a purely elastomeric and structured model. The fabricated pure elastomer highlights the hyper-elastic model curve under compression, while the flat sensor pad changes the modality of the elastomer curve.

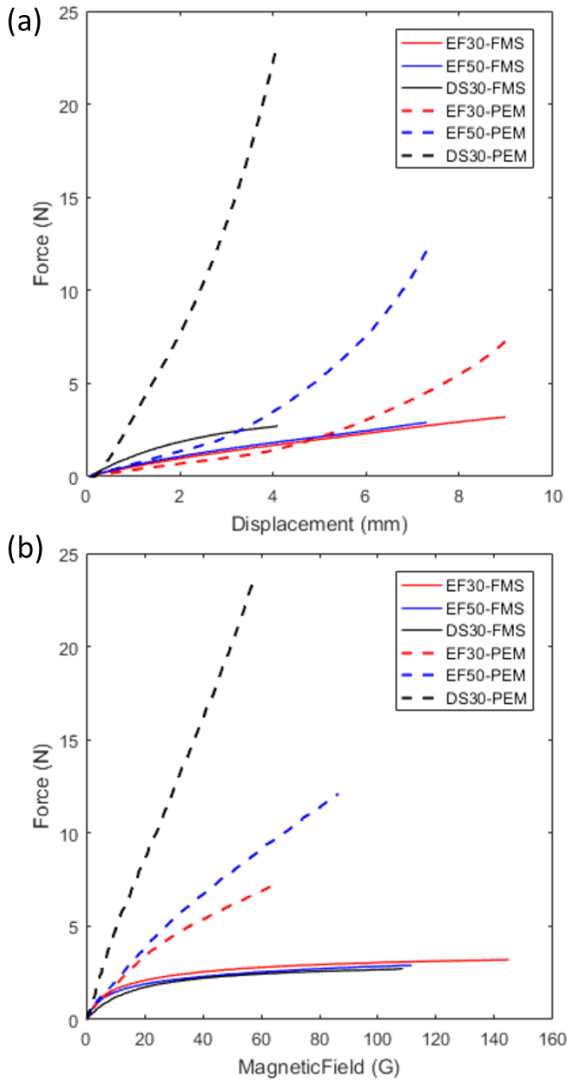

Figure 6.2.9 Comparison between pure elastomer model (PEM) and flat magnetic sensor (FMS at 3 psi) for all three elastomer materials. (a) Force against displacement; (b) Force against Magnetic Field. (EF30 = EcoFlex™ 00-30; EF50 = EcoFlex™ 00-50; DS30 = DragonSkin™ 30A)

6.2.5 Conclusion

In this study, a novel flat soft tactile sensor capable of variable mechanical compliance and shape change was designed and studied with the developed SPIC fabrication technique. The development highlights the fabrication method used to create a dynamically robust sensitive force measurement in a calibrated operating range based on different elastomeric material and induced pressures. Possible future work from this study could potentially include: (1) introducing of actual cavities for active/portable sensing pads; (2) structural inflation at a planar motion for sensitivity instead of balloon/spherical inflation. The work presented here can be applied towards surface to skin-like sensing applications and active tactile pads for force measurements. The study also notes that the use of equipment (load cell) described here was not available during the progression of Chapter 5.

6.3 Case Study – 03: Soft Planar Inflatable Composite Robots

In this study, the soft planar inflatable composite (SPIC) fabrication technique developed in Chapter 3 is used to design a series of 'robots' as proof-of-concepts to further highlight the potential of SPICs. Going back to the initial development of SPIC, the conceptual design depicts its morphology to be controlled through embedded mechanical programming with the use of strain-limiting material (constraint layer) and/or its overall material embodiment. The development of SPICAs and SPIDA enforces the use of design parameters classified in Chapter 5. By configuring the layer ratio (L_r) of the overall composite material, the inflation of the actuators exhibited expansion over a single surface due to the difference in layer thickness. However, as the actuator and cavity width (A_w and C_w) increases, a ballooning effect is still exhibited when inflated while cavity ratio (Cr) is maintained. Case studies 1 and 2 incorporated the use of a fabric mesh acting as the embedded strain-limiting material. The inflation of these fabricated composites showed a form of embedded mechanical programming to control the inflation expansion of the elastomers. However, elasticity and stretch ability of the composite is significantly reduced due

to the strain-constraint in fabric. Expanding the concept of embedded mechanical programming, a stiffer and less elastic elastomer is proposed to be used as a strain-limiting mechanism. By reconfiguring the selective layers of materials, a multi-material layered elastomeric inflatable composite with elastomer based embedded mechanical programming could further showcase the extensive possibility within the developed SPIC fabrication and soft robotic composites.

6.3.1 Conceptual Design and Development

The proposed development aims to incorporate the use of multi-material layering of elastomeric materials to include an overall material embodiment of inflation and embedded mechanical programming. To accomplish this, three robotic planar designs ((1) Cube; (2) Petal; and (3) Quadrupedal robot) of increasing complexity in overall shape and cavity geometry is developed to showcase the adaptability of the SPIC fabrication technique. Figure 6.3.1 illustrates the conceptual design of the soft planar inflatable composite robots (SPICRs). Referencing the design parameters described in Chapter 5, the SPICRs is set to the layer ratio (L_r) of 0.2 with a total composite thickness of 1 mm. However, its selective material layering is set to include a multi-material layering method consisting of an elastomer based strain-limiting layers. Its structural geometry variation (cavity design) is modified from possible and/or potential geometrical cavity designs inspired within the research and literature without the use of soft modelling approaches.

The designs of SPICRs follow several distinct geometrical attributes, such as channel width (1 mm wide), actuator size (width and length) and cavity ratio ($0.5>C_r<1.5$). The cube and petal design is intended to showcase self-folding from a planar design into a 3D shape when inflated (actuated). While the quadrupedal robot design is intended to mimic Shepard *et al*. soft quadrupedal robot of a similar design but differ in size, cavity complexity and fabrication technique [35]. The SPICRs were not assessed by soft modelling approaches, including channel configuration to assess pneumatic distribution and feasibility of cavity design inflation were not characterised and is based on creativity of the envisioned SPICR designs.

Without the aid of soft modelling and optimisation, the efficacy of SPICRs rely on the layer configuration of elastomers as a fundamental point of development. The

fabrication of the SPICRs is as presented in Chapter 3, while the intended elastomer materials to be used are EcoFlex™ 00-50 and DragonSkin™ 30A. Based on the stiffness (shore hardness) of the material property, EcoFlex™ 00-50 is used to encapsulate the cavity and the point of inflation, while DragonSkin™ 30A acts as the strain-limiting layer to control the inflation profile of the cavity at opposing sides with different thicknesses. This configuration is opted to adjust the tensile ability of the inflation profile and to control the expansion of EcoFlex™ 00-50 material as shown in previous studies. The elastomer layer configuration schematic for each intended material is as described in Figure 6.3.1, along with the SPICRs designs and dimensions.

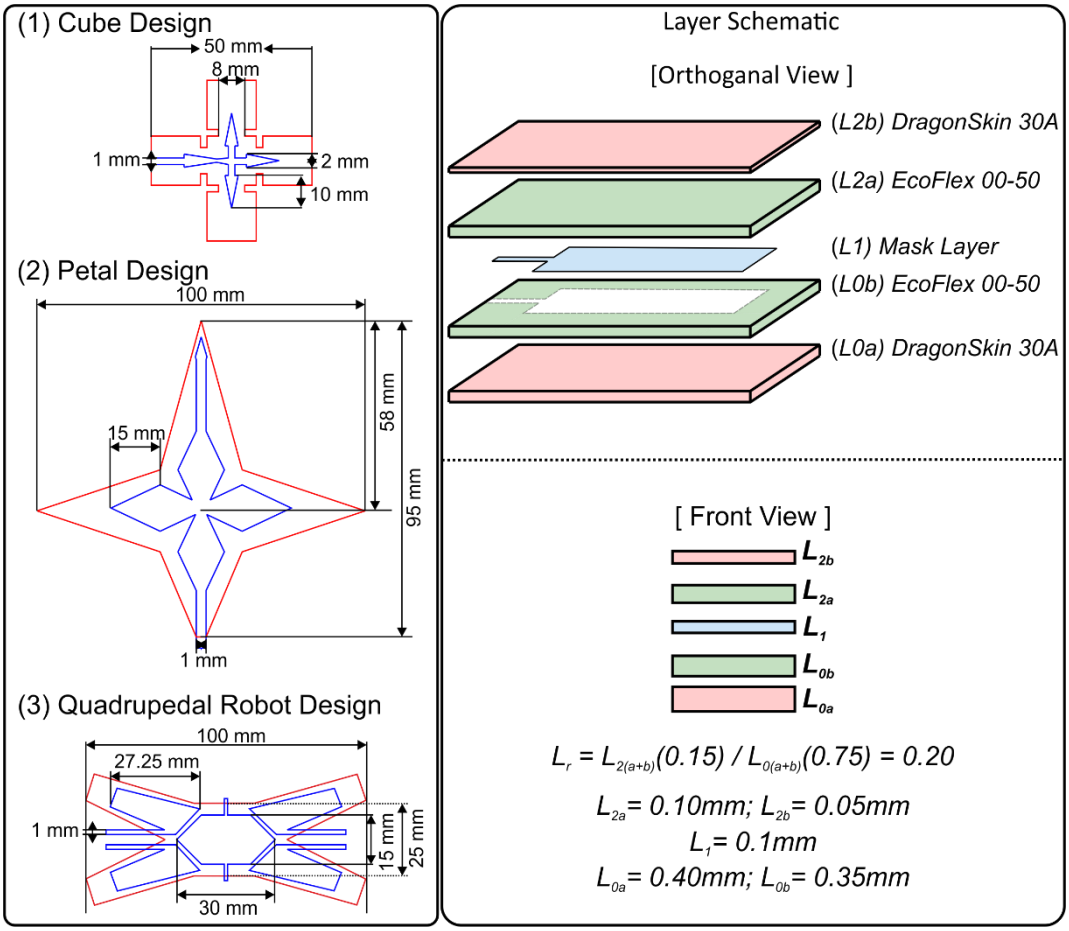

Figure 6.3.1 (Left) Soft planar inflatable composite robotic designs for (1) Cube Design; (2) Petal Design; (3) Quadrupedal Robot Design. (Red Outline: Robot geometry design; Blue Outline: Cavity design). (Right) Layer schematic design of soft planar inflatable composite configuration. Multiple materials (EcoFlex™ 00-30 and DragonSkin™ 30A) is configured at different thicknesses depending on its listed layer ratio (L_r)

6.3.2 Results and Discussion

A custom pneumatic control set-up was assembled to inflate the fabricated SPIC robots and record its effects when pressurised with air. The SIPCRs were pressured across a range of controlled input pressures through a pneumatic control unit operated by electronic servo-valves (SMC ITV0010-15 PSI Pressure Regulator, SMC, Japan). The internal pressure within each SPICR were monitored and regulated using an analogue absolute pressure transducer (15 PSI SCC series absolute pressure transducer, HoneyWell, USA). The SPICRs were pressured across a range of 0 psi to 10 psi in 2 psi increments based on preliminary tests to avoid over-expansion and exceeding the elastomeric material strain limit at the fabricated layer configuration. A schematic diagram of the pneumatic control set-up can be found in Appendix 2. To capture and record the effects of pressure and motion of the SPICRs, a high definition camera (D5300, Nikon, Japan) was set-up directing towards a custom stage fitted with a measurable calibrated backing pattern (5 mm x 5 mm Grid).

Further analysis of the SPICRs, such as inflation profile, speed, and lifting force, was not considered as the aim of the study was to showcase the SPIC fabrication technique and the use of multi-material layering to incorporate elastomeric based stain-limiting layer configuration for soft robotic applications.

Figure 6.3.2 presents the recorded motion of the SPIC fabricated cube design across the intended range of pressures. Starting from Fig. 6.3.2 (1) at zero psi, the cube composite design is laid flat on the surface with no visible inflation. As the cube is inflated, inflation is induced and a single-side of the cube starts to fold towards the centre of the design. The inflation profile exhibited intended results, as inflation is directed towards a single planar side where the stiffness of DragonSkin™ 30A is thinner as compared to its opposing side. However, as pressure increases, the propagation of inflation to other cavities only exhibits when a single-cavity point has reached its material strain limit, this effect is visible at Fig. 6.3.2 (4 – 6). The results suggests that an increase or reduction in layer thickness at L_2 configuration, between EcoFlex™ 00-50 and DragonSkin™ 30A, could inhibit the large inflation profile exhibited and control the propagation of pressure across the cavities.

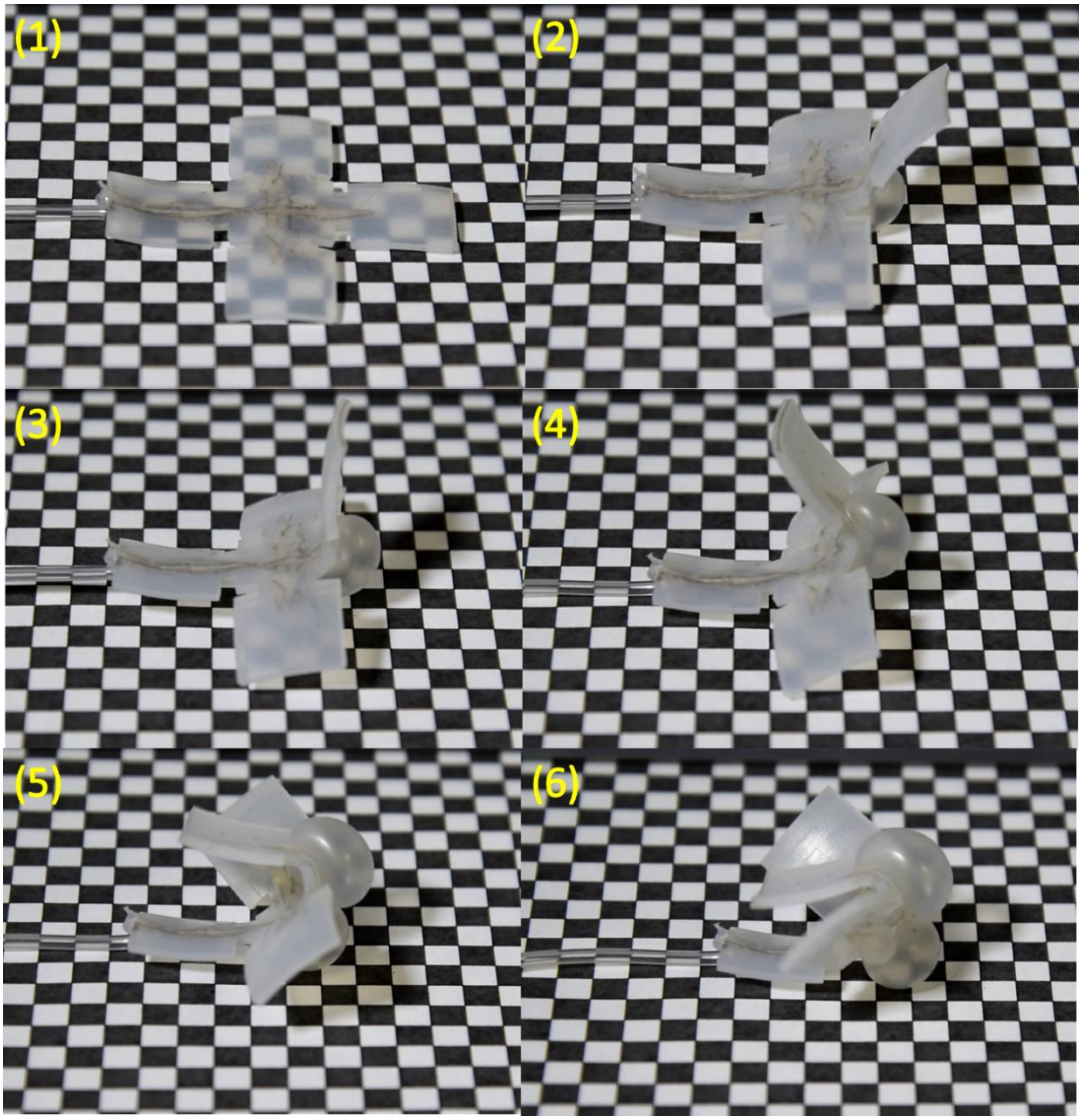

Figure 6.3.2 Inflation result of Cube design at 2 psi interval control up to 10 psi. (1) 0 psi; (2) 2 psi; (3) 4 psi; (4) 6 psi; (5) 8 psi; (6) 10 psi (maximum pressure input)

In the case of the petal design shown in Figure 6.3.3, the inflation shows a proportional distribution of pressure across all four sides. The is plausible as the design features a central-connected cavity as compared to channel propagation in the cube design. As the pressure is increased, the inflation of the cavities is shown to exhibit a similar ballooning effect as the shape changes morphology from 2D planar to a 3D structure. This result further suggest the lack of mechanical strain induced by DragonSkin™ 30A at layer configuration L_2, while little to no inflation is shown at layer configuration L_0 with DragonSkin™ 30A.

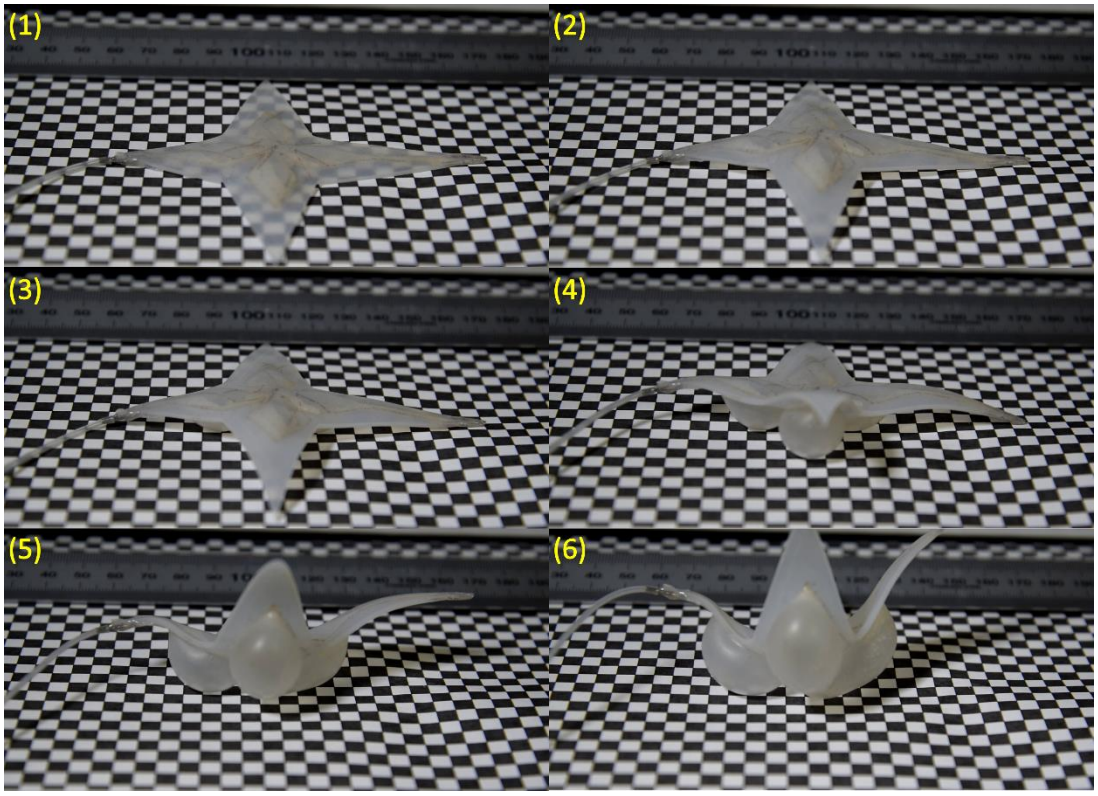

Figure 6.3.3 Inflation result of Petal design at 2 psi interval control up to 10 psi. (1) 0 psi; (2) 2 psi; (3) 4 psi; (4) 6 psi; (5) 8 psi; (6) 10 psi (maximum pressure input)

Despite a large inflation profile exhibited, the SPICR designs were capable of self-folding and shape change from a planar composite to a 3D structure. A single pressure input was used to inflate the initial cube and petal SPICRs. In the case of the quadrupedal robot, a 5-way pneumatic valve manifold at 10 psi input, is connected to each of the robot cavity component (limbs) of the design. This method of actuation is intended to produce a systematic control and in result a gait-like actuation. Shown in Figure 6.3.4, the actuation of the quadrupedal robot starts off with no pressure at a rest position. This is followed by a constant pressure of the central cavity of the robot to induce life motion when its limbs are actuated. Figure 6.3.4 (3 – 6) is then actuated in a gait-like manner to induce a walking motion. However, minimal motion is recorded over a period of 3 minutes of actuation. Post-processing of the recorded motion indicated a 2 mm/minute walking motion in a single direction.

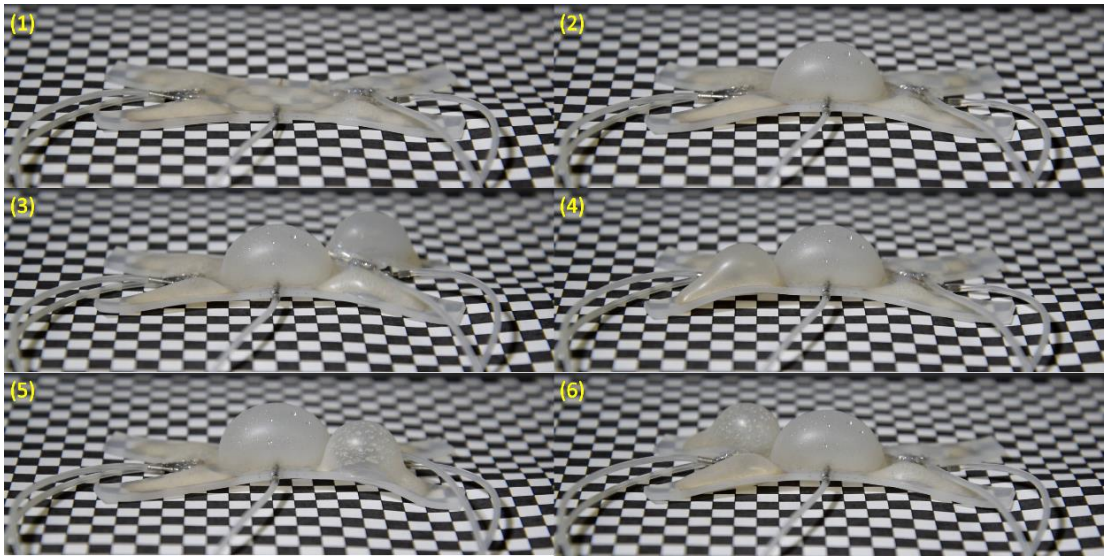

Figure 6.3.4 Actuation of Quadrupedal robot design in a gait-like manner. (1) Zero pressure is provided to show the rest position of the robot; (2) Central cavity is inflated to allow robot to lift-up; (3 - 6) Limbs of the robots are actuated in a gait-like manner to induce motion.

Several changes to the control time-step to induce a gait motion was implemented. Despite this, the recorded motion did not improve. The input pressure was then increased to 15 psi, as the inflation profile of the cavities did not indicate exceeding material strain to induce a larger gait-motion. However, the increase in pressure exceeded the material strain and in result caused a tear on the surface and input channel of the quadrupedal robot. At this stage, the quadrupedal robot design was concluded to be insufficient to produce a gait-motion based on its current design. Compared to existing variations of quadrupedal robots in literature, the distinct difference in working principle of this study refers to the cavity design; and layer configuration.

Due to its single-shaped cavity design, there is insufficient lifting-force generated by its limb during inflation as compared to a rib-like cavity structure with propagating force to induce a bending structure as introduced by Shepherd *et al*. [35]. Exhibiting a similar inference to the previous cases, the stiffer material (DragonSkin™ 30A) introduced at the bottom layer (L_{0a}, Figure 6.3.1), was sufficient in limiting expansion. However, the inflation profile at the top layer resulted in expansion at a non-uniform

and uncontrolled state despite presence of a DragonSkin™30A at L_{2b} (Figure 6.3.1). This would then result in an un-even distribution of forces associated with the cavity design and layer configuration.

From the overall results of the designed and fabricated SPICRs, it is evident that an elastomeric material of stiffer property can be used to act as a strain-limiting layer to induce mechanical programming based on the designed layer configuration. This can be seen in all SPICRs, as inflation is induced to a single side of the planar composite. Despite a large inflation profile exhibited in all SPICRs, the results showcased a series soft robotic composite designs of multi-material elastomeric layering of SPIC fabrication and the use of elastomeric material properties to create embedded mechanical programming.

The study did not include soft modelling and optimisation techniques, as such possible solutions to enhance the performances of the designed SPICRs in this study could potentially include modelling of strain-limiting layers into FEA techniques to enable further advancements of SPICRs to be developed. However, based on the current understanding, cavity design is still sought to be first designed and optimised. This is followed with its layer configuration along with its elastomeric counterparts to ensure feasibility of the development.

6.3.3 Conclusion

In this study, a series of soft planar inflatable composite robot, SPICR, designs were developed using the SPIC fabrication technique. Three robotic designs (Cube, Petal and Quadrupedal robot) were subjected to showcase actuation from a planar 2D-composite design to a 3D structure for self-folding or gait-actuation. The development showcased the use of multi-material layering of elastomer material of different material properties (EcoFlex™ 00-50 and DragonSkin 30A), as oppose to a single material embodiment or the use of external material (fabric mesh) as previously investigated.

The SPICR's layer schematic and ratios is configured towards fundamental tensile ability of material and stiffness due to layer thickness. The results exceeded

expectations as the designed SPICRs were capable of active shape-change upon actuation. Despite no soft modelling approach used to optimise the SPICRs, it is evident that an elastomeric material of stiffer property can be used to enable strain-limiting capabilities depending on its layer configuration and ratio. Possible future work from this study would include (1) soft modelling techniques to optimise all parametric design and material layers; and (2) different strain-limiting materials to enhance and control structural inflation profile within the overall elastomeric material embodiment, .to produce the next generation of soft robotic composites.

Chapter 7 Discussion and Conclusion

The research in this thesis has displayed the development of a soft fabrication technique towards soft, planar, inflatable composites. The work presented in this thesis proposes a novel approach of building elastomeric materials layered in a planar manner to create functional inflatable components. In addition, a wider challenge of designing, fabrication and characterisation has been carried out as the development progresses. This chapter will discuss the overall research in general and the chapters within the thesis.

This chapter considers key features and approaches of the research aim. The objectives of the research are assessed in reflection to the aims of the research and has made a number of significant contributions to the soft robotics field, notably:

1. *Novel fabrication approach though lamination of soft elastomeric material in a planar manner.*
2. *Design and modelling approach of soft laminar composites to create soft actuators based on a proposed design scheme.*
3. *Several applications made possible through the fabrication technique to create functional composites.*

A conclusion is then presented to summarise the overall research.

7.1 Discussion

Following the review of the literature, the field of soft robotics is still predominantly 'growing', as development approach towards design methodology and fabrication methods for building these soft machines are still under-developed. Soft robotic devices to date are typically developed at larger (centimetre) scales and limited by its production through bespoke manufacturing methods. As the field continues to mature, the technological impact is found to be closely tied to the development of new manufacturing methods and materials [11, 19]. It is believed that the true potential of soft robotic devices lies within the fundamental geometry and properties of its constituent materials. Despite existing soft robotic applications across different scales, it is believed that the potential of soft planar devices has yet to be fully explored.

Although a number of advance fabrication techniques have enabled intriguing and innovative soft robotic devices, there is a distinct lack of fully elastomeric and inflatable based soft robotic composites fabricated from composite layering techniques. Existing planar based soft robotic devices often comprise of semi-rigid structures and extensible layers for articulation while actuation is adapted and not integrated [37, 84, 85, 87, 93, 97, 172, 173]. The material build mostly comprises of semi-compliant (paper, thermoplastic, fabric) materials, which allows architecture structures to take shape due to the material innate properties. This can be seen in composite structures such as, thermoplastic configured composite structures by Overvelde *et al.*, and fabric composed inflatable composites by Ou *et al.,* [62, 96].

Taking inspiration from existing developments, a novel fabrication approach was designed to create soft planar inflatable composites (SPIC). The technique is based on film application of elastomeric materials to build soft composites through a layer-by-layer fabrication process. Developments of similar attributes have supported this type of fabrication technique, such as planar capacitive sensors by [174], and microstructures for fluidic actuation [165]. However, these developments were created to adhere to applications as compared to a distinct fabrication approach to create inflatable and deformable soft composites.

The conceptual design drove the development of the SPIC fabrication method, which aims to exploit layer based configuration of elastomeric sheets. Film application technology was adopted based on its ability to produce controlled coating of soft materials at desired uniform thicknesses. However, commercial automatic film applicators were costly and were not designed to enable a continuous step-repeat fabrication design. As such, a manual casting knife applicator was commercially obtained to enable the desired fabrication effects. The choice film applicator was based on a number of set criteria as described in Section 3.4. A bespoke platform was then assembled to automate the fabrication process to enable consistent, repeatable and uniform production of elastomeric sheets at two distinct factors: (1) applicator spread speed and (2) applied pressure/direction across a substrate. The bespoke applicator platform emulates commercial automatic applicators functionality with adjustable speeds through a linear drive actuator and provide a levelled robust plane to ensure uniform coating is achieved. Commercial automated film applicators are sold at the price point range of 2,000£ to 4,000£, with the choice of upgrades that includes vacuum test beds, and upgradable functionality to include a wider range of applicators. However, the bespoke applicator platform built in this study would cost no more than 500£. Despite the need to design, assemble and characterise the platform, the clear difference in price point favoured the choice of an open-source build.

Despite high manufacturing tolerances of film applicators, a characterisation study was conducted to evaluate the effects of elastomeric material and feasibility of the technique. It is noted that film applicators are governed by the theoretical wet film thickness phenomena for coating of materials. Despite the use of non-common application materials associated towards coatings, the use of standard practices (e.g. ASTM D823-95 standard practice) can be used to characterise material into films [135]. Similar fabrication techniques of published data and industry standards have also reported exact common factors that can affect the quality and fundamental mechanics of the fabricated films [174-176]. These factors persists in all types of film applicators and are highly dependent on material viscosity as described in Section

4.1. Based on the experimental results for characterisation of film applicator, the results collected reflects industry standard tolerances of rated viscous materials. As such, a repeat-step-compensation method was opted to produce the desired elastomer thickness as depicted in industry and similar developed fabrication approaches within the research community [90, 174, 176]. Initial development was aimed to produce a predictive metric to set the applicator thickness for precise production of desired thickness of elastomeric films. The characterisation results shows potential in producing this, however, this is currently not possible due to the limitation of non-contact measurement techniques for elastomeric translucent surfaces.

The SPIC fabrication technique introduced the concept of laser ablation of elastomeric material for removal and patterning of fabricated composites. The fabrication tool was characterised to enabled precise control of cutting and patterning of elastomeric materials through differential power and speed settings of the laser. Existing published works have reported similar fabrication approach, however, no existing power-speed library for controllable depth cutting by laser ablation is available for common elastomeric materials used in the research community [141, 177, 178]. This is due to the technique not widely adopted due to the formation of soot and debris during ablation and patterning, of which can cause deformations to the device in development. Extension of technique is often used towards final stage of fabrication. Currently, characterisation of laser ablation on common elastomeric materials (EcoFlex™, DragonSkin™ and Elastosil®) have been conducted based on laser power and speed settings. The ability to vary the laser power and speed settings enabled depth controlled ablation and cutting of elastomer and is being utilised in the SPIC fabrication. A definitive laser setting metric on existing elastomeric material is proposed in future works to push and aid soft robotic research.

Presented in Chapter 5, the design parameters based on the conceptual design of SPIC introduced a design scheme to model, simulate soft inflatable composites via FEA techniques. Compared to existing soft modelling FEA approaches, the design study taken is introduced in a simplified comprehensive manner as compared to

references [42, 43, 45, 179]. The design scheme was inspired by Ranzani *et al*., in differentiating geometry cavity design and layer configuration [165]. However, the work done by Ranzani *et al.*, is linked towards micro-structures, where the presented work here differs in approach, scale, material and fabrication technique [165].

The parametric design and FEA approach mainly focused on the feasibility of soft modelling and inflation behaviour simulation, as compared to trial and error fabrication of designs generated from creativity. As such, a series of continuous bending actuators, SPICAs, were introduced. The produced models where evaluated in inflation behaviour and visual efficacy as compared to its fabricated counterpart due to the use of published hyper-elastic data. The collected data from published works only serve as a reference point to enable the modelling approach, as there is currently no established library of elastomeric materials and hyper-elastic coefficients commonly used within the research community. A soft planar inflatable discrete bending actuator, SPIDA, was also developed featuring a joint-like bending actuator. Differing in cavity geometry shape and cavity parameters from SPICAs, angle-like bending can be emulated with elastomeric material without a large inflation profile to induce shape deformation as shown in Section 5.3.

A series of case studies were also performed to further present the efficacy and validity of the SPIC fabrication technique. Case study 1 presented preliminary investigation to create soft layered pneumatic actuators based on empirical design of conventional soft pneumatic bending actuators. The study showed potential in miniaturisation of actuator size and optimisation in cavity design, which had led to the developed SPICAs introduced in Chapter 5. This is followed by Case study 2, where the SPIC fabrication technique is used to dynamically create a novel flat soft tactile sensor capable of variable mechanical compliance and shape change. The study presented highlights the potential of skin-like sensing application and active tactile pads capable of rivalling existing technologies [24, 176, 180, 181].

A series of soft planar inflatable composite robots is introduced in Case study 3. Based on the parametric design scheme for SPIC fabrication, three robotic designs were showcased to exhibit self-folding from a planar 2D design to a 3D structure. The study employed multi-material layering of elastomers with different material

properties as opposed to a single-material embodiment or the inclusion of external strain-limiting materials. Despite no modelling approach were used to optimise the geometric structure of the cavities, the results yielded were expected and further study on the design parameters of SPIC could potentially invoke new soft planar inflatable composite robots.

7.2 Assessment of Research Objectives

The aim of this PhD was to develop a fabrication technique towards inflatable composites embodied in soft material and in a planar manner. The vision in hindsight was towards functional designs within a composite as a building blocks towards inflatable and shape reconfigurable structures. Section 1.3 presented several objectives that were set at the initial stage of the research. The following details the objectives have been successfully achieved.

1. To study the literature and state-of-the-art soft robotics technologies which would highlight the available techniques and progression within the field of research.

A literature review surrounding soft fabrication was identified in Chapter 2 as a starting point to understand and identify a research gap surrounding soft fabrication for soft robots. The review provided a general introduction to soft robotics by identifying soft fabrication techniques and the need for bespoke fabrication methods and advance techniques to embody and incorporate soft material. Through a systematic review approach, the fabrication of current state-of-the-art soft robotic applications were vetted to identify their fundamental fabrication methods. Through this review, the trend of soft robotic research was found to favour additive manufacturing in terms of 3D printing. It was evident that within the soft robotic community, the depth of composite layering applications have yet to see a fully soft and compliant device. As such, applications through composite layering was found to be an intriguing point of development as a research gap. Thus, the development of a soft planar inflatable composite was initiated.

2. Develop a bespoke soft fabrication tool and technique for manufacturing to advance and/or aid the development of soft robotic systems.

This thesis introduced a novel bespoke fabrication technique to develop thin, soft, inflatable composites through a layer-by-layer process in a planar manner in Chapter 3. The technique adapted from existing additive manufacturing technique of composite layering and introduces mask layers for inflatable cavity and embedded strain-limiting layers for shape change and material integrity. Fabricated composites can then be patterned and cut to planar shapes via laser cutting and ablation to create actuators, sensors and possible applications for medical use. To enable the introduced fabrication technique, a bespoke fabrication tool was built to assist the fabrication technique of elastomer film application. Compared to commercial available variants of the technique, the bespoke platform benefitted from a higher range and resolution of driving speeds, adjustable workspace and flexible configuration for integrated techniques. In addition, the bespoke applicator platform is significantly cost effective compared to its commercial available counterparts.

3. Development of a design method for soft planar inflatable composites in the form of soft actuators and robots.

In Chapter 3, the conceptual design initially brought about the design parameters of (1) Selective material layering and (2) Structural geometry variation. Selective material layering depicts the material layers to form a composite, while structural geometry variation points to the design of the mask layer for inflation and/or actuation. In Chapter 5, the design parameters were implemented into a design scheme to create soft planar inflatable actuators (SPIA). The initial development focused on the creation of soft planar inflatable continuous (bending) actuators (SPICAs), followed by introducing soft planar inflatable discrete (bending) actuator (SPIDA). The design scheme reduces the need for trial and error fabrication and provided an design approach based on the introduced design parameters to enable modelling and simulation of soft bending actuators prior to fabrication. The design approach enabled the creation of SPIDA, a joint-like soft bending actuator capable of articulated angle during inflation.

4. Understand elastomeric material properties through the characterisation of its fabrication method and applications.

In Chapter 4, a characterisation method to gauge the production capabilities for thin, elastomeric films were conducted. The technique evaluated a range of readily available and commonly used elastomers in the field of soft robotics. Varying with viscosity, the range of elastomers were subjected to a series of experimental test to evaluate the efficacy of the film applicator in terms of applicator set thickness, applicator spread speed and curing temperature of elastomer as a thin film. The results concluded that a step-repeat compensation method provided a robust method to overcome material viscosity and the theoretical wet film thickness affecting the production of desired set applicator thickness. In Chapter 5, through modelling and simulation approaches, hyper-elastic model of elastomeric material properties was necessary to enable the development. During the time of study, it was not possible to build a complete the library of hyper-elastic models due to limitation of equipment. As such, published data of hyper-elastic material is used for modelling and simulation. While the work still requires further progression, the approach has provided key insight into understanding elastomeric material properties and the use of hyper-elastic model properties.

5. Model, simulate and potentially optimise the behaviour of soft planar inflatable composite designs using digital modelling approaches through Finite Element Analysis method.

Chapter 5 investigates the approach towards modelling and simulation using finite element analysis. The chapter brought forward the design parameters introduced in Chapter 3 and produced a design scheme to model and simulate soft bending actuators. The actuator designs were then fabricated for evaluation with its model counterpart in terms of behaviour and feasibility. The design approach removed the need for trial and error design and fabrication (blind fabrication) and introduced a novel design approach to model and simulate soft inflatable composites. The result introduced a joint-like bending soft actuator capable of articulated angle during inflation. Comparing the fabricated and simulated results, it was concluded that

further research is still required to provide a complete accurate representation of both modalities.

6. Evaluate and demonstrate how soft planar inflatable composites can be leveraged for soft robotic applications through evaluation of case studies based on soft fabrication methods and applications.

Several case studies were presented in Chapter 6 to highlight the use of the developed fabrication technique. Section 6.1 introduced an empirical design approach to conventional soft robotic bending actuators. The development sets itself apart from the design scheme introduced in Chapter 5. Section 6.2 then introduced an adjustable stiffness sensor based on existing soft-magnetic based sensor development within the research group. The sensors were introduced as inflatable composites of different elastic materials to produce a range of stiffness and sensing resolution. Section 6.3 introduced a series of soft composite robotic designs with multi-material layer configurations that extends the parametric study of SPIC presented in Chapter 5. The results further elaborate and showcase the potential of SPIC fabrication technique, while highlighting a need to expand on cavity geometric designs and soft modelling for optimisation as potential future developments.

7.3 Concluding Remarks

This thesis has demonstrated the development of a soft fabrication technique to build on inflatable soft robots in a planar manner. The work presented in this thesis details a novel approach and development of soft planar inflatable composites. To enable the development, a fabrication process was formulated based on existing soft fabrication techniques and invoke advance manufacturing methods. To assist the developed fabrication technique, a bespoke fabrication platform was developed to enable creation of thin elastomer films to be configured into functional composites. The bespoke platform was also evaluated in its efficacy to create elastomeric sheets of desired thickness. This is further presented with a characterisation study on the proposed SPIC fabrication processes. Based on the conceptual design of SPIC, a parametric design study was performed to create soft planar inflatable actuators. Expanding on design methodologies, finite element method approach was utilised to modelled and simulated soft robotic components to further expand the development. A series of case studies were presented, to showcase the efficacy and capabilities of the developed SPIC fabrication technique for soft robotic development. The case studies results highlighted many exciting possibilities and potential for SPIC fabrication. While there is always a need for further improvements, optimisation and development, the current research has reached to a concluding point .

Chapter 8 Future Work

This chapter provides an overview on the main aspects to this PhD which would benefit from further development and improvements. This research has given an insight into the development of a fabrication technique to create soft planar inflatable composites. As such, aspects of improvements needed to further optimise and increase efficacy to develop new methods and techniques for fabrication in a planar manner and design morphology for functional inflatable composites.

8.1 Elastomer Film Measurement Technique

In chapter 4, the characterisation of the elastomeric films produced were measured manually through a modified digital thickness gauge. While resolution of the thickness gauge was within suitable range for the development, a higher resolution, accuracy, robust and possibly automated measurement technique may be required. Tactile based measurement techniques (e.g. thickness gauge) may not be an ideal choice for elastomeric materials, as forces (including gravitational) acting upon the contact point may hinder results. Current light and image based depth analysis are still being developed and experimented on. However, the use of light and image depth analysis resulted in constant reflection of material surface and inaccurate measurements. A further exploration of measurement techniques on translucent surfaces is suggested in the future. This is to further enhance and provide a higher measurement accuracy to the elastomeric films being produced. A definitive characterisation of applicator settings would enable creation of a predictive library to produce elastomeric films at a controlled set thickness depending on the material.

8.2 Bespoke Applicator Platform

The developed bespoke applicator platform as the fabrication tool in this study holds many potentials to further advance soft composite fabrication. The existing machined aluminium build plate requires a complete re-design to incorporate smaller fabrication features and alignment features. Furthermore, a higher manufacturing tolerance would aid the fabrication of controlled production of elastomeric films. As the research progresses, automation and an all-in-one package may be the key that would attract many researchers as to 3D printers. Reflecting to the developed fabrication process, components such as heated bed platform, embedded laser cutter and an enclosed dispensing and cleaning system, may be incorporated into the applicator platform. However, incorporation of all the listed components would pose a great challenge not just at a cost level; especially at designing an enclosed dispensing and cleaning system.

8.3 Elastomer Characterisation for Hyper-elastic Model Constants

During the time of study, published data of hyper-elastic model coefficients were reviewed and used to enable finite element analysis modelling and simulation of soft robotic components. Limitations in testing equipments and in-depth insight within the area. While the fundamental understanding of material fabrication and characterisation were undertaken, the use of a video-extensometer was not available during the time of study. An expansive material library of hyper-elastic models is still under-progression and would benefit the soft robotic research field. Further extension of this work can then be utilised to expand on the study conducted in Chapter 5, and invoke definitive intricate and bespoke soft inflatable composite robots as well as pushing the boundaries of the developed soft planar inflatable composite fabrication method.

References

1. Albu-Schaffer, A. et al. Soft robotics. *IEEE Robotics & Automation Magazine.* 2008, **15**(3), pp.20-30.
2. Pfeifer, R. et al. The challenges ahead for bio-inspired 'soft' robotics. *Commun. ACM.* 2012, **55**(11), pp.76-87.
3. Trivedi, D. et al. Soft Robotics: Biological Inspiration, State of the Art, and Future Research. *Applied Bionics and Biomechanics.* 2008, **5**(3).
4. Ilievski, F. et al. Soft Robotics for Chemists. *Angewandte Chemie International Edition.* 2011, **50**(8), pp.1890-1895.
5. Kim, S. et al. Soft robotics: a bioinspired evolution in robotics. *Trends in Biotechnology.* 2013, **31**(5), pp.287-294.
6. Lipson, H. Challenges and Opportunities for Design, Simulation, and Fabrication of Soft Robots. *Soft Robotics.* 2013, **1**(1), pp.21-27.
7. Bao, G. et al. Soft Robotics: Academic Insights and Perspectives Through Bibliometric Analysis. *Soft Robotics.* 2018, **5**.
8. Majidi, C. Soft Robotics: A Perspective - Current Trends and Prospects for the Future. *Soft Robotics.* 2014, **1**(1), pp.5-11.
9. Laschi, C. and Cianchetti, M. Soft Robotics: New Perspectives for Robot Bodyware and Control. *Frontiers in bioengineering and biotechnology.* 2014, **2**, p.3.
10. Rus, D. and Tolley, M.T. Design, fabrication and control of soft robots. *Nature.* 2015, **521**(7553), pp.467-475.
11. Laschi, C. et al. Soft robotics: Technologies and systems pushing the boundaries of robot abilities. *Science Robotics.* 2016, **1**(1).
12. Robotiq. [Online]. [Accessed 4 September]. Available from: https://robotiq.com/.
13. Shintake, J. et al. Soft Robotic Grippers. *Advanced Materials.* 2018, **30**(29), p.1707035.
14. Brown, E. et al. Universal robotic gripper based on the jamming of granular material. *Proceedings of the National Academy of Sciences.* 2010, **107**(44), pp.18809-18814.
15. DeccanChronicle. [Online]. 2016. [Accessed 4 September]. Available from: https://www.deccanchronicle.com/technology/in-other-news/130716/first-bio-inspired-underwater-robot.html.
16. Marchese, A.D. et al. Autonomous Soft Robotic Fish Capable of Escape Maneuvers Using Fluidic Elastomer Actuators. *Soft Robotics.* 2014, **1**(1), pp.75-87.
17. Laschi, C. et al. Soft Robot Arm Inspired by the Octopus. *Advanced Robotics.* 2012, **26**(7), pp.709-727.
18. Iida, F. and Laschi, C. Soft Robotics: Challenges and Perspectives. *Procedia Computer Science.* 2011, **7**, pp.99-102.
19. Schmitt, F. et al. Soft Robots Manufacturing: A Review. *Frontiers in Robotics and AI.* 2018, **5**(84).

20. Tse, Z.T.H. et al. Soft Robotics in Medical Applications. *Journal of Medical Robotics Research.* 2018, **03**(03n04), p.1841006.
21. Johnson, M. et al. Fabricating biomedical origami: a state-of-the-art review. *International Journal of Computer Assisted Radiology and Surgery.* 2017, pp.1-10.
22. Polygerinos, P. et al. Soft Robotics: Review of Fluid-Driven Intrinsically Soft Devices; Manufacturing, Sensing, Control, and Applications in Human-Robot Interaction *Advanced Engineering Materials.* 2017, pp.e201700016-n/a.
23. Tolley, M.T. et al. A Resilient, Untethered Soft Robot. *Soft Robotics.* 2014, **1**(3), pp.213-223.
24. Follmer, S. et al. Jamming user interfaces: programmable particle stiffness and sensing for malleable and shape-changing devices. In: *Proceedings of the 25th annual ACM symposium on User interface software and technology*: ACM, 2012, pp.519-528.
25. Lu, N. and Kim, D.H. Flexible and Stretchable Electronics Paving the Way for Soft Robotics. *Soft Robotics.* 2014, **1**(1), pp.53-62.
26. Mosadegh, B. et al. Control of soft machines using actuators operated by a Braille display. *Lab on a Chip.* 2014, **14**(1), pp.189-199.
27. Robinson, S.S. et al. Integrated soft sensors and elastomeric actuators for tactile machines with kinesthetic sense. *Extreme Mechanics Letters.* 2015, **5**, pp.47-53.
28. Robert J. Webster, I. and Jones, B.A. Design and Kinematic Modeling of Constant Curvature Continuum Robots: A Review. *Int. J. Rob. Res.* 2010, **29**(13), pp.1661-1683.
29. Nurzaman, S.G. et al. *Soft robotics on the move: scientific networks, activities, and future challenges*. Mary Ann Liebert, Inc. 140 Huguenot Street, 3rd Floor New Rochelle, NY 10801 USA, 2014.
30. Paik, J. Soft Components for Soft Robots. In: Verl, A. et al. eds. *Soft Robotics: Transferring Theory to Application*. Berlin, Heidelberg: Springer Berlin Heidelberg, 2015, pp.272-281.
31. Wang, L. and Iida, F. Deformation in Soft-Matter Robotics: A Categorization and Quantitative Characterization. *IEEE Robotics & Automation Magazine.* 2015, **22**(3), pp.125-139.
32. Rieffel, J. et al. Growing and Evolving Soft Robots. *Artificial Life.* 2014, **20**(1), pp.143-162.
33. Suzumori, K. et al. Applying a flexible microactuator to robotic mechanisms. *IEEE Control Systems.* 1992, **12**(1), pp.21-27.
34. Klute, G.K. et al. McKibben artificial muscles: pneumatic actuators with biomechanical intelligence. In: *1999 IEEE/ASME International Conference on Advanced Intelligent Mechatronics (Cat. No.99TH8399)*, *19-23 Sept. 1999*, 1999, pp.221-226.
35. Shepherd, R.F. et al. Multigait soft robot. *Proceedings of the National Academy of Sciences.* 2011, **108**(51), pp.20400-20403.
36. Mosadegh, B. et al. Pneumatic Networks for Soft Robotics that Actuate Rapidly. *Advanced Functional Materials.* 2014, **24**(15), pp.2163-2170.
37. Park, Y.L. et al. A soft wearable robotic device for active knee motions using flat pneumatic artificial muscles. In: *2014 IEEE International Conference on*

Robotics and Automation (ICRA), *May 31 2014-June 7 2014*, 2014, pp.4805-4810.
38. Shen, H. Meet the soft, cuddly robots of the future. *Nature.* 2016, **530**(7588), pp.24-26.
39. Sun, Y. et al. Characterization of silicone rubber based soft pneumatic actuators. In: *2013 IEEE/RSJ International Conference on Intelligent Robots and Systems*, *3-7 Nov. 2013*, 2013, pp.4446-4453.
40. Hughes, J. et al. Soft Manipulators and Grippers: A Review. *Frontiers in Robotics and AI.* 2016, **3**(69).
41. Polygerinos, P. et al. Modeling of Soft Fiber-Reinforced Bending Actuators. *IEEE Transactions on Robotics.* 2015, **31**(3), pp.778-789.
42. Agarwal, G. et al. Stretchable Materials for Robust Soft Actuators towards Assistive Wearable Devices. *Scientific Reports.* 2016, **6**, p.34224.
43. Moseley, P. et al. Modeling, Design, and Development of Soft Pneumatic Actuators with Finite Element Method *Advanced Engineering Materials.* 2016, **18**(6), pp.978-988.
44. Shahzad, M. et al. Mechanical Characterization and FE Modelling of a Hyperelastic Material. *Materials Research.* 2015, **18**, pp.918-924.
45. Case, J.C. et al. Soft Material Characterization for Robotic Applications. *Soft Robotics.* 2015, **2**(2), pp.80-87.
46. Manti, M. et al. Stiffening in Soft Robotics: A Review of the State of the Art. *IEEE Robotics & Automation Magazine.* 2016, **23**(3), pp.93-106.
47. Cho, K.-J. et al. Review of manufacturing processes for soft biomimetic robots. *International Journal of Precision Engineering and Manufacturing.* 2009, **10**(3), p.171.
48. Someya, T. et al. The rise of plastic bioelectronics. *Nature.* 2016, **540**(7633), pp.379-385.
49. Studart, A.R. Additive manufacturing of biologically-inspired materials. *Chem Soc Rev.* 2016, **45**(2), pp.359-76.
50. Taylor, D.L. and in het Panhuis, M. Self-Healing Hydrogels. *Advanced Materials.* 2016, **28**(41), pp.9060-9093.
51. Suzumori, K. et al. Flexible microactuator for miniature robots. In: *[1991] Proceedings. IEEE Micro Electro Mechanical Systems*, *30 Jan-2 Feb 1991*, 1991, pp.204-209.
52. Daerden, F. and Lefeber, D. Pneumatic artificial muscles: actuators for robotics and automation. *European journal of mechanical and environmental engineering.* 2002, **47**(1), pp.11-21.
53. Kim, S. et al. Smooth Vertical Surface Climbing With Directional Adhesion. *IEEE Transactions on Robotics.* 2008, **24**(1), pp.65-74.
54. Cham, J.G. et al. Fast and Robust: Hexapedal Robots via Shape Deposition Manufacturing. *The International Journal of Robotics Research.* 2002, **21**(10-11), pp.869-882.
55. Truby, R.L. and Lewis, J.A. Printing soft matter in three dimensions. *Nature.* 2016, **540**(7633), pp.371-378.
56. Zolfagharian, A. et al. Evolution of 3D printed soft actuators. *Sensors and Actuators A: Physical.* 2016, **250**, pp.258-272.
57. Wallin, T.J. et al. 3D printing of soft robotic systems. *Nature Reviews Materials.* 2018.

58. Wang, Z. et al. Soft robotics for engineers. *HKIE Transactions.* 2015, **22**(2), pp.88-97.
59. Kim, S. et al. iSprawl: Design and Tuning for High-speed Autonomous Open-loop Running. *The International Journal of Robotics Research.* 2006, **25**(9), pp.903-912.
60. Yap, H.K. et al. High-Force Soft Printable Pneumatics for Soft Robotic Applications. *Soft Robotics.* 2016, **3**(3), pp.144-158.
61. Bryan, N.P. et al. 3D printing antagonistic systems of artificial muscle using projection stereolithography. *Bioinspiration & Biomimetics.* 2015, **10**(5), p.055003.
62. Overvelde, J.T.B. et al. A three-dimensional actuated origami-inspired transformable metamaterial with multiple degrees of freedom. *Nature Communications.* 2016, **7**.
63. Firouzeh, A. et al. Soft pneumatic actuator with adjustable stiffness layers for Multi-DoF Actuation. In: *2015 IEEE/RSJ International Conference on Intelligent Robots and Systems (IROS)*, *Sept. 28 2015-Oct. 2 2015*, 2015, pp.1117-1124.
64. Martinez, R.V. et al. Elastomeric Origami: Programmable Paper-Elastomer Composites as Pneumatic Actuators. *Advanced Functional Materials.* 2012, **22**(7), pp.1376-1384.
65. Meller, M.A. et al. Reconsidering the McKibben muscle: Energetics, operating fluid, and bladder material. *Journal of Intelligent Material Systems and Structures.* 2014, **25**(18), pp.2276-2293.
66. Marchese, A.D. et al. A Recipe for Soft Fluidic Elastomer Robots. *Soft Robotics.* 2015, **2**(1), pp.7-25.
67. Wakimoto, S. and Suzumori, K. Fabrication and basic experiments of pneumatic multi-chamber rubber tube actuator for assisting colonoscope insertion. In: *2010 IEEE International Conference on Robotics and Automation*, *3-7 May 2010*, 2010, pp.3260-3265.
68. Zhao, H. et al. Scalable manufacturing of high force wearable soft actuators. *Extreme Mechanics Letters.* 2015, **3**, pp.89-104.
69. Julien, G. et al. Microinjection molding of thermoplastic polymers: a review. *Journal of Micromechanics and Microengineering.* 2007, **17**(6), p.R96.
70. Han, D.D. et al. Light-Mediated Manufacture and Manipulation of Actuators. *Advanced Materials.* 2016, pp.8328-8343.
71. Chossat, J.B. et al. A Soft Strain Sensor Based on Ionic and Metal Liquids. *IEEE Sensors Journal.* 2013, **13**(9), pp.3405-3414.
72. Cheng, N.G. et al. Thermally Tunable, Self-Healing Composites for Soft Robotic Applications. *Macromolecular Materials and Engineering.* 2014, **299**(11), pp.1279-1284.
73. MacCurdy, R. et al. Printable hydraulics: A method for fabricating robots by 3D co-printing solids and liquids. In: *2016 IEEE International Conference on Robotics and Automation (ICRA)*, *16-21 May 2016*, 2016, pp.3878-3885.
74. Miriyev, A. et al. Soft material for soft actuators. *Nature Communications.* 2017, **8**(1), p.596.
75. Merz, R., Prinz, F.B., Ramaswami, K., Terk, M. and Weiss, L.E. Shape Deposition Manufacturing. *Proceedings of the 1994 Solid Freeform Fabrication Symposium.* 1994.

76. Kim, S. et al. Whole body adhesion: hierarchical, directional and distributed control of adhesive forces for a climbing robot. In: *Proceedings 2007 IEEE International Conference on Robotics and Automation*, *10-14 April 2007*, 2007, pp.1268-1273.
77. Dollar, A.M. et al. Embedded Sensors for Biomimetic Robotics via Shape Deposition Manufacturing. In: *The First IEEE/RAS-EMBS International Conference on Biomedical Robotics and Biomechatronics, 2006. BioRob 2006.*, *20-22 Feb. 2006*, 2006, pp.763-768.
78. Gafford, J. et al. Shape Deposition Manufacturing of a Soft, Atraumatic, Deployable Surgical Grasper1. *Journal of Medical Devices.* 2014, **8**(3), pp.030927-030927-3.
79. Park, Y.L. et al. Fingertip force control with embedded fiber Bragg grating sensors. In: *2008 IEEE International Conference on Robotics and Automation*, *19-23 May 2008*, 2008, pp.3431-3436.
80. Hoover, A.M. and Fearing, R.S. Fast scale prototyping for folded millirobots. In: *2008 IEEE International Conference on Robotics and Automation*, *19-23 May 2008*, 2008, pp.886-892.
81. Hawkes, E. et al. Programmable matter by folding. *Proceedings of the National Academy of Sciences.* 2010, **107**(28), pp.12441-12445.
82. Whitney, J.P. et al. Pop-up book MEMS. *Journal of Micromechanics and Microengineering.* 2011, **21**(11), p.115021.
83. Baisch, A.T. and Wood, R.J. Pop-up assembly of a quadrupedal ambulatory MicroRobot. In: *2013 IEEE/RSJ International Conference on Intelligent Robots and Systems*, *3-7 Nov. 2013*, 2013, pp.1518-1524.
84. Yao, L. et al. PneUI: pneumatically actuated soft composite materials for shape changing interfaces. In: *Proceedings of the 26th annual ACM symposium on User interface software and Technology*: ACM, 2013, pp.13-22.
85. Niiyama, R. et al. Pouch Motors: Printable/inflatable soft actuators for robotics. In: *2014 IEEE International Conference on Robotics and Automation (ICRA)*, *May 31 2014-June 7 2014*, 2014, pp.6332-6337.
86. Gorissen, B. et al. Flexible pneumatic twisting actuators and their application to tilting micromirrors. *Sensors and Actuators A: Physical.* 2014, **216**(Supplement C), pp.426-431.
87. Russo, S. et al. An Additive Millimeter-Scale Fabrication Method for Soft Biocompatible Actuators and Sensors. *Advanced Materials Technologies.* 2017, **2**(10).
88. Kow, J.W. et al. Thin soft layered actuator based on a novel fabrication technique. In: *2018 IEEE International Conference on Soft Robotics (RoboSoft)*, *24-28 April 2018*, 2018, pp.176-181.
89. Lee, D.Y. et al. Design of deformable-wheeled robot based on origami structure with shape memory alloy coil spring. In: *Ubiquitous Robots and Ambient Intelligence (URAI), 2013 10th International Conference on*, *Oct. 30 2013-Nov. 2 2013*, 2013, pp.120-120.
90. Atalay, A. et al. Batch Fabrication of Customizable Silicone-Textile Composite Capacitive Strain Sensors for Human Motion Tracking. *Advanced Materials Technologies.* 2017, **2**(9), pp.1700136-n/a.

91. Miyashita, S. et al. An untethered miniature origami robot that self-folds, walks, swims, and degrades. In: *2015 IEEE International Conference on Robotics and Automation (ICRA)*, *26-30 May 2015*, 2015, pp.1490-1496.
92. Shigemune, H. et al. Origami Robot: A Self-folding Paper Robot with an Electrothermal Actuator Created by Printing. *IEEE/ASME Transactions on Mechatronics.* 2016, **PP**(99), pp.1-1.
93. Li, S. et al. Fluid-driven origami-inspired artificial muscles. *Proceedings of the National Academy of Sciences.* 2017.
94. Strobl, H. *Snaplogy.* [Online]. 2010. [Accessed 4 September]. Available from: http://www.knotologie.de/.
95. Miyashita, S. et al. Ingestible, controllable, and degradable origami robot for patching stomach wounds. In: *2016 IEEE International Conference on Robotics and Automation (ICRA)*, *16-21 May 2016*, 2016, pp.909-916.
96. Ou, J. et al. aeroMorph - Heat-sealing Inflatable Shape-change Materials for Interaction Design. In: *Proceedings of the 29th Annual Symposium on User Interface Software and Technology*, *Tokyo, Japan*. 2984520: ACM, 2016, pp.121-132.
97. Rainier, N. et al. A Reconfigurable Pneumatic Bending Actuator with Replaceable Inflation Modules. *Soft Robotics.* 2018, **5**(3), pp.304-317.
98. Niiyama, R. et al. Pouch Motors: Printable Soft Actuators Integrated with Computational Design. *Soft Robotics.* 2015, **2**(2), pp.59-70.
99. Xia, Y. and Whitesides, G.M. Soft Lithography. *Angewandte Chemie International Edition.* 1998, **37**(5), pp.550-575.
100. Yazdi, A.A. et al. 3D printing: an emerging tool for novel microfluidics and lab-on-a-chip applications. *Microfluidics and Nanofluidics.* 2016, **20**(3), pp.1-18.
101. Qin, D. et al. Soft lithography for micro- and nanoscale patterning. *Nat. Protocols.* 2010, **5**(3), pp.491-502.
102. Morin, S.A. et al. Using “Click-e-Bricks” to Make 3D Elastomeric Structures. *Advanced Materials.* 2014, **26**(34), pp.5991-5999.
103. Stokes, A.A. et al. A Hybrid Combining Hard and Soft Robots. *Soft Robotics.* 2013, **1**(1), pp.70-74.
104. Choi, J.-W. et al. Multi-material microstereolithography. *The International Journal of Advanced Manufacturing Technology.* 2010, **49**(5), pp.543-551.
105. Jiang, Y. and Wang, Q. Highly-stretchable 3D-architected Mechanical Metamaterials. *Scientific Reports.* 2016, **6**, p.34147.
106. Patel, D.K. et al. Highly Stretchable and UV Curable Elastomers for Digital Light Processing Based 3D Printing. *Advanced Materials.* 2017, pp.1606000-n/a.
107. Frutiger, A. et al. Capacitive soft strain sensors via multicore-shell fiber printing. *Advanced Materials.* 2015, **27**(15), pp.2440-2446.
108. Shepherd, R.F. et al. Soft Machines That are Resistant to Puncture and That Self Seal. *Advanced Materials.* 2013, **25**(46), pp.6709-6713.
109. Morin, S.A. et al. Elastomeric Tiles for the Fabrication of Inflatable Structures. *Advanced Functional Materials.* 2014, **24**(35), pp.5541-5549.
110. Drotman, D. et al. 3D printed soft actuators for a legged robot capable of navigating unstructured terrain. In: *2017 IEEE International Conference on Robotics and Automation (ICRA)*, *May 29 2017-June 3 2017*, 2017, pp.5532-5538.

111. Muth, J.T. et al. Embedded 3D Printing of Strain Sensors within Highly Stretchable Elastomers. *Advanced Materials.* 2014, **26**(36), pp.6307-6312.
112. Lewis, J.A. Direct Ink Writing of 3D Functional Materials. *Advanced Functional Materials.* 2006, **16**(17), pp.2193-2204.
113. Carrico, J.D. et al. Fused filament additive manufacturing of ionic polymer-metal composite soft active 3D structures. In: *ASME 2015 Conference on Smart Materials, Adaptive Structures and Intelligent Systems, SMASIS 2015*, 2015.
114. Hardin, J.O. et al. Microfluidic Printheads for Multimaterial 3D Printing of Viscoelastic Inks. *Advanced Materials.* 2015, **27**(21), pp.3279-3284.
115. Raney, J.R. and Lewis, J.A. Printing mesoscale architectures. *MRS Bulletin.* 2015, **40**(11), pp.943-950.
116. Sydney Gladman, A. et al. Biomimetic 4D printing. *Nat Mater.* 2016, **15**(4), pp.413-418.
117. Schaffner, M. et al. 3D printing of robotic soft actuators with programmable bioinspired architectures. *Nature Communications.* 2018, **9**(1), p.878.
118. Coulter, F.B. and Ianakiev, A. 4D Printing Inflatable Silicone Structures. *3D Printing and Additive Manufacturing.* 2015, **2**(3), pp.140-144.
119. Wehner, M. et al. An integrated design and fabrication strategy for entirely soft, autonomous robots. *Nature.* 2016, **536**(7617), pp.451-455.
120. Truby, R.L. et al. Soft somatosensitive actuators via embedded 3D printing. *Advanced Materials.* 2018, **30**(15), p.1706383.
121. Wu, W. et al. Omnidirectional Printing of 3D Microvascular Networks. *Advanced Materials.* 2011, **23**(24), pp.H178-H183.
122. Melchels, F.P.W. et al. Hydrogel-based reinforcement of 3D bioprinted constructs. *Biofabrication.* 2016, **8**(3).
123. Shin, S.R. et al. A Bioactive Carbon Nanotube-Based Ink for Printing 2D and 3D Flexible Electronics. *Advanced Materials.* 2016, **28**(17), pp.3280-3289.
124. Morrow, J. et al. Directly Fabricating Soft Robotic Actuators With an Open-Source 3-D Printer. *IEEE Robotics and Automation Letters.* 2017, **2**(1), pp.277-281.
125. Osman Dogan Yirmibesoglu et al. Direct 3D Printing of Silicone Elastomer Soft Robots and Their Performance Comparison with Molded Counterparts. In: *RoboSoft'18*, *24th April 2018*, *Livorno, Italy*. 2018, p.6.
126. Sun, Y. et al. Design and fabrication of a shape-morphing soft pneumatic actuator: Soft robotic pad. In: *2017 IEEE/RSJ International Conference on Intelligent Robots and Systems (IROS)*, *24-28 Sept. 2017*, 2017, pp.6214-6220.
127. ElMaraghy, W. et al. Complexity in engineering design and manufacturing. *CIRP annals.* 2012, **61**(2), pp.793-814.
128. Ion, A. et al. Digital Mechanical Metamaterials. In: *Proceedings of the 2017 CHI Conference on Human Factors in Computing Systems*, *Denver, Colorado, USA*. 3025624: ACM, 2017, pp.977-988.
129. Roche, E.T. et al. Soft robotic sleeve supports heart function. *Science Translational Medicine.* 2017, **9**(373).
130. Morimoto, T.K. and Okamura, A.M. Design of 3-D Printed Concentric Tube Robots. *IEEE Transactions on Robotics.* 2016, **32**(6), pp.1419-1430.
131. Lee, C. et al. Soft robot review. *International Journal of Control, Automation and Systems.* 2017, **15**(1), pp.3-15.

132. Sonar, H.A. and Paik, J. Soft Pneumatic Actuator Skin with Piezoelectric Sensors for Vibrotactile Feedback. *Frontiers in Robotics and AI.* 2016, **2**(38).
133. Larson, C. et al. Highly stretchable electroluminescent skin for optical signaling and tactile sensing. *Science.* 2016, **351**(6277), pp.1071-1074.
134. Wang, Y. et al. Stretchable Thin Film Materials: Fabrication, Application, and Mechanics. *Journal of Electronic Packaging.* 2016, **138**(2), pp.020801-020801-22.
135. YING-YU, L. and QUI-DONG, W. ASTM D 823: standard practice for producing films of uniform thickness of paint, varnish, and related products on test panels. *Annual Book of ASTM Standards. West Conshohocken.* 1995.
136. ISO, E. Paints and Varnishes–Determination of Film Thickness. *ISO 2808.* 2007.
137. Quatman, C. *Calculating and Measuring Wet Film Thickness*. 2017.
138. ASTM-F2256-05R15. *Standard Test Method for Strength Properties of Tissue Adhesives in T-Peel by Tension Loading.* West Conshohocken, PA: ASTM International, 2015.
139. ASTM. Standard Test Method for Peel or Stripping Strength of Adhesive Bonds. 1983.
140. ASTM. Standard test methods for rubber property—Adhesion to rigid substrates. 1998.
141. Ben-Yehoshua, L. et al. Rapid fabrication of 3D elastomeric structures via laser-machining and vacuum deformation. In: *2015 Transducers - 2015 18th International Conference on Solid-State Sensors, Actuators and Microsystems, TRANSDUCERS 2015*, 2015, pp.1299-1302.
142. Wang, Z. et al. Interaction forces of soft fiber reinforced bending actuators. *IEEE/ASME Transactions on Mechatronics.* 2016, **22**(2), pp.717-727.
143. Krishnan, G. et al. Kinematics of a generalized class of pneumatic artificial muscles. *Journal of Mechanisms and Robotics.* 2015, **7**(4), p.041014.
144. Hiller, J. and Lipson, H. Automatic Design and Manufacture of Soft Robots. *IEEE Transactions on Robotics.* 2012, **28**(2), pp.457-466.
145. Yahya Elsayed, A.V., Constantina Lekakou, Tao Geng, C. M. Saaj, Tommaso Ranzani, Matteo Cianchetti, and Arianna Menciassi. Finite Element Analysis and Design Optimization of a Pneumatically Actuating Silicone Module for Robotic Surgery Applications. *Soft Robotics.* 2014, **1**(4), pp.255-262.
146. Mooney, M. A theory of large elastic deformation. *Journal of applied physics.* 1940, **11**(9), pp.582-592.
147. Boresi, A.P. et al. *Elasticity in engineering mechanics.* John Wiley & Sons, 2010.
148. Elgström, E. *Practical implementation of hyperelastic material methods in FEA models*. 2014.
149. Ogden, R. et al. Fitting hyperelastic models to experimental data. *Computational Mechanics.* 2004, **34**(6), pp.484-502.
150. Martins, P. et al. A comparative study of several material models for prediction of hyperelastic properties: Application to silicone-rubber and soft tissues. *Strain.* 2006, **42**(3), pp.135-147.
151. Bhashyam, G.R. ANSYS mechanical—a powerful nonlinear simulation tool. *Ansys, Inc.* 2002, **1**(1), p.39.

152. BARANOWSKI, P. et al. Rubber structure under dynamic loading–computational studies. *Engineering Transactions.* 2013, **61**(1), pp.33–46.
153. Ogden, R.W. Large deformation isotropic elasticity–on the correlation of theory and experiment for incompressible rubberlike solids. *Proceedings of the Royal Society of London. A. Mathematical and Physical Sciences.* 1972, **326**(1567), pp.565-584.
154. Yeoh, O.H. Some Forms of the Strain Energy Function for Rubber. *Rubber Chemistry and Technology.* 1993, **66**(5), pp.754-771.
155. Arruda, E.M. and Boyce, M.C. A three-dimensional constitutive model for the large stretch behavior of rubber elastic materials. *Journal of the Mechanics and Physics of Solids.* 1993, **41**(2), pp.389-412.
156. Kilian, H.-G. et al. The use of the van der Waals model to elucidate universal aspects of structure-property relationships in simply extended dry and swollen rubbers. *Colloid and Polymer Science.* 1986, **264**(10), pp.866-876.
157. Standard, I. and ISO, B. Rubber, vulcanized or thermoplastic—Determination of tensile stress-strain properties. *International Organization for Standardization, Geneva.* 2005.
158. ASTM. Standard test methods for vulcanized rubber and thermoplastic elastomers-tension. *ASTM D412-16.* 2006.
159. Standardization, I.O.f. *ISO 7743: 2011: Rubber, Vulcanized Or Thermoplastic. Determination of Compression Stress-strain Properties.* ISO, 2011.
160. ASTM. Standard test methods for rubber properties in compression. 2012.
161. Holland, D.P. et al. The soft robotics toolkit: Strategies for overcoming obstacles to the wide dissemination of soft-robotic hardware. *IEEE Robotics & Automation Magazine.* 2017, **24**(1), pp.57-64.
162. Alici, G. An effective modelling approach to estimate nonlinear bending behaviour of cantilever type conducting polymer actuators. *Sensors and Actuators B: Chemical.* 2009, **141**(1), pp.284-292.
163. Elgeneidy, K. et al. Bending angle prediction and control of soft pneumatic actuators with embedded flex sensors–a data-driven approach. *Mechatronics.* 2018, **50**, pp.234-247.
164. Galloway, K.C. et al. Mechanically programmable bend radius for fiber-reinforced soft actuators. In: *2013 16th International Conference on Advanced Robotics (ICAR)*: IEEE, 2013, pp.1-6.
165. Ranzani, T. et al. Increasing the Dimensionality of Soft Microstructures through Injection-Induced Self-Folding. *Advanced Materials.* 2018, **0**(0), p.1802739.
166. Sun, Y. et al. A miniature soft robotic manipulator based on novel fabrication methods. *IEEE Robotics and Automation Letters.* 2016, **1**(2), pp.617-623.
167. Khin, P. et al. Soft haptics using soft actuator and soft sensor. In: *Biomedical Robotics and Biomechatronics (BioRob), 2016 6th IEEE International Conference on*: IEEE, 2016, pp.1272-1276.
168. Polygerinos, P. et al. Towards a soft pneumatic glove for hand rehabilitation. In: *2013 IEEE/RSJ International Conference on Intelligent Robots and Systems, 3-7 Nov. 2013*, 2013, pp.1512-1517.
169. Wang, H. et al. Design Methodology for Magnetic Field-Based Soft Tri-Axis Tactile Sensors. *Sensors.* 2016, **16**(9), p.1356.

170. Boer, G.d. et al. Design Optimisation of a Magnetic Field Based Soft Tactile Sensor. *Sensors.* 2017, **17**(11), p.2539.
171. Azim, S. et al. Soft tactile sensors with variable compliance. In: *2017 IEEE SENSORS*, *Oct. 29 2017-Nov. 1 2017*, 2017, pp.1-3.
172. Ou, J. et al. jamSheets: thin interfaces with tunable stiffness enabled by layer jamming. In: *Proceedings of the 8th International Conference on Tangible, Embedded and Embodied Interaction*, *Munich, Germany*. 2540971: ACM, 2013, pp.65-72.
173. Weng, M. et al. Multiresponsive Bidirectional Bending Actuators Fabricated by a Pencil-on-Paper Method. *Advanced Functional Materials.* 2016, **26**(40), pp.7244-7253.
174. L., W.E. et al. Low-Cost, Facile, and Scalable Manufacturing of Capacitive Sensors for Soft Systems. *Advanced Materials Technologies.* 2017, **2**(9), p.1700072.
175. Chossat, J.-B. et al. Soft Tactile Skin Using an Embedded Ionic Liquid and Tomographic Imaging. *Journal of Mechanisms and Robotics.* 2015, **7**(2), pp.021008-021008-9.
176. Wu, Y. et al. A skin-inspired tactile sensor for smart prosthetics. *Science Robotics.* 2018, **3**(22).
177. Yuen, M.C. and Kramer, R.K. Fabricating microchannels in elastomer substrates for stretchable electronics. In: *ASME 2016 11th International Manufacturing Science and Engineering Conference, MSEC 2016*, 2016.
178. Liu, Z. et al. A rapid prototyping technique for microfluidics with high robustness and flexibility. *Micromachines.* 2016, **7**(11).
179. Veale, A.J. et al. Modeling the Peano fluidic muscle and the effects of its material properties on its static and dynamic behavior. *Smart Materials and Structures.* 2016, **25**(6).
180. Suh, C. et al. Soft Pneumatic Actuator skin with embedded sensors. In: *2014 IEEE/RSJ International Conference on Intelligent Robots and Systems*, *14-18 Sept. 2014*, 2014, pp.2783-2788.
181. Booth, J.W. et al. OmniSkins: Robotic skins that turn inanimate objects into multifunctional robots. *Science Robotics.* 2018, **3**(22).

Appendix 1: Gantt Chart

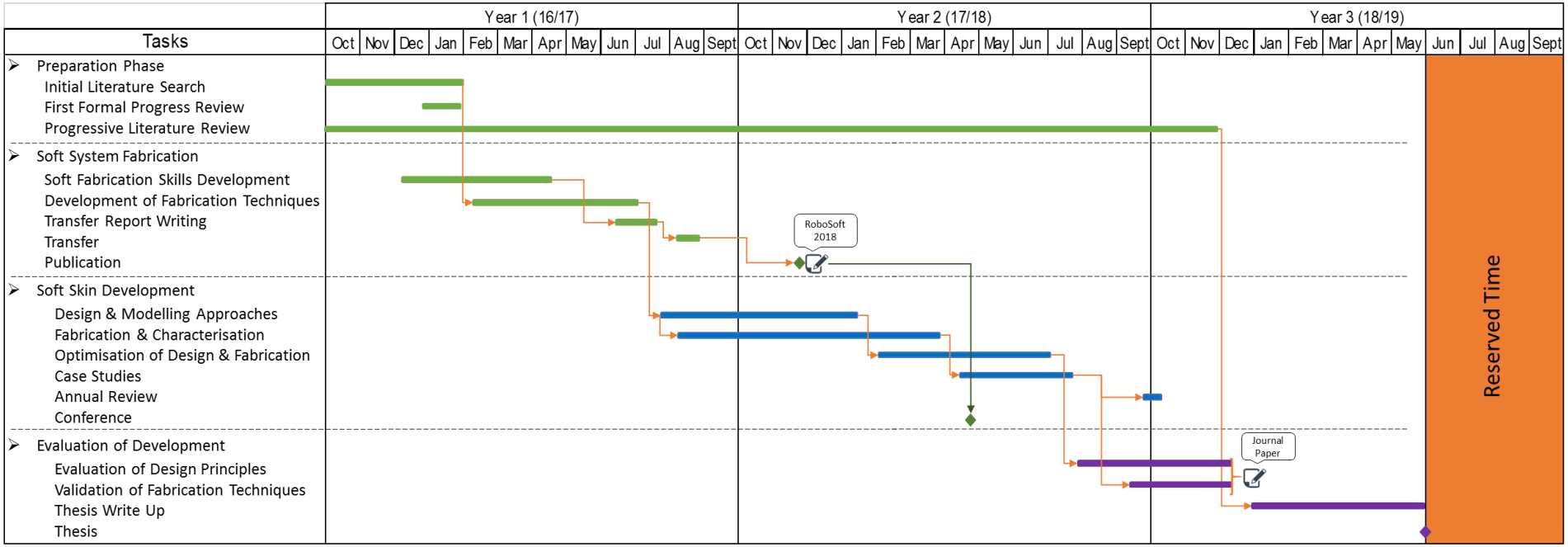

Appendix 1 Gantt Chart of Research Study

Appendix 2 Custom Pneumatic Set-Up

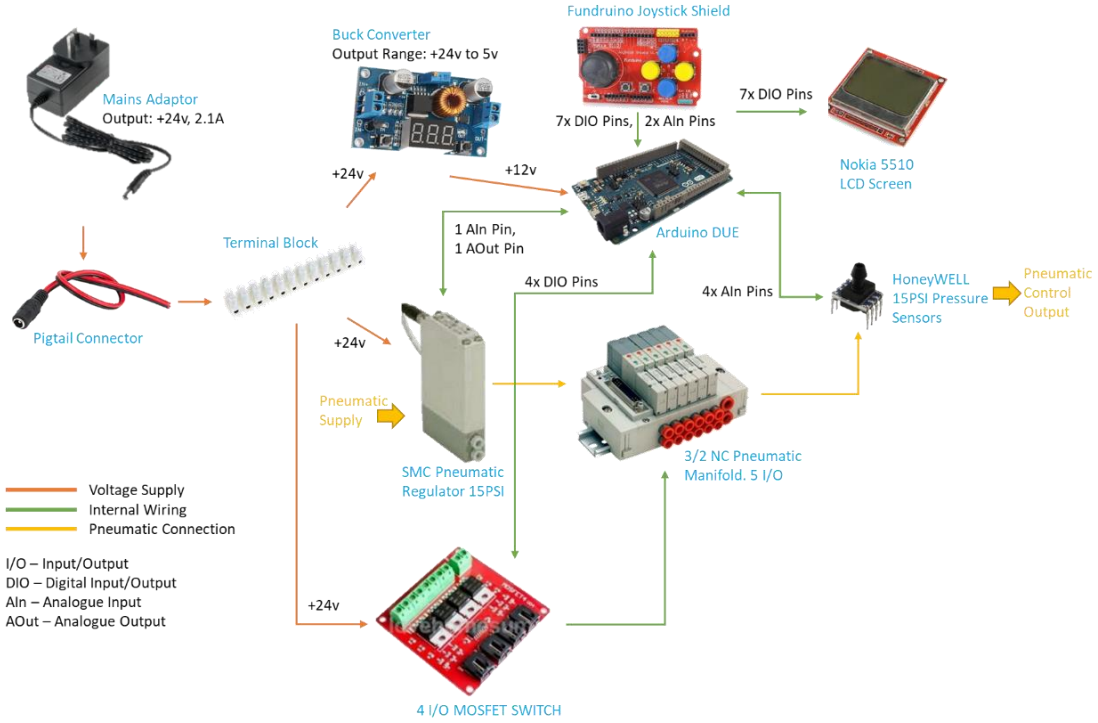

Appendix 2.1 Custom pneumatic control set-up assembly and build. Build of materials and components is listed in Appendix 2.2

No.	Part Name	Qty	Description	
1	RS Pro ACDC Adaptor 144-0962	1	Mains Adaptor AC – DC, Output 24V 2A.	https://bit.ly/2y6WoXQ
2	Droking Adjustable Step Down Converter	1	Buck Converter 24v to 5v	https://bit.ly/2Ue6crE
3	Arduino Due Microcontroller	1	Microcontroller	https://bit.ly/39fjXuu
4	Fundruino Joystick Shield	1	Joystick Shield for User Interaction	https://bit.ly/3bu7apz
5	Nokia 5510 LCD Screen	1	LCD Screen	https://bit.ly/2J9WzDW
6	SMC ITV0010-0200CL	1	Pneumatic Regulator 15PSI	https://bit.ly/2QKQemJ
7	5 I/O Pneumatic Valves	1	3/2 Normally Closed Pneumatic Manifold	https://bit.ly/2xkTcY7
8	4 I/O MOSFET Switchboard	1	MOSFET Switchboard	https://amzn.to/2y6D8K0
9	HoneyWELL SSCDANN015PAAA5	1	15PSI Absolute Pneumatic Sensor	https://bit.ly/2J9mhZn
10	Terminal Block	1	Non-fused Terminal Blocks	-
11	Pigtail Connector	3	Aux Adapter 3.5mm Audio Male/Female	https://amzn.to/2Uhd0F2
12	Pneumatic Tubing 4mm ϕ and 3m length	1	Pneumatic Tubing	-

Appendix 2.2 Build of materials and components for custom pneumatic set-up in reference to Appendix 2.2

Appendix 3 Bespoke Applicator Build

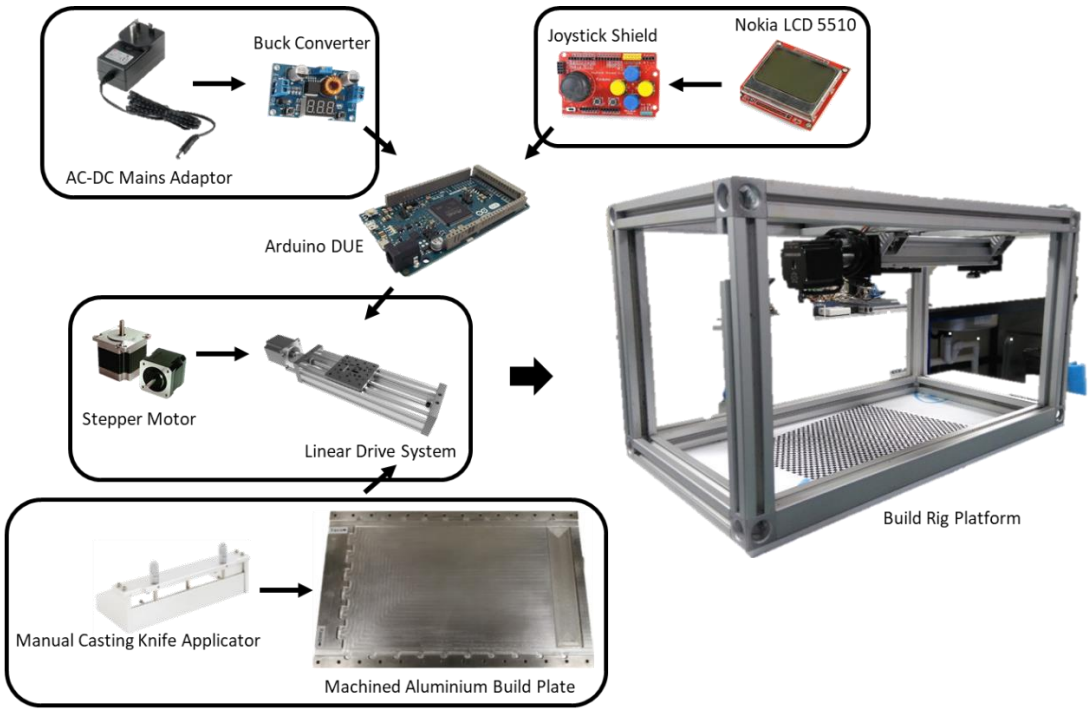

Appendix 3.1 Build and assembly of bespoke applicator platform. Build of materials and components is listed in Appendix 3.2

No.	Part Name	Qty	Description	
1	RS Pro ACDC Adaptor 144-0962	1	Mains Adaptor AC – DC, Output 24V 2A.	https://bit.ly/2y6WoXQ
2	Droking Adjustable Step Down Converter	1	Buck Converter 24v to 5v	https://bit.ly/2Ue6crE
3	Arduino Due Microcontroller	1	Microcontroller	https://bit.ly/39fjXuu
4	Fundruino Joystick Shield	1	Joystick Shield for User Interaction	https://bit.ly/3bu7apz
5	NEMA 17 Stepper Motor	2	Stepper Motor	https://bit.ly/2WErYGr
6	Digital Stepper Controller 2DM542	2	Stepper Controller Board	https://amzn.to/3dtEvCA
7	Elcometer Casting Knife Applicator	1	20cm wide Casting Knife Applicator	https://bit.ly/2UyfbTn
8	Open Build Linear Drive System	2	40cm length Linear Drive System	https://bit.ly/2WErYGr
9	Machined Aluminum (5083) Plate	1	Aluminum 5083	-
10	Rexroth Bars (Various Lengths)	1	Platform Assembly	-

Appendix 3.2 Build of materials and components for bespoke applicator platform in reference to Appendix 3.1

Appendix 4 Chapter 4 Characterisation Results

Appendix 4.1 Thickness Graphs

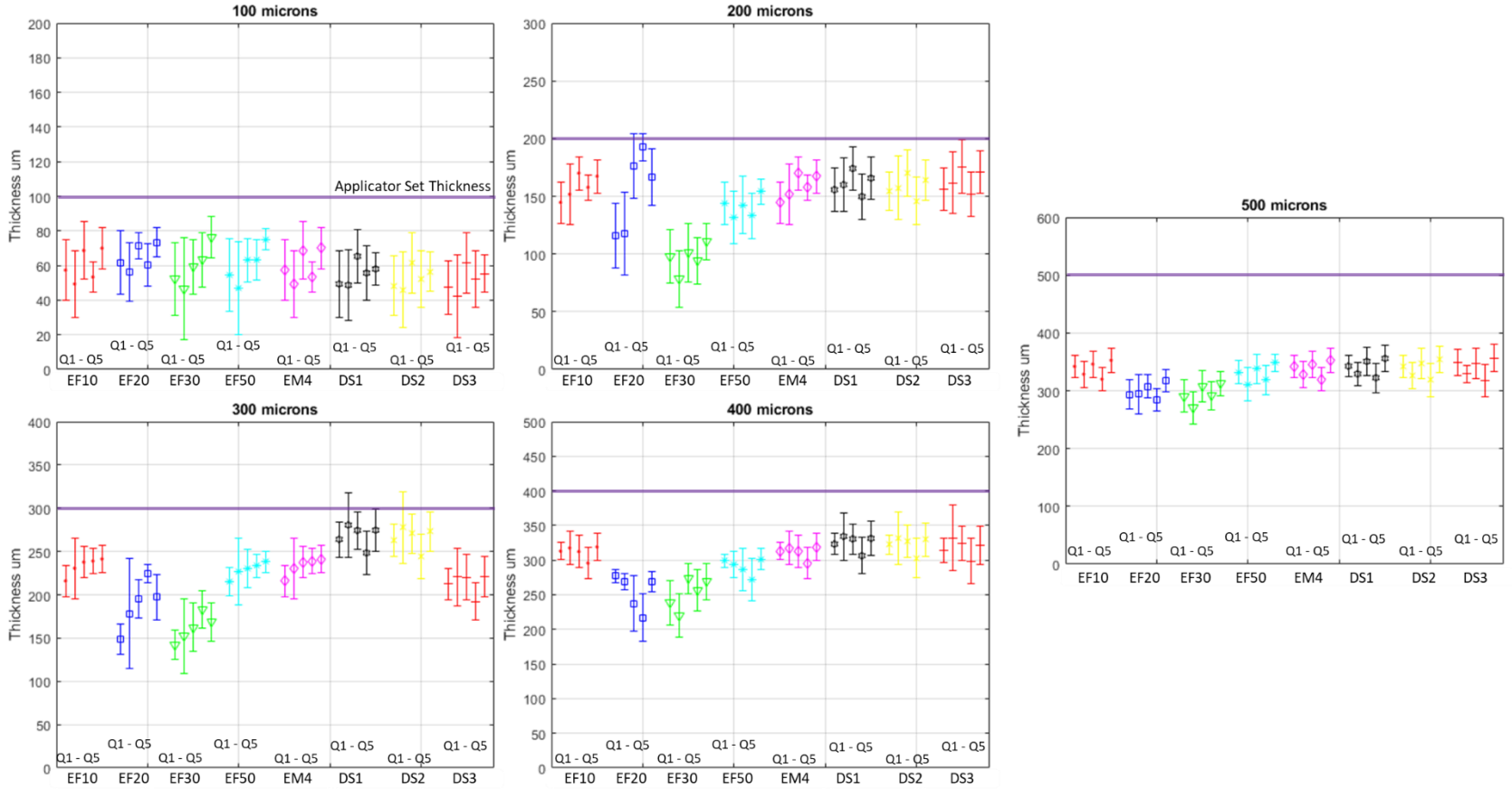

Appendix 4.1.1 Characterisation of applicator set thickness (gap) from 100 microns to 500 microns. Full list of material reflected from Section 4.1.2.

Appendix 4.2 Speed Graphs

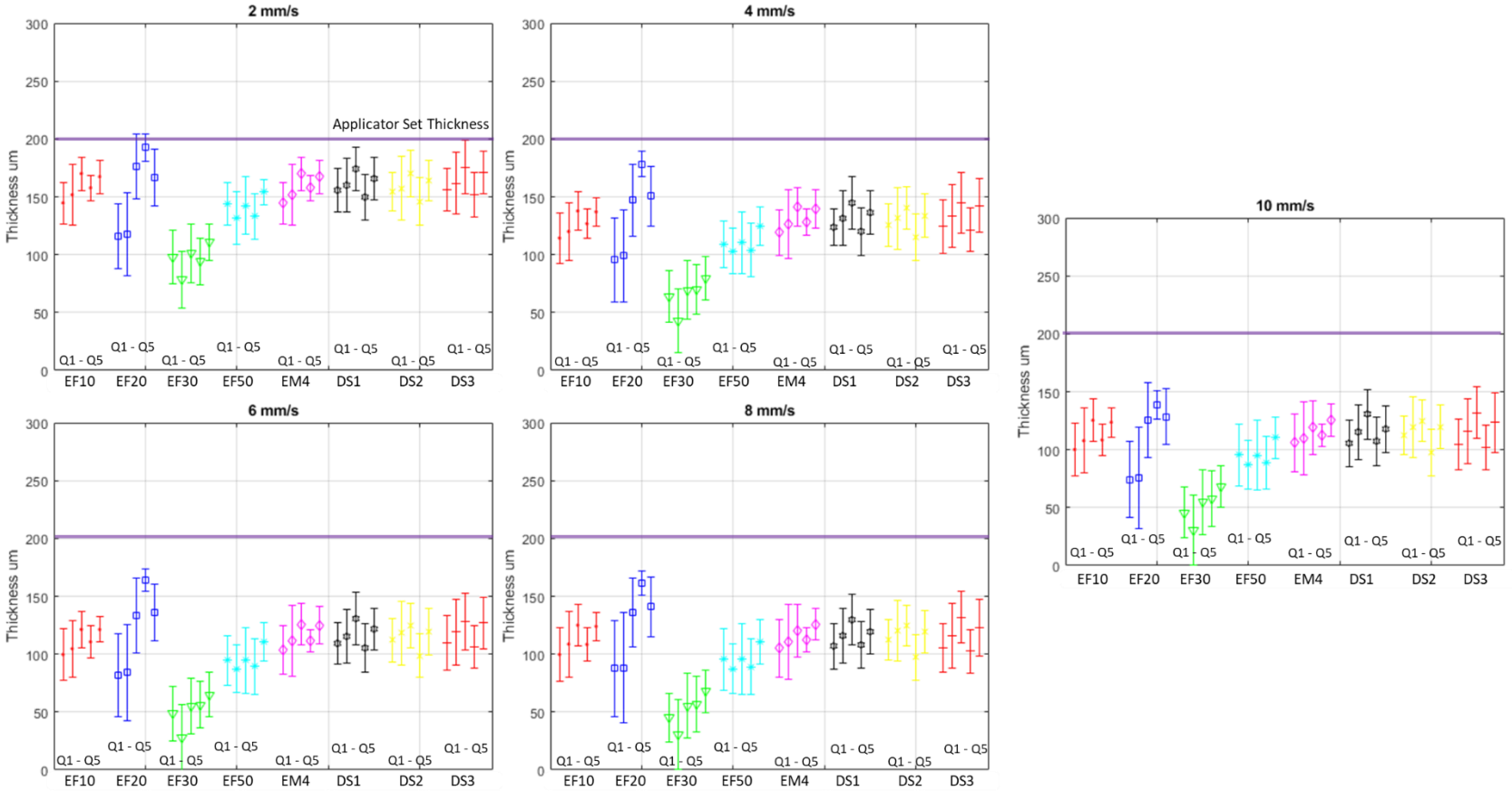

Appendix 4.2.1 Characterisation of applicator spread speed from 2mm/s to 10mm/s in 2mm/s intervals for 200-micron designated applicator layer.

Appendix 4.3 Temperature Graphs

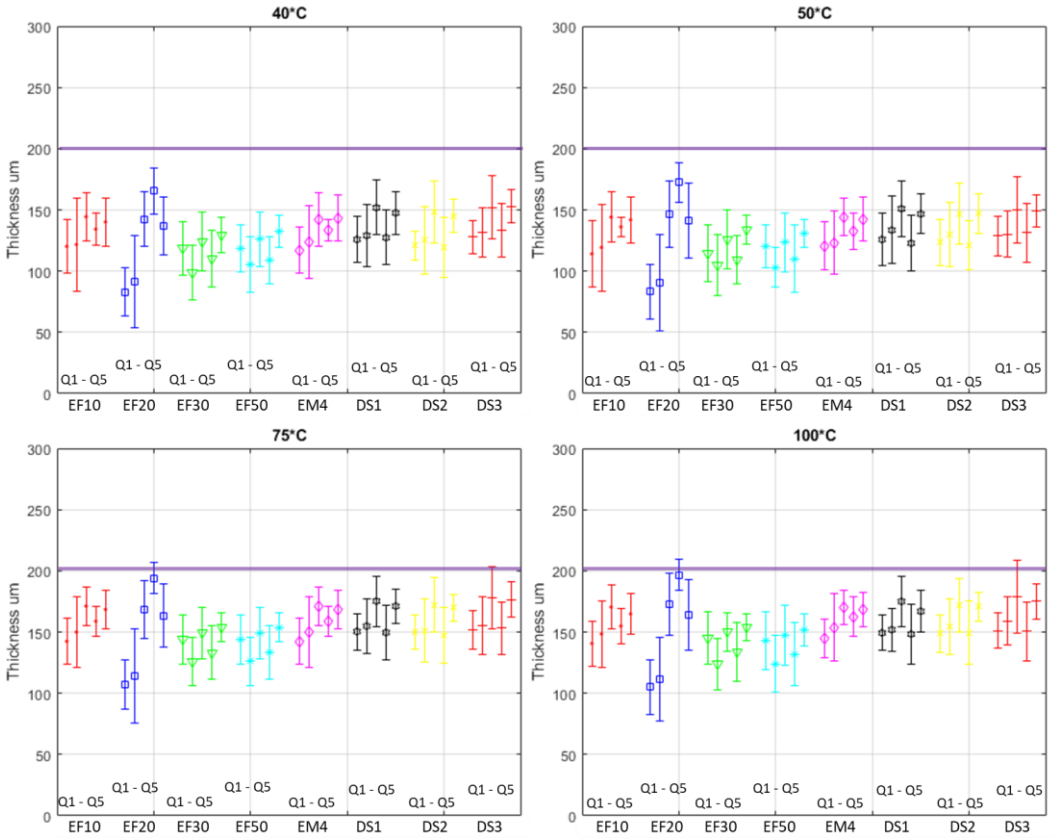

Appendix 4.3.1 Characterisation of curing temperature from 40°C, 50°C, 75°C and 100°C for 200-micron designated applicator layer.

Appendix 4.4 Tensile Graphs

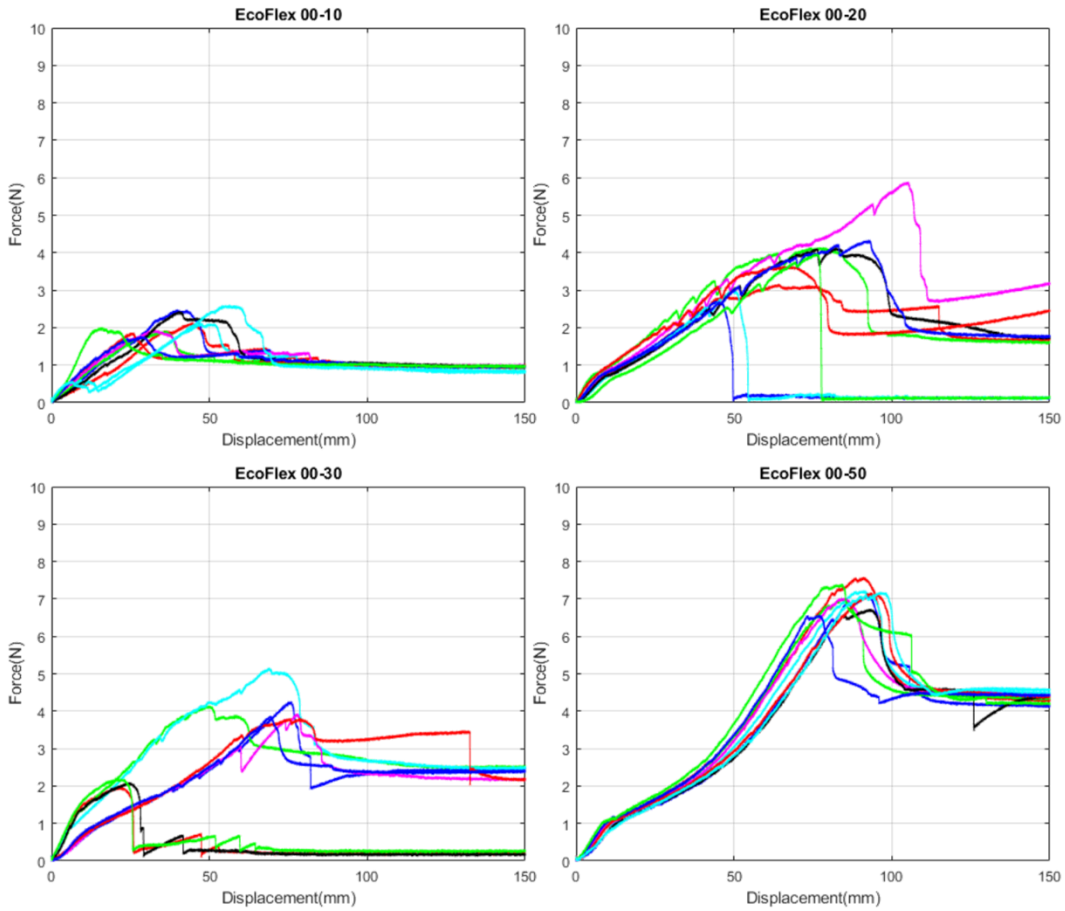

Appendix 4.4.1 Force against displacement result for all available elastomers (EcoFlex® Series)

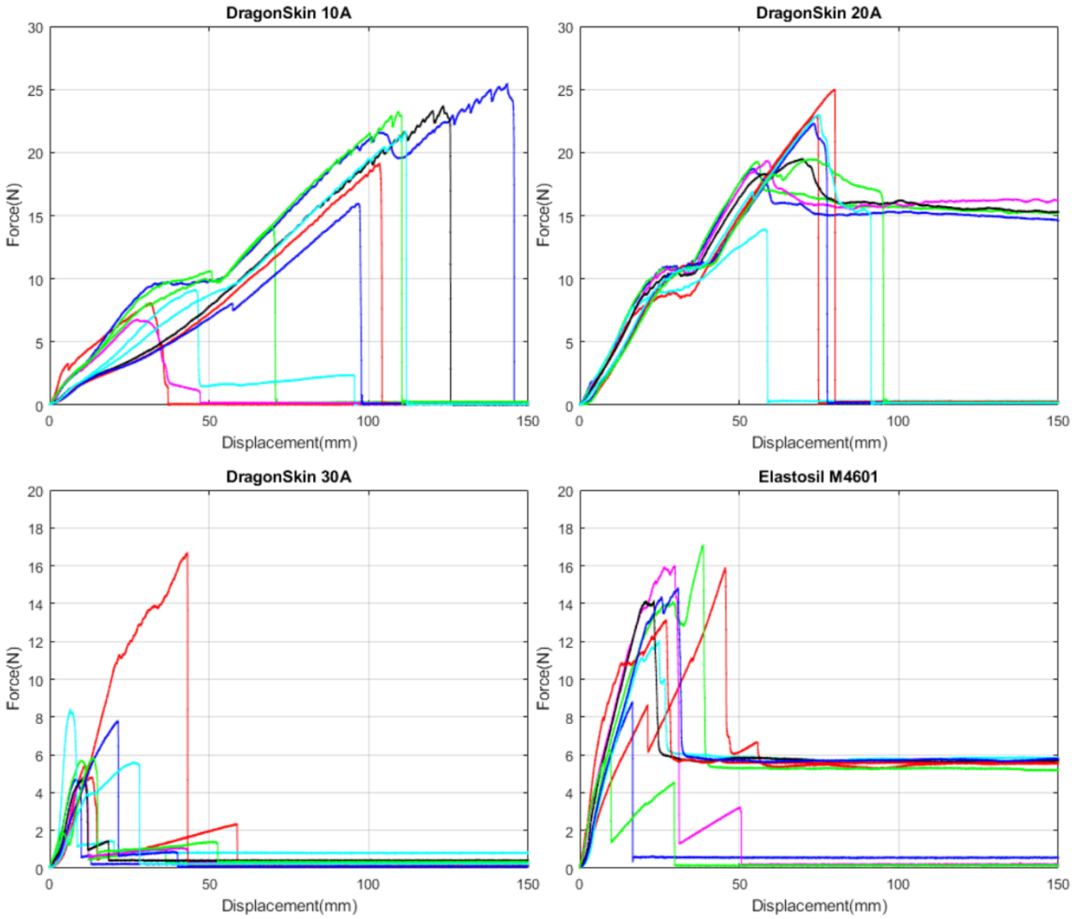

Appendix 4.4.2 Force against displacement result for all available elastomers (DragonSkin™ Series and Elastosil M4601)

Appendix 4.5 Recorded Depth Analysis of Laser Ablation

	Speed	EcoFlex™00-30														
Power	1%	5%	10%	15%	20%	25%	30%	35%	40%	45%	50%	60%	70%	80%	90%	100%
1%	0.06	0.08	0.02	0	0.05	0.02	0.05	0.04	0.07	0.07	0.05	0.08	0.09	0.06	0.02	0.08
5%	1.50	0.53	0.53	0.5	0.28	0.21	0.28	0.22	0.27	0.24	0.15	0.18	0.07	0.09	0.07	0.03
10%	1.20	0.34	0.13	0.13	0.11	0.12	0.08	0.11	0.12	0.07	0.33	0.19	0.15	0.08	0.13	0.09
15%	2.14	0.81	0.59	0.49	0.49	0.49	0.44	0.48	0.49	0.25	0.26	0.24	0.15	0.08	0.07	0.04
20%	1.84	0.86	0.49	0.42	0.29	0.25	0.24	0.21	0.24	0.24	0.3	0.21	0.15	0.11	0.10	0.09
25%	2.43	1.05	0.66	0.55	0.52	0.48	0.43	0.44	0.42	0.36	0.37	0.31	0.25	0.26	0.24	0.17
30%	2.92	1.25	0.76	0.63	0.64	0.59	0.49	0.42	0.44	0.46	0.45	0.4	0.31	0.36	0.28	0.32
35%	2.96	1.19	0.64	0.45	0.5	0.41	0.33	0.27	0.25	0.26	0.14	0.18	0.05	0.1	0.08	0.07
40%	3.53	1.44	1.12	0.81	0.72	0.67	0.54	0.4	0.39	0.32	0.33	0.27	0.17	0.23	0.08	0.1
45%	3.54	1.47	0.99	0.73	0.74	0.62	0.53	0.48	0.61	0.41	0.37	0.38	0.38	0.32	0.27	0.32
50%		1.84	1.18	0.84	0.78	0.72	0.58	0.47	0.45	0.43	0.32	0.29	0.24	0.19	0.1	0.16
60%		2.08	1.28	0.93	0.87	0.71	0.59	0.54	0.51	0.52	0.41	0.41	0.35	0.39	0.36	0.34
70%		2.51	1.47	1.18	0.93	0.85	0.7	0.64	0.64	0.57	0.54	0.5	0.39	0.37	0.29	0.23
80%		2.6	1.62	1.01	0.87	0.76	0.71	0.64	0.61	0.64	0.62	0.45	0.37	0.33	0.34	0.37
90%		2.72	1.6	1.43	1.16	1.02	0.86	0.70	0.68	0.62	0.59	0.52	0.37	0.27	0.22	0.13
100%		2.89	1.61	1.42	1.26	1.05	0.85	0.66	0.66	0.58	0.59	0.40	0.33	0.29	0.16	0.22

Appendix 4.5.1 Recorded depth analysis of laser ablation for EcoFlex™00-30

	Speed	EcoFlex™00-50														
Power	1%	5%	10%	15%	20%	25%	30%	35%	40%	45%	50%	60%	70%	80%	90%	100%
1%	0.06															
5%	1.44	0.52	0.45	0.45	0.22	0.20	0.19	0.19	0.19	0.18	0.09	0.09	0.03	0.03	0.02	0.02
10%	1.20	0.30	0.13	0.10	0.08	0.08	0.08	0.08	0.08	0.04	0.30	0.10	0.07	0.07	0.07	0.02
15%	2.09	0.79	0.54	0.47	0.43	0.42	0.42	0.42	0.42	0.17	0.17	0.15	0.09	0.08	0.07	0.04
20%	1.76	0.77	0.47	0.33	0.29	0.25	0.21	0.20	0.20	0.20	0.21	0.15	0.09	0.09	0.08	0.08
25%	2.39	1.03	0.62	0.50	0.46	0.42	0.38	0.36	0.35	0.35	0.35	0.29	0.22	0.18	0.17	0.17
30%	2.89	1.19	0.67	0.59	0.56	0.53	0.47	0.43	0.42	0.42	0.35	0.33	0.29	0.27	0.27	0.28
35%	2.91	1.14	0.58	0.39	0.41	0.38	0.33	0.26	0.22	0.20	0.15	0.10	0.04	0.05	0.04	0.05
40%	3.52	1.42	1.06	0.77	0.68	0.60	0.45	0.41	0.38	0.31	0.29	0.20	0.16	0.14	0.04	0.03
45%	3.51	1.40	0.99	0.72	0.66	0.60	0.44	0.45	0.56	0.39	0.37	0.36	0.30	0.25	0.22	0.23
50%	4.39	1.81	1.14	0.80	0.76	0.66	0.52	0.47	0.39	0.35	0.31	0.27	0.21	0.10	0.08	0.07
60%		2.03	1.26	0.93	0.79	0.70	0.54	0.52	0.50	0.48	0.40	0.36	0.33	0.35	0.29	0.28
70%		2.46	1.47	1.11	0.89	0.82	0.70	0.60	0.59	0.56	0.53	0.47	0.31	0.28	0.24	0.19
80%		2.53	1.58	0.99	0.83	0.76	0.62	0.58	0.57	0.57	0.56	0.39	0.35	0.33	0.34	0.33
90%		2.61	1.58	1.35	1.11	0.96	0.79	0.69	0.59	0.55	0.51	0.44	0.31	0.25	0.16	0.13
100%		2.62	1.59	1.37	1.18	0.98	0.81	0.65	0.58	0.54	0.49	0.40	0.26	0.19	0.13	0.16

Appendix 4.5.2 Recorded depth analysis of laser ablation for EcoFlex™00-50

	Speed	Elastosil®M4601														
Power	1%	5%	10%	15%	20%	25%	30%	35%	40%	45%	50%	60%	70%	80%	90%	100%
1%	0.07															
5%	0.78	0.02	0.02	0.01												
10%	1.19	0.13	0.05	0.04	0.02											
15%	1.43	0.32	0.09	0.02	0.01											
20%	1.69	0.36	0.13	0.07	0.04	0.03	0.03	0.02								
25%	1.84	0.79	0.46	0.37	0.33	0.30	0.23	0.19	0.15	0.15	0.14	0.09	0.04	0.02	0.02	
30%	1.29	0.43	0.14	0.08	0.08	0.09	0.03	0.02	0.01							
35%	1.81	0.79	0.37	0.24	0.19	0.24	0.13	0.07	0.04	0.02	0.01	0.02	0.01	0.01		
40%	1.67	0.77	0.34	0.19	0.11	0.13	0.08	0.04	0.04	0.02						
45%	2.34	1.18	0.72	0.52	0.47	0.40	0.35	0.32	0.29	0.26	0.27	0.21	0.18	0.17	0.15	
50%	2.55	1.50	0.87	0.66	0.60	0.51	0.36	0.36	0.31	0.29	0.21	0.12	0.09	0.08	0.08	
60%	3.08	1.04	0.72	0.38	0.39	0.33	0.26	0.19	0.13	0.16	0.16	0.14	0.14	0.38	0.30	0.21
70%	3.29	1.03	0.88	0.62	0.51	0.44	0.30	0.24	0.18	0.16	0.15	0.04	0.04			
80%	3.34	1.07	0.98	0.78	0.67	0.60	0.48	0.42	0.37	0.32	0.19	0.15	0.13	0.15	0.13	0.81
90%	3.38	1.35	1.18	0.99	0.77	0.64	0.54	0.47	0.43	0.41	0.31	0.24	0.14	0.90	0.70	0.50
100%		1.30	1.03	0.94	0.72	0.60	0.47	0.41	0.38	0.33	0.27	0.24	0.12	0.15	0.12	0.11

Appendix 4.5.3 Recorded depth analysis of laser ablation for Elastosil®M4601

	Speed	DragonSkin™30A														
Power	1%	5%	10%	15%	20%	25%	30%	35%	40%	45%	50%	60%	70%	80%	90%	100%
1%	0.08															
5%	0.81	0.04														
10%	1.33	0.31	0.18	0.13	0.14	0.11	0.07	0.03	0.02	0.02						
15%	1.47	0.48	0.24	0.14	0.15	0.13	0.09	0.04	0.02	0.02	0.02					
20%	1.37	0.54	0.21	0.11	0.08	0.06	0.04	0.03	0.05	0.03	0.02					
25%	1.88	1.01	0.52	0.38	0.33	0.30	0.20	0.12	0.08	0.05	0.04	0.04	0.02	0.02		
30%	1.84	1.02	0.61	0.45	0.42	0.36	0.28	0.24	0.24	0.19	0.12	0.07	0.03	0.02		
35%	2.09	0.97	0.71	0.50	0.42	0.36	0.27	0.22	0.21	0.15	0.12	0.08	0.02	0.01		
40%	2.04	1.04	0.84	0.63	0.54	0.46	0.37	0.31	0.24	0.22	0.10	0.05	0.04	0.01	0.01	
45%	1.78	0.76	0.61	0.52	0.39	0.33	0.23	0.22	0.12	0.11	0.09	0.05	0.04	0.02	0.02	
50%	2.10	0.78	0.64	0.61	0.53	0.46	0.41	0.36	0.26	0.28	0.25	0.22	0.14	0.12	0.10	0.08
60%	2.19	0.81	0.78	0.76	0.61	0.53	0.44	0.37	0.31	0.34	0.34	0.29	0.23	0.20	0.16	0.14
70%	2.51	1.21	1.06	0.86	0.76	0.62	0.53	0.44	0.42	0.39	0.27	0.18	0.11	0.10	0.09	0.07
80%	3.21	1.27	1.28	0.94	0.74	0.61	0.56	0.43	0.39	0.37	0.33	0.24	0.17	0.13	0.12	0.08
90%	3.26	1.23	1.13	0.91	0.67	0.56	0.49	0.38	0.31	0.27	0.18	0.14	0.06	0.02	0.03	0.02
100%		1.36	0.84	0.80	0.82	0.70	0.55	0.45	0.36	0.35	0.33	0.21	0.09	0.04	0.04	0.03

Appendix 4.5.4 Recorded depth analysis of laser ablation for DragonSkin™30A

Appendix 5

Appendix 5.1 List of hyper-elastic model coefficients

Coefficients	Elastomeric Material					
(MPa)	Elastosil® M4601	EcoFlex™ 00-30	EcoFlex™ 00-50	DragonSkin™ 20A	DragonSkin™ 30A	Sylguard™ 184
Yeoh						
$C10$	0.112	0.008	0.015	0.048	0.043	0.0493
$C20$	0.019	0	0	0.016	0.015	0.0211
$C30$	0	4.03×10^{-7}	-1.62×10^{-7}	-3.04×10^{-5}	0	-5.854
Ogden						
μ_1	-3.646	0.024	2.95×10^{-6}	-5.46×10^{-7}	-1.37×10^{-6}	-3.58×10^{-7}
μ_2	0.619	6.67×10^{-5}	4.64×10^{-6}	3.39×10^{-6}	2.89×10^{-6}	5.07×10^{-6}
μ_3	7.00×10^{-6}	4.54×10^{-4}	-2.10×10^{-6}	-8.90×10^{-7}	-1.73×10^{-6}	-9.77×10^{-6}
α_1	2.49×10^{-6}	1.714	0.0196	-1	-2.892	3.073
α_2	3.39×10^{-6}	7.068	0	0.094	0.246	0.041
α_3	2.34×10^{-6}	-3.366	0.0094	0.999	2	-3.039

Appendix 5.2 System Units (SI) to be used in FEM software Abaqus

Dimensions	Units
Length	mm
Force	N
Time	s
Pressure	MPa
Stress	MPa
Mass	$1 \times 10^3\ Kg$
Volume	$1 \times 10^{-9}\ m^3$
Density	$1 \times 10^{12} kg/m^3$
Energy	mJ
Velocity	$1 \times 10^{-3} m/s$
Acceleration	$1 \times 10^{-3} m/s^2$

Usage example: If Density = 1000 kg/m3, FEA Software will specify the density as 1000e-12.

Appendix 5.3 Actuator Matrix

Actuator Width [*Aw*] 5mm, 10mm, 20mm Thickness Layer Ratio [*Lr*]	*Aw* *Cw* 5mm: = 1mm 10mm: = 6mm 20mm: = 16mm *Cb* = 0.5mm	*Aw* *Cw* 5mm: = 1mm 10mm: = 6mm 20mm: = 16mm *Cr* = 1mm	*Aw* *Cw* 5mm: = 1mm 10mm: = 6mm 20mm: = 16mm *Cr* =1.5mm	*Aw* *Cw* 5mm: = 1mm 10mm: = 6mm 20mm: = 16mm *Cb* = 2mm
L2: 0.45mm L0: 0.45mm *Lr* =1.00	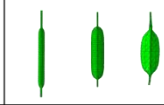	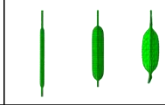	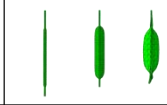	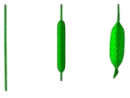
L2: 0.35mm L0: 0.55 mm *Lr* = 0.63				
L2: 0.25mm L0: 0.65 mm *Lr* = 0.38				
L2: 0.15mm L0: 0.75 mm *Lr* = 0.20				
L2: 0.10mm L0: 0.80 mm *Lr* = 0.125				

[Note: Each box represents the three modelled SPICAs of different Actuators Widths (A_w) for 5 mm, 10mm, and 20 mm (Left to Right) in an inflated state at 10 psi]

Appendix 6 (Thin Soft layered Actuator Based on a Novel Fabrication Technique.)

2018 IEEE International Conference on Soft Robotics (RoboSoft)
Livorno, Italy, April 24-28, 2018

Thin Soft Layered Actuator Based on a Novel Fabrication Technique

Jun Wai Kow *Student Member, IEEE*, Peter Culmer, *Member, IEEE*, and Ali Alazmani, *Member, IEEE*

Abstract— **This paper presents a novel fabrication method for constructing thin soft layered actuators. The method is based on building up thin layers of elastomeric material with embedded strain-limiting and mask layers using a bespoke film applicator. This enables the fabrication of millimetre-scale soft actuators with complex integrated masks and/or strain-limiting layers, as demonstrated in a series of proof of concept prototypes. The prototype actuators can be cut into a desired shape via laser cutting the laminated sheet. This paper shows the feasibility of the fabrication method and the value of its use in creating thin soft layered actuators for application in soft robotics. The technique can be further developed to fabricate multi-material composite soft actuators which are thin, compact, flexible and stretchable.**

I. Introduction

There have been great advances in the field of soft robotics since its inception, founded to bridge the gap between nature and the state of the art 'rigid' robotic systems of the day. There is increasing demand for soft robotic technology due to factors including the innate compliance, safety, and adaptability which such systems possess. To date, soft robotic systems have typically operated at centimetre or larger scales, largely limited by the fabrication processes involved in their manufacture. However, there is growing demand for smaller, more precise and more dexterous soft robotic systems which can address challenges in diverse areas including healthcare, manipulation and search and rescue [1-3]. Thus, the development of new high-precision fabrication techniques is crucial to support the advancement and expansion of soft robotics.

Since its inception, soft robotic fabrication has seen a shift from conventional 'moulding and casting' methods to explore a range of rapid prototyping techniques including 3D printing [4-6], soft lithography [7-9], shape deposition manufacturing [10, 11], and combinative techniques [12-17]. These techniques have all been exploited to build soft robotic actuators and inflatable surfaces [18-22]. Soft actuators such as pneumatic networks (PneuNet) [23] and fiber-reinforced pneumatic artificial muscles (FPAM) [24] have inspired variants of soft pneumatic actuator (SPA)'s designs over the years, all of which uses a form of moulding or casting in their fabrication process. Attempts have been made to build small SPAs based on 3D printed moulds, however, despite the feasibility, due to design and geometrical constraints of moulding techniques, the ability of these actuators to operate in applications with narrow and limited space are somewhat limited [3, 25, 26]. Moreover, moulding-based fabrication techniques are inherently limited in the geometries they can produce which consequently limits the functionality of the actuators they produce.

In order to address the shortcomings of conventional SPAs, there is a need for more flexible fabrication methods that can easily produce soft actuators at small scales with precise features and functionalities that can be easily designed.

In this paper, we describe a novel thin Soft Layered Composition (tSLC) fabrication technique to develop millimetre-scale thin Soft Layered Actuators (tSLA) with precise millimetre features. The technique derives from laminating and stacking thin precision-cut laminar materials which can include soft elastomers as inflatable layers, strain-limiting layers, and mask layers. The regions covered by the mask layer (between strain-limiting layer and inflatable layers) define inflatable 'zero-volume' cavities that can be selectively actuated through fluid inlets. This fabrication method enables the creation of complex, articulated mechanisms with submillimetre scale mechanical features with a range of potential applications in soft robotic research.

The remainder of the study is organised as follows: Section II describes the conceptual design for the tSLA and its production using our new tSLC fabrication method. The characterisation and test results of the actuator are then discussed in Section. III. Followed by, a discussion of the fabrication technique and conclusion in Section. IV and V respectively.

II. Actuator Design and Fabrication Method

A. Conceptual Design

Our proposed tSLA consists of thin soft elastomeric layers, strain-limiting layers, and mask layers stacked on top of each other to form a compound system, as shown in Fig. 1(a) and 1(b). Portions of the strain-limiting layer and the elastomeric layer can be selectively adhered to each other based on the mask layer features. This forms an inflatable structure with zero-volume chambers. The elastomeric material layers enable expansion of the inflatable cavities and channels as well as adhesion between layers when applied in a pre-polymer form. The stiffness of this layer must be less than that of the strain-limiting layer such that it bends or deforms more

J.W. Kow, P. Culmer, and A. Alazmani are with the School of Mechanical Engineering, University of Leeds, Leeds LS2 9JT, United Kingdom (Tel: +44 (0)113 343 2178, e-Mail: a.alazmani@leeds.ac.uk).

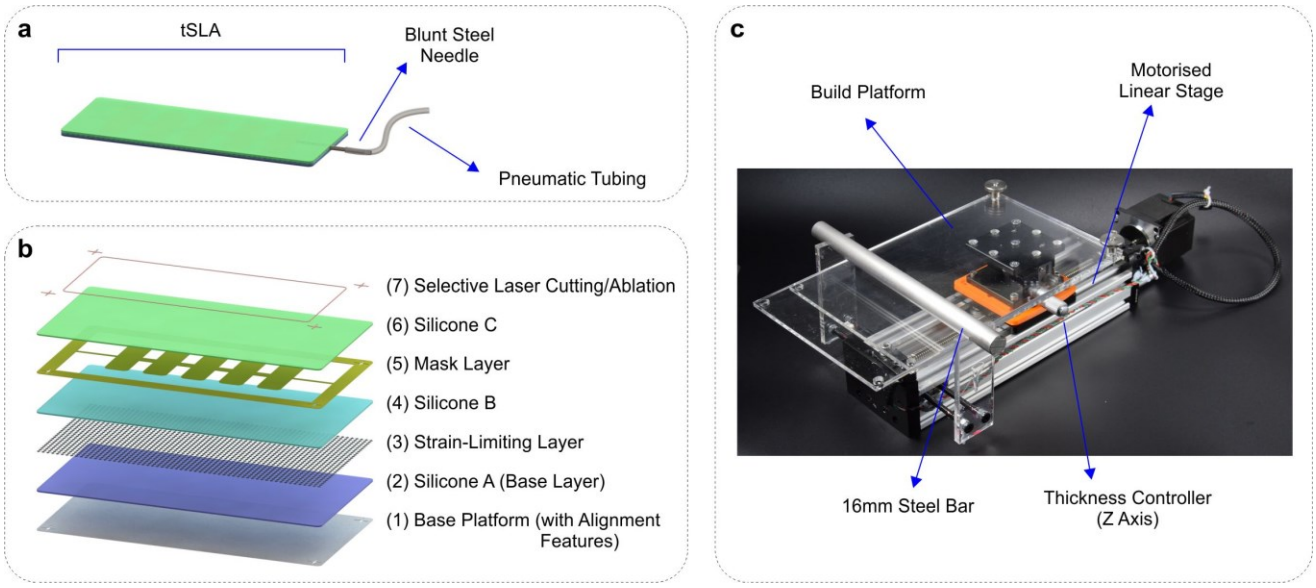

Figure 1. (a) Conceptual design for the tSLA, (b) Schematic diagram of the tSLC fabrication steps to create tSLA (orthogonal view). This includes base platform with alignments features, elastic layers (i.e. silicone), strain-limiting layer (i.e fabric, paper), mask layer produced via laser cutting, and final selective laser cutting to pattern and/or separating the tSLA from the base platform sheet, (c) Bespoke thin film applicator to apply thin and uniform prepolymer silicone.

readily compared to the strain-limiting layer. A stiffer elastomer or inextensible material (i.e. fabric, paper, and polyethylene terephthalate (PET) film) can be used for strain-limiting layers. This layer acts to resist various types of strains in one or multi directions until its yield strength is reached. Upon actuation, expansion of the inflatable layer is directed by the strain-limiting layer, causing a bending motion or resultant force which can be exploited for actuation.

Using this concept, the stiffness, overall thickness, inflation profile and geometry of the soft actuator can be manipulated layer by layer, with the selection of appropriate materials and profiles and consideration of their configuration relative to each other. This can then be utilised to develop tSLAs with a range of pre-programmed behaviours and geometries.

B. Fabrication Technique

The conceptual tSLA design drove the development of our tSLC fabrication method which aims to exploit a combination of thin laminar structures, created here using a bespoke film applicator as shown in Fig. 1(c), which can be precisely cut or etched using a laser-cutter. The applicator consists of a linear actuating stage (C-Beam® Linear Actuator, Open Build) of 175 mm travel distance with a manual vertical stage (MAZ-40-10 Z-axis Vertical Stage, Optics Focus Solutions) to control the height of the applicator platform made of extruded acrylic (W: 250 mm, L: 150 mm). A metal rod of 16 mm Ø is mounted at a set height of 10 mm from the base of the rod to the applicator platform. The translational stage is able to move the film platform relative to the rod from 1 up to 10 mm/s. The vertical stage is then manually calibrated to adjust the rod-plate separation and thus produce films sheets of desired thicknesses ranging from 0.1 mm to 1 mm.

The tSLC fabrication process, is as follows: (i) the applicator is set to the desired layer thickness while pre-polymer silicone is poured onto the centre of the platform. (ii) The platform is then actuated at a desired set speed; spreading the silicone across the platform to produce the desired thickness. (iii) Once the silicone has spread, the platform is then removed and placed into an oven to cure for a set time depending on the type of silicone. (iv) Strain-limiting materials (i.e fabric or pre-polymer silicone) or laser cut masks layers are then added to the layer before and/or after the silicone has been cured. (v) Further layers of silicone or embedded material are introduced by repeating stages (i)-(iv) based on the desired layer configuration. Once completed, the composite structure is aligned onto a backing paper, using pre-defined alignment features, and placed into a 50W laser cutter (VLS3.50 Universal Laser Systems) to cut out the desired shape, as shown in Fig. 2(a). The fabricated actuators are cleaned (using isopropanol), integrated with pneumatic airlines and are then ready to be tested and used.

The selective laser cutting process can be used not only to cut the tSLA and separate it from the base build platform, but also to cut individual layers and/or patterns to produce desirable features for the tSLA. The profile of these patterns can be controlled in Z-axis direction by adjusting power and speed settings of the laser beam. Alignment features are utilised to align each layer on the laser's cutting platform. The layer is cleaned using an airgun and then a sonicator to remove any debris and soot from the layer. This will provide a clean surface and make sure good bonds can be created when other layers are added in the tSLC process [27, 28].

C. Fabrication of tSLA

A range of prototype tSLAs were developed to evaluate their performance and the characteristics and efficacy of the underlying fabrication method.

As illustrated in Fig 1(a) and 1(b), a layer-by-layer schematic was first designed to determine the sequential process for the actuator fabrication. The fabrication of each soft actuator are as followed: (i). the applicator is configured to produce the desired layer thickness. Pre-polymer silicone is prepared for all elastomeric layers, in this instance using Ecoflex 50 (Smooth-On Inc., USA) mixed at 2000 rpm for 90 seconds (ARE-310, Thinky Inc., Japan). Defoaming of the mixture was performed at 2200 rpm for the same time period. After mixing, the mixture was poured onto the platform and spread across using the film applicator to form a silicone sheet of 0.4 mm. A fabric mesh with 0.1 mm thickness (Soft 'n Sheer stabiliser, Sulky of America Inc.) is then placed on top of the pre-polymer silicone layer to embed the fabric as a strain-limiting layer. (ii). The platform is then removed from the stage and placed into the oven at 45°C for 10 to 15 minutes. This process speeds the curing of silicone and control the thickness of the film, while other elastomeric material may require longer curing times. (iii). Once the first layer has been cured, the platform is adjusted to compensate to the new height and another layer of 0.4 mm thick Ecoflex 50 is applied and cured in the oven. (iv). A mask layer of 0.1 mm thickness (Paper Solvy Water Soluble Stabiliser, Sulky of America Inc) is laser cut to the shape of the zero-volume cavity and then manually aligned on top of the cured layer of silicone. This is then followed by an application of a 1.5 mm layer of silicone to encapsulate the mask layer. (v). After the final layer of silicone is cured, the sheet is removed from the build platform onto an alignment sheet for laser cutting. The mask layers are made of water-soluble paper which are readily removed from the fabricated actuator by flushing with water, leaving a zero volume chamber for pneumatic inflation.

III. Characterisation and Results

A. Experimental Design

Preliminary characterisation of the prototype tSLAs were performed to consider the effect of two key design parameters on the actuator behaviour; channel configuration and cavity width. As shown in Fig. 2(a) and 2 (b), based on preliminary work a nominal spacing between cavities was set at 5 mm for two cavity width configurations of 5 mm and 3 mm. In addition, two channel configurations were designed to investigate the effect of placing pressure lines in different locations (DL: Dual-line channel, SL: Single-line channel), while the total channel width of 3 mm remained constant between different configurations.

A custom experimental test rig, shown in Fig. 3, was developed to measure block force and bending angle of each tSLAs across a range of controlled input pressures (0 to 5 psi). For each test, the prototype actuators are inflated using a custom syringe-driver consisting of a linear stage of 175 mm travel distance and a 50 ml syringe. An analogue absolute

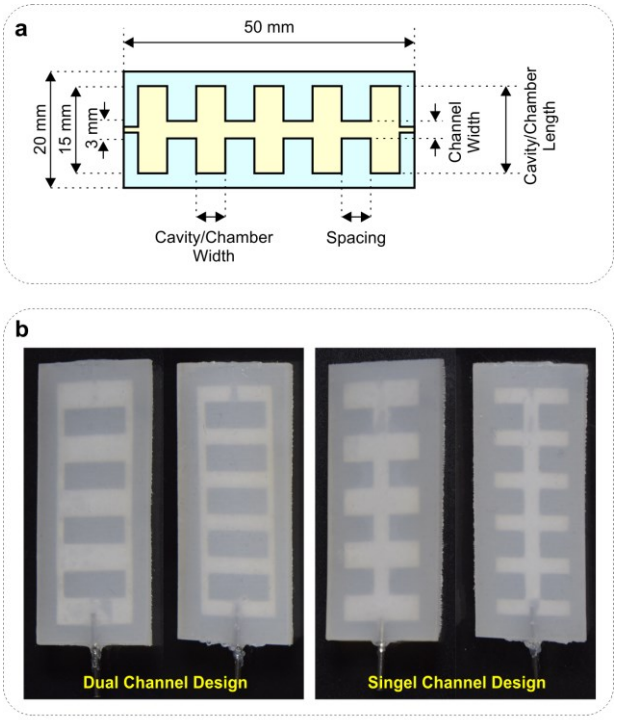

Figure 2. tSLA protoypes; (a) conceptual design and features, (b) fabricated tSLAs with different channel and cavity width configuration.

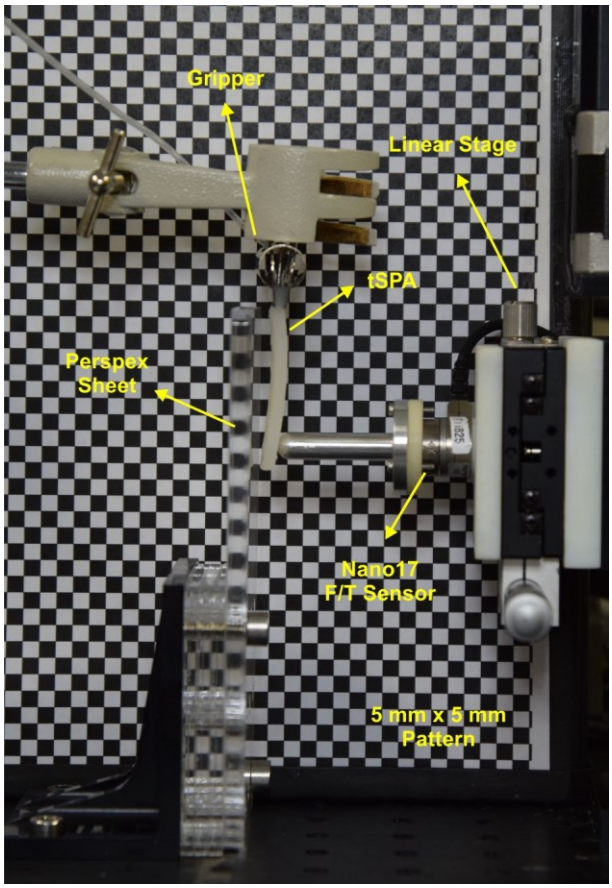

Figure 3. Experimental apparatus used to conduct block force and actuation angle experiments.

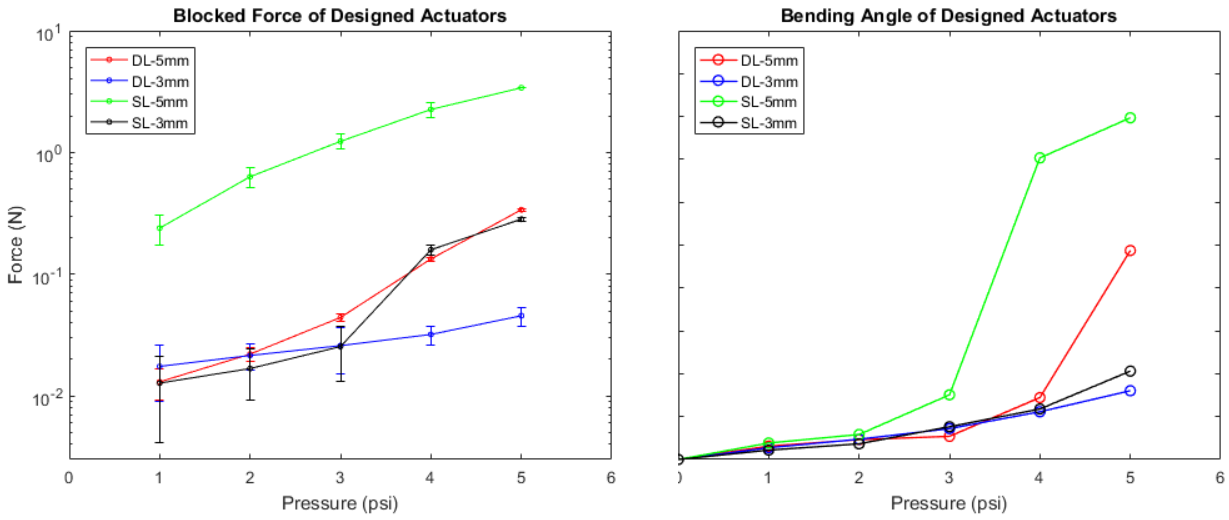

Figure 4. Results of the blocked force and tip bending angle response for the tSLAs at five static input pressures between 0 and 5 psi.

pressure transducer (30PSI SSC series absolute pressure transducer, HoneyWell, USA) was used to monitor and regulate the pressure applied to the actuator.

A 6-axis loadcell (Nano17, ATI Industrial Automation, USA) was used to measure the block force generated by the tSLAs. The actuator side surface was placed in contact with a rigid Perspex plate to minimise nonlinear effects due to bending. The pressure inside the actuator was then incrementally increased and normal force exerted by the tSLA's tip was recorded. Each experiment was repeated three times to assess accuracy and repeatability. A custom program was developed using LabVIEW (National Instruments, USA) to acquire the measurements from the loadcell and pressure transducer, while controlling the syringe pump at the set static input pressures.

The bending profile of the tSLAs at controlled input pressures were recorded by using a high definition camera (D5300, Nikon, Japan) along with a measurable calibrated backing pattern (5 mm × 5 mm grid). Intrinsic calibration of the system was conducted to mitigate lens distortion effects and verify measurement accuracy. Post processing of the images was performed using an open-source image analysis program (ImageJ, Image Processing and Analysis in Java) in which the Cartesian X and Y coordinates of the actuator tip were tracked and the resultant total bending angle was calculated.

B. Results

The range of prototype actuators were evaluated using static pressure tests in which the actuator's blocked force and bending angle were measured. All tSLAs were subjected to static pressure between 0 and 5 psi at 1 psi increments and all completed these tests without failure.

The experimental results for the blocked force of the tSLAs are shown in Fig. 3(a). In all designs, the blocked force generated by the tSLA increases with input pressure. The actuator showing the best performance (5 mm chamber width, single channel) showed a maximum blocked force of 3.5 N at 5 psi static input pressure. The tSLAs with 5 mm chamber width obtained significantly higher blocked force output when compared to the narrower 3 mm chamber design across all input pressures.

As shown in Fig. 4(a) and Table 1, the channel design (single line in the centre or double lines on the sides) can have significant influence on force generation. From our results, the blocked force increased by 10 fold for the 5 mm chamber width in the single-line channel design when compared to the double-line.

The free response of the actuators shows that the tSLA bending angle increases with pressure across all designs as shown in Fig. 4(b) and Table 1. Similar to the blocked force experiment, the bending angle of the tip is significantly higher for the 5 mm chamber width design. The channel design is also

TABLE 1. Results of the blocked force and tip bending angle response for the tSLAs at five static input pressures between 0 and 5 psi.

tSLA Designs	Blocked Force (N)					End Tip Angel (deg)				
	1 psi	2 psi	3 psi	4 psi	5 psi	1 psi	2 psi	3 psi	4 psi	5 psi
SL – 3 mm	0.0127	0.0168	0.0254	0.1586	0.2830	2.1890	3.6500	7.6480	11.7800	20.6160
SL – 5 mm	0.2390	0.6313	1.2340	2.2548	3.3974	3.8400	5.8300	15.0830	70.3470	79.6950
DL – 3 mm	0.0175	0.0215	0.0259	0.0320	0.0455	2.7440	4.7300	7.1930	11.1340	16.0420
DL – 5 mm	0.0130	0.0220	0.0441	0.1334	0.3381	3.1110	4.6280	5.4040	14.4450	48.7410

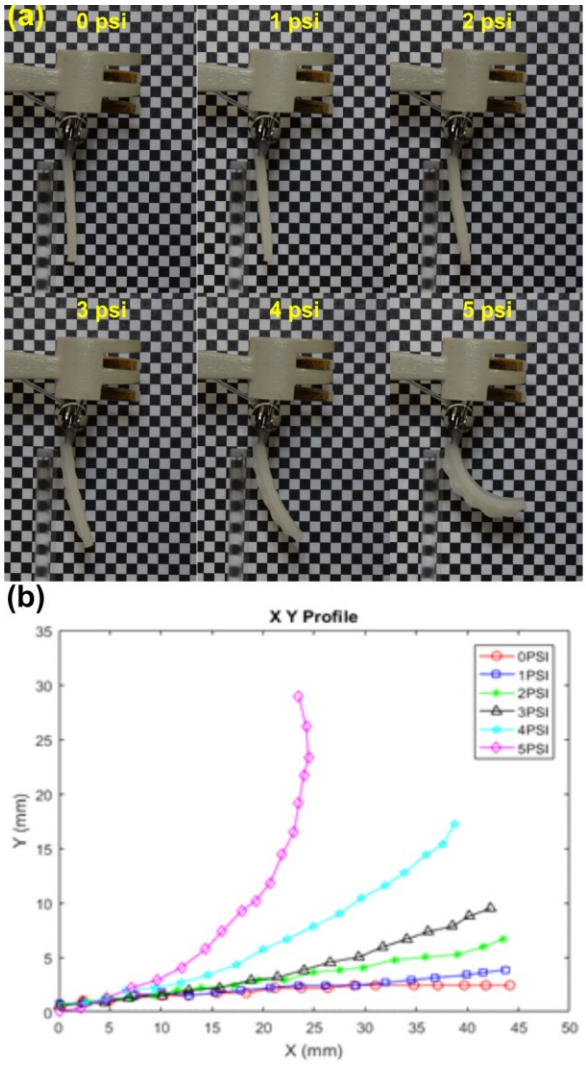

Figure 5. A prototype tSLA with 5 mm chamber width and single line channel design; (a) Side view of this actuator at 0 to 5 psi input pressures, (b) Calibrated X-Y profile of the actuator

influential, for the same cavity width, double lined configurations show lower bending. It was noted that there was expansion of the double channels at either side of the actuator which resisted the bending moment of the tSLA, hence constraining the bending of the actuator in comparison to a single channel configuration.

The sensitivity of the actuators to input pressure exhibits a noticeable non-linear response. For input pressures up to approximately 3 psi, small changes of bending angle were observed per unit pressure change. A possible explanation is that, in this pressure regime, the tSLAs stiffens by first expanding against the strain-limiting constraint fabric layer. Beyond this point, small changes in input pressure generate far larger changes in bending angle and these effects are amplified based on the cavity width.

Following these initial investigations we subjected the prototype tSLAs to additional testing to explore the bending characteristics across a range of pressures. The results for the 3 mm chamber width and single channel configurations are presented in Fig. 5 showing the Cartesian position of the actuator segments and corresponding images from which these measures were obtained. The non-linear response of the actuator across the pressure range is again evident in this response. For pressures up to 3 psi the actuator produces a near-linear response with low curvature. Beyond this, at 4 and 5 psi, there is a marked change in the form of the actuator, with higher curvature which increases toward the tip. Inspecting the images shown in Fig. 5(a) shows this is linked to expansion of the zero volume chambers and is a factor which could be controlled through manipulation of the constraint layer.

IV. Discussion

In this study, we introduced a novel thin Soft Layered Composition fabrication technique and demonstrated its capabilities through a series of proof of concept thin Soft Layered Actuators. The technique allows creation of thin laminar systems, ideally suited to actuators with zero-volume fluidic cavities but also applicable for different soft robotic devices with structural, actuation and sensing capabilities.

Using tSLC fabrication, the thickness of each layer can be carefully controlled using a film applicator (i.e. for prepolymer materials or pastes) and/or by choosing a readily available film/sheet (i.e. polyvinylidene chloride (PVDC), polyethylene terephthalate (PET), Kevlar) which can be incorporated in to the tSLC fabrication process without additional resizing or pre-processing. Use of thin "two dimensional" layers also allows the use of laser cutting and ablation techniques for the creation of precise patterns and features in/on each layer. These design features of tSLC fabrication aid repeatability of the process and enable smaller features to be embedded within soft robotic systems, hence, offering the possibility of reducing the overall scale of soft systems. This provides the opportunity for millimetre scale soft systems with precise operation which can be readily tailored for application specific requirements.

The tSLC fabrication approach can be easily extended to develop multi-material composite soft actuators consisting of multiple actuation layers in which the entire actuator is thin, small, soft flexible and stretchable. In our work to date we have produced a range of elastomeric sheets using Ecoflex series and Dragonskin series silicones. In our early designs presented here, there is no constraint layer limiting the inflation profile of the top layer during actuation. In some cases, the cavity pressure may exceed the elastic layer's yield point. This can be controlled by adding an additional constraint layer (made of a stiffer material compared to that of the inflatable layer, e.g. stiffer silicone) on top of the inflatable layer (Silicone C in Fig. 1(b)). For small gaps (< 1 mm) between chambers/features, elastic layers start to delaminate at pressures above 5 psi due to failure of the bonding mechanism. Isopropanol can be used to clean the surface before application of another layer. This was used to produce a strong bond and stop the delamination of the layers. Using this technique, tSLAs of 0.5 mm to 5 mm actuators can be produced.

tSLAs fabricated using the tSLC technique provide distinct advantages compared to similarly sized soft robotic actuators. The thin form factor of each layer allows the stacked combination of multiple layers, each bringing different functionalities (i.e. structural elements, sensing layers) without significantly increasing the thickness of the overall composite actuator. Thin soft robotic actuators are particularly interesting as they can be designed to form 3D shapes (or surfaces) from 2D structures when actuated [20]. Unlike other soft robotic actuators, their "2D" nature make tSLAs lightweight and portable, eliminating much of the material 'bulk' evident in alternatives like pneuNets.

V. Conclusion

A novel tSLC fabrication technique was proposed and used to develop a range of tSLA. The tSLAs are soft layered actuators consisting of planar 2D geometrical designs, fabricated layer by layer via lamination of silicone and used to create thin pneumatic networks. As demonstrated by our preliminary results, this fabrication technique can be used to create tSLAs in a highly controlled way with several potential applications (i.e. biomedical, search and rescue, manipulation). Although further work is required to develop design and optimization tools for these systems, the prototypes here demonstrate the many exciting opportunities for future application of this work.

Acknowledgment

The Authors would like to thank Mr. Dominic Jones and Mr Will Stokes from the Surgical Technologies Laboratory and Mr. David Readman for their technical support with LabVIEW programming of the film applicator.

References

1. Miyashita, S. et al. Ingestible, controllable, and degradable origami robot for patching stomach wounds. In: *2016 IEEE International Conference on Robotics and Automation (ICRA)*, *16-21 May 2016*, 2016, pp.909-916.
2. Russo, S. et al. Soft pop-up mechanisms for micro surgical tools: Design and characterization of compliant millimeter-scale articulated structures. In: *2016 IEEE International Conference on Robotics and Automation (ICRA)*, *16-21 May 2016*, 2016, pp.750-757.
3. Sun, Y. et al. A miniature soft robotic manipulator based on novel fabrication methods. *IEEE Robotics and Automation Letters.* 2016, **1**(2), pp.617-623.
4. Wu, W. et al. Omnidirectional Printing of 3D Microvascular Networks. *Advanced Materials.* 2011, **23**(24), pp.H178-H183.
5. Muth, J.T. et al. Embedded 3D Printing of Strain Sensors within Highly Stretchable Elastomers. *Advanced Materials.* 2014, **26**(36), pp.6307-6312.
6. Mutlu, R. et al. Effect of flexure hinge type on a 3D printed fully compliant prosthetic finger. In: *IEEE/ASME International Conference on Advanced Intelligent Mechatronics, AIM*, 2015, pp.790-795.
7. Marchese, A.D. et al. A Recipe for Soft Fluidic Elastomer Robots. *Soft Robotics.* 2015, **2**(1), pp.7-25.
8. Bryan, N.P. et al. 3D printing antagonistic systems of artificial muscle using projection stereolithography. *Bioinspiration & Biomimetics.* 2015, **10**(5), p.055003.
9. Patel, D.K. et al. Highly Stretchable and UV Curable Elastomers for Digital Light Processing Based 3D Printing. *Advanced Materials.* 2017, pp.1606000-n/a.
10. Park, Y.L. et al. Fingertip force control with embedded fiber Bragg grating sensors. In: *2008 IEEE International Conference on Robotics and Automation*, *19-23 May 2008*, 2008, pp.3431-3436.
11. Gafford, J. et al. Shape Deposition Manufacturing of a Soft, Atraumatic, Deployable Surgical Grasper1. *Journal of Medical Devices.* 2014, **8**(3), pp.030927-030927-3.
12. Shepherd, R.F. et al. Multigait soft robot. *Proceedings of the National Academy of Sciences.* 2011, **108**(51), pp.20400-20403.
13. Martinez, R.V. et al. Robotic Tentacles with Three-Dimensional Mobility Based on Flexible Elastomers. *Advanced Materials.* 2013, **25**(2), pp.205-212.
14. Chossat, J.B. et al. A Soft Strain Sensor Based on Ionic and Metal Liquids. *IEEE Sensors Journal.* 2013, **13**(9), pp.3405-3414.
15. Stokes, A.A. et al. A Hybrid Combining Hard and Soft Robots. *Soft Robotics.* 2013, **1**(1), pp.70-74.
16. Zhao, H. et al. Scalable manufacturing of high force wearable soft actuators. *Extreme Mechanics Letters.* 2015, **3**, pp.89-104.
17. Wehner, M. et al. An integrated design and fabrication strategy for entirely soft, autonomous robots. *Nature.* 2016, **536**(7617), pp.451-455.
18. Martinez, R.V. et al. Elastomeric Origami: Programmable Paper-Elastomer Composites as Pneumatic Actuators. *Advanced Functional Materials.* 2012, **22**(7), pp.1376-1384.
19. Onal, C.D. and Rus, D. A modular approach to soft robots. In: *2012 4th IEEE RAS & EMBS International Conference on Biomedical Robotics and Biomechatronics (BioRob)*, *24-27 June 2012*, 2012, pp.1038-1045.
20. Ou, J. et al. aeroMorph - Heat-sealing Inflatable Shape-change Materials for Interaction Design. In: *Proceedings of the 29th Annual Symposium on User Interface Software and Technology*, *Tokyo, Japan*. 2984520: ACM, 2016, pp.121-132.
21. Pikul, J.H. et al. Stretchable surfaces with programmable 3D texture morphing for synthetic camouflaging skins. *Science.* 2017, **358**(6360), pp.210-214.
22. Stanley, A.A. and Okamura, A.M. Deformable Model-Based Methods for Shape Control of a Haptic Jamming Surface. *IEEE Transactions on Visualization and Computer Graphics.* 2017, **23**(2), pp.1029-1041.
23. Mosadegh, B. et al. Pneumatic Networks for Soft Robotics that Actuate Rapidly. *Advanced Functional Materials.* 2014, **24**(15), pp.2163-2170.
24. Park, Y.L. et al. A soft wearable robotic device for active knee motions using flat pneumatic artificial muscles. In: *2014 IEEE International Conference on Robotics and Automation (ICRA)*, *May 31 2014-June 7 2014*, 2014, pp.4805-4810.
25. Khin, P. et al. Soft haptics using soft actuator and soft sensor. In: *Biomedical Robotics and Biomechatronics (BioRob), 2016 6th IEEE International Conference on*: IEEE, 2016, pp.1272-1276.
26. Morimoto, T.K. and Okamura, A.M. Design of 3-D Printed Concentric Tube Robots. *IEEE Transactions on Robotics.* 2016, **32**(6), pp.1419-1430.
27. Yuen, M.C. and Kramer, R.K. Fabricating microchannels in elastomer substrates for stretchable electronics. In: *ASME 2016 11th International Manufacturing Science and Engineering Conference, MSEC 2016*, 2016.
28. Atalay, A. et al. Batch Fabrication of Customizable Silicone-Textile Composite Capacitive Strain Sensors for Human Motion Tracking. *Advanced Materials Technologies.* 2017, **2**(9), pp.1700136-n/a.